Electrochemical Studies in Room Temperature Ionic Liquids

Debbie Sue Silvester

St John's College

University of Oxford

DPhil Thesis

Trinity Term 2008

Physical and Theoretical Chemistry

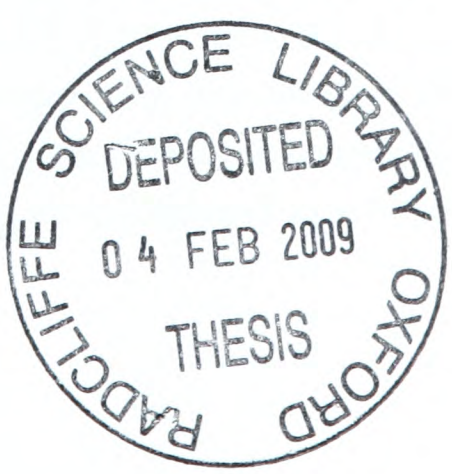

Electrochemical Studies in Room Temperature Ionic Liquids

A Thesis Submitted for the Degree of DPhil in Chemistry

by Debbie Sue Silvester

St John's College, University of Oxford

Trinity Term 2008

The work presented in this thesis involves the application of room temperature ionic liquids (RTILs) as solvents for use in electrochemical experiments. Initially, the fundamentals of electrochemistry is presented, followed by a comprehensive overview of RTILs in terms of their properties, applications and their behaviour as electrochemical solvents compared to conventional aprotic solvents. The results of 8 original studies are then presented as follows:

- X-Ray photoelectron spectroscopy is used to quantify the concentration of bromide ions in an ionic liquid, and is independently confirmed by potential-step chronoamperometry
- The reaction mechanisms and kinetics for the electrochemical reduction of some aromatic nitro compounds (namely nitrobenzene and 4-nitrophenol) are determined
- The electrochemistry of phosphorus trichloride and phosphorus oxychloride is studied in detail for the first time, due to the unusual stability of these highly reactive compounds in RTILs
- The reductions and oxidations of sodium and potassium nitrate are studied, giving rise to 'melt'-like behaviour. The electrodeposition of sodium oxide on platinum is also demonstrated
- The electrochemical oxidation of nitrite and the oxidation and reduction of the toxic gas, nitrogen dioxide, is presented
- The oxidation of hydrogen gas is studied in ten RTILs with a range of different cations and anions, and contrasting interactions with the RTIL anions are seen
- The electrochemical oxidation of ammonia gas is studied in five RTILs with different anions and a general reaction mechanism is suggested
- The reduction of benzoic acid is studied in six RTILs, and the kinetics of the dissociation step are found to be very fast

The first five studies are all carried out in one particular ionic liquid, and the reactions and mechanisms are compared to that observed in conventional aprotic solvents. The last three studies employ several RTILs with different cations and anions to look at the contrasting interaction of protons with the RTIL cation/anion and ultimately help to understand the pH properties of the solvent. The overall findings from the work in this thesis are that some reactions and mechanisms (*e.g* bromide, nitro derivatives and ammonia) are generally the same in RTILs as in conventional aprotic solvents, but other species (*e.g.* nitrates, phosphorus derivatives) show remarkably different behaviour. It has also been demonstrated that RTILs are suitable media for the detection of nitrogen dioxide, hydrogen and ammonia gases. This suggests that RTILs could potentially offer many advantages when employed as solvents in electrochemical reactions and in amperometric gas sensors.

Acknowledgements

First and foremost, I would like to thank Professor Richard G. Compton for welcoming me into his research group for three years and for letting me accompany him to several enjoyable conferences. It has been a pleasure to work with such a great supervisor, both on an academic and personal level, and I am grateful of all the opportunities he has given me.

I would also like to thank my co-workers who have made the work in this thesis possible. To Professor Christopher Hardacre, Dr. Cristina Lagunas and Leigh Aldous at QUILL in Belfast for providing all of the ionic liquid samples used throughout this thesis, and many helpful answers to my countless questions. To Dr. Alison Crossley at the Materials Department, Oxford University for carrying out the XPS experiments and taking a huge gamble putting a liquid into her expensive spectrometer.

I would also like to thank *all* members of the Compton group, past and present, for making my three years in Oxford so enjoyable. Special mentions go to Emma Rogers for her love of chips, cheese and beans, glamming up for guest dinners, climbing, simulations, being a dab hand with CorelDraw and being a true intellectual; Laura Barrosse-Antle for the carrot, the sleepover, losing her hat, superglue, various encounters with duct tape and for proof-reading Chapter 2; Tessa Broder for lunchtime Neighbours, wrestling, throwing the rat in my drink and generally being abusive; Aoife O'Mahony for her amusing Irish phrases, climbing, botox, Basildon and keeping me entertained even after presenting her talk to me 12 times; Jenny Long for disney songs, amusing secret santa gifts and the memorable head injury; Weisi He for the yellow pig, owning so many mobile phones and getting drunk after just one vodka and orange(!); Kass Toghill for ladies nights, talking about nothing in particular and having the perfect body to be Lara Croft; Andy Wain for being a great mentor and falling off the chair; Greg Wildgoose for taking it like a man, the contact lens solution 'incident' and answering simple questions in far too much detail; Xiaobo Ji for his positivity, enthusiasm and for attempting to outdrink Paul at the pirate party; Biljana for always being so nice and for taking us to dinner at Keble; Behzad (Roohollah Torabi) for allerting the terrorism police and driving us through a marsh; Sarah Ward Jones for being a great dancer and accompanying me to Winnipeg; Lei for recovering the rat and thinking that Belfast was in Amsterdam; Neil Rees for group gossip; Denis for waking up Moscow; and to various Part II's and summer students (Andy, Alex, Edmund, Chris, Darren, Kris, Ben and Martin) for many enjoyable sessions in the Flag and college bar.

Finally, I would like to thank my family and in particular, my husband Paul, for all their support and encouragement over the last few years. I look forward to starting a new life with Paul in Australia.

Contents

Glossary

Table 1: List of symbols commonly used throughout this thesis.

Symbol	Definition
α	charge transfer coefficient
δ	diffusion layer thickness
η	dynamic viscosity
κ	specific conductivity
ρ	density
τ	dimensionless time parameter
ϕ	work function of the spectrometer
ϕ_{m}	electrostatic potential of the electrode (metal)
ϕ_{OHP}	electrostatic potential at the Outer Helmholtz Plane
ϕ_{s}	electrostatic potential of the solution
υ	scan rate
a	hydrodynamic radius
c	concentration
C	homogeneous chemical reaction step
$\mathrm{c_{bulk}}$	bulk concentration
C_{dl}	double layer capacitance
D	diffusion coefficient
D_∞	constant corresponding to hypothetical diffusion coeficient at infinite temperature
$\frac{\partial c}{\partial x}$	direction of concentration gradient
$\frac{\partial \phi}{\partial x}$	direction of potential gradient
$\frac{dE}{dt}$	variation in potential with time
δt	time interval
δx	distance
dx	width
e^-	electron
E	heterogeneous electron transfer step
E	potential
E_1	begin potential
E_2	end potential where voltammogram is reversed
$E_{1/2}$	half wave potential
E_0	standard electrode potential
$E_{\mathrm{a,D}}$	diffusional activation energy
E_{app}	applied potential
E_{binding}	energy of electrons emitted from a one-electron configuration within the atom
$E_{\mathrm{f}}{}^0$	formal electrode potential
E_{kinetic}	kinetic energy of emitted electron

Table 2: List of symbols commonly used throughout this thesis contd....

Symbol	Definition
E_{photon}	energy of X-ray photons
ΔE_{pp}	peak-to-peak separation
E_{RE}	potential difference across the reference electrode/solution interface
E_{WE}	potential difference across the working electrode/solution interface
F	Faraday constant (96485 C mol^{-1})
f	fraction of wave heights for 'split wave'
i	current
i_0	standard exchange current
i_{b}	current for the backward process
i_{c}	charging or capacitative current
i_{d}	diffusion limited current in a chronoamperometric experiment
i_{f}	current for the forward process
i_{p}	peak current at a macroelectrode
i_{ss}	steady state limiting current
J	flux
J_{d}	diffusional flux
J_{m}	migratory flux
k_1	forward rate constant for a homogeneous chemical step
k_{-1}	backward rate constant for a homogeneous chemical step
k_{b}	backward rate constant
k_{B}	Boltzmann constant (1.38×10^{-23} J K^{-1})
k_{f}	forward rate constant
k_0	standard heterogeneous rate constant
K_{eq}	equilibrium constant
M	molar mass
n	number of electrons or a real integer > 0
n_{rd}	number of electrons transferred in the rate determining step
O	general solution species prone to undergoing a one-electron reduction
$[\text{O}]_0$	concentration of species O at the electrode surface
R	general solution species prone to undergoing a one-electron oxidation
R	universal gas constant (8.314 J mol^{-1} K^{-1})
$[\text{R}]_0$	concentration of species R at the electrode surface
R^2	least-squares correlation coefficient
r_{d}	radius of disk electrode
r_{hemi}	hemispherical radius of disk electrode
R_{s}	uncompensated resistance
t	time
Δt	time interval
T	absolute temperature
T_0	ideal gas temperature
u	ionic mobility
x	direction
Δx	length interval
z	charge

Table 3: List of units commonly used throughout this thesis.

Unit	Definition
A	amp
atm.	atmospheric pressure
C	coulomb
cP	centipoise
cm	centimetre
d.p.	decimal places
eV	electron volt
K	Kelvin
kV	kilo volt
M	molar mass
m	metre
mm	millimetre
mM	millimolar
mS	millisiemens
μm	micrometre
nA	nanoamp
nm	nanometre
ppb	parts per billion
ppm	parts per million
s	seconds
V	volt

Table 4: List of abbreviations commonly used throughout this thesis.

Abbreviation	Definition
A^-	solvent anion
AFM	atomic force microscopy
BDD	boron doped diamond
BE	binding energy
BQ/H_2Q	benzoquinone/hydroquinone
BZA	benzoic acid
Cc/Cc^+	cobaltocene/cobaltocenium
EPR	electron paramagnetic resonance
ESR	electron spin resonance
EW	electrochemical window
3-D	three dimensional
DBCH	dibromocyclohexane
DCM	dichloromethane
DEA	diethylamino
DMA	dimethylamino
DMF	*N*,*N*-dimethylformamide
DMSO	dimethyl sulfoxide
DPP^+	2,6-diphenylpyrylium cation
Fc/Fc^+	ferrocene/ferrocenium
HA	proton solvated by solvent anion
IL	ionic liquid
IUPAC	International Union of Pure and Applied Chemistry
MeCN	acetonitrile
NM	nitromethane
NMR	nuclear magnetic resonance
OHP	outer Helmholtz plane
PTFE	polytetrafluoroethylene
PC	propylene carbonate
PVC	polyvinylchloride
PZC	potential of zero charge
QUILL	Queens University Ionic Liquids Laboratory
rds	rate determining step
RE	reference electrode
RTIL	room temperature ionic liquid
TBAP	tetra-*n*-butylammonium perchlorate
TMPD	N, N, N', N'-tetramethylphenylenediamine
THF	tetrahydrofuran
UHV	ultra-high vacuum
vdW	van der Waals
VOCs	volatile organic compounds
VTF	Vogel-Tammann-Fulcher
XPS	X-ray photoelectron spectroscopy
WE	working electrode

Chapter 1

Fundamentals of Electrochemistry

Electrochemistry is the study of the interface between an electrode (an electronic conductor) and an electrolyte (an ionic conductor), and falls into two distinct categories. The first is known as 'equilibrium electrochemistry' and occurs when a potential difference is established between the electrode and electrolyte without the passage of a sustained current. This can yield a wealth of thermodynamic information such as reaction free energies, entropies and enthalpies, equilibrium constants, activities and solution pHs.[1] The second is known as 'dynamic electrochemistry' and involves the study of electron transfer reactions between an electrode (usually metallic) and a reactant molecule (a species usually in the solution phase). A potential difference is applied between the electrode and electrolyte and the current is monitored as a function of the applied potential. The resulting plot is known as a voltammogram and provides both kinetic and thermodynamic information on the electron transfer process.[2]

In this thesis we are mostly concerned with the second type of electrochemical process, *i.e.* the study of the reactions occuring between a solid electrode and an electrolyte solution. The rest of this chapter serves as an introduction to the fundamental electrochemical principles and methods relevant to the work reported in this thesis. A more detailed account can be found in several standard Electrochemistry textbooks.[3–7]

1.1 The Electrode/Solution Interface

In voltammetry, a potential is applied between an electrode and an electrolyte solution to induce a current, the magnitude of which is measured as a function of that potential. Before we can design and successfully interpret the observations made during electrochemical experiments, it is important to first consider the structure of the electrode/solution interface and the types of

current that may be induced to flow across it.

1.1.1 Structure of the Interfacial Region

In an electrochemical experiment, the electrode acts as a source or sink of electrons. When immersed in an electrolyte solution, a potential difference develops across the interface as a result of charge separation between the electrode and solution. This causes the ions in the immediate vicinity of the electrode surface to re-orientate themselves in an effort to achieve the most energetically stable arrangement and to maintain electroneutrality. As a result, ions of opposite charge are attracted to the electrode surface and ions of the same charge are repelled. An electric field gradient is established extending out towards the bulk solution, and this region is termed the 'double layer'.

There have been various models proposed to describe the structure of the double layer. Helmholtz[8,9] first proposed a relatively simple model where two rigid layers of equal and opposite charge are formed at each side of the electrode-electrolyte interface, confined to a region known as the Outer Helmholtz Plane (OHP). A more realistic model was then proposed by Gouy[10] and Chapman,[11] who treated the ions as point charges and proposed that the potential dropped exponentially over a 'diffuse layer', tending to the bulk solution value. Stern[12] then developed a new model (shown in Figure 1.1) that eliminated weaknesses of the two earlier models. He suggested that the double layer was indeed comprised of an OHP which was opposite (but not equal) in charge to the electrode surface, as well as a diffuse layer of ions treated as spheres of realistic dimensions, rather than point charges. In this model, the potential drops linearly between the electrode (ϕ_{m}) and OHP (ϕ_{OHP}) and then exponentially decreases to the bulk solution (ϕ_{s}). Further refinements to the model were then made by Bockris *et al.*[13] and Grahame,[14] although the Stern approach is generally adequate to describe the interfacial region.

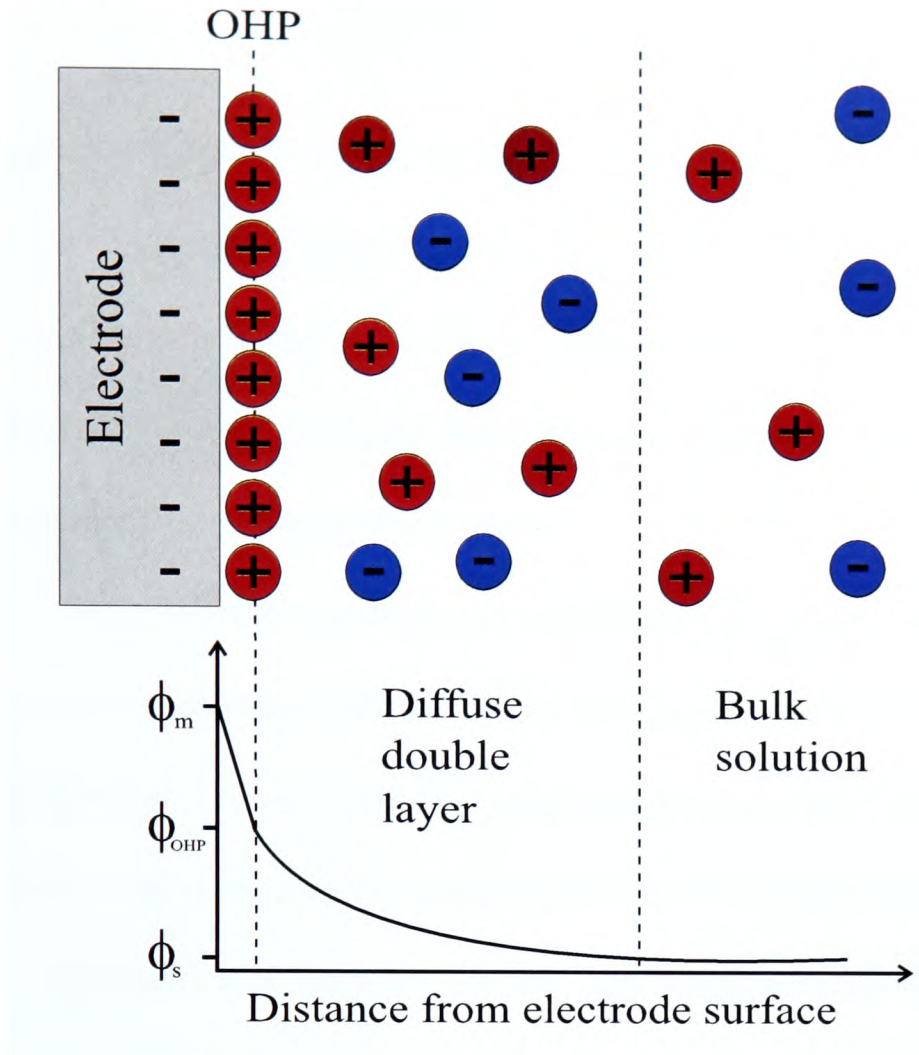

Figure 1.1: A schematic diagram of the Stern[12] double layer model and the variation of electrical potential against distance from the electrode surface.

1.1.2 Faradaic and Nonfaradaic Processes

Two types of activity can take place at an electrode surface and contribute to the measured current. The first is termed 'faradaic' (after Sir Michael Faraday)[15] and involves the transfer of electrons between the metal electrode and electroactive species in solution. Depending on the direction of the flow of electrons, the species can either be oxidised or reduced, and the amount converted by electrolysis is proportional to the amount of charge passed. For one mole of electrons, the charge passed is 96485.4 C, known as the Faraday constant, F. In the absence of any additional processes, one Faraday of charge is passed per one mole of reactant consumed (assuming n=1).

The second type of process is termed 'non-faradaic' and can be caused by adsorption/desorption processes and changes in the interfacial structure as the potential is varied, resulting in charge and discharge of current. This type of charging current, i_c, (sometimes called capacitative current) can be described by:

$$i_c = AC_{dl}\frac{dE}{dt} = AC_{dl}\upsilon \tag{1.1}$$

where A is the electrode area, C_{dl} is the double layer capacitance, $\frac{dE}{dt}$ is the variation in potential with time and υ is the scan rate. Non-faradaic charging currents can be undesirably large when the scan rate is high (*e.g.* kV s^{-1}, often used in 'fast scan' voltammetry), so electrodes of small diameter (microelectrodes) are required in such experiments to avoid the faradaic response being swamped by capacitative currents.

Although both faradaic and non-faradaic processes contribute to the overall measured current response, experimental conditions are usually designed so that non-faradaic contributions are minimised, and only faradaic processes are recorded. The magnitude of any faradaic current is mainly dependent on the following factors: the rate of mass transport of an electroactive species to and from the electrode surface, any heterogeneous electron transfer between the electrode and solution at the interface, and any homogeneous chemical reactions ocurring before or after the electron transfer. These topics will be addressed in the following sections.

1.2 Mass Transport

In order for an electrode process to occur, a fresh supply of electroactive material must be transported from the bulk solution to the electrode surface. The motion of molecules and ions in solution can generally be divided into three main categories; diffusion, migration and convection, each of which will be described below.

1.2.1 Diffusion

Diffusion is the movement of species in solution from an area of high concentration to an area of low concentration due to the presence of a concentration gradient. When an electroactive species is depleted near the electrode surface (by electrochemical oxidation or reduction), a significant concentration gradient is formed, driving the movement of fresh material to replenish

the exhausted region. This effect is described mathematically by Fick's first law:[16]

$$J_d = -D\frac{\partial c}{\partial x} \tag{1.2}$$

where J_d is the flux due to the diffusion of a species with concentration c in direction x, $\frac{\partial c}{\partial x}$ is the concentration gradient in the direction from x to a plane surface and D is the measure of the ease with which the species diffuses, known as the diffusion coefficient of the species, given by:

$$D = \frac{(\delta x)^2}{2\delta t} \tag{1.3}$$

where δt is the time interval in which a particle moves a distance of δx. The value of D in aqueous solution typically varies between 10^{-9} and 10^{-10} m^2 s^{-1} at 298 K,[7] and is dependent on factors such as molecular size of the diffusing species, solvent viscosity and temperature. The negative sign in equation 1.2 arises because the flux of the species tends to oppose the concentration gradient.

In order to describe the variation of concentration with time, we first consider the flux of material in and out of an element with width dx, as shown below:

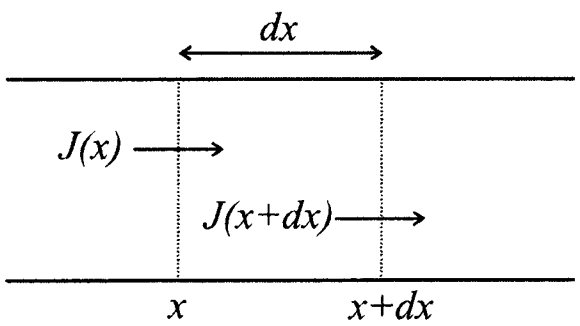

Figure 1.2: Flux in and out a region of width dx.

The rate of change of concentration with time within this region is given by:

$$\frac{\partial c}{\partial t} = \frac{J(x) - J(x+dx)}{dx} \tag{1.4}$$

By differentiating equation 1.2 and substituting into equation 1.4, we obtain Fick's second law of diffusion:

$$\frac{\partial c}{\partial t} = D\frac{\partial^2 c}{\partial x^2} \tag{1.5}$$

which can be written for a three-dimensional system to describe transport in each direction:[2]

$$\frac{\partial c}{\partial t} = D\frac{\partial^2 c}{\partial x^2} + D\frac{\partial^2 c}{\partial y^2} + D\frac{\partial^2 c}{\partial z^2} \tag{1.6}$$

This equation enables the prediction of concentration changes of an electroactive material close to the electrode surface.

1.2.2 Convection

Convection is the movement of species due to a mechanical force acting on the solution. There are two types; 'natural' convection, which arises from thermal gradients and/or density differences within the solution, and 'forced' convection, which occurs through external forces, such as gas bubbling through a solution, pumping, stirring or motion of the electrode. 'Natural' convection forces are often undesirable and difficult to predict, but are not significant on short timescales ($<$ 10 seconds) and only become important when slow voltage scan rates are employed. Under such conditions, forced convection (which is several orders of magnitude greater and more predictable than natural convection) may be introduced to overwhelm the effects of natural convection, improving the reliability and reproducibility of experimental results.

1.2.3 Migration

Migration is the movement of a charged species due to the presence of an electric field.[4] When a potential is applied to a solution, an electric potential gradient is established in the interfacial region between the electrode and the solution, inducing the migration of charged species towards the electrode. The migratory flux, J_m, can be expressed mathematically by:[2]

$$J_m = -uc\frac{\partial \phi}{\partial x} \tag{1.7}$$

where u is the ionic mobility, c is the concentration and $\frac{\partial \phi}{\partial x}$ is the direction of the potential gradient. The mobility is given by the Einstein relation:[4]

$$u = \frac{|z|FD}{RT} \tag{1.8}$$

where z is the charge, R is the universal gas constant, F is the Faraday constant and T is the temperature. Unfortunately, migration can have unpredictable and complicated effects on voltammetry,[3] but can be overcome by introducing a large excess of chemically and electrochemically inert 'background electrolyte' in the solution. The concentration of background electrolyte must be at least 30 times greater than that of the electroactive species, usually satisfied by 0.1 M.[3] The excess of ions near the interfacial region creats an 'atmosphere' that ensures that electric fields do not build up beyond the double layer, essentially maintaining electroneutrality during electrolysis.

In addition to this, there are other advantages to using a supporting electrolyte. Firstly, the abundance of ions results in the compression of the double layer to a very small region (*ca.* 10-20 Å), facilitating electron transfer *via* quantum mechanical tunneling. Secondly, the solution conductivity is increased and results in reduced Ohmic drop effects, which can distort (stretch or slant) voltammetry due to electrical resistance of the solvent to the passage of current. Thirdly, the activity coefficient of the electroactive material becomes fixed, which is important since changing the activity coefficient is likely to have a dramatic and undesirable effect on voltammetry.

1.2.4 The Diffusion Coefficient

In the last sections, the diffusion coefficient has been introduced as a measure of the ease with which a species diffuses, or alternatively the rate at which material moves down a concentration gradient. In practice, it is more useful to think of the diffusion coefficient in terms of hydrodynamic theory, which relates D to the inverse of solvent viscosity according to the Stokes-Einstein relation:[7]

$$D = \frac{k_{\mathrm{B}}T}{6\eta\pi a} \tag{1.9}$$

where k_B is the Boltzmann constant, T is the temperature, η is the viscosity and a is the hydrodynamic radius of the diffusing species (which encompasses the radius of the molecule and its solvation shell).

There are also other ways to experimentally calculate D, including using the steady-state limiting current at a microdisk electrode (see section 1.6.2.2), the Randles-Sevčik method[17,18] (see section 1.6.2.1) and the Cottrell equation[19] (see section 1.6.1). The variation of the diffusion coefficient with temperature is given by the following Arrhenius relationship:

$$D = D_\infty \exp\left(\frac{-E_{a,D}}{RT}\right) \tag{1.10}$$

where D_∞ is a constant corresponding to the hypothetical diffusion coefficient at infinite temperature, R is the universal gas constant and $E_{a,D}$ is the diffusional activation energy of the electroactive species.

1.3 Heterogeneous Electron Transfer

In the last sections, the processes by which electroactive material is transported to an electrode surface has been described. We now move on to consider the faradaic currents produced from an electron transfer reaction in terms of electron transfer kinetics.

1.3.1 The Butler-Volmer Model

There have been several attempts to rationalise the rate of heterogeneous electron transfer, but the most widely accepted treatment is that proposed by Butler[20] and Volmer,[21] and is assumed for all the work reported hereafter in this thesis. To explain this model, it is useful to consider the simple one-electron reduction of a species, O, to its reduced form, R:

$$O + e^- \underset{k_b}{\overset{k_f}{\rightleftharpoons}} R \tag{1.11}$$

where k_f and k_b are the forward and backward rate constants for the heterogeneous electrochemical processes, respectively.

Any current flow is proportional to the rate constant and the concentration of species A and B at the electrode surface. Therefore, at a given potential, the overall current can be expressed as the sum of currents for the forward and reverse processes:

$$i = i_b + i_f = FAk_b[R]_0 - FAk_f[O]_0 \tag{1.12}$$

where F is Faraday's constant, A is the electrode area and $[R]_0$ and $[O]_0$ are the concentrations of species R and O at the electrode surface. Using transition state theory, the two rate constants can be expressed as:

$$k_f = k_0 \exp\left(-\frac{\alpha F(E - E_f{}^0)}{RT}\right) \tag{1.13}$$

$$k_b = k_0 \exp\left(\frac{(1-\alpha)F(E - E_f{}^0)}{RT}\right) \tag{1.14}$$

where k_0 is the standard electrochemical rate constant, $(E - E_f{}^0)$ is the overpotential (the difference between the potential and the formal potential) and α is the transfer coefficient. When no overpotential is applied (*i.e.* $E = E_f{}^0$), the standard electrochemical rate constant is the value of k_f and k_b, and has the same dimensions. The transfer coefficient, α, is a measure of the symmetry of the energy barrier for electron transfer.[2] It is a dimensionless quantity with a value between 0 and 1, usually close to 0.5, reflecting the fact that the transition state lies 'midway' between species A and species B.

By substituting equations 1.13 and 1.14 into equation 1.12, we arrive at the Butler-Volmer equation:

$$i = FAk_0\left[[R]_0 \exp\left(\frac{(1-\alpha)F(E - E_f{}^0)}{RT}\right) - [O]_0 \exp\left(-\frac{\alpha F(E - E_f{}^0)}{RT}\right)\right] \tag{1.15}$$

This equation can be combined with equations for mass transport to give a theoretical treatment for the current response to the applied potential (see section 1.7).

1.3.2 Electrochemical Reversibility

The term 'reversibility' provides an indication of the rate of the electron transfer kinetics of a redox couple. An 'electrochemically reversible' system is one where electron transfer is sufficienly fast that equilibrium is achieved on a short timescale and maintained as the potential is varied. Under these conditions, equation 1.15 simplifies to the Nernst equation:[1]

$$E = E_f{}^0 + \frac{RT}{F}\ln\frac{[R]_0}{[O]_0} \tag{1.16}$$

This describes how the electrode potential varies with electrolyte composition at the electrode surface under equilibrium conditions.[1] In the other extreme, a system with relatively slow electrode kinetics is classed as 'irreversible'. In this case, equilibrium is not attained at potentials close to $E_f{}^0$ on the timescale of the experiment, and a significant overpotential must be applied to drive a reaction. Systems displaying intermediate electrode kinetics are termed 'quasi-reversible'.

For irreversible reactions, between the limiting current plateau of a voltammogram and the equilirium potential there is a region of potential where the current depends exponentially on potential, described by the following form of the Butler-Volmer equation:

$$i = i_0 \exp\left(\frac{-\alpha F(E - E_f^0)}{RT}\right) \tag{1.17}$$

where i_0 is the standard exchange current. This equation can be arranged to give the 'Tafel' equation:[2,4,5]

$$\ln i = \ln i_0 - \frac{\alpha F(E - E_f^0)}{RT} \tag{1.18}$$

Using the above equation, the exchange current and transfer coefficient may be determined.

1.4 Homogeneous Processes

When an electrochemical process is coupled with homogeneous chemical reactions, the effect on voltammetric behaviour can be significant, and electrochemical methods can be employed to study kinetics and mechanisms. A simple notation used to describe such processes was proposed by Testa and Reinmuth,[22] with the letter '**E**' used to describe an electrochemical step, and the letter '**C**' for a chemical process. These terms are combined in the order in which they occur in the reaction mechanism. The types of reactions most relevant to this thesis include EC, ECE and CE mechanisms, which are briefly introduced below.

1.4.1 EC Mechanism

In an EC process, the product of the electrochemical step (E) is unstable and undergoes a follow-up chemical step (C) to yield a species which is electrochemically inert in the potential window of interest. An example of this type of mechanism is the one-electron reduction of the 2,6-diphenylpyrylium cation (DPP^+) in acetonitrile:[23]

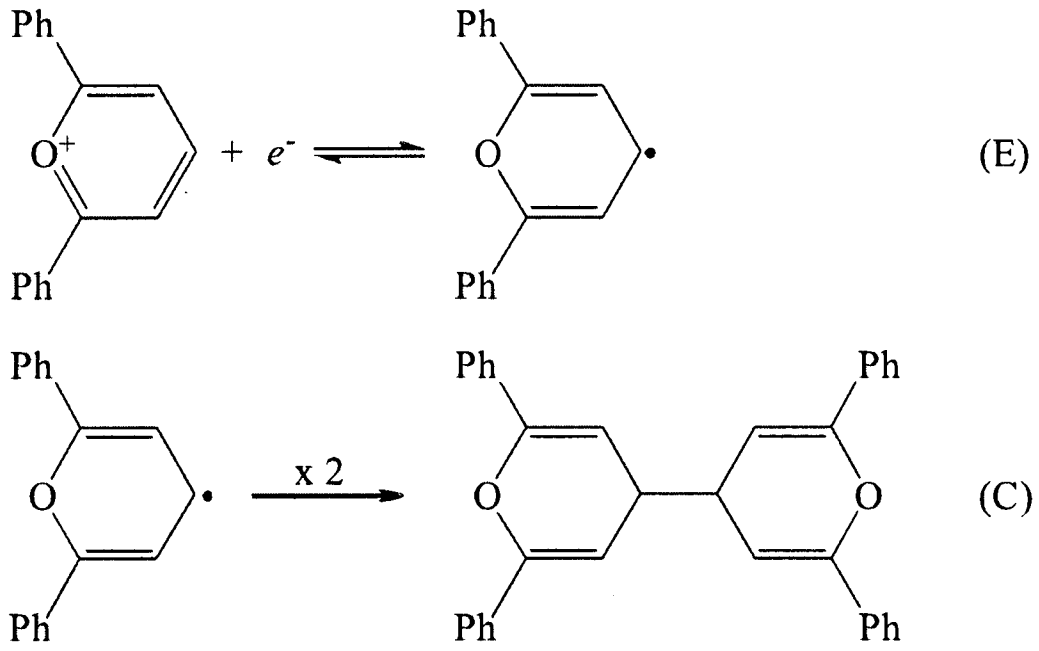

In this process, the parent molecule (DPP^+) is reduced by one electron to form a highly reactive radical species, which then rapidly dimerises in solution. The chemical step is second order, so in this case the mechanism is denoted as EC_2.

1.4.2 ECE Mechanism

An ECE reaction is essentially the same as an EC reaction, except the product formed is electrochemically active in the potential window under study and is itself immediately reduced or oxidized. An example is the reduction of 4-nitrosophenol in aqueous solution:[24]

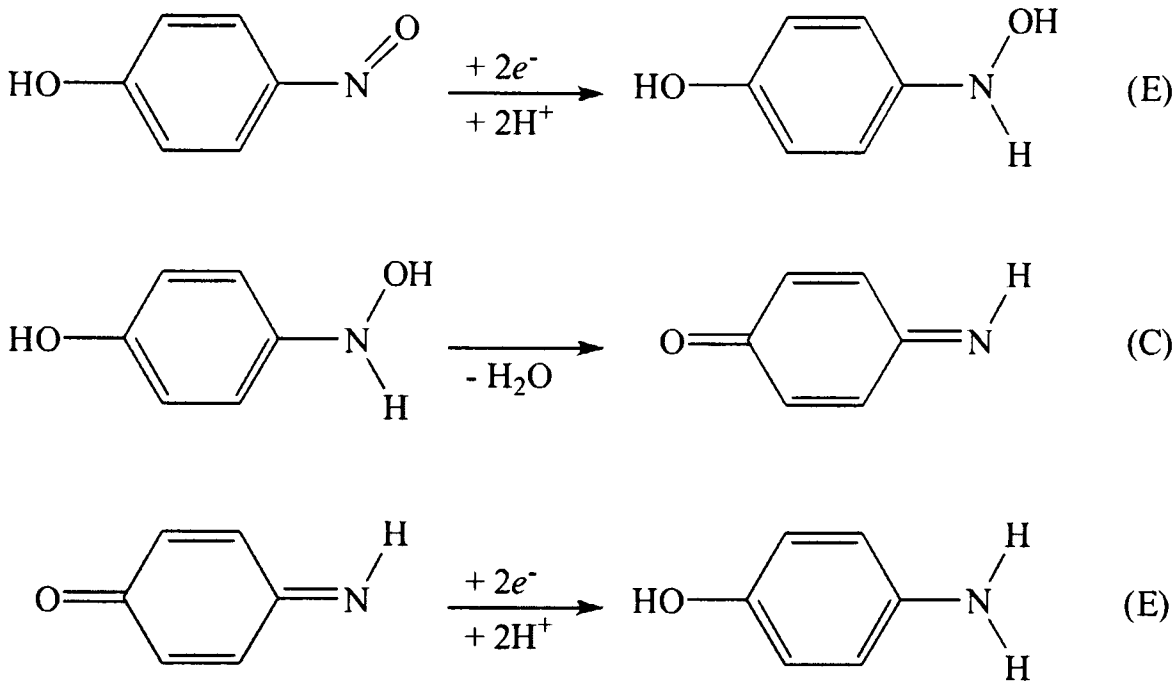

In this reaction, the nitroso-group is reduced by two electrons to hydroxylamine, which then dehydrates to 4-benzoquinoneimine, and is then rapidly electrochemically reduced to 4-aminophenol.

1.4.3 CE Mechanism

In a CE process, the parent molecule undergoes a homogeneous chemical step (C) prior to electron transfer (E). An example of this is the reduction of a weak acid such as acetic acid:[25]

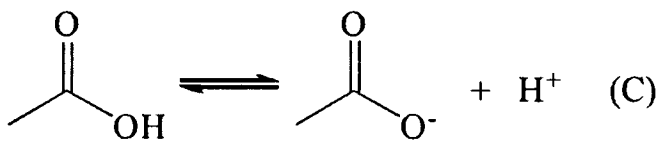

$$H^+ + e^- \rightleftharpoons {}^1/_2\, H_2 \qquad (E)$$

In this reaction, acetic acid dissociates into acetate and a proton. The proton is then electrochemically reduced by one-electron to form hydrogen. The kinetics of the dissociation step (C) determines the current, and thus can be studied using electrochemical techniques. This type of analysis is presented in Chapter 11 for the reduction of benzoic acid.

1.5 Practical Electrochemistry

The last few sections have outlined the basis of electrochemical processes in terms of well-established theory. We next move on to consider the practical aspects associated with measuring the various parameters that have been introduced. The initial focus is on the design of cells for electrochemical experiments, and the types of electrodes employed.

1.5.1 Electrochemical Cells

An electrochemical cell is a device consisting of two half-cells that are in electrical contact. In dynamic electrochemistry, we are usually only interested in faradaic processes taking place at a single working electrode (WE), where one half-cell reaction occurs. In order to complete the electrochemical circuit, a second electrode called a 'counter electrode' is added to the cell, which acts to balance the injection of charge in the solution at the WE, and this is where the second half-cell reaction takes place. It is important to ensure that a counter electrode process does not interfere with a process occuring at the WE, as this can have significant complications in understanding voltammetric behaviour.

Experimentally, it is common to use a third electrode, called a 'reference electrode' (RE) in a three-electrode arrangement with the working and counter electrodes. The voltage of the WE is then measured relative to the RE. The potential of the RE remains fixed throughout the experiment, and any changes in the externally applied potential are directly related to those at the WE. The applied potential, E_{app}, is given by:[2]

$$E_{\text{app}} = E_{\text{WE}} - E_{\text{RE}} - iR_{\text{s}} \tag{1.19}$$

where E_{WE} and E_{RE} are the potential differences across the WE/solution and RE/solution interface, respectively, i is the current and R_{s} is the uncompensated resistance of the electrolyte solution. The final term in equation 1.19 is called 'Ohmic drop', and can result in the appearance of stretched or 'slanted' voltammetry. Ohmic drop is usually small (particularly in highly

conducting solutions containing a large concentration of supporting electrolyte *e.g.* 0.1 M) and in many cases is negligible. If present, it can be minimised either by reducing the distance between the working and reference electrodes, or by decreasing the size of the working electrode such that only small currents are passed (*e.g.* to micron sized dimensions). In the latter case, the reference and counter electrodes can be combined to give a two-electrode set-up, with the second electrode acting both as a reference and counter electrode, termed a 'quasi-reference electrode'.

There are a variety of WE geometries routinely used in electrochemical experiments, but the most prolific is the disk (described in detail in the next section). Counter electrodes are typically good electronic conductors (*e.g.* metals) with a large surface area, so as not to limit electron transfer at the WE. There are four main types of RE (described in section 1.5.3).

1.5.2 Disk Electrodes

Microdisk and macrodisk electrodes are a very popular type of working electrode in electrochemical experiments and are used extensively throughout this thesis. One of the reasons for their widespread use is their ease of fabrication; a conducting metal wire is sealed into an insulating material (such as glass or PTFE) and a cross-section of the wire is exposed. In addition, the symmetry of the disk serves to simplify mass transport considerations, and disk electrodes can be considered theoretically in two-dimensions.

There are two types of diffusion that can occur at a disk electrode. 'Planar' diffusion takes place at all points normal to the disk surface, and 'convergent' diffusion takes place at the disk edges, illustrated graphically in Figure 1.3a. When the disk size is large (a so called 'macro-electrode'), convergent diffusion is negligible and planar diffusion dominates. The mathematical expression for linear (planar), one-dimensional diffusion is given by:[7]

$$\sqrt{D\pi t} << r_{\mathrm{d}} \tag{1.20}$$

where D is the diffusion coefficient, t is the time and r_{d} is the radius of the disk electrode.

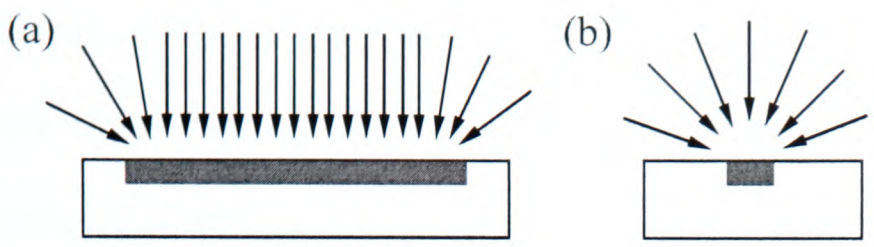

Figure 1.3: Comparison of diffusion patterns at (a) macrodisk and (b) microdisk electrodes.

When the disk radius is sufficiently small (less than *ca.* 50 μm, called an 'ultramicroelectrode' or more simply a 'microelectrode') convergent diffusion dominates, and the linear component is negligible (at conventional voltage scan rates). This type of diffusion is called 'hemispherical' and is depicted in Figure 1.3b. At higher scan rates, planar diffusion can become significant at microelectrode, since the diffusion layers formed at the electrode surface are very small, similar in size to the electrode itself. At very short experimental timescales, or in the presence of a very slow diffusing species (*e.g* in highly viscous media), the currents recorded at microelectrodes may be purely attributed to planar diffusion. The appearance of steady-state or transient behaviour can be predicted using the following parameter, p:[7]

$$p = \sqrt{\frac{Fr_d{}^2\upsilon}{RTD}} \tag{1.21}$$

where $p << 1$ corresponds to steady-state behaviour, and $p >> 1$ corresponds to transient behaviour.

Practically, both types of electrode have unique benefits. Macroelectrodes are widely commercially available, easy to use and are commonly employed in many types of electrochemical experiment. Their larger size result in higher overall currents, and diffusion to macroelectrodes is simpler and can be theoretically simulated in one dimension. In addition, since the diffusional behaviour at macroelectrodes is predominantly planar, this allows the study of reaction mechanisms by observation of volatmmetric 'peaks' rather than limiting current plateaus. Microelectrodes on the other hand have significant advantages. The rate of mass transport to a microelectrode is much faster compared to a macroelectrode, making them particularly useful for the measurement of fast electrochemical processes. Other benefits include a larger current

density, reduced capacitance and lower ohmic drop. Due to the smaller overall current, it is also possible to simplify the experimental arrangement by employing a two-electrode set-up (as described above), which is useful when only small quantities of solvent are available.

1.5.3 Reference Electrodes

For most electrochemical experiments, it is a requirement for there to be a 'reference' electrode that provides a stable potential relative to the voltage of the working electrode. In conventional solvents, there are four main types. The first are based on potential determining equilibria such as $Ag^+ + e^- \rightleftharpoons Ag$ or $\frac{1}{2}Cl_2 + e^- \rightleftharpoons Cl^-$, where for 'cationic electrodes', equilibrium is established between atoms or molecules and their corresponding cations in solution, or for 'anionic electrodes', their corresponding anions. The second type of reference electrode consists of three phases, with a metal covered by a layer of its sparingly soluble salt, which is immersed in a solution containing the anion of this salt. Examples include $Hg/Hg_2Cl_2/Cl^-$ (saturated calomel electrode) and $Ag/AgCl/Cl^-$. The third type of reference electrode involves the use of a redox couple. In this case, an inert, non-reactive metal such as platinum or gold, is immersed in a solution containing both species contributing to a redox couple. For example in water: $\frac{1}{2}BQ + e^- + H^+ \rightleftharpoons \frac{1}{2}H_2Q$, where BQ is benzoquinone and H_2Q is hydroquinone, or in aprotic solvents: $Fc^+ + e^- \rightleftharpoons Fc$, where Fc is ferrocene and Fc^+ the ferrocenium cation. The fourth type is called a 'quasi'-reference (sometimes called 'pseudo'-reference) electrode. These usually consist of just a metal wire, such as silver or platinum, placed directly in the solution. The main advantage of using this type of electrode is that the solvent volume can be minimized to microlitre quantities, since a two-electrode arrangement can be employed and the distance between the electrodes can be minimized. However, the potential of quasi-reference electrodes are not stable and can shift over the course of an experiment. This can be overcome by calibrating the potential *vs* an internal reference couple, either before an experiment (in cases where there is little change in

electrolyte composition and where the potential is not expected to shift), or *in-situ* (involving the introduction of a redox couple into the same solution, provided that there is no interference with the electrochemical system being studied). IUPAC recommend the use of either the ferrocene/ferrocenium, Fc/Fc^+ couple,[26] or alternatively the cobaltocene/cobaltocenium Cc^+/Cc has been suggested.[27,28] Quasi-reference electrodes are the most commonly used in this thesis, and where necessary, peak potentials have been reported *vs* either the ferrocene/ferrocenium or cobaltocenium/cobaltocene redox couples.

1.6 Voltammetric Techniques

Voltammetry is the study of the current response when a voltage is applied to an electrode. Two approaches may be considered; either the potential is stepped to a fixed value and the current is measured as a function of time, or the potential is swept linearly through a range and the current is measured. The following sections introduce the different voltammetric techniques that are relevant to the experiments reported within this thesis in the context of disk geometry under diffusion-only conditions. For simplicity, it is assumed in both cases that the electrolyte solution contains an electroactive species, A, which can be converted to species B in a simple one-electron oxidation, as shown below:

$$\mathrm{A} \underset{k_\mathrm{b}}{\overset{k_\mathrm{f}}{\rightleftharpoons}} \mathrm{B} + e^- \tag{1.22}$$

where k_f and k_b are the forward and backward rate constants for the electrochemical process.

1.6.1 Potential Step Chronoamperometry

The study of the variation of the current response with time under potentiostatic control is called chronoamperometry.[5] In a chronoamperometric experiment, the potential is instantaneously stepped from an initial value, E_1, (usually where no current flows) to a final value, E_2, (where the electron transfer process occurs) as depicted in Figure 1.4. A large current is initially

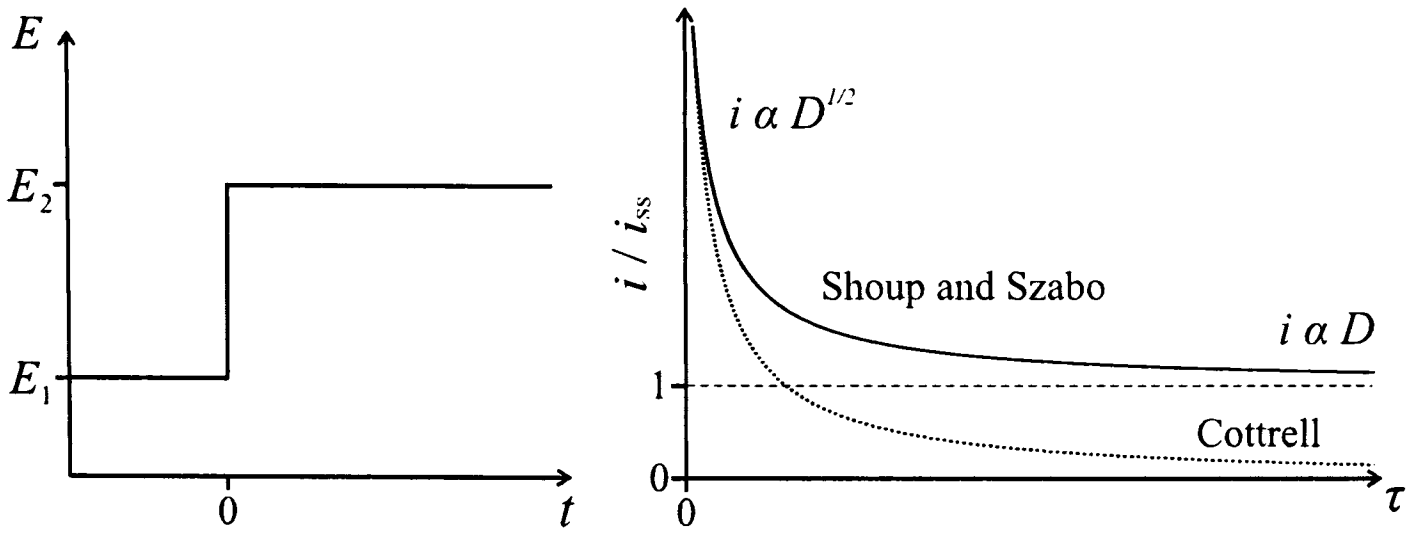

Figure 1.4: A potential waveform applied during a chronoamperometric experiment and the experimental output on a microdisk electrode (Shoup and Szabo equation) compared to a macrodisk (Cottrell equation).

recorded, which then falls steadily with time due to the depletion of species A at the electrode surface. For processes where planar diffusion dominates (*e.g.* macroelectrodes), the diffusion limited current, i_d, tends to zero (see Figure 1.4) and is given by the Cottrell equation:[19]

$$i_d = \frac{nFAD^{\frac{1}{2}}c}{\pi^{\frac{1}{2}}t^{\frac{1}{2}}} \tag{1.23}$$

where n is the number of electrons transferred, F is Faraday's constant, A is the electrode surface area, c is the concentration of the electroactive species, and t is the time. A plot of i versus $\frac{1}{\sqrt{t}}$ should result in a linear line through zero from which the diffusion coeffcient can be calculated. The Cottrell equation is only valid in systems subject to the following boundary conditions: (a) only species A is present in solution at t=0, (b) the solution is sufficiently large that far from the electrode surface the concentration of A approaches the bulk value, and (c) the concentration of A is reduced to zero immediately after the potential step.

When convergent diffusion dominates (*e.g.* a microelectrode), the problem becomes more complex and must be considered in two dimensions. The experimental transient obtained at a microelectrode decays to a limiting current (see Figure 1.4), as opposed to zero for Cottrellian behaviour. In this case, the current can be described as a function of a dimensionless parameter,

τ:[29]

$$i = 4nFr_{\mathrm{d}}Dcf(\tau) \tag{1.24}$$

where

$$\tau = \frac{4Dt}{{r_{\mathrm{d}}}^2} \tag{1.25}$$

Here, n is the number of electrons transferred, F is the Faraday constant, D is the diffusion coefficient, c is the initial concentration of parent species, r_{d} is the radius of the disk electrode, and t is the time. Aoki and Osteryoung[29] used two different expressions for $f(\tau)$. At short times when τ is less than 1.44:

$$f(\tau) = \sqrt{\frac{\pi}{4\tau}} + \frac{\pi}{4} + 0.094\sqrt{\tau} \tag{1.26}$$

whereas at longer times when τ is greater than 0.82:

$$f(\tau) = 1 + 0.71835\tau^{-\frac{1}{2}} + 0.05626\tau^{-\frac{3}{2}} - 0.00646\tau^{-\frac{5}{2}} \tag{1.27}$$

However, since this was not sufficient to describe the variation of i with τ over the full range of τ, Shoup and Szabo[30] derived a single expression to describe the current over the entire range, with a maximum error of less than 0.6 %:

$$f(\tau) = 0.7854 + 0.8862\tau^{-\frac{1}{2}} + 0.2146\exp(-0.7823\tau^{-\frac{1}{2}}) \tag{1.28}$$

In some systems, 'double potential step' chronoamperometry can also be performed to calculate the diffusion coefficient of species B. This usually involves stepping the potential from E_1 to E_2, then back to E_1 and measuring the current decay for both processes. At a microelectrode, the first step can be analysed by the Shoup and Szabo[30] expression, and the second step by an exponentially expanding time grid described by Klymenko *et al.*[31]

It should be noted that chronoamperometric transients cannot provide any information on the electrode kinetics of a reaction, since the position of the potential step is chosen to be more negative than the formal potential for the reduction process, such that the mass transport is rate limiting.

1.6.2 Linear Sweep and Cyclic Voltammetry

'Linear sweep voltammetry' involves the measurement of current as the potential is varied (usually linearly) from an initial value, E_1, to a final value, E_2, at a fixed scan rate, ν. It is common to then reverse the sweep and record the current when the potential is swept back to E_1 at the same scan rate. This process is termed 'cyclic voltammetry' and is depicted in Figure 1.5.

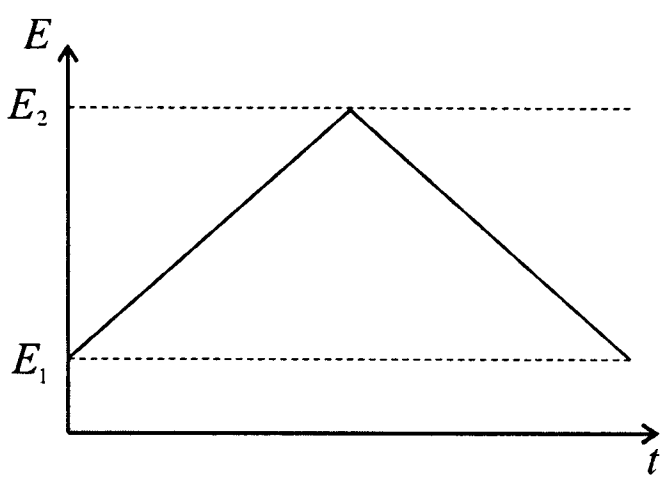

Figure 1.5: Triangular potential 'ramp' used in cyclic voltammetry, showing the variation of applied potential with time.

The experimental output from a cyclic voltammetric experiment is a plot of current, i, *vs* potential, E, called a 'voltammogram'. The shape and position of the voltammogram is influenced by various factors including the type of mass transport operating and the size of the working electrode. As a result, the characteristic voltammetry obtained at macro and microelectrodes is very different, and will be discussed below.

1.6.2.1 Voltammetry at Macroelectrodes

Typical characteristic cyclic voltammetric waveshapes on large electrodes where planar diffusion dominates are depicted in Figure 1.6. The three voltammograms shown correspond to 'reversible', 'quasi-reversible' and 'irreversible' electron transfer processes with the same formal potential, $E_f{}^0$.

For the reversible case, the voltammogram has an $E_f{}^0$ close to half way between the oxidation and reduction peak potentials, $E_p{}^{Ox}$ and $E_p{}^{Red}$.[3] The shape of the curve can be understood as follows. Initially, the applied potential is not large enough to induce electron transfer, so no current is recorded. As the potential is swept positively, the current increases approximately

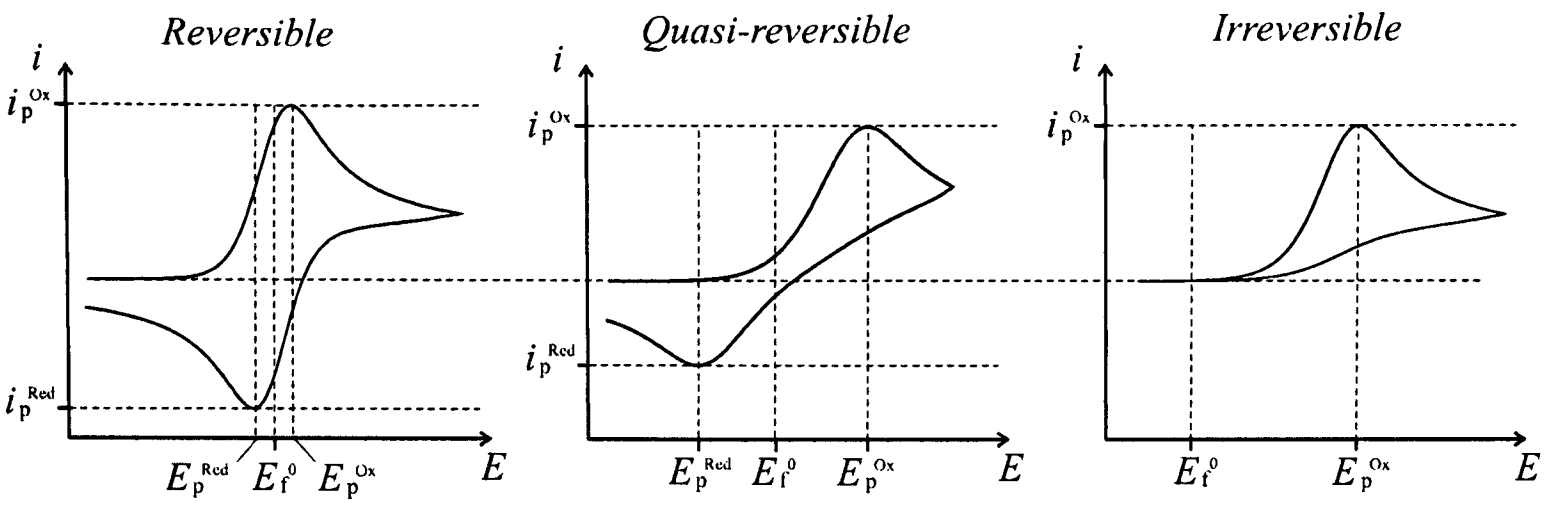

Figure 1.6: A comparison of cyclic voltammetric wave-shapes representing planar diffusion at a macrodisk electrode.

exponentially as species A is oxidised. At higher potentials, the current begins to fall off as mass transport to the electrode becomes limiting. Eventually, a maximum current (peak) is observed as a result of the balance between electron transfer and diffusion. The current then falls off after reaching a maximum since the diffusion layer becomes thicker, and species A has further to diffuse to the electrode. The peak current, i_p, at 298 K can be calculated using the Randles-Sevčik equation:[17,18]

$$i_p = (2.69 \times 10^5) n^{\frac{3}{2}} A D^{\frac{1}{2}} \nu^{\frac{1}{2}} c_{bulk} \tag{1.29}$$

where n is the number of electrons, A is the area of the electrode, D is the diffusion coefficient, ν is the scan rate and c_{bulk} is the concentration of the electroactive species in bulk solution.

When the voltammogram is reversed, species B (the oxidised form of A) is in a high concentration local to the electrode surface and is reduced at the electrode to give the back-wave shown in Figure 1.6. When the system is fully reversible, the forward and reverse peaks are separated by $2.218\frac{RT}{nF}$ (corresponding to $\frac{57}{n}$ mV at 298 K), and the peak potentials are independent of scan rate. At high scan rates (shorter experimental timescale), there is less depletion of material at the electrode surface, resulting in a smaller diffusion layer and consequently a steeper concentration gradient. This results in more flux of material towards the electrode surface and hence higher peak currents. As a result, the peak currents for the forward and reverse peaks

increase with increasing scan rate with i_p linearly proportional to the square root of scan rate for a diffusional process.

If the electron transfer is sufficiently slow, the resulting voltammogram is classed as 'irreversible' and a wave shape similar to that in Figure 1.6 is seen. The wave is more broad than for the fully reversible case, and accordingly the peak current is less than that predicted by equation 1.29. For an irreversible system, the peak current at 298 K is given by:[5]

$$i_p = (2.99 \times 10^5) n(\alpha n_{rd})^{\frac{1}{2}} A D^{\frac{1}{2}} \nu^{\frac{1}{2}} c_{bulk} \qquad (1.30)$$

where n_{rd} is the number of electrons transferred in the rate determining step and α is the charge transfer coefficient. As with the reversible case, the peak current scales linearly with the square root of scan rate. The are, however, some differences compared to the fully reversible case. Firstly, although the electrode process has the same ${E_f}^0$, a larger overpotential is required to drive the electron transfer, resulting in the oxidation peak appearing at a more positive potential. Secondly, the absence of a voltammetric back peak suggests that if the reverse process takes place, it does so at a sufficiently negative potential outside of the potential window shown. It could also be the result of a rapid chemical reaction after the electron transfer step (as mentioned previously).

For intermediate 'quasi-reversible' systems, the shape of the voltammogram appears more 'drawn out' (see Figure 1.6), and the peak separations are greater that 59 mV since the kinetics of the electron transfer are not fast enough to maintain a full Nernstian equilibrium. The peak currents are also smaller than for the fully reversible case. When the scan rate is increased, peak to peak separations vary (unlike for a reversible system), and the peak current is not proportional to the square root of scan rate. Matsuda and Ayabe have classified reversible, quasi-reversible and irreversible voltammetry according to the magnitude of k_0 relative to the voltammetric scan rate, as shown in Table 1.1.

Table 1.1: Criteria for classification of reversibility according to electron transfer and scan rates.

Electrochemical Process	Criteria
Reversible	$k_0 \geq 0.3\ \upsilon^{\frac{1}{2}}$ cm s^{-1}
Quasi-reversible	$0.3\ \upsilon^{\frac{1}{2}} > k_0 > 2 \times 10^{-5}\ \upsilon^{\frac{1}{2}}$ cm s^{-1}
Reversible	$k_0 \leq 2 \times 10^{-5}\ \upsilon^{\frac{1}{2}}$ cm s^{-1}

1.6.2.2 Voltammetry at Microelectrodes

When the electrode diameter is sufficiently small (*ca.* $\leq$ 50 μm), convergent diffusion takes place at the electrode surface. The resulting voltammogram is sigmoidal in shape (as shown in Figure 1.7) and reaches a limiting current plateau, in contrast to the peak-shaped behaviour obtained at macroelectrodes. This type of behaviour is called 'steady-state', and occurs because the rate of mass transport to a microelectrode is sufficiently fast that the concentration of electroactive species at the electrode surface is continually replenished over the whole potential range. In this case, the concentration profile at a given potential is independent of time.

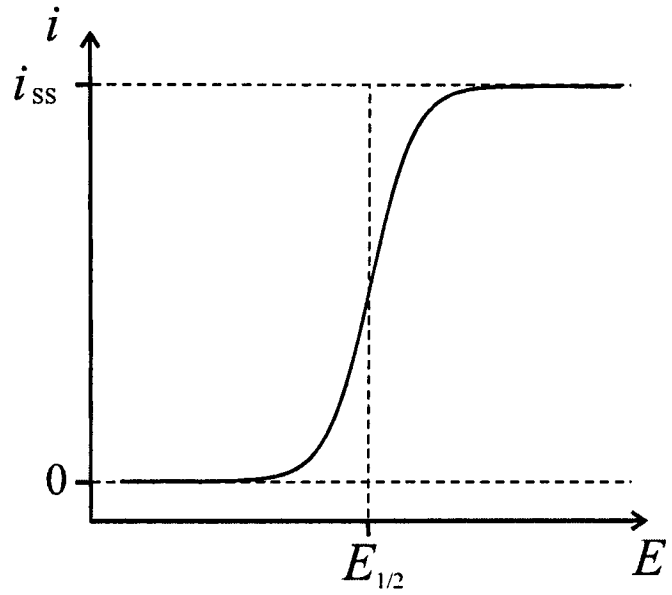

Figure 1.7: Steady-state voltammetry at a microdisk electrode.

The voltammogram is characterised both by the limiting current and the half wave potential, $E_{1/2}$. In systems where the electrode kinetics are fast, $E_{1/2}$ is close to the formal potential for the redox couple, but deviates significantly when the electron transfer is slow. Depending on the reversibility, it is also possible to extract heterogeneous information from the curvature of the wave.[32]

The steady-state limiting current, i_{ss}, can be used to electrochemically calibrate the radius,

r_d, of a microdisk electrode using:

$$i_{ss} = -4nFDcr_d \tag{1.31}$$

where F is Faraday's constant, c is the concentration, and D is the diffusion coefficient of the electroactive species (characterised independently). Alternatively, the diffusion coefficient of an electroactive species can be calculated from i_{ss} by knowledge of the electrode radius.

It should also be noted (as mentioned previously) that planar diffusion can still dominate at microelectrodes at sufficiently high scan rates or in cases of species with low diffusion coefficients (*e.g.* in highly viscous media such as room temperature ionic liquids, which will be explored throughout this thesis).

1.7 Modelling Electrochemical Processes

Although electrochemical experiments provide a wealth of information about processes taking place near the electrode surface and in solution, it is often useful to use theoretical models to fit experimental data and predict the outcome of voltammetric experiments. In simulating voltammetric data, numerical methods are often employed as analytical techniques cannot be solved exactly. There are various strategies, but the type used in several places throughout this thesis is based on the *Fast Implicit Finite Difference* method,[33] using the commercially available software package DigiSim®.[34]

Finite difference methods are based on solving the partial differential equations associated with mass transport. It is common to approximate the the continuous space and time dimensions as discrete variables, depending on the number of spatial dimensions involved. For a simple 1-dimensional case, the x coordinate can be divided into small intervals of length Δx, and the time t divided into small time steps Δt. This is shown pictorially in Figure 1.8. At each point on the grid, the concentration of the species of interest is approximated by assuming that the concentration between adjacent points varies linearly. By solving these now linear equations

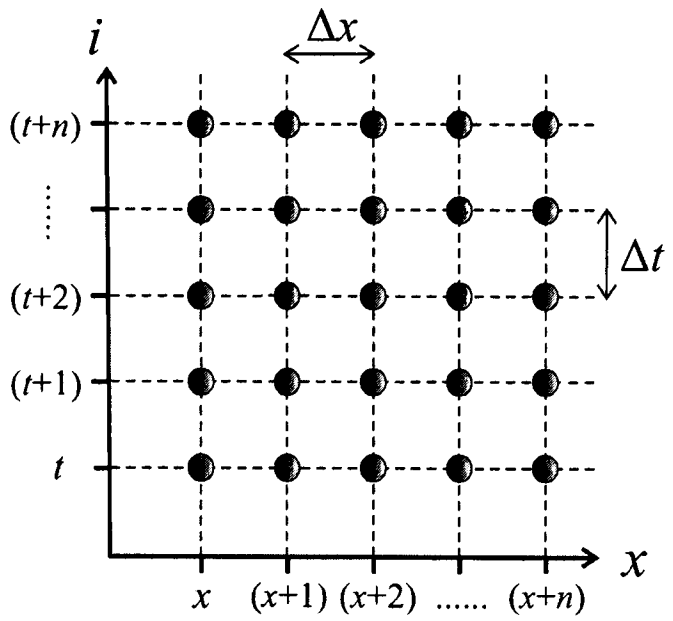

Figure 1.8: A grid representing the discretisation of the variables x and t.

generates a concentration profile, and a time-dependent current curve can be calculated for the region immediately adjacent to the electrode surface.

DigiSim® is a versatile simulation program, as it allows the simple input of a wide range of fixed parameters such as the scan rate, potential range, electrolyte concentration, diffusion coefficients and electrode area. It is then possible to select and optimise parameters for the electron transfer rate constant, the transfer coefficient, the half wave potential (for heterogeneous steps) and the forward rate constants and equilibrium constants (for homogeneous steps). It is noted that when simulating responses at a microdisk (where hemispherical diffusion takes place), the hemispherical radius, r_{hemi}, should be used instead of the disk radius.[35] r_{hemi} is related to r_{d} by the following expression:[35]

$$r_{\text{hemi}} = \frac{2r_{\text{d}}}{\pi} \tag{1.32}$$

1.8 X-Ray Photoelectron Spectroscopy

Although not an electrochemical technique *per se*, X-ray photoelectron spectroscopy (XPS) has been used in various places throughout this thesis to provide additional information about the elements present both in a room temperature ionic liquid solution (Chapter 4) and on a solid electrode surface (Chapter 7). This section will provide a brief introduction to the technique,

but a more comprehensive account can be found in several textbooks.[36–38]

XPS is a quantitative spectroscopic technique that provides information on the elemental composition, empirical formula, chemical state and electronic state of the elements within a material. The technique works by irradiating a material (usually a solid) with a beam of aluminium or magnesium X-rays while simultaneously measuring the kinetic energy and number of electrons that escape from the top 10 nm of the surface. Because the energy of a particular X-ray wavelength is a known quantity, the electron binding energy of each of the emitted electrons can be calculated from the following equation:

$$E_{\text{binding}} = E_{\text{photon}} - E_{\text{kinetic}} - \phi \tag{1.33}$$

where E_{binding} is the energy of the electron emitted from one electron configuration within the atom, E_{photon} is the energy of the X-ray photons being used, E_{kinetic} is the kinetic energy of the emitted electron as measured by the instrument and ϕ is the work function of the spectrometer (not the material). The binding energy of the peaks are characteristic of each element and are used to determine which elements are present. The composition of each element can then be determined from the peak areas after employing appropriate sensitivity factors. All elements with an atomic number between those of lithium and lawrencium can be detected (not hydrogen and helium), and the sensitivity is usually in the parts per thousand range. Detection limits of parts per million (ppm) are possible, but often require a very long collection time. XPS requires ultra-high vacuum (UHV) conditions, and as a result, it is very rarely used to study the composition of liquids. Chapter 4 presents one of the first XPS studies on liquids, by employing a low-volatility 'room temperature ionic liquid'.

This chapter has outlined the fundamental electrochemical principles that are relevant to this thesis. The next chapter introduces room temperature ionic liquids as a class of solvents, which are used in all electrochemical experiments reported throughout this thesis.

References

[1] Compton, R. G. and Sanders, G. H. W., *Electrode Potentials*, Oxford University Press, Oxford, UK, 1998.

[2] Fisher, A. C., *Electrode Dynamics*, Oxford University Press, Oxford, UK, 1998.

[3] Bard, A. J. and Faulkner, L. R., *Electrochemical Methods: Fundamentals and Applications, 2nd ed.*, John Wiley and Sons: New York, USA, 2001.

[4] Rieger, P. H., *Electrochemistry, 2nd ed.*, Chapman and Hall, Inc. New York, USA, 1994.

[5] Brett, C. M. A. and Brett, A. M. O., *Electrochemistry: Principles, Methods and Applications*, Oxford University Press, Oxford, UK, 1994.

[6] Bond, A. M., *Broadening Electrochemical Horizons*, Oxford University Press, Oxford, UK, 2002.

[7] Compton, R. G. and Banks, C. E., *Understanding Voltammetry*, World Scientific, Singapore, 2007.

[8] von Helmholtz, H. L. F., *Ann. Physik.*, 1853, **165**, 211–233.

[9] von Helmholtz, H. L. F., *Ann. Physik.*, 1879, **243**, 337–382.

[10] Gouy, G., *Compt. Rend.*, 1910, **149**, 654.

[11] Chapman, D. L., *Phil. Mag.*, 1913, **25**, 475.

[12] Stern, O., *Z. Elektrochem. Angew. Phys. Chem.*, 1924, **30**, 508–516.

[13] Bockris, J. O. M.; Devanathan, M. A. V. and Mueller, K., *Proc. Phys. Soc. Ser. A*, 1963, **274**, 55–79.

[14] Grahame, D. C., *Chem. Rev.*, 1947, **41**, 441–501.

[15] Faraday, M., *Experimental Researches in Electricity*, Bernard Quaritch, London, UK, 1839.

[16] Fick, A., *Phil. Mag.*, 1855, **10**, 30.

[17] Randles, J. E. B., *Trans. Faraday Soc.*, 1948, **44**, 327–338.

[18] Sevčik, A., *Collect. Czech. Chem. Commun.*, 1948, **13**, 349–377.

[19] Cottrell, F. G., *Z. Physik. Chem.*, 1903, **42**, 385–431.

[20] Butler, J. A. V., *Trans. Faraday Soc.*, 1924, **19**, 729–733.

[21] Erdey-Gruz, T. and Volmer, M., *Z. Physik. Chem.*, 1930, **150**, 203–213.

[22] Testa, A. C. and Reinmuth, W. H., *Anal. Chem.*, 1961, **33**, 1320–1324.

[23] Amatore, C. A.; Jutand, A. and Pfluger, F., *J. Electroanal. Chem.*, 1987, **218**, 361–365.

[24] Alberts, G. S. and Shain, I., *Anal. Chem.*, 1963, **35**, 1859–1866.

[25] Daniele, S.; Lavagnini, I.; Baldo, M. A. and Magno, F., *Anal. Chem.*, 1998, **70**, 285–294.

[26] Grützner, G. and Kuta, J., *Pure Appl. Chem.*, 1984, **56**, 461–466.

[27] Stojanovic, R. S. and Bond, A. M., *Anal. Chem.*, 1993, **65**, 56–64.

[28] Hultgren, V. M.; Mariotti, A. W. A.; Bond, A. M. and Wedd, A. G., *Anal. Chem.*, 2002, **74**, 3151–3156.

[29] Aoki, K. and Osteryoung, J., *J. Electroanal. Chem.*, 1981, **122**, 19–35.

[30] Shoup, D. and Szabo, A., *J. Electroanal. Chem. Interfacial Electrochem.*, 1982, **140**, 237–245.

[31] Klymenko, O. V.; Evans, R. G.; Hardacre, C.; Svir, I. B. and Compton, R. G., *J. Electroanal. Chem.*, 2004, **571**, 211–221.

[32] Mirkin, M. V. and Bard, A. J., *Anal. Chem.*, 1992, **64**, 2293–2302.

[33] Rudolph, M., *J. Electroanal. Chem.*, 1991, **314**, 13–22.

[34] Rudolph, M.; Reddy, D. P. and Feldberg, S. W., *Anal. Chem.*, 1994, **66**, 589A–600A.

[35] Alden, J. A.; Hutchinson, F. and Compton, R. G., *J. Phys. Chem. B*, 1997, **101**, 949–958.

[36] Moulder, J. F.; Stickle, W. F.; Sobol, P. E. and Bomben, K. D., *Handbook of X-ray Photoelectron Spectroscopy*, Eden Prairie, MN, USA, 1992.

[37] Briggs, D. and Seah, M. P., Eds., *Practical Surface Analysis, Vol 1: Auger and X-Ray Photoelectron Spectroscopy*, John Wiley and Sons: Chichester, UK, 1994.

[38] Brown, J. M., *Molecular Spectroscopy*, Oxford University Press, Oxford, UK, 1998.

Chapter 2

Introduction to Room Temperature Ionic Liquids

All of the experiments reported in this thesis are performed using a group of solvents classed as 'room temperature ionic liquids' (RTILs). These are liquids composed entirely of ions, and possess several architypal properties such as high intrinsic conductivity, high thermal stabilty, low volatility, wide liquid range, high polarity, high viscosity and wide electrochemical windows. There is much interest in the use of RTILs at many academic (and now industrial) research institutes; this is illustrated by the rapid growth in the number of publications on ionic liquids found from a literature search on Sci Finder® Scholar during the last 15 years (see Figure 2.1). A 100-fold increase is observed from 1992 to 2007, which shows the hugely increasing interest in these media.

This chapter aims to introduce room temperature ionic liquids as solvents, with particular focus on their physical properties, applications and the voltammetric/electrochemical behaviour of species dissolved in RTILs compared to conventional molecular solvents (*e.g.* acetonitrile). Small sections of this chapter were published in a review paper entitled *"Electrochemistry in Room Temperature Ionic Liquids: A Review and Some Possible Applications"* in *Z. Phys. Chem.*,[1] but much of it has been re-written and updated to include significant new developments.

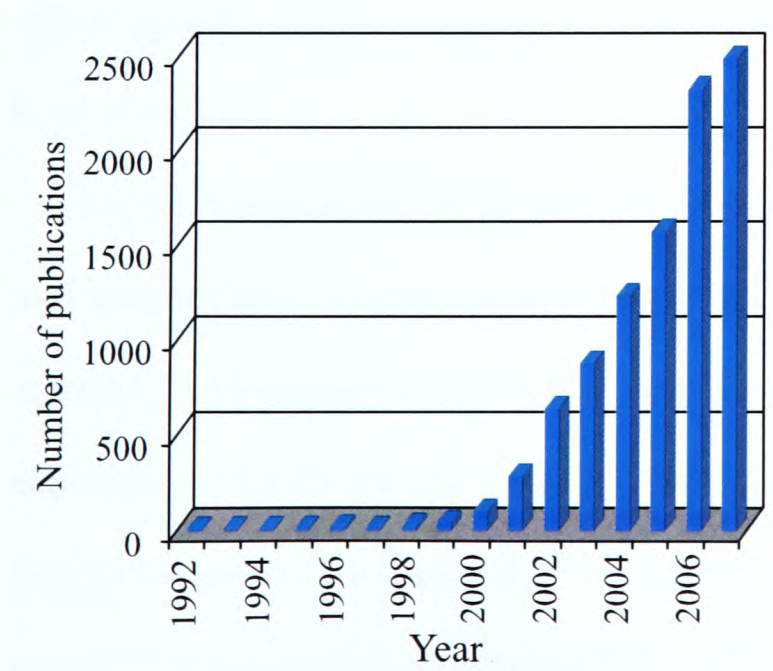

Figure 2.1: Exponential growth of room temperature ionic liquid publications over the last 15 years. Data obtained from a literature search using SciFinder® Scholar 2007.

2.1 Introduction

Although there is no exact definition, ionic liquids are most commonly defined as materials that are composed solely of ions and melt at temperatures of 373 K or less.[2] The advantage of this type of liquid is that reactions can be performed at much more 'ambient' temperatures compared to reactions in molten salts (*e.g.* NaCl, melting point of 1073 K, or LiCl-KCl, melting point of 628 K), and the equipment employed at moderate temperatures may be used. The first ionic liquid reported in the literature (ethylammonium nitrate) was discovered in 1914.[3] However, relatively little was reported about these solvents in the open literature until 1951, when Hurley and Wier reported the electrodeposition of metals such as aluminium in ethylpyridinium bromide.[4,5] It was in 1982 that a new 'class' of ionic liquid that incorporated the 'haloaluminate' anion (*e.g.* $[AlCl_4]^-$) was synthesized.[6] Several papers were subsequently published on this type of solvent, but the ionic liquids' high sensitivity to air and moisture resulted in much effort and expensive experimental equipment required to maintain the essentially 'anhydrous' conditions necessary (*e.g.* a glove box). The introduction of apparently 'air and moisture stable' ionic liquids,[7] which possess many significant advantages over their haloaluminate counterparts, resulted in the increase in the number of publications in the early 1990's. The interest in ionic liquids has surged since around 1999, coinciding with the publication of a review paper by Welton,[8] which appears to be the most cited ionic liquid paper to date (more than 3400 citations at the time of writing).

The next sections will introduce some of the main physical properties of ionic liquid solvents, and some of their key applications. Focus will then turn to the use of RTILs as electrochemical solvents, the purpose for which they were originally conceived.[9,10] For a more comprehensive summary of RTILs for use in other applications, the reader is directed to several interesting review papers on catalysis,[8,11–13] 'green' chemistry,[14–16] organic reactivity,[17,18] analytical uses,[19–22] biocatalysis and enzymes[23,24] and applications in the chemical industry.[2]

2.2 Classes of Ionic Liquids

Although there is not (as yet) an accepted method of grouping ionic liquids into category's based on their properties, it can loosely be stated that they fall into three main, arbitrary classes. The first generation, as mentioned above, are based around haloaluminate anions such as $[AlCl_4]^-$ but have major drawbacks due to their high sensitivity to moisture, requiring them to be handled under anhydrous conditions (*i.e.* glove box).[6] The second generation based on anions such as tetrafluoroborate ($[BF_4]^-$) or hexafluorophosphate ($[PF_6]^-$),[25] are less reactive with water but still absorb moisture, changing the physical and chemical properties of the liquids, which in turn alters their behaviour. The more 'modern' ionic liquids are composed of more hydrophobic anions such as bis(trifluoromethylsulfonyl)imide ($[NTf_2]^-$) or perfluoroalkylphosphate ($[FAP]^-$), and are less moisture sensitive than their predecessors. These are thought to belong in an intermediate class, somewhere between second and third generation. The third generation are so-called 'task-specific' ILs (first invented by Davis *et al.*)[26–28] where the ionic liquid contains functional groups. Finally, there are other ILs which are difficult to categorize according to the definitions above, containing anions such as dicyanamide $[N(CN)_2]^-$, thiocyanate $[SCN]^-$ and methyl sulphate $[MeSO_4]^-$. Some of these unclassified RTILs are halide free or possess physical properties such as lower viscosity and high conductivity. Common cations include imidazolium ($[C_n mim]$), pyrrolidinium ($[C_n mpyrr]$), pyridinium ($[C_n py]$), tetraalkylammonium ($[N_{a,b,c,d}]$) and tetraalkylphosphonium ($[P_{a,b,c,d}]$). Figure 2.2 shows the structures of some commonly used cations and anions that make up non-haloaluminate RTILs. The nature of the cation and anion can be varied to allow for 'tuneable' solvents for specific purposes;[29] theoretically, there are up to *ca.* 10^{18} combinations possible![30] Table 2.1 gives some examples of the types of ionic liquid cations and anions already synthesized, and the range of molecules is growing rapidly each year. Since many of these compounds being synthesized are new, there is much work needed to understand their physical properties before they can be considered for specific applications.

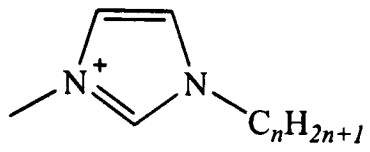

Imidazolium, $[C_nmim]^+$

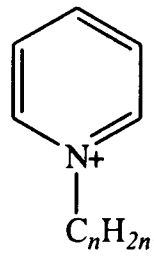

Pyridinium, $[C_npy]^+$

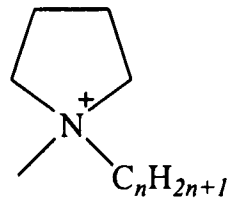

Pyrrolidinium, $[C_nmpyrr]^+$

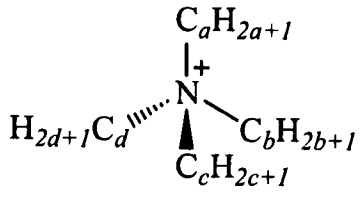

Tetraalkylammonium, $[N_{a,b,c,d}]^+$

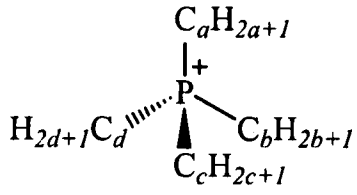

Tetraalkylphosphonium, $[P_{a,b,c,d}]^+$

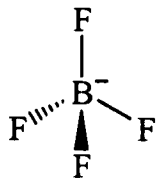

Tetrafluoroborate $[BF_4]^-$

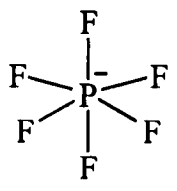

Hexafluorophosphate, $[PF_6]^-$

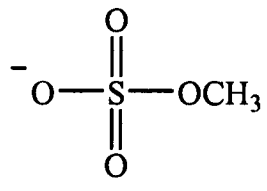

Methyl sulphate $[MeSO_4]^-$

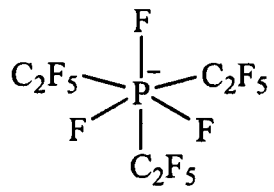

Trifluorotris(pentafluoroethyl)phosphate, $[FAP]^-$

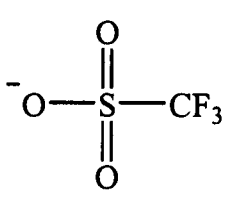

Trifluoromethylsulfonate, $[OTf]^-$

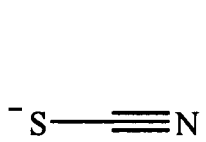

Thiocyanate $[SCN]^-$

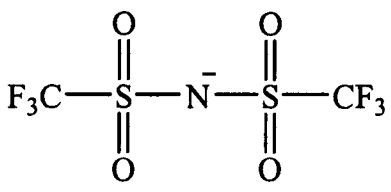

Bis(trifluoromethylsulfonyl)imide, $[NTf_2]^-$

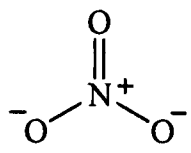

Nitrate $[NO_3]^-$

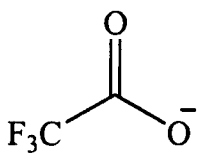

Trifluoroacetate $[TFA]^-$

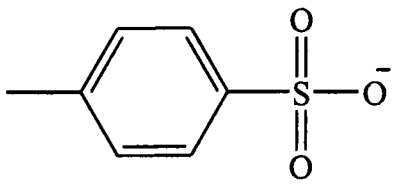

Tosylate $[Ts]^-$

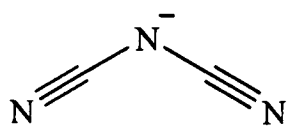

Dicyanamide $[N(CN)_2]^-$

Figure 2.2: Molecular structures of some common cations and anions employed in room temperature ionic liquids, and the nomenclature used throughout this thesis.

Table 2.1: Examples of cations and anions that have been employed as non-haloaluminate ionic liquids.

Cations	Ref.	Anions	Ref.
1,3-dialkylimidazolium	25,31,32	$[BF_4]^-$	32,33
1,2,3-trialkylimidazolium	31,34	$[PF_6]^-$	7,32,34
1,3,4-trialkylimidazolium	31	$[NTf_2]^-$	31,34
1-alkyl-3-methoxyalkylimidazolium	31	$[OTf]^-$	31,35
1-(ω-phenylalkyl)-3-methylimidazolium	36	$[FAP]^-$	37
1-methyl-3-[2,6-(S)-dimethylocten-2-yl]imidazolium	38	$[NO_3]^-$	39
N, *N*-dialkylpyrrolidinium	40–42	$[SCN]^-$	43
tetraalkylammonium	44,45	$[AsF_6]^-$	32,34,46
methoxyalkyltrialkylammonium	47	$[N(CN)_2]^-$	43,48
tetraalkylphosphonium	49	$[H(HF)_n]^-$	42,50
N-alkylpyridinium	51	$[MeSO_4]^-$	52
trialkylsulfonium	53	$[TFA]^-$	31
N, *N*-dialkylpiperidinium	42	$[CTf_3]^-$	46
hydrazinium	54	$[Ts]^-$	48
1-alkyl-3-methylbenzotriazolium	48	$[Co(CO)_4]^-$	55
1-alkyl-2-methylpyrrolinium	56	$[DNA]^-$	57

2.2.1 Task-Specific Ionic Liquids

The ability to change the combination of cation and anion is highly advantageous, as the physical properties of an ionic liquid can be 'fine-tuned' for a specific purpose. A review by Davis[27] suggests a huge number of feasible anions and cations are possible, simply by adding an additional functional group to the cation or anion. Figure 2.3 shows the structures of some cations and anions that have been employed as 'task-specific' ionic liquids. In particular, the imidazolium ring can be functionalized with a reactive functional group for a specific purpose. For example, a primary amine functionalized imidazolium cation has been used to separate CO_2 from gas streams,[58] while ionic liquids with appended sulfonic acid groups have been used as a solvent-catalyst for esterifications.[59] Zwitterionic liquids, where the anion and cation are tethered together in a single structure have also been used for electrochemical applications.[60] Despite the possibility of such a huge library of ionic liquid structures possible and the exponential growth in the number of publications in ionic liquids, studies have mostly been limitied to a relatively small number of ionic liquids. This could be due to the unfavourable effects that adding functional groups has on the physical properties of the ionic liquid *e.g.* increased reactiv-

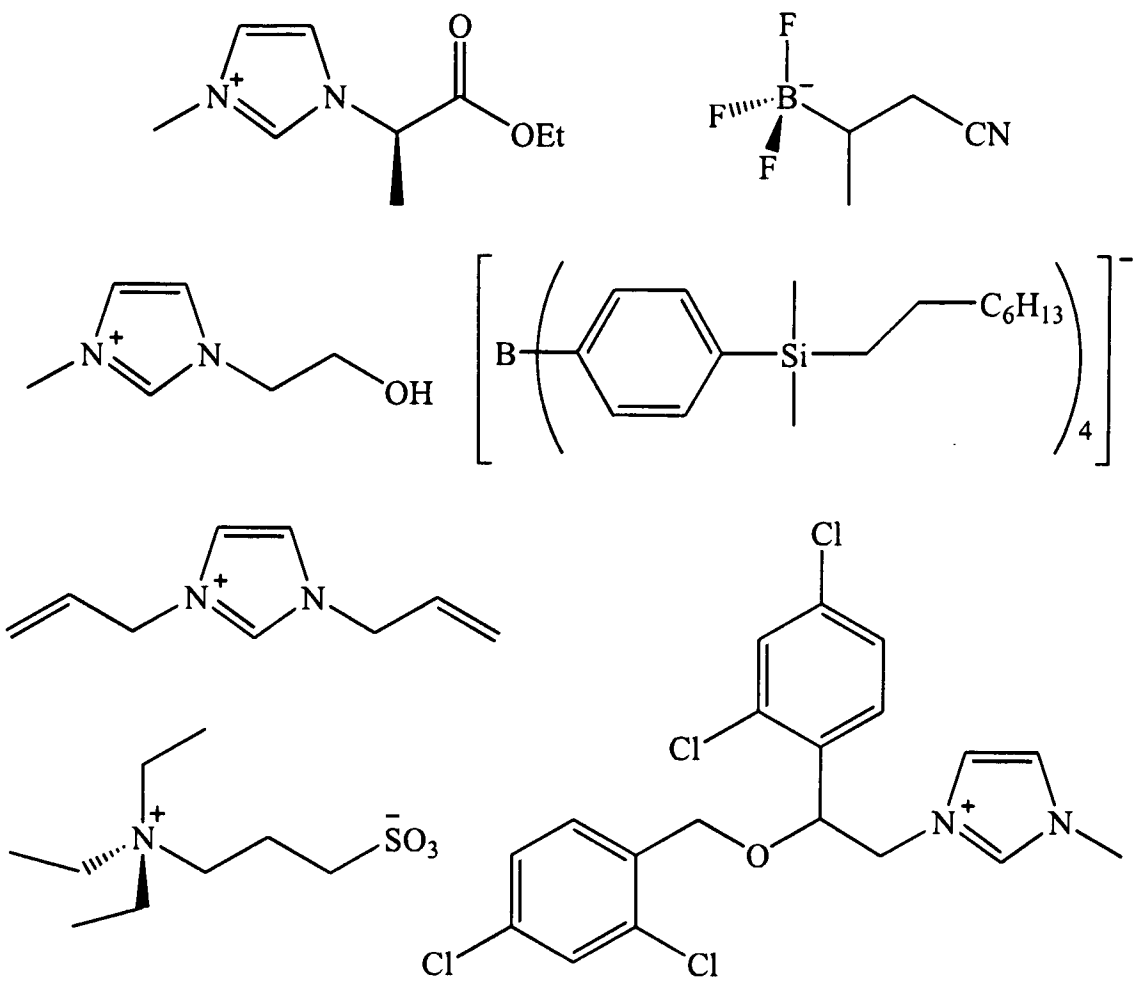

Figure 2.3: Examples of some 'task-specific' ionic liquids and 'zwitterionic liquids', taken from the literature.[27,66,67]

ity with species in solution, a narrower electrochemical window and a much more complicated synthetic and purification procedure.

The rest of this chapter will focus on the properties and applications of the second and third generation RTILs with anions such as bis(trifluormethylsulfonyl)imide, tetrafluoroborate and hexafluorophosphate, as these are the types used in the experiments reported in this thesis. Comprehensive accounts of haloaluminate[6,46,61–64] and task-specific[26–28,65] ionic liquids can be found in the literature.

2.2.2 Synthesis of RTILs

Most imidazolium-based ionic liquids are synthesized following the method given in Figure 2.4. In this reaction, the cation is initially formed by alkylation of an imidazole using an alkyl halide. The ionic liquid is then formed by a metathesis reaction with an alkali metal or silver salt of

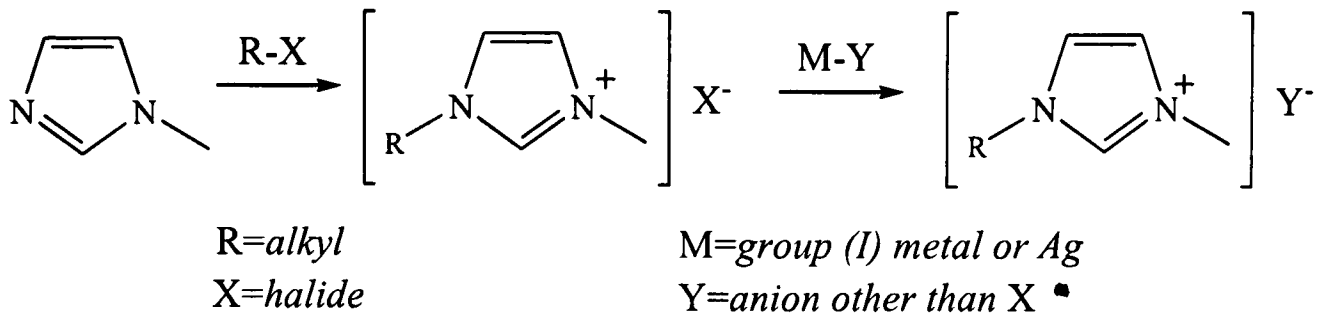

Figure 2.4: Reaction scheme for the synthesis of an imidazolium RTIL.[31] A similar method is followed for pyrrolidinium, tetraalkylammonium and tetraalkylphosphonium ionic liquids.[40,41,43,44,49]

the desired anion, leaving the alkali metal or silver halide as a by-product. A similar two-step procedure is used for the synthesis of pyrrolidinium, tetraalkylammonium and tetraalkylphosphonium ionic liquids.[40,41,43,44,49] In all cases, if the second step does not go to completion, unreacted halide ions from the first step are left in the ionic liquid as impurities, and must be removed in additional purification steps. The removal of halide impurities is very important, as halides can increase the viscosity and have significant effects on the electrochemical window of the solvent and outcome of synthetic routes (see section 2.4.2).

2.3 Properties of RTILs

Before considering a solvent for use as a reaction medium or in an electrochemical experiment, it is important to understand its physical and chemical properties. As a class of solvent, ionic liquids generally have high viscosities, densities greater than water, high intrinsic conductivities, wide electrochemical windows, high thermal stabilities, high polarities and solvating properties similar to those of conventional aprotic solvents. This section will examine each of these properties individually.

2.3.1 Viscosity

The viscosity of a solvent is an important physical property, since high viscosities form barriers for many applications and slow down the rate of diffusion-controlled chemical reactions.[68] Ionic

liquids have viscosities comparable to that of oils, *i.e.* two to three orders of magnitude higher than conventional molecular solvents. Table 2.2 compiles a list of some physical properties of some commonly used RTILs and conventional aprotic solvents, with viscosity values given in the second column. Viscosities of most RTILs are generally in the range of 30–450 cP at ambient temperature (with a few more viscous ionic liquids known that include halide anions, *e.g.* $[C_4mim]I$ and $[C_6mim]Cl$). The high viscosity of ionic liquids is obviously a disadvantage for use in industrial applications for the reasons described later, explaining the quest for new ionic liquids exhibiting lower viscosities. Viscosities can be lowered by the addition of small amounts of organic cosolvents,[69] but this tends to cause the solvent to lose some of its favourable properties such as low-volatility and thermal stability.

The viscosity of ionic liquids is primarily determined by van der Waals (vdW) forces and hydrogen bonding.[10,11,79] For example, ionic liquids with the $[C_2mim]^+$ cation exhibit lower viscosities than $[C_4mim]^+$, as increasing the length of the carbon chain on the imidazolium cation results in increased van der Waals interactions. Increased vdW forces results in more energy being necessary for molecular motions. The addition of fluoride functional groups on the imidazolium carbon chain also results in a higher viscosity due to an increase in hydrogen bonding.[11,31] The identity of the anion has a greater effect on viscosity than does the composition of the cation. For example, anions containing a greater number of fluoride ligands (*e.g.* $[BF_4]^-$ and $[PF_6]^-$) form much more viscous ionic liquids than the weakly basic $[NTf_2]^-$ anion (where the negative charge is delocalized over the two sulfoxide groups) due to the increased number of strong H—F interactions.

The viscosities of ionic liquids are highly temperature dependent, with a 20 % change over 5 K not uncommon around room temperature.[32] Okoturo and VanderNoot[71] report the viscosity of 23 RTILs over a temperature range of 283–343 K. They found that although some ionic liquids fit well to an Arrhenius relationship over the whole temperature range, those with symmetric cations

Table 2.2: Viscosity (η), density (ρ), conductivity (κ) and accessible electrochemical windows (EW) at a platinum electrode of some commonly used RTIL and molecular electrochemical solvents.

Ionic Liquid	η at 293 K/cP	ρ at 293 K/g cm^{-3}	κ at 293 K/mS cm^{-1}	EW†/V
$[C_2mim][NTf_2]$	34[31]	1.53[70]	8.8[31]	4.3
$[C_4mim][NTf_2]$	52[31]	1.44[70]	3.9[31]	4.8
$[C_8mim][NTf_2]$	74[36]	1.33[70]	-	5.0
$[C_4dmim][NTf_2]$	105[71]	1.42[70]	2.0[72]	5.2
$[C_6mim][FAP]$	74[37]	1.56[70]	1.3[37]	5.3
$[C_4mpyrr][NTf_2]$	89[71]	1.40[70]	2.2[40]	5.2
$[C_4mim][OTf]$	90[31]	1.30[31]	3.7[31]	4.9
$[C_4mim][BF_4]$	112[71]	1.21[73]	1.7[74]	4.7
$[N_{6,2,2,2}][NTf_2]$	167[44]	1.27[44]	0.67[75]	5.4
$[C_4mim][NO_3]$	266[73]	1.16[73]	-	3.7
$[C_4mim][PF_6]$	371[73]	1.37[73]	1.5[74]	4.7
$[P_{14,6,6,6}][NTf_2]$	450[49]	1.07[70]	-	5.0
$[P_{14,6,6,6}][FAP]$	464[70]	1.18[70]	-	5.6
$[C_4mim]I$	1110[76]	1.49[70]	-	2.1
$[C_6mim]Cl$	7453[37]	1.05[70]	-	3.2
Acetonitrile	0.34[77]	0.79[77]	§7.6[77]	§5.0[78]
Dichloromethane	0.44[77]	1.33[77]	-	§3.5[78]
N,*N*-Dimethylformamide	0.92[77]	0.94[77]	§4.0[77]	§4.3[78]
Dimethylsulfoxide	1.99[77]	1.10[77]	§2.7[77]	§4.4*
Propylene carbonate	2.5[77]	1.21*	-	§4.7[78]

§ containing 0.1 M TBAP at 295 K
† obtained from our own studies on blank RTILs using a 10 μm diameter Pt electrode and Pt quasi reference electrode. Electrochemical windows defined by the voltage range where the current is less than 1 nA.

or cations with functional groups fit better to the Vogel-Tammann-Fulcher (VFT) relationship (given below):[80–82]

$$\kappa = A\sqrt{T}e^{-B(T-T_0)} \tag{2.1}$$

where κ is conductivity, A and B are emperically derived constants, and T_0 is the ideal glass temperature at which the conductivity drops to zero. Some ionic liquids did not fit well to either equation.[71]

2.3.2 Density

Ionic liquids are typically more dense than organic solvents and water and generally fall in the range of 1 to 1.6 g cm^{-3} (see third column, Table 2.2).[83] The density decreases with increasing length of the alkyl chain on the imidazolium cation[13] and increases with the molecular mass of the anion in the approximate order $[BF_4]^- < [OTf]^- < [PF_6]^- < [NTf_2]^- < [FAP]^-$. Most density values are reported at around room temperature. However, several researchers have recorded densities as a function of temperature and have reported an approximately linear decrease of density with temperature.[36,84,85] Typical values for the volume expansion coefficient of *ca.* 5×10^{-4} K^{-1} were found,[84] which are significantly lower than those of common organic solvents (*e.g.* toluene, *ca.* 11×10^{-4} K^{-1}). This knowledge may be useful for employing RTILs in applications at higher temperatures, where extraction of reaction products is important.

2.3.3 Intrinsic Conductivity

In electrochemical experiments, the conductivity of a solvent is of vital importance. Ionic liquids have reasonably good conductivities, comparable to those of organic solvents with additional supporting electrolyte (*e.g.* 0.1 M TBAP). Some examples of measured conductivities of ionic liquids and conventional solvents at 293 K are shown in the fourth column of Table 2.2. Based on the fact that ionic liquids are composed entirely of charged ions, it is expected that they should have high conductivities. However, conductivity depends upon both the number of charge carriers and their mobilities. The high viscosity and large size of constituent ions result in reduced ion mobility and average conductivities. The conductivities of ionic liquids are often approximately inversely proportional to viscosity, and the lower viscosity ionic liquids such as $[C_2mim][NTf_2]$ and $[C_4mim][NTf_2]$ have reasonably high conductivities of 8.8 and 3.9 mS cm^{-1}, as compared to 7.6 and 4.0 mS cm^{-1} for acetonitrile and DMF, respectively. At increased temperatures, the conductivity increases,[35,75] due to the increased mobility resulting from a decrease in viscosity.

The variation of ionic liquid conductivity with temperature follows the Vogel-Tammann-Fulcher (VTF) relationship.[32,75,86,87] Vila *et al.*[87] reported the variation of conductivity with temperature in nine imidazolium based ionic liquids and showed that this relationship applies with a high level of precision. They also observed that conductivity decreases as the cation alkyl chain length is increased. However, conductivity was found to be less dependent on anion size, where the greatest conductivity was observed at an 'optimal' anion size, *i.e.* $[BF_4]^-$.

It is also worth mentioning a few reports of ionic liquids with higher conductivities than those reported in Table 2.2. For example, Hagiwara *et al.*[42,50,88] have synthesized a range of ionic liquids with conductivites ranging from 12 mS cm^{-1} to as high as 110 mS cm^{-1}.[50] These ionic liquids were made by reacting *n*-alkylimidazolium chlorides with anhydrous hydrogen fluoride (HF) and are described by the formula $[C_n mim][F(HF)_m]$ (where m= 2 or 3). They were reported to have viscosities as low as 4.9 cP and modest electrochemical windows of *ca.* 2.5-3.5 V.[50] However, these ionic liquids have not been extensively investigated as solvents, probably due to the extremely harsh conditions employed in their synthesis and their possible degradation to hazardous species such as HF.

2.3.4 Electrochemical Window

The electrochemical window of a solvent is defined by the voltage difference between the anodic and cathodic decomposition potentials of the molecules/ions that make up the solvent.[6] This voltage range is very narrow (approximately 1.5 V) in aqueous solutions on various electrode surfaces,[78] due to the oxidation and reduction of water. However, the electrochemical window in aprotic solutions containing supporting electrolytes is much wider *e.g.* 5.0 V for acetonitrile, 3.5 V for dichloromethane and 4.4 V for dimethylsulfoxide.[78] Ionic liquids have also been shown to possess wide electrochemical windows, in the range of *ca.* 4.0–6.0 V,[9] due to the robustness of the cations and anions that make up their structure. The window size is dependent

on the specific cation and anion combination used. The wide electrochemical windows have been exploited in electrodeposition studies (discussed in section 2.5.6), where certain metals and semi-conductors have been deposited that are out of the range of traditional solvents.[10,89] When voltage differences larger than their electrochemical window are applied, ionic liquids have been shown to decompose to products such as methylpyrrolidine, octanes, octenes, 2-butanol, dibutylmethylamine and butylpyrrolidine (in the case of $[C_4mpyrr][NTf_2]$), and to 1-butyl-3-methylimidazolium radicals (in the case of $[C_4mim][BF_4]$).[90]

The electrochemical windows given in the literature tend to differ from one report to another for a number of reasons, such as the presence of impurities, which can narrow the electrochemical window (see section 2.4), or the choice of electrode material. In addition, many researchers use different reference electrode materials, with many electrochemical windows reported *vs* a quasi-reference electrode such as a Pt/Ag wire. It is useful to know both the cathodic and anodic potential windows when choosing an ionic liquid for a particular electrochemical experiment, and voltages should be reported *vs* a stable reference couple. It has been suggested[91,92] that either ferrocene or cobaltocenium hexafluorophosphate may be suitable for such a purpose, as they have both been shown to have a potential independent of electrode composition, analyte concentration and scan rate.[92]

The final column of Table 2.2 shows the measured electrochemical windows on a Pt micro-electrode (diameter 10 μm) for a range of commonly used RTILs, compared to conventional aprotic solvents containing 0.1 M TBAP as supporting electrolyte. It can be seen that most ionic liquids have electrochemical windows of *ca.* 3.7–5.6 V, with the widest window seen in $[P_{14,6,6,6}][FAP]$. It is commonly thought that the reduction potentials of imidazolium-containing ionic liquids are slightly reduced due to the removal of the acidic proton attached to the ring carbon between the two heteroatoms.[9,31] Indeed, when the proton is replaced with a methyl group, the reductive window is extended (5.2 V for $[C_4dmim][NTf_2]$ compared to 4.8 V for

[C_4mim][NTf_2]). In addition, when the alkyl chain length on the imidazolium ring is extended, wider electrochemical windows are observed, but these are narrowed when functionalized groups are introduced *e.g.* with an alkyl-ether chain.[93] Alternatively, when the imidazolium cation is replaced with either pyrrolidinum,[40] tetraalkylammonium[44] or tetraalkylphosphonium,[37] wider electrochemical windows are observed. The nature of the anion is also known to influence the electrochemical window. Slightly wider electrochemical windows are observed for $[NTf_2]^-$ anions compared to $[BF_4]^-$, $[PF_6]^-$, although the difference is not a significant, being only of the order 0–300 mV. Narrower electrochemical windows are observed for ionic liquids containing chloride and iodide (see Table 2.2), due to the lower oxidation potential of the halide anions compared to $[BF_4]^-$, $[PF_6]^-$ and $[NTf_2]^-$. The most stable anion to oxidation is believed to be tris(pentafluoroethyl)trifluorophosphate ($[FAP]^-$) and a very wide electrochemical window of 7.0 V was reported for tetrabutylammonium [FAP] ([$N_{4,4,4,4}$][FAP]). It has also been shown that the anodic electrochemical window of acetonitrile can be extended by *ca.* 0.8 V with the addition of $[FAP]^-$ based ionic liquids as supporting electrolytes.[94] This additional potential range may allow the observation of voltammetric peaks, which would otherwise have been obscured by the decomposition of supporting electrolyte.

2.3.5 Thermal Stability

The thermal stability of a solvent is defined as the upper limit of the liquidus range[13] and is an important physical property to consider when using ionic liquids for reactions at high temperatures. Most decomposition temperatures reported in the literature are 573–674 K, with some ionic liquids thermally stable at temperatures up to 725 K.[76] The stability of the solvent is believed to depend on the strength of the heteroatom-carbon and heteroatom-hydrogen bonds.[11] For ionic liquids, thermal stability has been found to increase with increasing anion size, in the order: halide < $[BF_4]^-$ < $[NTf_2]^-$ < $[PF_6]^-$,[85,95] and with increasing alkyl chain length on the

imidazolium cation (*e.g.* from $[C_2mim]^+$ to $[C_8mim]^+$).[95] In addition, imidazolium ionic liquids were found to be more stable than those containing tetraalkylammonium cations.[95] These ionic liquids have little vapour pressure up to their decomposition, providing a wide liquid range with no vapour pressure.

The exact decomposition temperatures reported in the literature tend to vary drastically, possibly due to the presence of impurities in the ionic liquid and the experimental methods used. It has recently been suggested that many of the reported temperatures may be inaccurate.[10,96] Both reports suggest that such high temperatures are only tolerated by most liquids for a short time, and that long term exposure to temperatures above *ca.* 473 K inevitably leads to decomposition. However, for most applications, such as gas sensing (see section 2.5.4), this temperature is far above that required and so poses no real problem in terms of decomposition of the solvent.

2.3.6 Polarity and Solvating Properties

A key property of a solvent is how it will interact with potential solutes. For molecular solvents, this is commonly recorded as the 'polarity' of the pure liquid, and is generally expressed by its dielectric constant. However, determining the polarity of ionic liquids is more complicated than determining that of molecular solvents due to additional interactions such as hydrogen bonding, coulombic interactions and electron donating/accepting properties.[17] The simplest qualitative definition of a polar solvent is one that will dissolve and stabilize dipolar or charged solutes.[8] Based on this definition and on the fact that ionic liquids are composed entirely of ions, it is generally thought that ionic liquids will be highly polar, but this has shown to be an overstatement.[97] In fact, ionic liquids are capable of dissolving a wide range of solutes, both polar and non-polar, and usually exhibit fairly low 'polarity' values.[98] Several methods, such as using solvatochromic dyes *e.g.* Reichardt's dye,[36] betaine dye[98] and Nile Red,[36,99] electron paramag-

netic resonance (EPR),[100] association with water,[101] Fourier transform infra-red spectroscopy[102] and microwave dielectric spectroscopy,[103] have been used to quantify polarity in RTILs. The recorded polarity values, as with many other physical properties of RTILs, tend to vary from one laboratory to another, possibly due to the presence of impurities, or the exact experimental method used.

Taking into account these variations, the polarity of ionic liquids has been briefly compared to conventional solvents. For example, Carmichael and Seddon[99] suggested that ionic liquids based on the $[C_n mim]^+$ cation, with $[PF_6]^-$, $[BF_4]^-$, $[NTf_2]^-$ and $[NO_3]^-$ anions, have a similar polarity to 2-aminoethanol, but a lower polarity than alcohols such as methanol, ethanol and butanol. Aki *et al.*[51] indicated that $[C_4mim][PF_6]$, $[C_8mim][PF_6]$, $[C_4mim][NO_3]$ and $[C_4py][BF_4]$ are more polar than acetonitrile but less polar than methanol.

Having established that the polarity of ionic liquids is not easy to predict, it is useful to briefly look at the experimentally reported solubilities of solids, liquids and gases in ionic liquids compared to conventional solvents. For any experiment, the reactions and properties of a solute can only be investigated if dissolved to a sufficient quantity in a solvent. While there are many reports on the solubility of gases in ionic liquids, there are only a few articles[104] on the solubility of solids and liquids (excluding water and co-solvents, which are widely reported).[105,106] In general, it has been found that simple aliphatic compounds are sparingly soluble in ionic liquids,[11] while olefins[11,74,107] and carbohydrates[108] show a much higher solubility, and aldehydes can be completely miscible.[109] A similar trend is observed for gas solubilities. Gases such as carbon dioxide and sulfur dioxide are exceptionally soluble,[110,111] carbon monoxide and methane less soluble,[83] and oxygen and hydrogen only slightly soluble.[83] The contrasting solubilities can be exploited in reactions such as hydrogenation and hydrocarbonylation, allowing for relatively easy separation of products and/or unreacted substrates.

2.4 Effect of Impurities

Despite many ionic liquids being labelled as 'hydrophobic', it is well known that all ionic liquids absorb water to some extent. The presence of other impurities, such as chloride, dissolved gases, and species left over from the synthesis of RTILs (resulting in coloured solutions) are also important considerations and are briefly assessed below. As mentioned in the previous sections, it is likely that differing amounts and the nature of such impurities may account for the large variation of data reported concerning the physical properties of ionic liquids.

2.4.1 Water

Water impurities in RTILs have been shown to significantly decrease the viscosity,[112] increase the conductivity,[113] decrease the density[76] and significantly reduce the electrochemical window.[38] Schröder *et al.*[38] studied the effect of water on the diffusion of *N*, *N*, *N'*, *N'*-tetramethylphenylene-diamine (TMPD) in $[C_4mim][PF_6]$. It was shown that the diffusion coefficient of a neutral TMPD molecule nearly doubles and the potential window is significantly decreased in the presence of *ca.* 5 wt.% of water. Both cathodic and anodic features have been observed in the voltammetry of an ionic liquid which has been exposed to moist air for some time (see Figure 2.5).[1] These features can be comparable in size to any electroactive species under study, hence the need for vacuum techniques to remove these impurities. Since even 'hydrophobic' RTILs absorb moisture to some extent, this is obviously an important factor when employing these liquids as electrochemical solvents.

In all of the experiments reported in this thesis, the ionic liquid has been evacuated under vacuum for an extended period of time before the recording of voltammograms to minimise the effects of impurities (see Figure 2.5). In order to further illustrate the effectiveness of vacuum techniques to remove water/moisture from RTILs, Table 2.3 shows the measured[114] water contents using the Karl Fischer Titration method in both air-equilibrated and vacuum

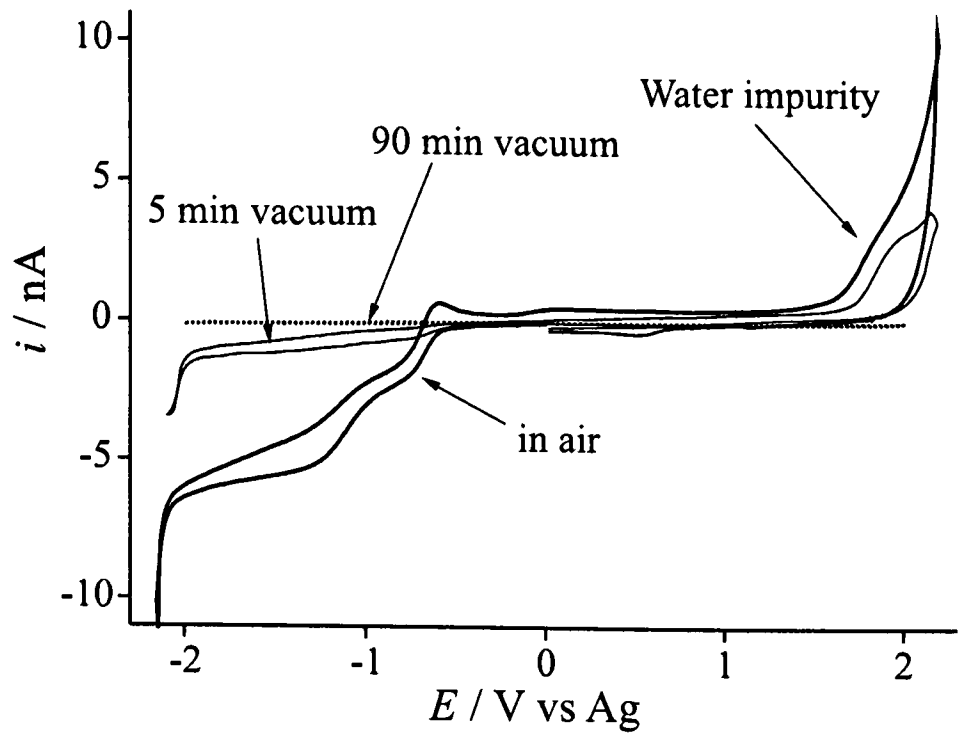

Figure 2.5: Cyclic voltammetry of a blank sample of $[C_4mim][OTf]$ on a gold microdisk electrode (diameter 25 μm) at 298 K, showing both cathodic and anodic features when exposed to air and when vacuum techniques have been used to remove these impurities.[1]

dried ionic liquids. It is clear from this table that every ionic liquid has a different affinity to water and that the 'hydrophobic' ionic liquids appear to have the lowest water contents, with the halide ionic liquids being most hydrophilic. It has been reported that ionic liquids containing the $[NTf_2]^-$ anion and the 1,3-dialkylimidazolium salt have a saturated water content of less than 2 %,[31,44] whereas some ionic liquids are known to be totally miscible with water.[76] It can also be seen from the table that the water content in the ionic liquids can be decreased by vacuum purging the solvent before use. For example, the water content of $[C_2mim][NTf_2]$ decreases by a factor of *ca.* 32 when purged under vacuum at 333 K for 24 hours.

2.4.2 Halides

Due to the methods used in the synthesis of most RTILs (see section 2.2.2), halide impurities can be introduced into the ionic liquid. Seddon *et al.*[115] studied the effect of halide impurities in imidazolium-based RTILs and reported a notable increase in viscosity with chloride content. In addition, the accessible potential window is decreased when halide impurities are present, since halides are more easily oxidised than many anions used in non-haloluminate RTILs. Figure 2.6 shows the voltammetry obtained for a 'pure' RTIL on a gold electrode. A sharp chloride-induced

Table 2.3: Water contents (air equilibrated and vacuum dried for 24 hours at 333 K) of some commonly used RTILs, calculated using the Karl Fischer titration method.

Ionic Liquid	Water content[114] /ppm (air equilibrated)	Water content[114] /ppm (vacuum dried)
$[P_{14,6,6,6}][FAP]$	328	-
$[C_4mpyrr][NTf_2]$	406	133
$[C_6mim][FAP]$	417	203
$[C_4mim][NTf_2]$	491	144
$[C_4dmim][NTf_2]$	504	295
$[N_{6,2,2,2}][NTf_2]$	1,150	167
$[C_4mim][PF_6]$	2,119	268
$[C_2mim][NTf_2]$	3,385	105
$[C_4mim][BF_4]$	5,083	119
$[C_4mim]I$	11,349	1,050
$[C_4mim][OTf]$	15,227	250
$[C_6mim]Cl$	61,049	2,231

gold stripping peak is observed due to the presence of small amounts of chloride impurity left over from the synthesis. This is due to the oxidation of gold surface chloride,[116,117] and can often decrease the anodic window by 0.9 V or more. Halide impurities have also been known to affect the outcome of synthetic routes. For example, Gallo *et al.*[118] reported that the rates of nickel, iron and ytterbium catalysed Michael additions were significantly affected by the presence of halide impurities, with a complete inhibition of the reaction containing iron and ytterbium. Trace quantities of chloride have also been shown to deactivate the catalyst in some transition metal catalysed reactions such as hydrogenation.[119,120] These few examples highlight the importance of chloride quantification in ionic liquid samples, and there are several methods, such as ion chromatography,[121,122] capillary electrophoresis,[123] and electrochemistry,[124] employed for this purpose. For example, an electrochemical method based on cathodic stripping voltammetry at a silver electrode has been used in the analytical determination of trace chloride to the parts per billion level.[124]

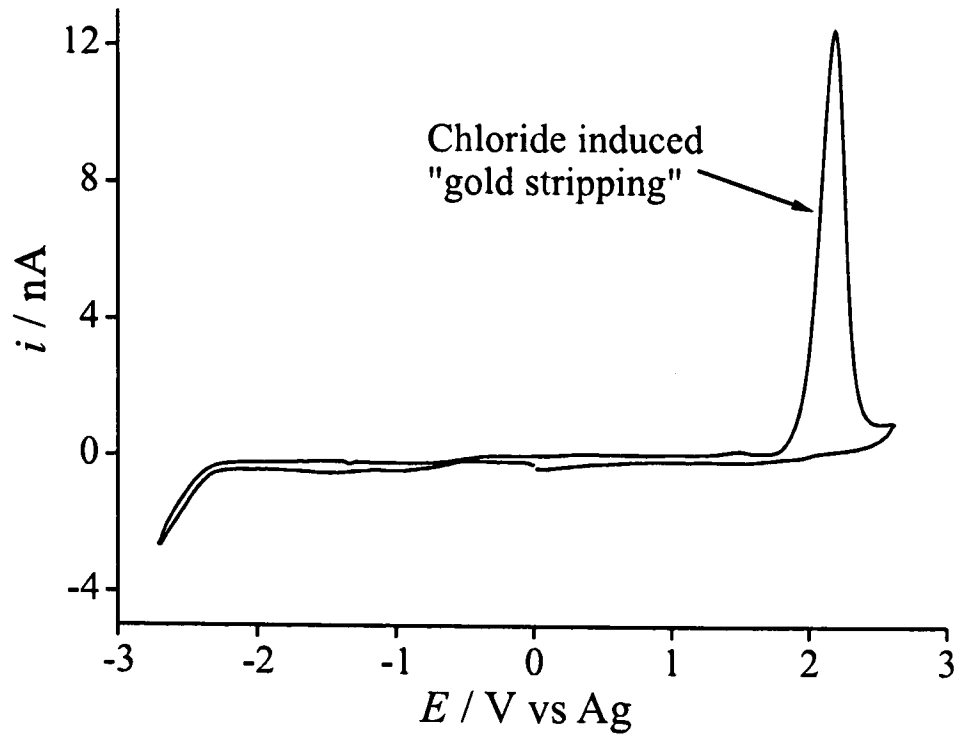

Figure 2.6: Cyclic voltammetry of a blank sample of $[C_4mpyrr][NTf_2]$ at 298 K on a gold microdisk electrode (diameter 25 μm) at a scan rate of 100 mV s^{-1} after vacuum purging for 90 mins. The oxidation peak at +2.1 V is believed to be gold stripping,[116,117] induced by the presence of chloride.[1]

2.4.3 Air

Another important consideration is the presence of air impurities, particularly when using RTILs as solvents in electrochemistry or in reactions where atmospheric gases can interfere. In addition to dissolved water/moisture (see section 2.4.1), dissolved gases such as oxygen can influence the electrochemical window of a pure RTIL. Figure 2.5 (thick solid line) shows the electrochemical window of a blank ionic liquid in the presence of air. The reductive features are believed to be a combination of the reduction waves of oxygen to superoxide, and superoxide to peroxide, as well as the reduction wave of water.[1] Degassing of ionic liquid solvents, either by vacuum techniques or by purging with an inert gas such as argon, is generally required before the recording of voltammograms in many electrochemical experiments.

2.4.4 Coloured Ionic Liquids

It has been widely recognised that although ionic liquids should be colourless, they are frequently not.[125,126] The formation of the colour (typically yellowish to orange) has been attributed to the use of starting materials with colour, such as imidazole, or to excessive heating during the synthesis of *e.g.* the imidazolium salt.[125,127] Earle *et al.*[126] suggest that there is no evidence

that coloured impurities affect the chemical or physical properties of ionic liquids, even though the coloured impurities may be aesthetically displeasing. However, 'high quality' ionic liquids such as $[C_4mim][NTf_2]$, $[C_4mim][OTf]$, $[C_4mim][PF_6]$ and $[C_4mim][BF_4]$ have been reported to be colourless, even though they are not 100 % pure.[125] A number of precautions for synthesis of colourless ionic liquids have been described, and a procedure for the removal of colour from impure ionic liquids using acidic alumina and activated charcoal has also been proposed.[125,126]

2.5 Applications of RTILs

Due to their many favourable properties (as discussed above), RTILs are increasingly being used for a number of commercial applications, such as 'green' synthesis, catalysis and biosensing, and in electrochemical devices such as solar cells, capacitors, fuel cells, lithium batteries and gas sensors. They have also been used for electrosynthetic and electrodeposition reactions. The following sections will introduce RTILs in the context of some of these applications.

2.5.1 'Green' Synthesis and Catalysis

Ionic liquids have attracted a great deal of attention as possible replacements for conventional solvents in organic synthesis and organic/inorganic catalysis. They were originally called 'green' solvents[14,15] in early research papers because of their low volatility and inability to emit volatile organic compounds (VOCs). However, many ionic liquids have since been shown to be not as 'green' as first believed, and many questions have arisen with regards to their toxicity and degradation. For example, ionic liquids based on the $[PF_6]^-$ anion have been shown to degrade to hazardous hydrogen fluoride, HF.[128] It is also noted that volatile organic solvents are almost always used in the synthesis of ionic liquids.

Despite these concerns, many common ionic liquids have been found to be highly favourable solvents in many kinds of organic and catalytic reactions, in particular for biphasic reac-

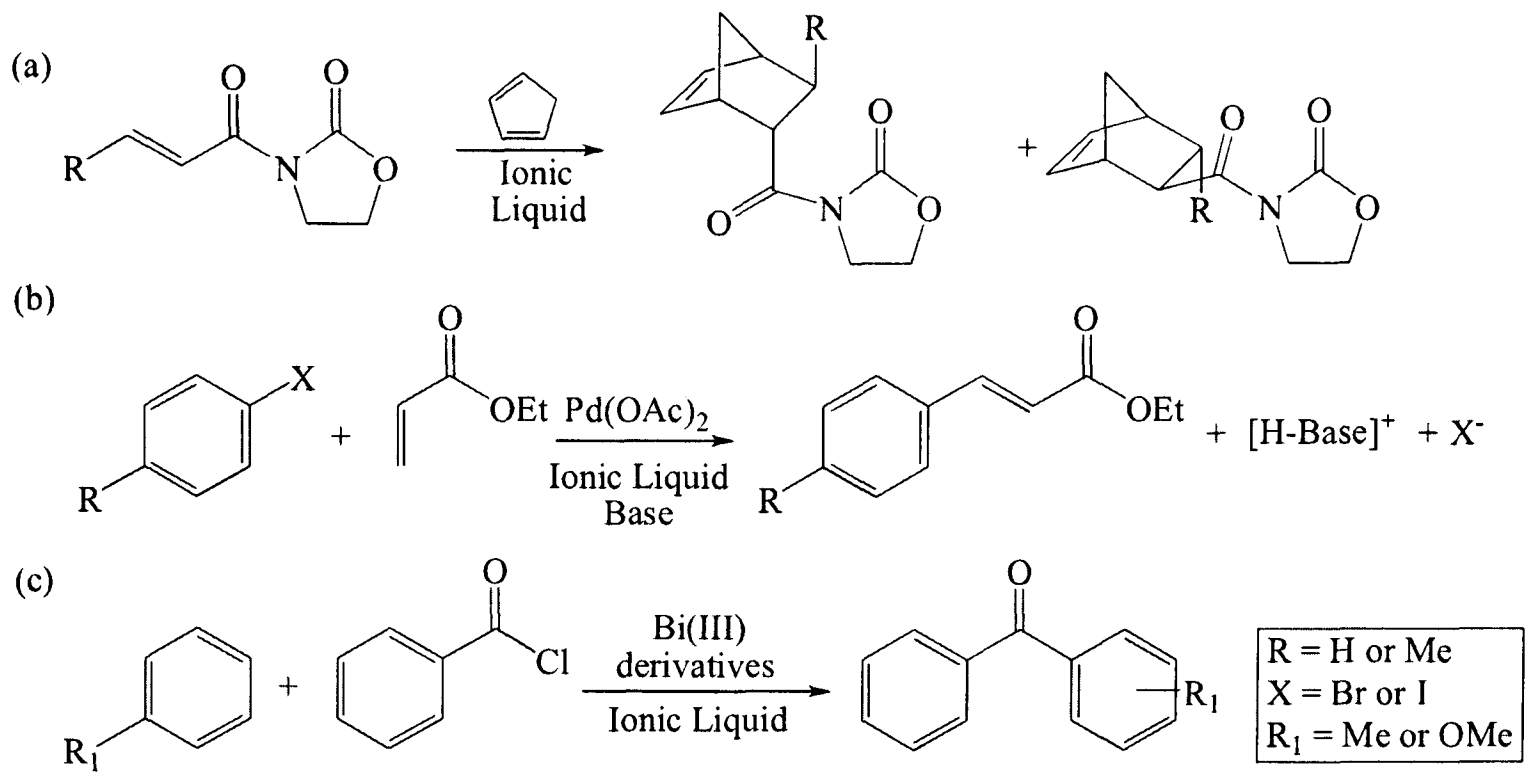

Figure 2.7: Mechanistic schemes for (a) Diels-Alder,[129] (b) Heck reaction[130] and (c) Friedel-Crafts reaction[131] using RTIL solvents.

tions,[63,119] in which the catalyst is isolated in one phase and the product remains in another. This opens up the possibility of recycling the solvent, reducing long-term costs and minimising waste. There are a vast number of reports on organic synthesis and catalysis in ionic liquids, and several review papers have been published.[8,11,12,74,107] A few specific examples of organic reactions in ionic liquids include the Diels-Alder,[129] Heck[130] and Friedel-Crafts[131] reactions, shown in Figure 2.7 a, b and c, respectively. In the first reaction (Figure 2.7a), excellent diastereoselectivity and enantioselectivity was achieved from performing a Diels-Alder reaction in imidazolium-based ionic liquids at room temperature, as opposed to the necessarily low temperatures (*ca.* 195 K) usually required to produce such good selectivities in conventional solvents. In the Heck reaction (Figure 2.7b), the coupling of aryl halides with alkenes was shown to produce excellent yields in ionic liquids, as the palladium catalyst dissolved well in the ionic liquid medium, and the product and by-products could be easily separated.[130] In the third example (Figure 2.7c), the activity of four bismuth(III) derivatives ($Bi(OTf)_3$, Bi_2O_3, $BiCl_3$ and BiOCl) was found to increase dramatically when they were dissolved in imidazolium-based ionic liq-

uids.[131] A catalyst loading of as low as 1 % was required for a clean, high-yielding acylation of a variety of benzene derivatives, and the possibility of recycling the solvent was suggested.[131]

It has also been reported that ionic liquids may not be completely inert under many reaction conditions and can themselves alter reactivity, catalytic activity and by-product formation. An extensive account of the reactivity *of* ionic liquids (as opposed to the reactivity *in* ionic liquids) has been written by Chowdhury *et al.*[18] and should be carefully considered before employing ionic liquids as reaction media for any organic or catalytic reaction.

2.5.2 Biochemical Applications: Enzyme Catalysis

Although enzyme reactions often take place in aqueous/buffered solutions (media in which enzymes are most soluble), many biocatalytic processes are performed in organic media to improve the solubility of hydrophobic reactants and/or products and to shift reaction equilibria from hydrolysis towards synthesis. However, many enzymes require a full hydration shell to be active, and it is often found that such enzymes are deactivated in organic media. Organic solvents are also known to damage bacterial cell membranes and to promote enzyme denaturation.

As an alternative to organic solvents, ionic liquids have been investigated as possible media in which to perform biochemical reactions, and a number of review papers have been published.[23,132–135] The most in-depth account to date appears to be a review written by van Rantwijk and Sheldon,[24] who describe in detail many biotransformations in ionic liquids and suggest that such media may be highly advantageous for enzyme catalysis. The reason for the interest in ionic liquids as solvents in biochemical reactions is largely due to their ability to stabilize enzymes. As with organic solvents, proteins are not soluble in most ionic liquids when the ionic liquids are used as a pure solvent. However, when small amounts of water are added to an ionic liquid, many enzymes can be sufficiently dissolved and still retain their stability due to the much lower water content (compared to a pure aqueous environment). For example,

Fujita *et al.*[136] showed that cytochrome *c* maintained its structure and activity after 6 months at room temperature in ionic liquids (with 20 wt % water), whereas inactivity occured after only 1 week in a buffered aqueous solution. A second important advantage of ionic liquids is that their moderately high polarity may be exploited for biotransformation reactions of highly polar species such as polysaccharides (which cannot be performed in water due to equilibrium limitations) and highly polar substrates such as carbohydrates and amino acids (which are sparingly soluble in common organic solvents). In addition, ionic liquids have been shown to enhance enantioselectivity and regioselectivity[135] and, in some cases, can be successfully recycled for further reactions without effecting the rate or yield of the process.[12]

It should be noted that not all ionic liquids are suitable for biocatalysis. For example, enzymes such as lipase were found to be active in ionic liquids containing $[NTf_2]^-$, $[BF_4]^-$ or $[PF_6]^-$ anions but inactive in ionic liquids with Cl^-, $[OTf]^-$, $[NO_3]^-$ or $[TFA]^-$ anions.[137] In addition, the low volatility of ionic liquids makes extracting solid or non-volatile products formed after a biocatalytic reaction difficult, and the contrasting hydrophilicity/hydrophobicity of ionic liquids means that it is also difficult to predict which precise cation/anion combination may be suitable for any particular reaction. Despite these challenges, the many advantages of ionic liquids have allowed their use in biochemical applications such as delivery of pharmaceutical chemicals[138] and controlled drug release,[139] and ionic liquids soon may be introduced into industrial scale biocatalytic processes.[24]

2.5.3 Electrochemical Devices

Many electrochemical devices are based on aqueous, gel or polymer electrolytes, the lifetimes of which are limited by the conductivity and stability of the solvent. Due to their favourable properties, ionic liquids are potentially attractive alternative electrolytes for use in many electrochemical devices.[140] There are various examples of the use of RTILs in applications such as con-

ducting polymer electrochemical devices,[141,142] actuators,[143] double-layer capacitors,[32,88,144–146] supercapacitors,[147] dye-sensitized solar cells,[148–151] lithium batteries,[72,152] fuel-cells,[153] channel field-effect transistors[154] and light-emitting electrochemical cells.[155,156] For example, Lu *et al.*[141] describe the use of two common ionic liquids ($[C_4mim][BF_4]$ and $[C_4mim][PF_6]$) as electrolytes for π-conjugated polymer devices based on polyaniline, polypyrrole and polythiophene. They show that such devices are stable over long periods of time with negligible loss of activity over one million cycles. In addition, this was possible without the use of an inert atmosphere (*i.e.* glove box), which is commonly required for stable preparation and operation of such devices.[141] Kawano and Wanatabe[151] showed that the high ionic strength of ionic liquids led to fast charge transport based on the exchange reaction of the I^-/I_3^- redox couple, which contributed to the high performance of their dye-sensitized solar cells. When using ionic liquids for fuel cell applications, de Souza *et al.*[153] achieved a high overall efficiency of 67 % with $[C_4mim][BF_4]$ in an open atmosphere at room temperature, but the efficiency was dependent on the exact nature of the RTIL used; only a 28 % efficiency was achieved with $[C_4mim][PF_6]$. The presence of impurities such as water are also important considerations, as it was shown that 10 % (by volume) of water decreased the efficiency of the two fuel cells from 67 % to 42 % (in $[C_4mim][BF_4]$) and from 28 % to 16 % (in $[C_4mim][PF_6]$). Another challenge when using ionic liquids in electrochemical devices is their high viscosity, resulting in their ion conductivity often falling short of that of solvent-based electrolytes,[140] To overcome this, Matsumoto *et al.*[157] used low viscosity ionic liquids such as $[C_2mim][F(HF)_m]$ (where m= 2 and 3) for solar cells, but the efficiency was only 2.1 % (less than that obtained using LiI/MeCN), and the hazardous nature of HF means that the use of such ionic liquids is unlikely to appeal commercially.

2.5.4 Gas Sensing

RTILs are potentially advantageous solvents for electrochemical gas sensors. Most amperometric sensors of gases (such as oxygen, carbon monoxide, sulfur dioxide, hydrogen sulfide, chlorine, nitrogen dioxide and nitric oxide) employ conventional solvents that cannot survive drastic temperature changes or extremely dry or humid conditions. The 'lifetime' of a sensor is often determined by how quickly the electrolyte dries out, and many conventional gas sensors use a H_2SO_4/H_2O mixture to approximately match 'usual' atmospheric conditions, but which may not be ideal for amperometric measurements. RTILs have the ability to withstand high temperatures and pressures, and most have a wide liquid temperature range, which allows them to perform under conditions where traditional solvents would struggle to remain physically or chemically unchanged. This, combined with the intrinsic conductivity (no need for supporting electrolyte) and wide potential windows of RTILs (to investigate compounds that may have been inaccessible otherwise) makes them advantageous media for use in the development of stable and robust amperometric gas sensors. The electrochemical mechanisms of a range of gases, including oxygen,[158,159] carbon dioxide,[160,161] ammonia,[162,163] hydrogen sulfide[164] and sulfur dioxide,[165] have been studied in various ionic liquids in our research group alone, and the use of RTILs in gas sensor design is assessed by Buzzeo *et al.*[166]

The solubility of gases in ionic liquids is important, since many applications focus on the use of these liquids as replacement solvents for reactions involving gaseous species. Experimentally, it has been found that many gases, including carbon dioxide,[111,167] are highly soluble in ionic liquids. Table 2.4 shows a comparison of the solubility of a several gases in ionic liquids and conventional solvents, measured by electrochemical methods. The solubilities of the non polar gases (hydrogen and oxygen) are relatively small in both RTILs and conventional solvents. The polar gases (hydrogen sulfide, H_2S, and sulfur dioxide, SO_2), however, are much more soluble in RTILs than other solvents. In particular, the solubility of H_2S is increased by a factor of *ca.*

Table 2.4: Solubilities of various gases (at 298 K and 1 atm. pressure) in room temperature ionic liquids and conventional molecular solvents.

Solvent	H_2 / mM	O_2 / mM	H_2S / mM	SO_2 / mM
$[C_2mim][NTf_2]$	4.2[168]	10.8[166]	530[164]	230[165]
$[C_4mim][BF_4]$	5.2[168]	3.7[169]	-	1600[165]
$[C_4mim][NO_3]$	4.8[168]	-	440[164]	3000[165]
$[C_4mim][PF_6]$	5.1[168]	3.6[169]	230[164]	250[165]
Water	0.8[170]	16[166]	74[171§]	1470[172]
MeCN	-	8.1[166]	-	-
DMF	1.1[170]	2.1[166]	-	-
DMSO	2.0[170]	4.8[166]	-	-

§ at 313 K

3-7 in ionic liquids compared to water, suggesting that RTILs may be very favourable media for H_2S sensing. It is also important to note that the solubilities can vary between each ionic liquid, an effect which is thought to be dependent mainly upon the nature of the RTIL anion.[111] This should be taken into consideration when choosing a suitable solvent for an electrolyte material.

Despite their many advantages, RTILs are still in the development stage as solvents in commercial gas sensors, as their high viscosity (resulting in slower mass transport and lower attainable currents) and sensitivity to moisture may limit their widespread use. However, with the synthesis of more hydrophobic and less viscous RTILs and the ability to 'fine-tune' the solvent for a specific purpose, these problems may soon become insignificant.

2.5.5 Electrosynthesis

As mentioned in section 2.5.1, several reports have highlighted the advantages of using RTILs for organosynthesis due to their potential recyclability and reuseability. They have been employed as solvents, for example, in transition metal catalysis,[11] Diels Alder[129] and Heck[130] reactions. However little has been detailed on electrosynthetic processes in this medium. Described below is an example of a model voltammetric study in RTILs that shows promise as an electro-organic

synthetic route in RTILs.

The oxidation of bromide was chosen as a 'model' system to compare the behaviour of electroactive species in RTILs to that of the same species in aprotic solvents. The oxidation of bromide was studied in the RTIL $[C_4mim][NTf_2]$ on both platinum macro and microelectrodes[173] and compared to a similar study in acetonitrile. In aprotic systems, the tribromide anion, Br_3^-, and molecular bromine Br_2, are generated upon oxidation of the halide. Two oxidation waves are observed and have been ascribed[174,175] to the following processes:

$$3Br^- \rightarrow Br_3^- + 2e^- \tag{2.2}$$

$$Br_3^- \rightarrow \frac{3}{2}Br_2 + e^- \tag{2.3}$$

The homogeneous reaction between bromide and the electrogenerated bromine is also known to form tribromide:

$$Br^- + Br_2 \rightleftharpoons Br_3^- \tag{2.4}$$

The voltammograms obtained in both MeCN and $[C_4mim][NTf_2]$ revealed two waves upon oxidation, with a linear relationship observed between limiting current and bromide concentration. The ratio of the limiting currents of the first and second oxidations was 2:3, and the diffusion coefficient of bromide in the ionic liquid was two orders of magnitude less than in MeCN.[173]

The reactivity of electrogenerated bromine with cyclohexene was studied in $[C_4mim][NTf_2]$ on a platinum microdisk electrode.[176] Micromolar additions of cyclohexene were made to a 20 mM $[C_2mim]Br/[C_4mim][NTf_2]$ solution, and linear sweep voltammograms were recorded at a platinum microdisk electrode. Two oxidative waves were observed, corresponding to the direct oxidation of bromide (equations 2.2 and 2.3 above). A new, third wave was also observed, which is believed to be due to direct oxidation of a product species, dibromocyclohexane (DBCH) formed *via* a bromination reaction (see Figure 2.8a). NMR analysis of the solution showed characteristic peaks for the protons on bromine substituted carbons. In order to further confirm this, the direct oxidation of DBCH was studied at a platinum microdisk electrode, and was found to overlay exactly with the third wave. In contrast, a similar study in MeCN did not yield

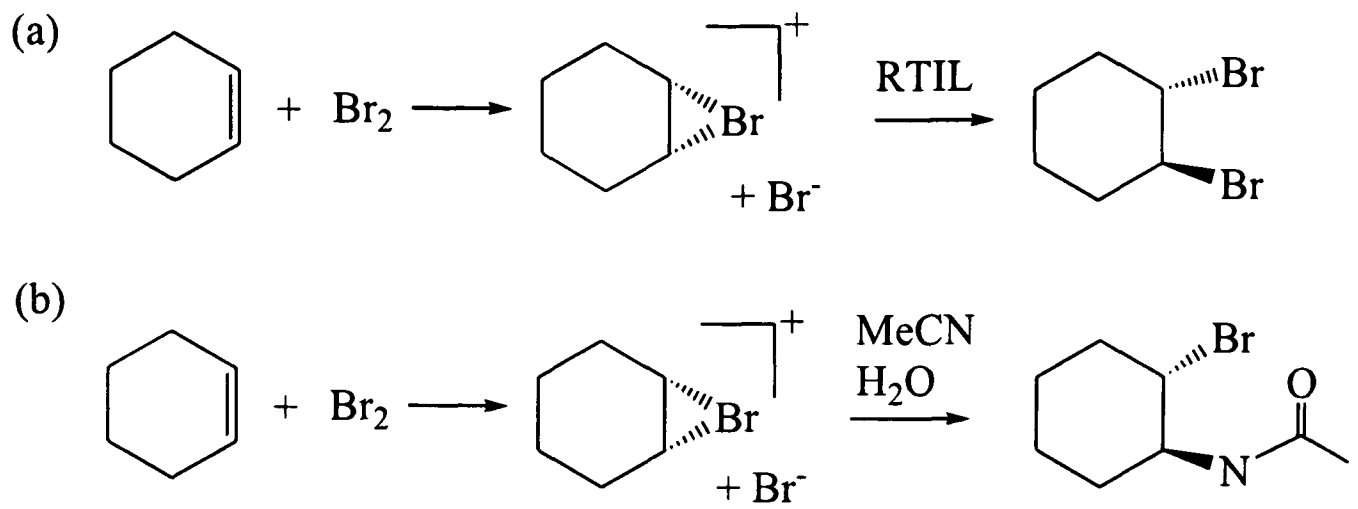

Figure 2.8: (a) Reaction of cyclohexene with electrogenerated bromine in $[C_4mim][NTf_2]$. The final reaction product is trans-1,1-dibromocyclohexane (DBCH). (b) Reaction of cyclohexene with electrogenerated bromine in acetonitrile, generating a solvent-incorporated acetamine.[173]

dibromocyclohexane, but instead a solvent-incorporated product (see Figure 2.8b), confirmed by bulk electrolysis and analysis of NMR spectra.

Other electrosynthetic processes worth mentioning include the cycloaddition of carbon dioxide to epoxides in several $[C_nmim]^+$-based ionic liquids under mild conditions,[177] as shown in Figure 2.9a, and the electrochemical pinacol coupling of acetophenone in three ionic liquid solvents, as shown in Figure 2.9b.[178] In the first process, the radical anion of CO_2 (formed by holding the potential at -2.4 V *vs* Ag/AgCl) reacts with the epoxide to form a cyclic carbonate.[177] In the second example, the use of RTILs as the electrochemical solvent not only simplifies the experimental setup and product extraction but also results in strong effects on both the stereoselectivity and kinetics of the reaction.[178]

Such processes could potentially be applied to large scale organic reactions, although reaction conditions and product extraction techniques would have to be carefully considered. With the advent of new recyclable and distillable RTILs,[179] it seems obvious that more electrosynthetic processes need to be investigated in these versatile and tuneable solvents, as RTILs may offer simpler and more efficient ways to synthesize a desired species than those offered by conventional solvents.

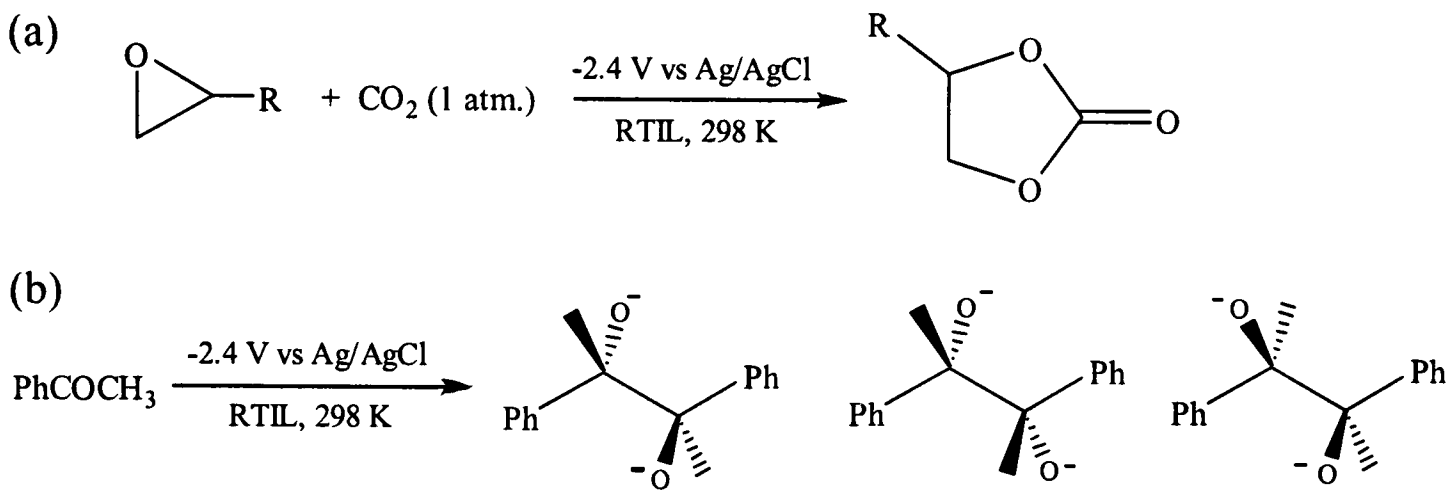

Figure 2.9: Reaction schemes for (a) the formation of a cyclic carbonate from an epoxide[177] and (b) the pinacol coupling of acetophenone[178] in RTIL solvents.

2.5.6 Electrodeposition

As mentioned in section 2.3.4, ionic liquids have very wide electrochemical windows compared to conventional molecular solvents, making them highly favourable for the electrodeposition of metals and semiconductors that are normally deposited out of the potential range of traditional solvents. In addition to the wider range of elements/compounds that can be deposited in RTILs, higher quality deposits with more variable morphologies are also possible due to the absence of the hydrogen evolution process, which takes place in aqueous media.[89] However, a major drawback to using RTILs as electrodeposition media is their sensitivity to moisture, requiring all experiments, including those employing non-haloaluminate RTILs, to be performed inside a glove box. Despite the more difficult experimental procedures required, the advantageous properties of RTILs have resulted in many reports of electrodeposition of a wide range of metals, alloys and semiconductors, with several review papers[89,180,181] and a recently published book[182] devoted entirely to the subject. For example, metals that have been deposited in ionic liquids include aluminium, copper, palladium, gold, zinc, manganese and tin. Less noble metals such as sodium, lithium, gallium and iron, semiconductors such as silicon and germanium, as well as several aluminium alloys containing elements such as iron, cobalt, nickel, copper and silver have also been reported (see the review paper by Endres[89] and references therein). In addition, it

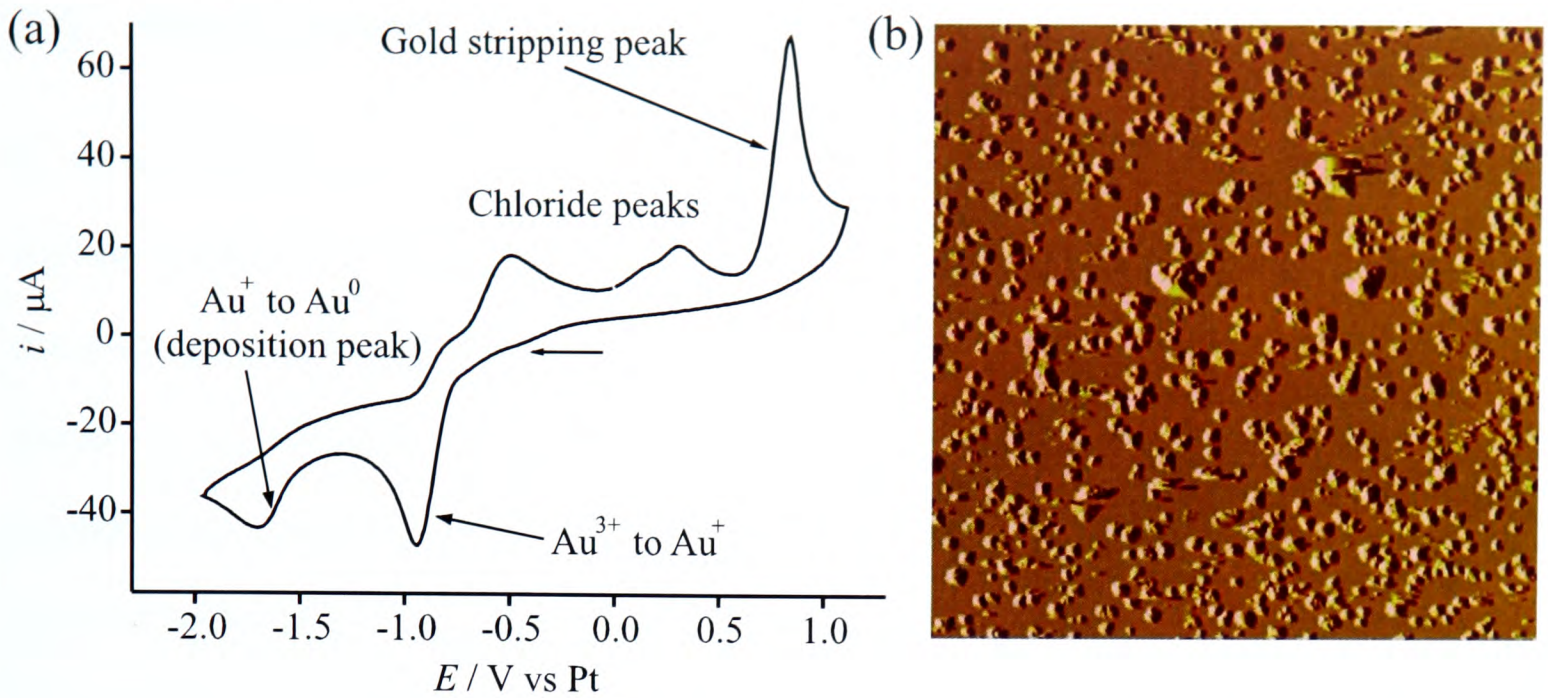

Figure 2.10: (a) Typical cyclic voltammetry for the reduction of *ca.* 5 mM $HAuCl_4$ in $[C_4mim][NTf_2]$ at 298 K on a BDD electrode at 100 mV s^{-1}. (b) Atomic Force Microscopy (AFM) image of gold nanoparticles deposited on a boron doped diamond electrode (BDD), from the same solution. Average size of the nanoparticles: diameter=208 (±64) nm, height=93 (±29) nm.[186]

has recently been demonstrated that other species such as uranium (as uranium oxide, UO_2),[183] cadmium telluride (CdTe)[184] and cadmium selenide (CdSe) quantum dots[185] can also be formed in RTIL media.

As a specific example of electrodeposition, Figure 2.10a shows typical cyclic voltammetry for the reduction of *ca.* 5 mM $HAuCl_4$ in $[C_4mim][NTf_2]$ on a 3 mm diameter boron doped diamond (BDD) electrode.[186] The potential was swept from 0 to -2.0 V and then held at -2.0 V for 60 seconds to enable deposition of gold onto the BDD electrode surface. The sharp reduction peak at *ca.* -0.9 V *vs* Pt corresponds to the reduction of Au(III) to Au(I), with a second reduction peak at -1.7 V assigned to the reduction of Au(I) to Au(0). The identities of all the remaining peaks have been explained in detail by Aldous *et al.*[187] and will not be included here. Figure 2.10b shows an atomic force microscopy (AFM) image of the electrode surface after deposition. As can be seen, many discrete gold deposits, which have an average diameter of 208 (±64) nm and average height of 93 (±29) nm, are formed on the electrode surface. This example demonstrates that RTILs can be easily employed as solvents in the electrodeposition of gold nanoparticles.

2.6 Fundamental Electrochemical Studies

In the previous section, it has been shown that RTILs can offer many advantages over conventional molecular solvents in various applications. However, before RTILs are employed in electrochemical applications (*e.g.* gas sensing, electrosynthesis and electrodeposition), it is important to understand their fundamental electrochemical behaviour as solvents. In particular, the behaviour of certain species in RTILs should be compared to their behaviour in conventional molecular solvents in order to ascertain whether these solvents behave analogously and if they can be treated accordingly. In this section, the focus will be on four main topics: voltammetry, mass transport, heterogeneous electron transfer kinetics and the electrical double layer in RTILs.

2.6.1 Voltammetry in Ionic Liquids

Once ionic liquids have been prepared and purified, there are no additional difficulties when employing them as solvents for electrochemical experiments (compared to conventional molecular solvents). In fact, their intrinsic conductivity means that no supporting electrolyte is required, which simplifies experimental setup and minimizes waste. Their wide electrochemical windows are also particularly beneficial when investigating peaks at very negative and positive potentials.

However, when studying cyclic voltammetry in RTILs, the high viscosity of the solvent must be taken into account, as this has significant consequences when interpreting voltammetric behaviour. In an early paper by Boxall *et al.*[188] entitled 'Apparent Anomaly During Rotating Disk Electrodes in Ionic Liquids', the authors studied the oxidation of ferrocene in $[C_4mim][PF_6]$ and noticed that the current maximum was not very reproducible. On closer inspection, they determined (as predicted by theory) that, due to the much higher viscosity of the RTIL, over 100 revolutions of the disk were required to approach the true Levich limiting current.[188]

This effect is important to understand before employing RTILs as electrochemical solvents, as the steady-state limiting current obtained from a microelectrode is often used to calculate

diffusion coefficients in traditional solvents. If a true steady-state condition is not achieved, the diffusion coefficients calculated using this method may not be an accurate measurement of the real values. According to the inequality given in equation 2.5, true steady-state behaviour will only be achieved at rather slow scan rates of 10 mV s^{-1} or below at a 5 μm radius disk, assuming $D = 1 \times 10^{-11}$ m^2 s^{-1} (typical for solid species in RTILs). Therefore, obtaining true limiting currents in these solvents is often far from trivial.

$$\nu << \frac{RTD}{nFr_d{}^2} \tag{2.5}$$

Here ν is the scan rate, R is the universal gas constant, T the absolute temperature, D the diffusion coefficient, F the Faraday constant and r_d the radius of the disk.[189]

A very good example of this behaviour is illustrated by the voltammetry of the reduction of oxygen in ionic liquids. Figure 2.11 shows the reduction of 1 atm. oxygen in the RTIL $[N_{6,2,2,2}][NTf_2]$ on a 10 μm diameter Pt electrode at 1 V s^{-1}.[158] The reduction peak is steady-state in nature and is dictated by convergent diffusion to the electrode surface, whereas the oxidation peak is highly transient due to a significant contribution from planar diffusion. This behaviour is attributed to the widely different diffusion coefficients of oxygen and superoxide (1.5×10^{-10} m^2 s^{-1} for O_2 and 4.7×10^{-12} m^2 s^{-1} for $O_2{}^{-\bullet}$) resulting in a single voltammogram demonstrating both steady-state and transient behaviour.[158]

As a result of this behaviour, many researchers commonly use a microelectrode to study the voltammetry of diffusing species. This has the advantages of producing macroelectrode ('transient') behaviour (useful for mechanistic and kinetic studies where peak shapes and potentials are important), but with the added benefits of high current density and low ohmic drop associated with microelectrodes. In addition, the volume of ionic liquid solvent can be minimised (to tens of microlitres) by using a two-electrode system, with a quasi-reference electrode (usually a metal wire) and a microelectrode as the working electrode.

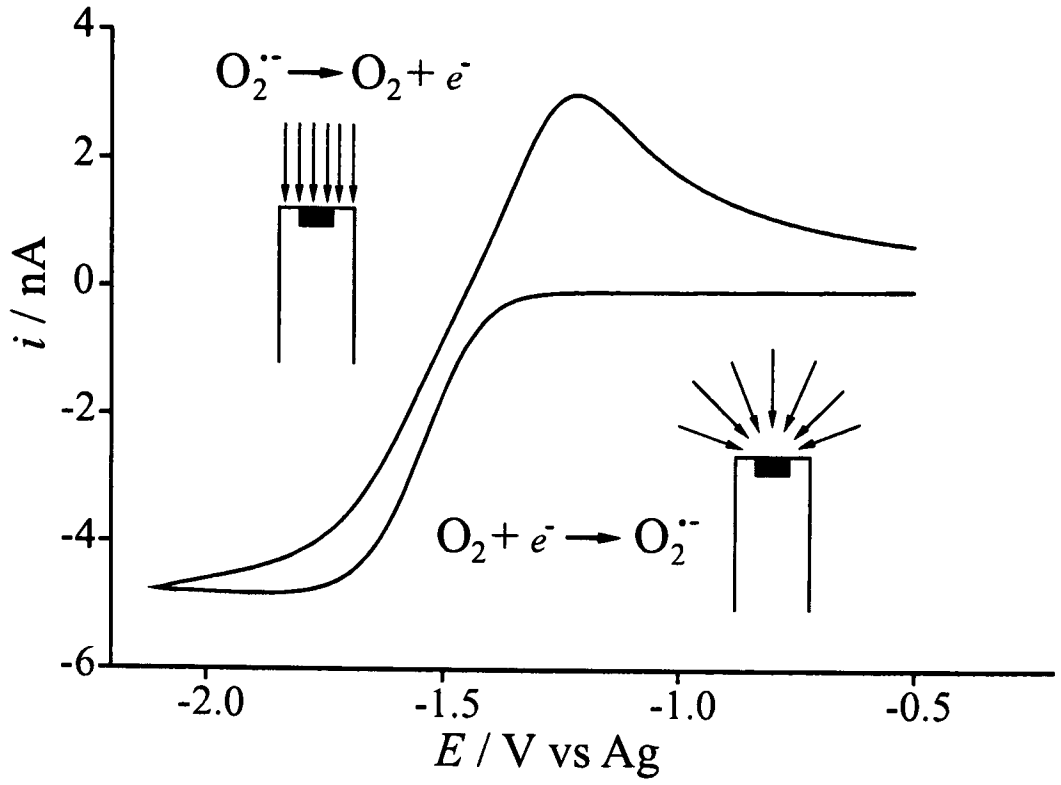

Figure 2.11: Cyclic voltammetry obtained for the reduction of 1 atm. oxygen gas in $[N_{6,2,2,2}][NTf_2]$ at 298 K on a 10 μm diameter Pt electrode at a scan rate of 1 V s^{-1}. Inset shows the hemispherical and planar diffusion responsible for the steady state and transient behaviour observed in the same voltammogram, due to a discrepancy in the diffusion coefficients.

2.6.2 Mass Transport

In a fundamental study designed to compare diffusional transport in RTILs with that observed in conventional aprotic solvents, the diffusion rate of N, N, N', N'-tetramethylphenylenediamine (TMPD) was studied[190,191] as a function of temperature (298-348 K) and charge on the diffusing species in the following solvents: $[C_2mim][NTf_2]$, $[C_4py][NTf_2]$, $[C_4mpyrr][NTf_2]$, $[C_{10}mim][NTf_2]$, $[P_{14,6,6,6}][NTf_2]$ and acetonitrile. To overcome the potential complication of conproportionation (a thermodynamically favoured process producing two $TMPD^{+\bullet}$ molecules from a reaction between TMPD and $TMPD^{2+}$), the voltammetry of the radical cation of TMPD was studied. Figure 2.12 shows a typical cyclic voltammogram obtained for the oxidation of $TMPD^{+\bullet}$ in $[C_4mpyrr][NTf_2]$. $TMPD^{+\bullet}$ is reversibly reduced to neutral TMPD at *ca.* -0.15 V *vs* Ag, and oxidized to $TMPD^{2+}$ at *ca.* +0.55 V. The diffusion coefficients of all three diffusing species were calculated using single and double-step chronoamperometry (described in more detail by Klymenko *et al.*).[192] It was found that the diffusion coefficient of the radical cation ($TMPD^{+\bullet}$)

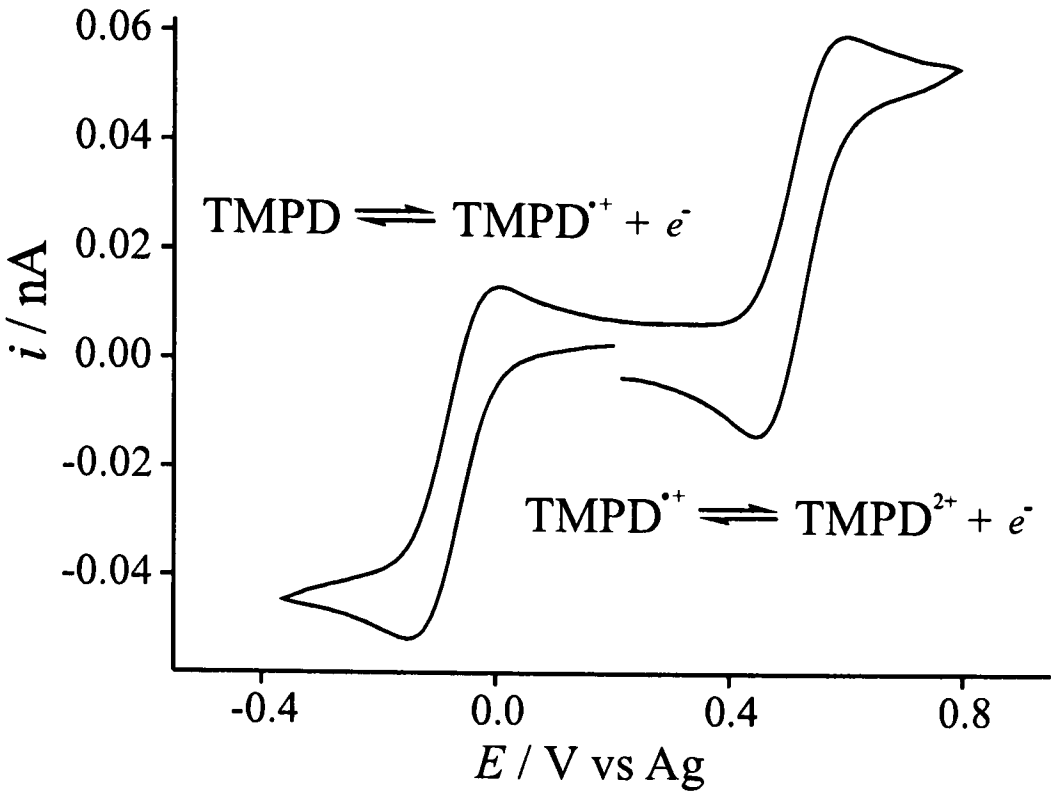

Figure 2.12: Cyclic voltammetry for the reduction of 2 mM $TMPD^{+\bullet}[BF_4]^-$ in $[C_4mpyrr][NTf_2]$ at 298 K on a Pt microelectrode (diameter 10 μm) at 100 mV s^{-1}.[191]

is only slightly diminished from that of the neutral species (ratio=0.88) in acetonitrile, but in RTILs the ratio was much closer to 0.5.[190] In addition, the diffusion coefficient of the dication ($TMPD^{2+}$) was found to be half that of the neutral species in MeCN (ratio of 0.51), but three times smaller in RTILs (ratio 0.33). A similar voltammetric and chronoamperometric study on the ferrocene/ferrocenium (Fc/Fc^+) and cobaltocenium/cobaltocene (Cc^+/Cc) redox couples was performed in the ionic liquids $[C_2mim][NTf_2]$, $[C_4mim][NTf_2]$, $[C_4mpyrr][NTf_2]$, $[C_4mim][OTf]$, $[C_4mim][BF_4]$, $[C_4mim][NO_3]$, $[C_4mim][PF_4]$ and $[P_{14,6,6,6}][FAP]$.[92] It was shown that the diffusion coefficient of the charged species was slower than that of the neutral species by a ratio of *ca.* 0.5–0.8 in seven of the ionic liquids, and in $[P_{14,6,6,6}][FAP]$ this ratio was reduced to *ca.* 0.1 and 0.3 for Fc^+/Fc and Cc^+/Cc, respectively. This demonstrates that, for modelling purposes, the assumption of equal diffusion coefficients (valid in MeCN)[193,194] is unwise in ionic liquid solvents.

In both of the above studies,[92,190] it was also shown that the Arrhenius relationship between D and T (temperature) is universally followed, with the diffusional activation energy approxi-

mately equal to the activation energy for viscosity in a particular RTIL, except in the case of the cobaltocenium ion in $[C_4mim][PF_6]$ (possibly due to the strong affinity of Cc^+ with $[PF_6]^-$). Furthermore, a qualitative conformity to the Stokes-Einstein relation was demonstrated, with diffusion coefficients linearly proportional to the inverse of viscosity, showing that RTILs can treated in the same way as conventional solvents, but with significantly slower diffusion. However, it should be noted that this is not true for all systems in RTILs, such as for the diffusion of small molecules, where Stokes-Einstein behaviour has been found to break down *e.g* for O_2,[159] H_2 (see Chapter 9), SO_2[165] and H_2S.[164]

2.6.3 Heterogeneous Electron Transfer Kinetics

Hapiot and coworkers have studied the heterogeneous electron transfer kinetics of a selection of nitro compounds[195] and of the electrogenerated radical cations[196] of veratrole (1,2-dimethoxybenzene), durene (1,2,4,5-tetramethylbenzene) and DTF-NO_2 (1,3-dithiol,4-methyl-5-(methylthio)-2-(4-nitrobenzene) ethylene). In the case of the nitro compounds,[195] they report that k_0 (standard electrochemical rate constant) values are decreased by two orders of magnitude for the fastest redox couples (nitrobenzene derivatives) when the solvent is changed from acetonitrile to RTIL. However, when the inner sphere contribution is more important, such as for the reduction of 2-methyl-2-nitropropane, there is very little variation between the k_0 values in both types of solvent. Such effects need to be taken into account, since some electrochemical processes that are fast in traditional organic solvents may become slow in RTILs, unless they were already slow due to inner sphere reorganisation. The study[196] of electrogenerated organic cation radicals reveals that the identity of the solvent (acetonitrile or RTIL) does not significantly affect the nature of the mechanisms of all species that were investigated. The authors noted a decrease in k_0 values of roughly one order of magnitude from acetonitrile to RTILs, which indicates a higher solvent reorganisation in RTILs during the charge transfer. Electrodimerisation

processes in RTILs were investigated, and it was found that the only other parameter affected in the kinetic analysis was the bimolecular kinetic rate constant. This was attributed to the high degree of ion-association in RTILs, resulting in a specific solvation of the reactants. On the whole, it was suggested that these preliminary experiments showed promise for the use of RTILs as new media for organic electrochemistry.

However, these two studies may not fully take into account both uncompensated resistance or 'ohmic drop' (which takes place in resistive solutions and may distort the voltammogram), and capacitative charging (which can be dominant at very fast scan rates). Since peak-to-peak separations were used to calculate the heterogeneous rate of electron transfer, these factors obviously need to be considered when calculating accurate rate constants. Subsequently, Fietkau *et al.*[197] looked at a series of ferrocene derivatives in $[C_2mim][NTf_2]$ using a high-speed channel electrode system with a microband electrode of width 12.5 μm. The use of such an electrode meant that the problems relating to capacitive currents were avoided, and those related to ohmic drop were minimised. Heterogeneous rate constants, k_0, were measured, and were found to be roughly one order of magnitude lower in the RTIL compared to acetonitrile, and there was no correlation found between the heterogeneous rate constant (k_0) and the hydrodynamic radius (a) in RTILs. Two subsequent studies by Belding *et al.*[198] on arenes and substituted anthracenes, and by Long *et al.*[199] on phenylenediamines in RTILs also found no correlation between k_0 and a. These results indicate that, in line with theoretical work by Lynden-Bell,[200,201] Marcus theory for outer sphere electron transfer does not apply in these solvents. Since Marcus theory is based on the reorganisation of solvent dipoles, it is unsurprising that this is the case in solvents that are made up entirely of ions.

2.6.4 Double Layer Capacitance

Another important property of a solvent in electrochemical experiments is the structure of the double layer at the electrode-solution interface, and its variation with potential, which can affect the rates of electrode processes. This effect cannot be neglected,[78] especially when the concentration of the electroactive species is very low, causing any charging current to be probably larger than the faradaic current for the reduction or oxidation reaction if the voltage is scanned at an appreciable rate. It is also important when considering RTILs for electrochemical capacitor applications.[144,145] There are only a few articles which deal with double layer studies in RTILs,[35,88,144,145] and these indicate that ionic liquids possess double-layer capacitances (C_{dl}) comparable to non-aqueous solvents with supporting electrolyte. For example, both Nanjundiah *et al.*[35] (on a mercury dropping electrode) and Ue *et al.*[88] (on an activated carbon electrode) report C_{dl} values of 15.1 μF cm^{-2} for 0.1 M KCl/H_2O and 14.6 μF cm^{-2} for 3 M H_2SO_4/H_2O, compared to 10.6-12.4 μF cm^{-2} for various $[C_2mim]^+$ ionic liquids close to the potential of zero charge (PZC). Lower C_{dl} values of 5.2-6.9 μF cm^{-2} were reported for $[C_2mim]^+$ and $[C_4mim]^+$ ionic liquids on a carbon electrode surface,[145] which indicates that the accessibility of the electrolyte to the carbon electrode surface limits the specific capacitance recorded. Nanjundiah *et al.*[35] suggest that although there are similarities between RTILs and aqueous systems at potentials close to the PZC, the Stern diffuse double-layer model,[78] usually applied in aqueous electrolyte systems, cannot be used to describe the process in RTILs. Instead, a multi-layer model was proposed, where the excess charge on the RTIL is located several layers deep within multi-layers of alternating positive and negative charge (cations and anions), in agreement with studies carried out in molten salts.[202] Two recent papers by Kornyshev[203,204] have discussed the electrical double layer in ionic liquids in more detail and concluded that the maximum capacitance coincides with the PZC if the molecule is 'symmetric' (similar size of cations and anions), but that the capacitance curve could be much more complicated for non-symmetric

systems.[204] Despite the contrasting behaviour of solutions in RTILs with aqueous solutions, RTILs are still seen as suitable electrolytes in electrochemical double-layer capacitors because of their high specific capacitance, excellent stability and wide electrochemical windows.[35,144,145]

2.7 Summary

This chapter has introduced room temperature ionic liquids as a relatively 'new' class of solvent. Due to their favourable physical properties, they have been found to offer many advantages over their volatile organic counterparts in many areas of research. For example, RTILs have higher densities than water, which can be useful for the extraction of reaction products that remain in different phases. They have high intrinsic conductivities (similar to aprotic solvents with added supporting electrolyte) resulting in a simplified experimental set-up, minimal waste and the possibility to recycle the solvent after an electrochemical reaction. They also have wide electrochemical windows (dictated by the high stability of the cation and anion) and additional voltammetric peaks can now be observed that were otherwise out of the range of traditional solvents. They have a low volatility and high thermal stability, and have found use as reaction media at higher temperatures where they will not evaporate (in contrast to traditional volatile organic solvents). They also have the ability to solubilise a wide range of polar and non-polar species. However, one drawback is the high viscosity of RTILs (typically 2-3 orders of magnitude greater than conventional molecular solvents) resulting in the slowing of diffusion coefficients and voltammetric response times. Other issues include their sensitivity to moisture, and the relatively high amounts of impurities (such as water, air, halide and unreacted starting material) compared to conventional solvents, both resulting in a significant effects on their physical properties and reactivity of species dissolved in RTILs.

The use of RTILs in applications such as green synthesis and catalysis, enzyme catalysis, in electrochemical devices, gas sensing, electrosynthesis and electrodeposition has been discussed.

In many of these fields, RTILs have been shown to be potentially superior over conventional solvents, but several factors need consideration if RTILs are to be used in large-scale commercial processes. For example, the separation of products, reactions *of* RTILs (as opposed to reactions *in* RTILs), high viscosity and slow response times (in amperometic gas sensors), and sensitivity to mositure may limit their widespread use. In addition, their toxicity needs to be extensively assessed and appropriate disposal methods should be developed. Despite these issues, ionic liquids have been successfully employed in several industrial applications,[2] and with the advent of 'edible' ionic liquids based on the choline cation,[24] there is scope for many more environmentally friendly applications.

In terms of their behaviour as electrochemical solvents, the mechanisms of electroactive species in RTILs have been found to be similar to that in conventional solvents. However, the voltammetry is characterised by extremely slow rates of diffusion, and a decrease in the rate of electron transfer kinetics has been consistently observed. It has also been observed that the diffusion coefficients of neutral and charged species can be significantly different (*e.g.* oxygen/superoxide or ferrocene/ferrocenium). It has been found that some solid molecules such as TMPD and ferrocene follow the Stokes-Einstein relation relating diffusion coefficients to the viscosity, but other small molecules (*e.g.* O_2, H_2S and SO_2) do not. It has also been shown that Marcus theory, which applies for most species in aprotic solvents, does not apply for the same species in RTILs. In addition, the electrical double layer in RTILs appears to be more complex than in traditional solvents, and more work is needed to fully understand its effect on the behaviour of species near the electrode surface. As a result of these findings, it may be more appropriate to assume that RTILs do *not* behave in the same way as traditional solvents (*e.g.* acetonitrile), but they should be treated as a completely unique class of solvent until well-established theories are tested.

2.8 Aims of the Work Reported in this Thesis

Most simply put, the work reported in this thesis aims to investigate the electrochemical behaviour of dissolved solid, liquid and gaseous species in ionic liquid media. This will be achieved by employing electrochemical methods such as cyclic voltammetry and potential-step chronoamperometry, and X-ray photoelectron spectroscopy (XPS) as a complementary technique.

The results in this thesis are split up into two main parts. The first half looks at the electrochemical reaction mechanisms of dissolved solid organic and inorganic species, such as bromide, nitro derivatives (nitrobenzene and 4-nitrophenol), sodium and potassium nitrates and nitrates, and nitrogen dioxide gas, and liquid solutes, such as phosphorus trichloride (PCl_3) and phosphorus oxychloride ($POCl_3$). It is also shown that the solubility of bromide in low-volatility RTILs can be successfully be quantified by XPS (a technique usually only applied to solids and gases). All of the work in the first part is undertaken in one chosen RTIL in order to demonstrate the concept that RTILs can successfully be used as an electrolyte medium in which to study a variety of species. Some of the findings are compared to the behaviour observed in conventional aprotic solvents such as acetonitrile. The second half then looks at the properties of the different RTILs themselves, in particular, by studying the behaviour of protons in RTILs with different anions and cations. It will be shown that the RTIL anion, depending on its identity, can have a very strong interaction with the dissolved proton (formed either electrochemically after the oxidation of hydrogen and ammonia gases or from the chemical dissociation of benzoic acid). It will also be demonstrated that RTILs may be favourable media for the amperometric detection of nitrogen dioxide, hydrogen and ammonia in gas sensors.

However, before turning to the results, the next chapter introduces the experimental methods and equipment commonly used throughout this thesis.

References

[1] Silvester, D. S. and Compton, R. G., *Z. Phys. Chem.*, 2006, **220**, 1247–1274.

[2] Plechkova, N. V. and Seddon, K. R., *Chem. Soc. Rev.*, 2008, **37**, 123–150.

[3] Walden, P., *Bull. Acad. Sci. St. Petersburg*, 1914, **1**, 405–422.

[4] Hurley, F. H. and Wier, Jr., T. P., *J. Electrochem. Soc.*, 1951, **98**, 203–206.

[5] Hurley, F. H. and Wier, Jr., T. P., *J. Electrochem. Soc.*, 1951, **98**, 207–212.

[6] Wilkes, J. S.; Levisky, J. A.; Wilson, R. A. and Hussey, C. L., *Inorg. Chem.*, 1982, **21**, 1263–1264.

[7] Fuller, J.; Carlin, R. T.; De Long, H. C. and Haworth, D., *J. Chem. Soc., Chem. Commun.*, 1994, **3**, 299–300.

[8] Welton, T., *Chem. Rev.*, 1999, **99**, 2071–2083.

[9] Buzzeo, M. C.; Evans, R. G. and Compton, R. G., *ChemPhysChem*, 2004, **5**, 1106–1120.

[10] Endres, F. and Zein El Abedin, S., *PhysChemChemPhys*, 2006, **8**, 2101–2116.

[11] Wasserscheid, P. and Keim, W., *Angew. Chem. Int. Ed.*, 2000, **39**, 3772–3789.

[12] Gordon, C. M., *App. Catal. A*, 2001, **222**, 101–117.

[13] Wilkes, J. S., *J. Mol. Catal. A*, 2004, **214**, 11–17.

[14] Earle, M. J. and Seddon, K. R., *Pure Appl. Chem.*, 2000, **72**, 1391–1398.

[15] Dupont, J.; Consorti, C. and Spencer, J., *J. Braz. Chem. Soc.*, 2000, **11**, 337–344.

[16] Zhao, H., *Chem. Eng. Commun.*, 2006, **193**, 1660–1677.

[17] Chiappe, C. and Pieraccini, D., *J. Phys. Org. Chem.*, 2005, **18**, 275–297.

[18] Chowdhury, S.; Mohan, R. S. and Scott, J. L., *Tetrahedron*, 2007, **63**, 2363–2389.

[19] Pandey, S., *Anal. Chim. Acta*, 2006, **556**, 38–45.

[20] Baker, G. A.; Baker, S. N.; Pandey, S. and Bright, F. V., *Analyst*, 2005, **130**, 800–808.

[21] Anderson, J. L.; Armstrong, D. W. and Wei, G., *Anal. Chem.*, 2006, **78**, 2893–2902.

[22] Wei, D. and Ivaska, A., *Anal. Chim. Acta*, 2008, **607**, 126–135.

[23] Sheldon, R. A.; Madeira Lau, R.; Sorgedrager, M. J.; Van Rantwijk, F. and Seddon, K. R., *Green Chem.*, 2002, **4**, 147–151.

[24] van Rantwijk, F. and Sheldon, R. A., *Chem. Rev.*, 2007, **107**, 2757–2785.

[25] Wilkes, J. S. and Zaworotko, M. J., *J. Chem. Soc., Chem. Commun.*, 1992, **1**, 965–967.

[26] Visser, A. E.; Swatloski, R. P.; Reichert, W. M.; Mayton, R.; Sheff, S.; Wierzbicki, A.; Davis J. H., J. and Rogers, R. D., *Chem. Commun.*, 2001, **1**, 135–136.

[27] Davis Jr., J. H., *Chem. Lett.*, 2004, **33**, 1072–1077.

[28] Davis Jr., J. H., *'Synthesis of Task-Specific Ionic Liquids' in Ionic Liquids in Synthesis*, John Wiley and Sons: New York, USA, 2003.

[29] Jork, C.; Kristen, C.; Pieraccini, D.; Stark, A.; Chiappe, C.; Beste, Y. A. and Arlt, W., *J. Chem. Thermodynamics*, 2005, **37**, 537–558.

[30] Visser, A. E.; Swatloski, R. P.; Reichert, W. M.; Mayton, R.; Sheff, S.; Wierzbicki, A.; Davis Jr., J. H. and Rogers, R. D., *Environ. Sci. Technol.*, 2002, **36**, 2523–2529.

[31] Bonhôte, P.; Dias, A.-P.; Papageorgiou, N.; Kalyanasundaram, K. and Grätzel, M., *Inorg. Chem.*, 1996, **35**, 1168–1178.

[32] McEwen, A. B.; Ngo, E. L.; LeCompte, K. and Goldman, J. L., *J. Electrochem. Soc.*, 1999, **146**, 1687–1695.

[33] Forsyth, S.; Golding, J.; MacFarlane, D. R. and Forsyth, M., *Electrochim. Acta*, 2001, **46**, 1753–1757.

[34] Koch, V. R.; Dominey, L. A.; Nanjundiah, C. and Ondrechen, M. J., *J. Electrochem. Soc.*, 1996, **143**, 798–803.

[35] Nanjundiah, C.; McDevitt, S. F. and Koch, V. R., *J. Electrochem. Soc.*, 1997, **144**, 3392–3397.

[36] Dzyuba, S. V. and Bartsch, R. A., *ChemPhysChem*, 2002, **3**, 161–166.

[37] Ignat'ev, N.; Welz-Biermann, U.; Kucheryna, A.; Bissky, G. and Willner, H., *J. Fluorine Chem.*, 2005, **126**, 1150–1159.

[38] Schröder, U.; Wadhawan, J. D.; Compton, R. G.; Marken, F.; Suarez, P. A. Z.; Consorti, C. S.; de Souza, R. F. and Dupont, J., *New J. Chem.*, 2000, **24**, 1009–1015.

[39] Cammarata, L.; Kazarian, S. G.; Salter, P. A. and Welton, T., *PhysChemChemPhys*, 2001, **3**, 5192–5200.

[40] MacFarlane, D. R.; Meakin, P.; Sun, J.; Amini, N. and Forsyth, M., *J. Phys. Chem. B*, 1999, **103**, 4164–4170.

[41] Golding, J.; Forsyth, S.; MacFarlane, D. R.; Forsyth, M. and Deacon, G. B., *Green Chem.*, 2002, **4**, 223–229.

[42] Matsumoto, K.; Hagiwara, R. and Ito, Y., *Electrochem. Solid-State Lett.*, 2004, **7**, E41–E44.

[43] MacFarlane, D. R.; Forsyth, S. A.; Golding, J. and Deacon, G. B., *Green Chem.*, 2002, **4**, 444–448.

[44] Sun, J.; Forsyth, M. and MacFarlane, D. R., *J. Phys. Chem. B*, 1998, **102**, 8858–8864.

[45] Abbott, A. P.; Capper, G.; Davies, D. L. and Rasheed, R., *Inorg. Chem.*, 2004, **43**, 3447–3452.

[46] Hagiwara, R. and Ito, Y., *J. Fluorine Chem.*, 2000, **105**, 221–227.

[47] Matsumoto, H.; Yanagida, M.; Tanimoto, K.; Nomura, M.; Kitagawa, Y. and Miyazaki, Y., *Chem. Lett.*, 2000, **8**, 922–923.

[48] Forsyth, S. A. and MacFarlane, D. R., *J. Mater. Chem.*, 2003, **13**, 2451–2456.

[49] Del Sesto, R. E.; Corley, C.; Robertson, A. and Wilkes, J. S., *J. Organometallic Chem.*, 2005, **690**, 2536–2542.

[50] Hagiwara, R.; Matsumoto, K.; Nakamori, Y.; Tsuda, T.; Ito, Y.; Matsumoto, H. and Momota, K., *J. Electrochem. Soc.*, 2003, **150**, D195–D199.

[51] Aki, S. N. V. K.; Brennecke, J. F. and Samanta, A., *Chem. Commun.*, 2001, **5**, 413–414.

[52] Sun, J.; MacFarlane, D. R. and Forsyth, M., *Solid State Ionics*, 2002, **147**, 333–339.

[53] Matsumoto, H.; Matsuda, T. and Miyazaki, Y., *Chem. Lett.*, 2000, **12**, 1430–1431.

[54] Belieres, J.-P. and Angell, C., *J. Phys. Chem. B*, 2007, **111**, 4926–4937.

[55] Brown, R. J. C.; Dyson, P. J.; Ellis, D. J. and Welton, T., *Chem. Commun.*, 2001, **18**, 1862–1863.

[56] Sun, J.; MacFarlane, D. R. and Forsyth, M., *Electrochim. Acta*, 2003, **48**, 1707–1711.

[57] Leone, A. M.; Weatherly, S. C.; Williams, M. E.; Thorp, H. H. and Murray, R. W., *J. Am. Chem. Soc.*, 2001, **123**, 218–222.

[58] Bates, E. D.; Mayton, R. D.; Ntai, I. and Davis Jr., J. H., *J. Am. Chem. Soc.*, 2002, **124**, 926–927.

[59] Cole, A. C.; Jensen, J. L.; Ntai, I.; Tran, K. L. T.; Weaver, K. J.; Forbes, D. C. and Davis, James H., J., *J. Am. Chem. Soc*, 2002, **124**, 5962–5963.

[60] Yoshizawa, M.; Narita, A. and Ohno, H., *Aust. J. Chem.*, 2004, **57**, 139–144.

[61] Hussey, C. L., *Adv. Molten Salt Chem.*, 1983, **5**, 185–230.

[62] Seddon, K. R., *J. Chem. Technol. Biotechnol.*, 1997, **68**, 351–356.

[63] Olivier, H., *J. Mol. Catal. A*, 1999, **146**, 285–289.

[64] Geetha, S. and Trivedi, D. C., *Bull. Electrochem.*, 2003, **19**, 37–48.

[65] Lee, S.-G., *Chem. Commun.*, 2006, **10**, 1049–1063.

[66] Ohno, H., *Bull. Chem. Soc. Japan*, 2006, **79**, 1665–1680.

[67] Xue, H.; Verma, R. and Shreeve, J. M., *J. Fluorine Chem.*, 2006, **127**, 159–176.

[68] Weingartner, H.; Sasisanker, P.; Daguenet, C.; Dyson, P.; Krossing, I.; Slattery, J. and Schubert, T., *J. Phys. Chem. B*, 2007, **111**, 4775–4780.

[69] Wang, J.; Tian, Y.; Zhao, Y. and Zhuo, K., *Green Chem.*, 2003, **5**, 618–622.

[70] Obtained from http : //ildb.merck.de/ionicliquids/en/startpage.htm, the official merck ionic liquids website.

[71] Okoturo, O. O. and VanderNoot, T. J., *J. Electroanal. Chem.*, 2004, **568**, 167–181.

[72] Wang, Y.; Zaghib, K.; Guerfi, A.; Bazito, F. F.; Torresi, R. M. and Dahn, J., *Electrochim. Acta*, 2007, **52**, 6346–6352.

[73] Seddon, K. R.; Stark, A. and Torres, M.-J., *ACS Symp. Ser.*, 2002, **819**, 34–39.

[74] Olivier-Bourbigou, H. and Magna, L., *J. Mol. Catal. A*, 2002, **182183**, 419–437.

[75] MacFarlane, D. R.; Sun, J.; Golding, J.; Meakin, P. and Forsyth, M., *Electrochim. Acta*, 2000, **45**, 1271–1278.

[76] Huddleston, J. G.; Visser, A. E.; Reichert, W. M.; Willauer, H. D.; Broker, G. A. and Rogers, R. D., *Green Chem.*, 2001, **3**, 156–164.

[77] Lide, D. R., Ed., *Handbook of Chemistry and Physics: 76th Edition*, CRC Press, Boca Raton, USA, 1996.

[78] Bard, A. J. and Faulkner, L. R., *Electrochemical Methods: Fundamentals and Applications, 2nd ed.*, John Wiley and Sons: New York, USA, 2001.

[79] Xu, W.; Wang, L. M.; Nieman, R. A. and Angell, C. A., *J. Phys. Chem. B*, 2003, **107**, 11749–11756.

[80] Vogel, H., *Physik. Z.*, 1921, **22**, 645–646.

[81] Tammann, G. and Veszi, G., *Z. Anorg. Allgem. Chem.*, 1926, **150**, 355–380.

[82] Fulcher, G. S., *J. Am. Ceram. Soc.*, 1925, **8**, 339–355.

[83] Jacquemin, J.; Husson, P.; Padua, A. A. H. and Majer, V., *Green Chem.*, 2006, **8**, 172–180.

[84] Gu, Z. and Brennecke, J. F., *J. Chem. Eng. Data*, 2002, **47**, 339–345.

[85] Fredlake, C. P.; Crosthwaite, J. M.; Hert, D. G.; Aki, S. N. and Brennecke, J. F., *J. Chem. Eng. Data*, 2004, **49**, 954–964.

[86] Vila, J.; Gines, P.; Pico, J. M.; Franjo, C.; Jimenez, E.; Varela, L. M. and Cabeza, O., *Fluid Phase Equilib.*, 2006, **242**, 141–146.

[87] Vila, J.; Varela, L. M. and Cabeza, O., *Electrochim. Acta*, 2007, **52**, 7413–7417.

[88] Ue, M.; Takeda, M.; Toriumi, A.; Kominato, A.; Hagiwara, R. and Ito, Y., *J. Electrochem. Soc.*, 2003, **150**, A499–A502.

[89] Endres, F., *ChemPhysChem*, 2002, **3**, 144–154.

[90] Kroon, M. C.; Buijs, W.; Peters, C. J. and Witkamp, G. J., *Green Chem.*, 2006, **8**, 241–245.

[91] Sukardi, S. K.; Zhang, J.; Burgar, I.; Horne, M. D.; Hollenkamp, A. F.; MacFarlane, D. R. and Bond, A. M., *Electrochem. Commun.*, 2008, **10**, 250–254.

[92] Rogers, E. I.; Silvester, D. S.; Poole, D. L.; Aldous, L.; Hardacre, C. and Compton, R. G., *J. Phys. Chem. C*, 2008, **112**, 2729–2735.

[93] Donato, R. K.; Migliorini, M. V.; Benvegnu, M. A.; Dupont, J.; Goncalves, R. S. and Schrekker, H. S., *J. Solid State Electrochem.*, 2007, **11**, 1481–1487.

[94] Buzzeo, M. C.; Hardacre, C. and Compton, R. G., *ChemPhysChem*, 2006, **7**, 176–180.

[95] Ngo, H. L.; LeCompte, K.; Hargens, L. and McEwen, A. B., *Thermochim. Acta*, 2000, **357-358**, 97–102.

[96] Kosmulski, M.; Gustafsson, J. and Rosenholm, J. B., *Thermochim. Acta*, 2004, **412**, 47–53.

[97] Deetlefs, M. and Seddon, K. R., *Chimica Oggi*, 2006, **24**, 16–23.

[98] Reichardt, C., *Green Chem.*, 2005, **7**, 339–351.

[99] Carmichael, A. J. and Seddon, K. R., *J. Phys. Org. Chem.*, 2000, **13**, 591–595.

[100] Kawai, A.; Hidemori, T. and Shibuya, K., *Chem. Lett.*, 2004, **33**, 1464–1465.

[101] Köddermann, T.; Wertz, C.; Heintz, A. and Ludwig, R., *Angew. Chem. Int. Ed.*, 2006, **45**, 3697–3702.

[102] Tao, G. H.; Zou, M.; Wang, X. H.; Chen, Z. Y.; Evans, D. G. and Kou, Y., *Aust. J. Chem.*, 2005, **58**, 327–331.

[103] Wakai, C.; Oleinikova, A.; Ott, M. and Weingärtner, H., *J. Phys. Chem. B*, 2005, **109**, 17028–17030.

[104] Blanchard, L. A. and Brennecke, J. F., *Ind. Eng. Chem. Res.*, 2001, **40**, 287–292.

[105] Freire, M. G.; Santos, L. M.; Fernandes, A. M.; Coutinho, J. A. P. and Marrucho, I. M., *Fluid Phase Equilib.*, 2007, **261**, 449–454.

[106] Freire, M. G.; Carvalho, P. J.; Gardas, R. L.; Marrucho, I. M.; Santos, L. M. and Coutinho, J. A. P., *J. Phys. Chem. B*, 2008, **112**, 1604–1610.

[107] Zhao, D.; Wu, M.; Kou, Y. and Min, E., *Catal. Today*, 2002, **74**, 157–189.

[108] Liu, Q.; Janssen, M. H. A.; Van Rantwijk, F. and Sheldon, R. A., *Green Chem.*, 2005, **7**, 39–42.

[109] Zhao, G.; Jiang, T.; Gao, H.; Han, B.; Huang, J. and Sun, D., *Green Chem.*, 2004, **6**, 75–77.

[110] Anderson, J. A.; Dixon, J. K.; Maginn, E. J. and Brennecke, J. F., *J. Phys. Chem. B*, 2006, **110**, 15059–15062.

[111] Cadena, C.; Anthony, J.; Shah, J.; Morrow, T.; Brennecke, J. and Maginn, E., *J. Am. Chem. Soc.*, 2004, **126**, 5300–5308.

[112] Widegren, J. A.; Laesecke, A. and Magee, J. W., *Chem. Commun.*, 2005, **12**, 1610–1612.

[113] Widegren, J. A.; Saurer, E. M.; Marsh, K. N. and Magee, J. W., *J. Chem. Thermodynamics*, 2005, **37**, 569–575.

[114] O'Mahony, A. M.; Silvester, D. S.; Aldous, L.; Hardacre, C. and Compton, R. G., *J. Chem. Eng. Data*, 2008, page In press.

[115] Seddon, K. R.; Stark, A. and Torres, M.-J., *Pure Appl. Chem.*, 2000, **72**, 2275–2287.

[116] Kavanoz, M.; Gülce, H. and Yildiz, A., *Turk. J. Chem.*, 2004, **28**, 287–297.

[117] Aldous, L.; Silvester, D. S.; Villagrán, C.; Pitner, W. R.; Compton, R. G.; Lagunas, M. C. and Hardacre, C., *New J. Chem.*, 2006, **30**, 1576–1583.

[118] Gallo, V.; Mastrorilli, P.; Nobile, C. F.; Romanazzi, G. and Suranna, G. P., *J. Chem. Soc.*, 2002, **23**, 4339–4342.

[119] Suarez, P. A. Z.; Dullius, J. E. L.; Einloft, S.; de Souza, R. F. and Dupont, J., *Inorg. Chim. Acta*, 1997, **255**, 207–209.

[120] Dyson, P. J.; Ellis, D. J.; Welton, T. and Parker, D. G., *Chem. Commun.*, 1999, **1**, 25–26.

[121] Villagrán, C.; Deetlefs, M.; Pitner, W. R. and Hardacre, C., *Anal. Chem.*, 2004, **76**, 2118–2123.

[122] Hao, F.; Haddad, P. R. and Ruther, T., *Chromatographia*, 2008, **67**, 495–498.

[123] Berthier, D.; Varenne, A.; Gareil, P.; Digne, M.; Lienemann, C.-P.; Magna, L. and Olivier-Bourbigou, H., *Analyst*, 2004, **129**, 1257–1261.

[124] Villagrán, C.; Banks, C. E.; Hardacre, C. and Compton, R. G., *Anal. Chem.*, 2004, **76**, 1998–2003.

[125] Farmer, V. and Welton, T., *Green Chem.*, 2002, **4**, 97–102.

[126] Earle, M. J.; Gordon, C. M.; Plechkova, N. V.; Seddon, K. R. and Welton, T., *Anal. Chem.*, 2007, **79**, 758–764.

[127] Scammells, P. J.; Scott, J. L. and Singer, R. D., *Aust. J. Chem.*, 2005, **58**, 155–169.

[128] Swatloski, R. P.; Holbrey, J. D. and Rogers, R. D., *Green Chem.*, 2003, **5**, 361–363.

[129] Meracz, I. and Oh, T., *Tetrahedron Lett.*, 2003, **44**, 6465–6468.

[130] Carmichael, A. J.; Earle, M. J.; Holbrey, J. D.; McCormac, P. B. and Seddon, K. R., *Org. Lett.*, 1999, **1**, 997–1000.

[131] Gmouh, S.; Yang, H. and Vaultier, M., *Org. Lett.*, 2003, **5**, 2219–2222.

[132] Kragl, U.; Eckstein, M. and Kaftzik, N., *Curr. Opin. Biotechnol.*, 2002, **13**, 565–571.

[133] Park, S. and Kazlauskas, R. J., *Curr. Opin. Biotechnol.*, 2003, **14**, 432–437.

[134] Song, C. E., *Chem. Commun.*, 2004, **9**, 1033–1043.

[135] Yang, Z. and Pan, W., *Enzyme and Microbial Technol.*, 2005, **37**, 19–28.

[136] Fujita, K.; Forsyth, M.; MacFarlane, D. R.; Reid, R. W. and Elliott, G. D., *Biotechnol. Bioeng.*, 2006, **94**, 1209–1213.

[137] Kaar, J. L.; Jesionowski, A. M.; Berberich, J. A.; Moulton, R. and Russell, A. J., *J. Am. Chem. Soc.*, 2003, **125**, 4125–4131.

[138] Hough, W. L.; Smiglak, M.; Rodriguez, H.; Swatloski, R. P.; Spear, S. K.; Daly, D. T.; Pernak, J.; Grisel, J. E.; Carliss, R. D.; Soutullo, M. D.; Davis Jr., J. H. and Rogers, R. D., *New J. Chem.*, 2007, **31**, 1429–1436.

[139] Jaitely, V.; Karatas, A. and Florence, A. T., *Int. J. Pharm.*, 2008, **354**, 168–173.

[140] Macfarlane, D. R.; Forsyth, M.; Howlett, P. C.; Pringle, J. M.; Sun, J.; Annat, G.; Neil, W. and Izgorodina, E. I., *Acc. Chem. Res.*, 2007, **40**, 1165–1173.

[141] Lu, W.; Fadeev, A. G.; Qi, B.; Smela, E.; Mattes, B. R.; Ding, J.; Spinks, G. M.; Mazurkiewicz, J.; Zhou, D.; Wallace, G. G.; MacFarlane, D. R.; Forsyth, S. A. and Forsyth, M., *Science*, 2002, **297**, 983–987.

[142] Lu, W.; Fadeev, A. G.; Qi, B. and Mattes, B. R., *Synth. Met.*, 2003, **135-136**, 139–140.

[143] Lu, W.; Norris, I. D. and Mattes, B. R., *Aust. J. Chem.*, 2005, **58**, 263–269.

[144] McEwen, A. B.; McDevitt, S. F. and Koch, V. R., *J. Electrochem. Soc.*, 1997, **144**, L84–L86.

[145] Lewandowski, A. and Galinski, M., *J. Phys. Chem. Solids*, 2004, **65**, 281–286.

[146] Sato, T.; Masuda, G. and Takagi, K., *Electrochim. Acta*, 2004, **49**, 3603–3611.

[147] Frackowiak, E.; Lota, G. and Pernak, J., *App. Phys. Lett.*, 2005, **86**, 1–3.

[148] Papageorgiou, N.; Athanassov, Y.; Armand, M.; Bonhote, P.; Pettersson, H.; Azam, A. and Gratzel, M., *J. Electrochem. Soc.*, 1996, **143**, 3099–3108.

[149] Wang, P.; Zakeeruddin, S. M.; Moser, J.-E. and Grätzel, M., *J. Phys. Chem. B*, 2003, **107**, 13280–13285.

[150] Wang, P.; Zakeeruddin, S. M.; Moser, J. E.; Humphry-Baker, R. and Grätzel, M., *J. Am. Chem. Soc.*, 2004, **126**, 7164–7165.

[151] Kawano, R. and Watanabe, M., *Chem. Commun.*, 2005, **16**, 2107–2109.

[152] Xu, K., *Chem. Rev.*, 2004, **104**, 4303–4417.

[153] de Souza, R. F.; Padilha, J. C.; Goncalves, R. S. and Dupont, J., *Electrochem. Commun.*, 2003, **5**, 728–731.

[154] Gajar, S. A. and Geis, M. W., *J. Electrochem. Soc.*, 1992, **139**, 2833–2840.

[155] Yang, C.; Sun, Q.; Qiao, T. and Li, Y., *J. Phys. Chem. B*, 2003, **107**, 12981–12988.

[156] Shao, Y.; Bazan, G. C. and Heeger, A. J., *Adv. Mat.*, 2007, **19**, 365–370.

[157] Matsumoto, H.; Matsuda, T.; Tsuda, T.; Hagiwara, R.; Ito, Y. and Miyazaki, Y., *Chem. Lett.*, 2001, **30**, 1430–1431.

[158] Buzzeo, M. C.; Klymenko, O. V.; Wadhawan, J. D.; Hardacre, C.; Seddon, K. R. and Compton, R. G., *J. Phys. Chem. A*, 2003, **107**, 8872–8878.

[159] Evans, R. G.; Klymenko, O. V.; Saddoughi, S. A.; Hardacre, C. and Compton, R. G., *J. Phys. Chem. B*, 2004, **108**, 7878–7886.

[160] Wadhawan, J. D.; Welford, P. J.; McPeak, H. B.; Hahn, C. E. W. and Compton, R. G., *Sens. Act. B*, 2003, **B88**, 40–52.

[161] Buzzeo, M. C.; Klymenko, O. V.; Wadhawan, J. D.; Hardacre, C.; Seddon, K. R. and Compton, R. G., *J. Phys. Chem. B*, 2004, **108**, 3947–3954.

[162] Giovanelli, D.; Buzzeo, M. C.; Lawrence, N. S.; Hardacre, C.; Seddon, K. R. and Compton, R. G., *Talanta*, 2004, **62**, 904–911.

[163] Buzzeo, M. C.; Giovanelli, D.; Lawrence, N. S.; Hardacre, C.; Seddon, K. R. and Compton, R. G., *Electroanalysis*, 2004, **16**, 888–896.

[164] O'Mahony, A. M.; Silvester, D. S.; Aldous, L.; Hardacre, C. and Compton, R. G., *J. Phys. Chem. C*, 2008, **112**, 7725–7730.

[165] Barrosse-Antle, L.; Silvester, D. S.; Aldous, L.; Hardacre, C. and Compton, R. G., *J. Phys. Chem. B*, 2008, **112**, 3398–3404.

[166] Buzzeo, M. C.; Hardacre, C. and Compton, R. G., *Anal. Chem.*, 2004, **76**, 4583–4588.

[167] Anthony, J. L.; Maginn, E. J. and Brennecke, J. F., *J. Phys. Chem. B*, 2002, **106**, 7315–7320.

[168] Silvester, D. S.; Ward, K. R.; Aldous, L.; Hardacre, C. and Compton, R. G., *J. Electroanal. Chem.*, 2008, **818**, 53–60.

[169] Rogers, E. I. and Compton, R. G., Manuscript in preparation, 2008.

[170] Barrette Jr., W. C. and Sawyer, D. T., *Anal. Chem.*, 1984, **56**, 653–657.

[171] Kuranov, G.; Rumpf, B.; Smirnova, N. and Maurer, G., *Ind. Eng. Chem. Res.*, 1996, **35**, 1959–1966.

[172] Douabul, A. and Riley, J., *J. Chem. Eng. Data*, 1979, **24**, 274–276.

[173] Allen, G. D.; Buzzeo, M. C.; Villagrán, C.; Hardacre, C. and Compton, R. G., *J. Electroanal. Chem.*, 2005, **575**, 311–320.

[174] Iwasita, T. and Giordano, M. C., *Electrochim. Acta*, 1969, **14**, 1045–1059.

[175] Magno, F.; Mazzocchin, G. A. and Bontempelli, G., *J. Electroanal. Chem. Interfacial Electrochem.*, 1973, **47**, 461–468.

[176] Allen, G. D.; Buzzeo, M. C.; Davies, I. G.; Villagrán, C.; Hardacre, C. and Compton, R. G., *J. Phys. Chem. B*, 2004, **108**, 16322–16327.

[177] Yang, H.; Gu, Y.; Deng, Y. and Shi, F., *Chem. Commun.*, 2002, **3**, 274–275.

[178] Lagrost, C.; Hapiot, P. and Vaultier, M., *Green Chem.*, 2005, **7**, 468–474.

[179] Earle, M. J.; Esperanca, J. M.; Gilea, M. A.; Canongia Lopes, J. N.; Rebelo, L. P.; Magee, J. W.; Seddon, K. R. and Widegren, J. A., *Nature*, 2006, **439**, 831–834.

[180] Endres, F.; Bukowski, M.; Hempelmann, R. and Natter, H., *Angew. Chem. Int. Ed.*, 2003, **42**, 3428–3430.

[181] Abbott, A. P. and McKenzie, K. J., *PhysChemChemPhys*, 2006, **8**, 4265–4279.

[182] Endres, F.; MacFarlane, D. and Abbot, A., *Electrodeposition from Ionic Liquids*, Wiley, Weinheim, Germany, 2008.

[183] Vasudeva Rao, P. R.; Venkatesan, K. A. and Srinivasan, T. G., *Prog. Nucl. Energy*, 2008, **50**, 449–455.

[184] Hsiu, S. I. and Sun, I. W., *J. Appl. Electrochem.*, 2004, **34**, 1057–1063.

[185] Newman, P. J. and MacFarlane, D. R., *Z. Phys. Chem.*, 2006, **220**, 1473–1481.

[186] Silvester, D. S. and Compton, R. G., Manuscript in preparation, 2008.

[187] Aldous, L.; Silvester, D. S.; Pitner, W. R.; Compton, R. G.; Lagunas, M. C. and Hardacre, C., *J. Phys. Chem. C*, 2007, **111**, 8496–8503.

[188] Boxall, D. L.; O'Dea, J. J. and Osteryoung, R. A., *J. Electrochem. Soc.*, 2002, **149**, E468–E471.

[189] Compton, R. G. and Banks, C. E., *Understanding Voltammetry*, World Scientific, Singapore, 2007.

[190] Evans, R. G.; Klymenko, O. V.; Price, P. D.; Davies, S. G.; Hardacre, C. and Compton, R. G., *ChemPhysChem*, 2005, **6**, 526–533.

[191] Rogers, E. I.; Silvester, D. S.; Jones, S. E. W.; Aldous, L.; Hardacre, C.; Russell, A. J.; Davies, S. G. and Compton, R. G., *J. Phys. Chem. C*, 2007, **111**, 13957–13966.

[192] Klymenko, O. V.; Evans, R. G.; Hardacre, C.; Svir, I. B. and Compton, R. G., *J. Electroanal. Chem.*, 2004, **571**, 211–221.

[193] Moharram, Y. I., *J. Electroanal. Chem.*, 2006, **587**, 115–126.

[194] Tsierkezos, N. G., *J. Mol. Liquids*, 2008, **138**, 1–8.

[195] Lagrost, C.; Preda, L.; Volanschi, E. and Hapiot, P., *J. Electroanal. Chem.*, 2005, **585**, 1–7.

[196] Lagrost, C.; Carrié, D.; Vaultier, M. and Hapiot, P., *J. Phys. Chem. A*, 2003, **107**, 745–752.

[197] Fietkau, N.; Clegg, A. D.; Evans, R. G.; Villagrán, C.; Hardacre, C. and Compton, R. G., *ChemPhysChem*, 2006, **7**, 1041–1045.

[198] Belding, S. R.; Rees, N. V.; Aldous, L.; Hardacre, C. and Compton, R. G., *J. Phys. Chem. C*, 2008, **112**, 1650–1657.

[199] Long, J. S.; Silvester, D. S.; Barnes, A. S.; Rees, N.; Aldous, L.; Hardacre, C. and Compton, R., *J. Phys. Chem. C*, 2008, **112**, 6993–6700.

[200] Lynden-Bell, R. M., *Electrochem. Commun.*, 2007, **9**, 1857–1861.

[201] Lynden-Bell, R. M., *J. Phys. Chem. B*, 2007, **111**, 10800–10806.

[202] Graves, A. D. and Inman, D., *J. Electroanal. Chem. Interfacial Electrochem.*, 1970, **25**, 357–372.

[203] Kornyshev, A. A., *J. Phys. Chem. B*, 2007, **111**, 5545–5557.

[204] Fedorov, M. V. and Kornyshev, A. A., *Electrochim. Acta*, 2008, **53**, 6835–6840.

Chapter 3

General Experimental Methods

This chapter presents general experimental details and methods for the various investigations reported in this thesis. Descriptions of any apparatus or experimental procedures that are specific to an individual study will be given in the relevant results chapter.

3.1 Chemical Reagents

All chemicals used throughout this thesis are listed in Table 3.1, and were used as received, without further purification. In addition, 4-nitrophenolate (sodium salt) and 4-nitrosophenol were dried under vacuum for 48 hours prior to use. PCl_3 and $POCl_3$ were kept under a constant stream of dried nitrogen, and $HNTf_2$ was kept under an argon atmosphere during and after use.

As ionic liquids have only recently entered the mainstream chemical manufacturing industries, many of the ionic liquids used in this work have been synthesized and purified 'in-house'. This has been achieved by a collaboration with the group of Professor Christopher Hardacre at the School of Chemistry and Chemical Engineering (QUILL, Queen's University Belfast);[1] the majority of preparations being performed by Leigh Aldous. Table 3.2 lists all ionic liquids used throughout this thesis, and a reference to the literature method followed in their synthesis. In most cases, the synthetic methods reported (shown in more detail in Chapter 2, Section 2.2.2) often introduce halide impurities into the ionic liquid. The water insoluble bis(trifluoromethylsulfonyl)imide RTILs can then be purified by repeated aqueous extraction, leaving halide contents of less than 100 ppm.

Most of the syntheses follow the literature methods closely. However, the synthesis of $[C_4mim][NO_3]$ was adapted from a previously published procedure.[4] $AgNO_3$ (5.36 g, 0.032 M) and $[C_4mim]Cl$ (5.00 g, 0.029 M) were dissolved separately in minimum amounts of ultrapure

Table 3.1: All purchased chemicals used in performing the experiments reported within this thesis, along with their purity and commercial source.

Name	Formula /Abbreviation	Supplier	Purity
Ferrocene	$Fe(C_5H_5)_2$ / Fc	Aldrich	98 %
Tetra-*n*-butylammonium perchlorate	TBAP	Aldrich	>99 %
Acetonitrile	MeCN	Fisher Sci.	>99.99 %
4-nitrophenol	$HOPhNO_2$	Aldrich	98 %
Nitrobenzene	$PhNO_2$	Aldrich	97 %
4-nitroanisole	$H_3COPhNO_2$	Aldrich	99 %
4-nitrotoluene	H_3CPhNO_2	Aldrich	99 %
Nitrosobenzene	PhNO	Aldrich	97 %
4-nitrophenolate (sodium salt)	$^-OPhNO_2\ Na^+$	Aldrich	20-30 % H_2O
4-nitrosophenol	HOPhNO	Aldrich	40 % H_2O
Cobaltocenium hexafluorophosphate	$Co(C_5H_5)_2PF_6$ / Cc^+	Acros Org.	98 %
Phosphorus trichloride	PCl_3	Aldrich	99.999 %
Phosphorus oxychloride	$POCl_3$	Aldrich	99 %
Sodium nitrate	$NaNO_3$	Aldrich	>99 %
Potassium nitrate	KNO_3	Aldrich	>99 %
Sodium nitrite	$NaNO_2$	Aldrich	≥97 %
Potassium nitrite	KNO_2	Aldrich	≥96 %
Sodium oxide	Na_2O	Aldrich	80 %
Sodium peroxide	Na_2O_2	Aldrich	97 %
Nitronium tetrafluoroborate	NO_2BF_4	Aldrich	>95 %
Bis(trifluoromethylsulfonyl)imide	$HNTf_2$	Fluka	>95 %
Ammonium nitrate	NH_4NO_3	BDH	98 %
Ammonium hexafluorophosphate	NH_4PF_6	Aldrich	>95 %
Benzoic acid	$PhCO_2H$ / BZA	BDH	99.5 %
4-methoxy benzoic acid	$MeOPhCO_2H$	Acros Org.	98 %
4-chloro benzoic acid	$BrPhCO_2H$	Aldrich	98 %
4-dimethylamino benzoic acid	Me_2NPhCO_2H	Aldrich	99 %
4-diethylamino benzoic acid	Et_2NPhCO_2H	Aldrich	99 %
Nitrogen	N_2	BOC gases	99.99 %
Hydrogen	H_2	BOC gases	99.995 %
Ammonia	NH_3	BOC gases	10 % (90% N_2)
Nitrogen dioxide	NO_2	Argo Int.	99.5 %
Argon	Ar	BOC gases	99.99 %

Table 3.2: The room temperature ionic liquids used in this thesis and a reference to the literature procedure employed in their synthesis.

Chemical Name	Formula	Reference
1-Ethyl-3-methylimidazolium bis(trifluoromethylsulfonyl)imide	$[C_2mim][NTf_2]$	Bonhôte *et al.*[2]
1-Butyl-3-methylimidazolium bis(trifluoromethylsulfonyl)imide	$[C_4mim][NTf_2]$	Bonhôte *et al.*[2]
1-Butyl-3-methylimidazolium chloride	$[C_4mim]Cl$	Bonhôte *et al.*[2]
1-Butyl-2,3-dimethylimidazolium bis(trifluoromethylsulfonyl)imide	$[C_4dmim][NTf_2]$	Bonhôte *et al.*[2]
N-Butyl-*N*-methylpyrrolidinium bis(trifluoromethylsulfonyl)imide	$[C_4mpyrr][NTf_2]$	MacFarlane *et al.*[3]
N-Butyl-*N*-methylpyrrolidinium chloride	$[C_4mpyrr]Cl$	MacFarlane *et al.*[3]
N-Butyl-*N*-methylpyrrolidinium bromide	$[C_4mpyrr]Br$	MacFarlane *et al.*[3]
1-Butyl-3-methylimidazolium tetrafluoroborate	$[C_4mim][BF_4]$	donated by Merck KGaA
1-Butyl-3-methylimidazolium trifluoromethylsulfonate	$[C_4mim][OTf]$	donated by Merck KGaA
1-Butyl-3-methylimidazolium hexafluorophosphate	$[C_4mim][PF_6]$	donated by Merck KGaA
1-Butyl-3-methylimidazolium nitrate	$[C_4mim][NO_3]$	Cammarata *et al.*[4]
1-Hexyl-3-methylimidazolium tris(pentafluoroethyl)trifluorophosphate	$[C_6mim][FAP]$	Ignat'ev *et al.*[5]
1-Hexyl-3-methylimidazolium chloride	$[C_6mim]Cl$	Bonhôte *et al.*[2]
N-Hexyltriethylammonium bis(trifluoromethylsulfonyl)imide	$[N_{6,2,2,2}][NTf_2]$	Bonhôte *et al.*[2]
Tris(*P*-hexyl)tetradecylphosphonium bis(trifluoromethylsulfonyl)imide	$[P_{14,6,6,6}][NTf_2]$	donated by Merck KGaA

water. The [C_4mim]Cl solution was then slowly added to the stirred $AgNO_3$ solution. After stirring overnight the solution was filtered to remove the AgCl precipitate, the water removed and the liquid dried under high vacuum at 343 K overnight. The ionic liquid was then dissolved in 400 mL dry methanol, small amounts of activated charcoal and acidic alumina were added as seeds for the remaining AgCl, and the solution left overnight in a freezer. This solution was then filtered and the process repeated. The methanol was removed, and the ionic liquid was dried under high vacuum conditions.

Four of the ionic liquids listed in Table 3.2 were kindly donated by Merck KGaA. [C_4mim][BF_4], [C_4mim][PF_6] and [$P_{14,6,6,6}$][NTf_2] were used as received. [C_4mim][OTf] was first diluted with CH_2Cl_2 and passed through a column consisting of alternating layers of neutral aluminium oxide and silica gel in order to remove residual acidic impurities. All ionic liquids were further dried for 24 hours under vacuum at 343 K to remove any residual atmospheric impurities.

3.2 Electrodes and Potentiostat

All electrochemical experiments reported in this thesis employed either platinum microelectrodes (of diameter 2, 10 and 100 μm), platinum macroelectrodes (0.5 mm and 6 mm diameter) or gold microelectrodes (of diameter 5, 10 and 25μm). The microdisk electrodes from 2-100 μm in diameter were purchased from Cypress Systems (ESA Biosciences). The macroelectrodes were either purchased (0.5 mm diameter Pt electrode from BAS technicol) or constructed in house (6 mm diameter Pt electrode). All microdisk and macrodisk working electrodes were polished on soft lapping pads (Buehler, Illinois) with an alumina slurry of decreasing size; 1.0 μm and 0.3 μm for the 2, 5, 10 μm, 0.5 mm and 6 mm diameter electrodes, and 9.5 μm, 4.5 μm, 1.0 μm and 0.3 μm for the 25 and 100 μm diameter electrodes. The steady-state voltammetry of a 2 mM solution of ferrocene in acetonitrile containing 0.1 M TBAP was used to calculate the exact electrode diameter of all the microdisk electrodes, adopting a value for the diffusion coefficient

of 2.3×10^{-9} m^2 s^{-1} at 298 K.[6]

In most experiments using a microdisk electrode, a 0.5 mm diameter Ag quasi-reference electrode (Goodfellow Cambridge Limited, UK) was used in a simple two-electrode arrangement. However, in some cases, a Ag/Ag^+ reference electrode was used, with a platinum coil wire (Goodfellow Cambridge Limited, UK) counter electrode. The reference electrode consisted of a 0.5 mm diameter silver wire immersed in a glass tube containing 0.01 M $AgNO_3$ in $[C_4mim][NO_3]$ ionic liquid, separated from the bulk solution by a Vycor plug. Experiments involving the 6 mm and 0.5 mm diameter Pt electrodes were performed in a three-electrode arrangement, with the nature of reference and counter electrodes given in the relevant results sections. All electrochemical experiments were performed using a computer-controlled μ-Autolab potentiostat (Eco-Chemie, Netherlands).

3.3 Apparatus

Routine electrochemical experiments using microdisk electrodes were performed in a 'T-cell', shown in Figure 3.1. The cell was specially designed[7] to maintain the sample within a controlled atmosphere, and has proven effective in removing atmospheric impurities which otherwise appear in the electrochemical window of a blank RTIL solvent which has been exposed to air.[8,9] Throughout the course of this work, the cell has been adapted slightly to fit 0.25 inch diameter PTFE tubing, required for the inlet and outlet pipes of highly toxic gases NO_2 and NH_3. The adaption involved attaching a small piece of 0.25 inch glass tubing to both horizontal arms of the cell, allowing connection of the PTFE tubing *via* a metal cajon fitting. As seen in Figure 3.1, the working and reference electrodes are slot into the bottom and top of the cell to complete a two-electrode electrochemical circuit.

The microdisk working electrode is modified with a section of disposable micropipette tip, into which microlitre quantities (typically 20–80 μL) of the blank RTIL solvent can be placed.

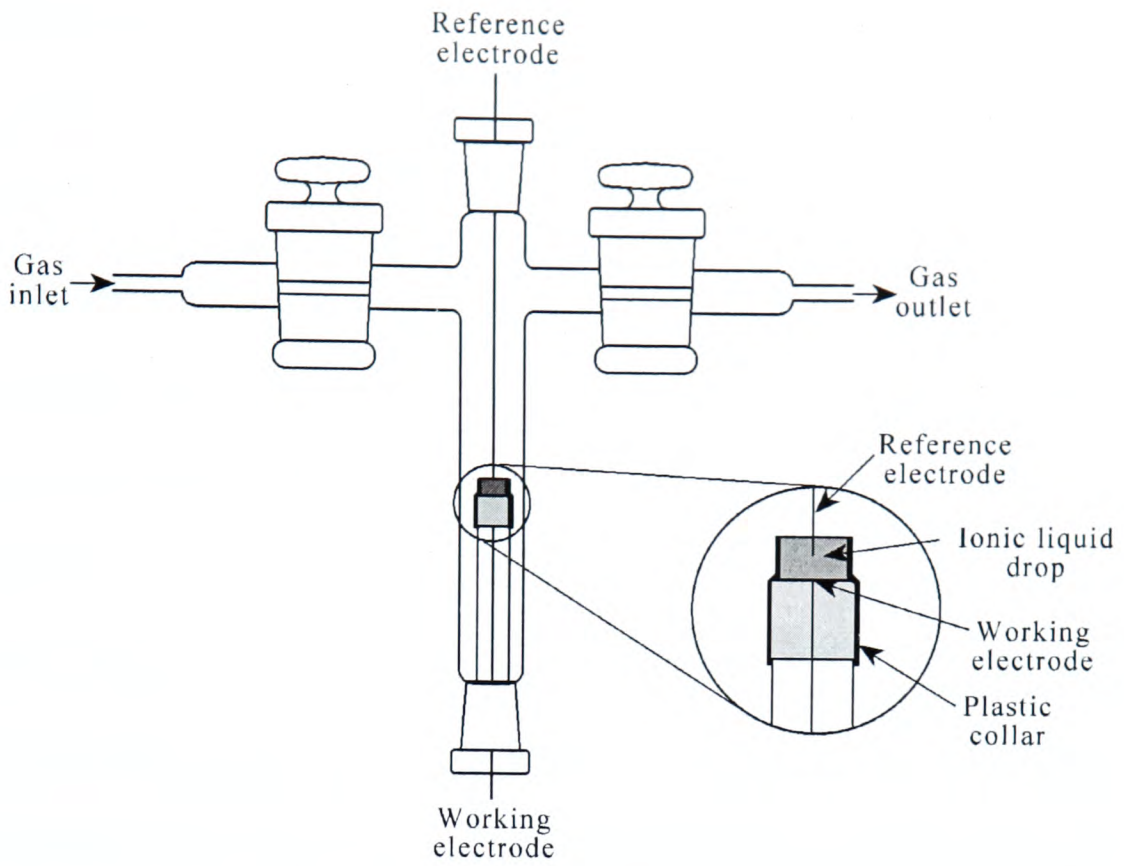

Figure 3.1: A cross section of the glass cell used to conduct electrochemical experiments on 20–80 μL samples of RTILs under conditions of controlled atmosphere.

For experiments involving the sensing of H_2, NO_2 and NH_3 gases, 20 μL of the RTIL solvent was purged under vacuum (Edwards High Vacuum Pump, Model ES 50, 0.05 Torr) for *ca.* 90 minutes, after which gas was introduced through one arm of the cell. An outlet gas line led from the cell into a fume cupboard. Before voltammetric scans were undertaken, the ionic liquid was saturated with gas (typically for 10–15 minutes for H_2, 20 minutes for NO_2 and 30 minutes for NH_3) as evidenced by stable maximum peak currents. For most other experiments, a 'solvent evaporation' procedure was used. Here, a stock solution was first made-up in acetonitrile to a known concentration (typically 10 or 20 mM). Small amounts of the stock solution could then be pipetted into the cell containing 20–80 μL blank RTIL. The acetonitrile is then evaporated, by purging first with N_2, then with vacuum, to leave the desired concentration of electroactive species in the RTIL. The preparation of other solutions are better placed and will be given in the relevant results chapters.

Two types of three-electrode cells were used for experiments involving the larger 100 μm,

0.5 mm and 6 mm diameter Pt electrodes and for the microdisk electrode experiments employing the Ag/Ag^+ reference electrode. The first cell was specially designed for volumes from 1–5 mL, to be used directly after removal from the vacuum/Schlenk-line. This consisted of a glass vial with a B 24 (24/29) vacuum connector, topped with a 15 mm thick cylinder of PTFE with four holes of specific diameter (three for the electrodes and one for the nitrogen line), so as to keep a closed system throughout the measurements. The second was a sealed five-necked flask, specifically used for experiments involving NO_2 on the 100 μm and 0.5 mm diameter Pt working electrodes. Two large syringe needles were attached to the inlet and outlet PTFE tubing and used to pierce the seals of two necks of the flask. This allowed a constant flow of NO_2 gas over the RTIL throughout the experiments. The remaining three necks of the flask were used to house the electrodes. Temperature controlled experiments were performed in a thermostated box (previously described by Evans *et al.*)[10] which also functioned as a Faraday cage. The temperature was accurate to $\pm$ 0.5 K.

3.4 Chronoamperometric Experiments

Chronoamperometric transients were achieved using a sample time of 0.01 s (0.001 s for all gases). In all experiments, the potential was stepped form a position of zero current to a potential after the voltammetric peak, and the current was measured for 10 s (0.5 s for all gases) after pre-equilibration for 20 seconds. The software package Origin 7.0 (Microcal Software Inc.) was used to fit the experimental data, after deletion of the initial 10 data points. The equations proposed by Shoup and Szabo[11] (below) were imported into the non linear curve fitting function, and the computer instructed to perform 100 iterations on the data, which are sufficient to give D and c within an error of 0.6 %.

$$I = -4nFDcr_{\mathrm{d}}f(\tau) \tag{3.1}$$

$$f(\tau) = 0.7854 + 0.8862\tau^{-\frac{1}{2}} + 0.2146\exp(-0.7823\tau^{-\frac{1}{2}}) \quad (3.2)$$

$$\tau = \frac{4Dt}{{r_d}^2} \quad (3.3)$$

where n is the number of electrons transferred, F is the Faraday constant, D is the diffusion coefficient, c is the initial concentration of parent species, r_d is the radius of the disk electrode, and t is the time. The value for the radius (previously calibrated) was fixed, and a value for the diffusion coefficient and the product of the number of electrons multiplied by concentration was obtained after optimisation of the experimental data. The accuracy of this method in aprotic and RTIL solvents has been been validated in a recent publication.[12]

3.5 XPS experiments

X-Ray photoelectron spectroscopy experiments were performed by Dr. Alison Crossley of the Materials Department at Oxford University using Mg X-ray excitation. The full experimental details are better placed, and are described individually, in Chapters 4 and 7.

The next chapter begins the presentation of research original to this thesis by exploiting the low-volatility nature of RTILs, studying the XPS spectrum of an ionic liquid with different amounts of dissolved bromide salt. The quantification of bromide present in the RTIL is verified independently by cyclic voltammetry and potential-step microdisk chronoamperometry.

References

[1] http : //quill.qub.ac.uk/.

[2] Bonhôte, P.; Dias, A.-P.; Papageorgiou, N.; Kalyanasundaram, K. and Grätzel, M., *Inorg. Chem.*, 1996, **35**, 1168–1178.

[3] MacFarlane, D. R.; Meakin, P.; Sun, J.; Amini, N. and Forsyth, M., *J. Phys. Chem. B*, 1999, **103**, 4164–4170.

[4] Cammarata, L.; Kazarian, S. G.; Salter, P. A. and Welton, T., *PhysChemChemPhys*, 2001, **3**, 5192–5200.

[5] Ignat'ev, N.; Welz-Biermann, U.; Kucheryna, A.; Bissky, G. and Willner, H., *J. Fluorine Chem.*, 2005, **126**, 1150–1159.

[6] Sharp, M., *Electrochim. Acta*, 1983, **28**, 301–308.

[7] Schröder, U.; Wadhawan, J. D.; Compton, R. G.; Marken, F.; Suarez, P. A. Z.; Consorti, C. S.; de Souza, R. F. and Dupont, J., *New J. Chem.*, 2000, **24**, 1009–1015.

[8] Evans, R. G.; Klymenko, O. V.; Hardacre, C.; Seddon, K. R. and Compton, R. G., *J. Electroanal. Chem.*, 2003, **556**, 179–188.

[9] Silvester, D. S. and Compton, R. G., *Z. Phys. Chem.*, 2006, **220**, 1247–1274.

[10] Evans, R. G.; Klymenko, O. V.; Price, P. D.; Davies, S. G.; Hardacre, C. and Compton, R. G., *ChemPhysChem*, 2005, **6**, 526–533.

[11] Shoup, D. and Szabo, A., *J. Electroanal. Chem. Interfacial Electrochem.*, 1982, **140**, 237–245.

[12] Paddon, C. A.; Silvester, D. S.; Bhatti, F. L.; Donohoe, T. J. and Compton, R. G., *Electroanalysis*, 2007, **19**, 11–22.

Chapter 4

Using XPS to Determine Solute Solubility in RTILs

In this chapter, X-Ray Photoelectron Spectroscopy (XPS) is used to quantify the amount of bromide ions present in two samples of [C_4mpyrr]Br (*N*-butyl-*N*-methylpyrrolidinium bromide) dissolved in the RTIL *N*-butyl-*N*-methylpyrrolidinium bis(trifluoromethylsulfonyl)imide ([C_4mpyrr][NTf_2]). One sample is of a known concentration (0.436 Br atom %); the other is a saturated solution. The results obtained from quantitative XPS analysis indicate that the saturated sample has a concentration, or solubility, of 0.90 Br atom % (746 mM) at 298 K, which is then independently confirmed by potential step chronoamperometry of the same solution.

The work described in this chapter was carried out with the assistance of Miss Tessa Broder, a fourth year undergraduate student at Oxford University, under the supervision of this author, and XPS experiments were performed by Dr. Alison Crossley, of the Materials Department at Oxford University. This work has been published in the Analyst.[1]

4.1 Introduction

X-Ray Photoelectron Spectroscopy (XPS) is a useful quantitative spectroscopic technique employed in a variety of industrial applications. It is used to determine the quantity of elements present (within 10 nm of the surface), the empirical formula of the material, the binding energy (BE) of one or more electronic states, the density of electronic states, and any contamination species.[2] To date, XPS has mainly been used to study solid species, and occasionally gases. Recently, various researchers[3–8] have used this technique to study room temperature ionic liquids (RTILs). Up until now, XPS studies on liquids has been impossible due to evaporation of the liquid under ultra-high vacuum conditions, but the unique non-volatility characteristics of RTILs means this is no longer a problem in this media.

XPS studies on RTILs are relatively rare, but a few recent reports show the technique to be useful for various purposes, and have focussed almost exclusively on pure RTILs. For example, Crespo *et al.*[4] first showed the use of RTILs in XPS experiments by testing the stability of RTILs in a supported liquid membrane. Caporali *et al.*[3] used XPS to show that the composition of the surface of $[C_4mim][NTf_2]$ (1-butyl-3-methylimidazolium bis(trifluoromethylsulfonyl)imide) is the same as the bulk, despite low energy ion scattering indicating that the outer layer is composed of F atoms. Licence and co-workers reported an XPS study of the chemical structure of the RTIL $[C_2mim][EtSO_4]$ (1-ethyl-3-methylimidazolium ethylsulfate),[8] and followed this with a more detailed study of 6 representative imidazolium-based RTILs,[7] showing that both the presence of alkyl substituents and the anion type does not affect the electron distribution of the imidazolium ring. Then, Kempter *et al.*[6] studied the electronic structure of $[C_2mim][NTf_2]$ using XPS among other techniques. Most recently, Wasserscheid *et al.*[5] used XPS to study the surface composition of $[C_2mim][EtSO_4]$ and detect silicon impurities left over from the synthesis of the RTIL.

These reports have generally focussed on the structure of the pure liquids, but to the best of our knowledge, there is only one specifically focussed on species knowingly dissolved in RTILs. That concerns using XPS to monitor the decay of a Pd complex in $[C_2mim][NTf_2]$.[8] We now demonstrate that this technique can be used to determine the solubility of dissolved salts (in the range 0.5 to 1.0 atom % of bromide) in these media, and we confirm these results using cyclic voltammetry and potential-step chronoamperometry to verify the concentrations found using XPS.

4.2 Experimental

The RTIL used in this study was $[C_4mpyrr][NTf_2]$ since the bromide salt was readily available, and the electrochemical window of this RTIL is wide (+5 V) and showed no obvious features

under vacuum. XPS experiments using Mg X-ray excitation were performed on two samples, one of a known concentration and one of a saturated solution of $[C_4mpyrr]Br$ in $[C_4mpyrr][NTf_2]$. Spectra obtained on several attempts showed well-defined characteristic emissions and no obvious degradation of the ionic liquid was observed during or after exposure to the X-ray source.

Solutions were made by dissolving appropriate amounts of the ionic liquid salt into approximately 400 μL of the ionic liquid. For the saturated solution, 200 μL of ionic liquid was used in order to minimise the amount of ionic liquid required. The solutions were stirred for approximately 24 hours to allow for full dissolution. XPS experiments on these solutions were performed as follows: samples of the ionic liquids were supported in shallow dish stubs, which were introduced into the instrument *via* a turbo molecular pumped entry lock. The entry lock was pumped for about 30 minutes before the sample was introduced into the analysis chamber. XPS was performed in an ion pumped UHV chamber equipped with a VG nine channel CLAM4 electron energy analyser (base pressure 5×10^{-9} torr). 250 Watt unmonochromated Mg X-ray excitation was used. The CLAM4 has variable slits for small area analysis. The largest slit (5 mm) was used in this case with no apertures selected. The analyser was operated at constant pass energy of 100 eV. Data was obtained using VGX900-W operating system. Peak areas were measured after background subtraction following the methods reported by Shirley.[9] For electrochemical experiments, solutions were prepared by diluting 10 μL of the RTIL samples used for XPS (0.436 Br atom % and saturated solution) up to 420 μL with $[C_4mpyrr][NTf_2]$, giving 8.6 and 17.8 mM solutions respectively. A conventional two-electrode arrangement was employed with a 10 μm diameter Pt working electrode and 0.5 mm Ag quasi-reference. All electrochemical experiments were performed inside a T-cell, as described in Chapter 3.

4.3 Results and Discussion

Figure 4.1 shows a typical XPS spectrum obtained from a 0.436 Br atom % solution of $[C_4mpyrr]Br$ in the RTIL $[C_4mpyrr][NTf_2]$. The figure is clearly labelled with the characteristic photoemission lines corresponding to C, N, O, F and S atoms present in the RTIL structure. Table 4.1 shows the quantification (atom %) obtained from the analysis of Figure 4.1, and also the results obtained for the saturated solution. In both cases, the elements that make up the RTIL are approximately present in the correct ratio as predicted from its structure. There is also a small peak at a binding energy of 69.0 eV, which corresponds to the Br 3d photoemission. Figure 4.2 shows a close-up view of this photoemission for both the 0.436 Br atom % (solid line) and the saturated Br solutions (dotted line). The saturated solution peak is clearly larger than that of the known concentration. The areas under the peaks are quantified to 2 d.p.[10] and are given in Table 4.1. The concentration obtained from XPS for the more dilute solution was 0.45 Br atom %, which agrees well with the actual value for the concentration (0.436 Br atom %). This therefore leads us to believe that the saturated solution has a concentration of *ca.* 0.90 Br atom %, giving the solubility of bromide in $[C_4mpyrr][NTf_2]$ as *ca.* 746 mM.

Table 4.1: Peak quantification (expressed as concentration, atom %) for each element present in both the 0.436 Br atom % and saturated solutions of $[C_4mpyrr]Br$ in the RTIL $[C_4mpyrr][NTf_2]$ at 298 K.

Solution	% C	% O	% N	% S	% F	% Br
0.436 Br atom %	42.71	15.77	7.74	8.80	24.52	0.45
Saturated Br	43.57	15.33	7.69	8.42	24.09	0.90

In order to further verify the concentrations obtained, cyclic voltammetry and potential-step microdisk chronoamperometry was performed on the two solutions. Both solutions were diluted up approximately 42 times, giving final concentrations (assuming that the XPS results for the saturated solution was correct) of 8.6 mM and 17.8 mM respectively, since the initial concentrations (361 mM and 746 mM) were too large for typical voltammetric analy-

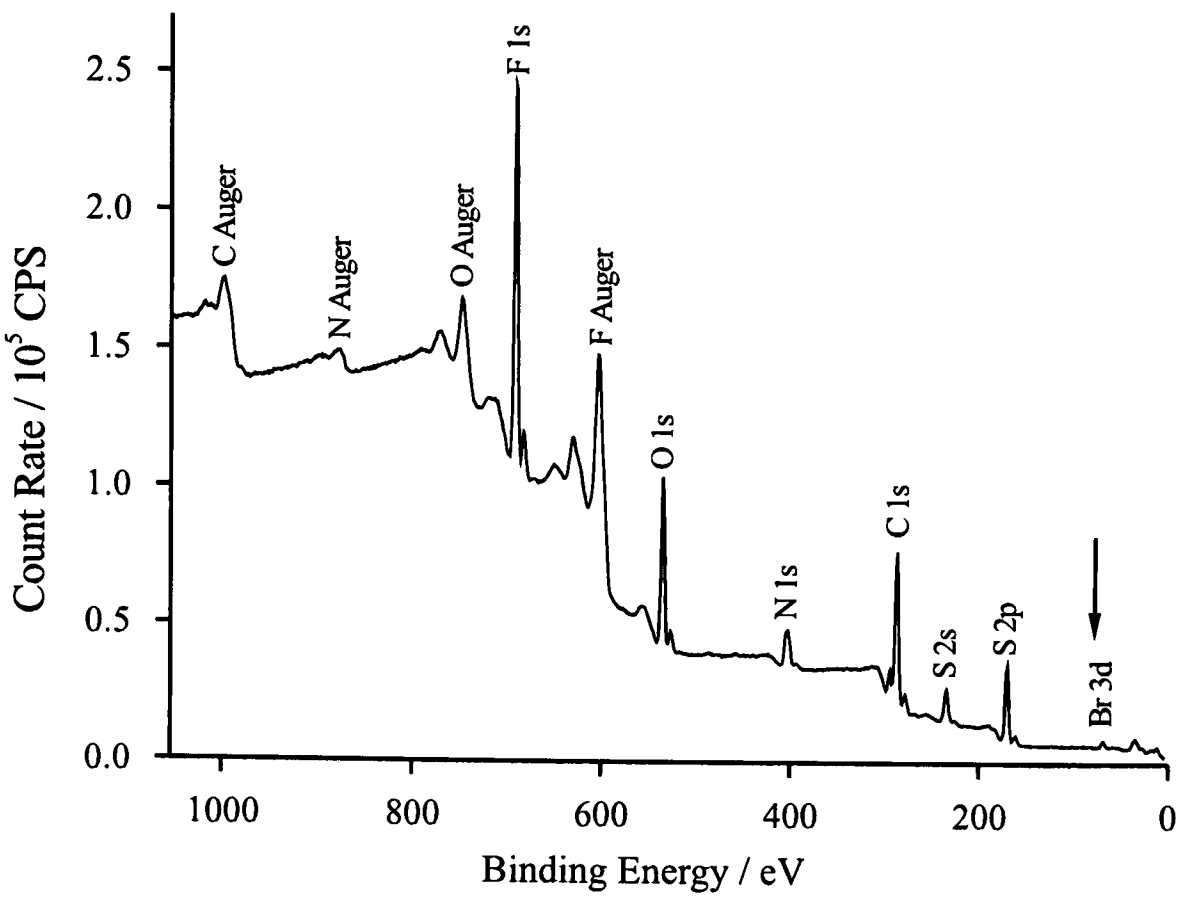

Figure 4.1: Survey scan XPS spectrum of a 0.436 Br atom % solution of $[C_4mpyrr]Br$ in $[C_4mpyrr][NTf_2]$.

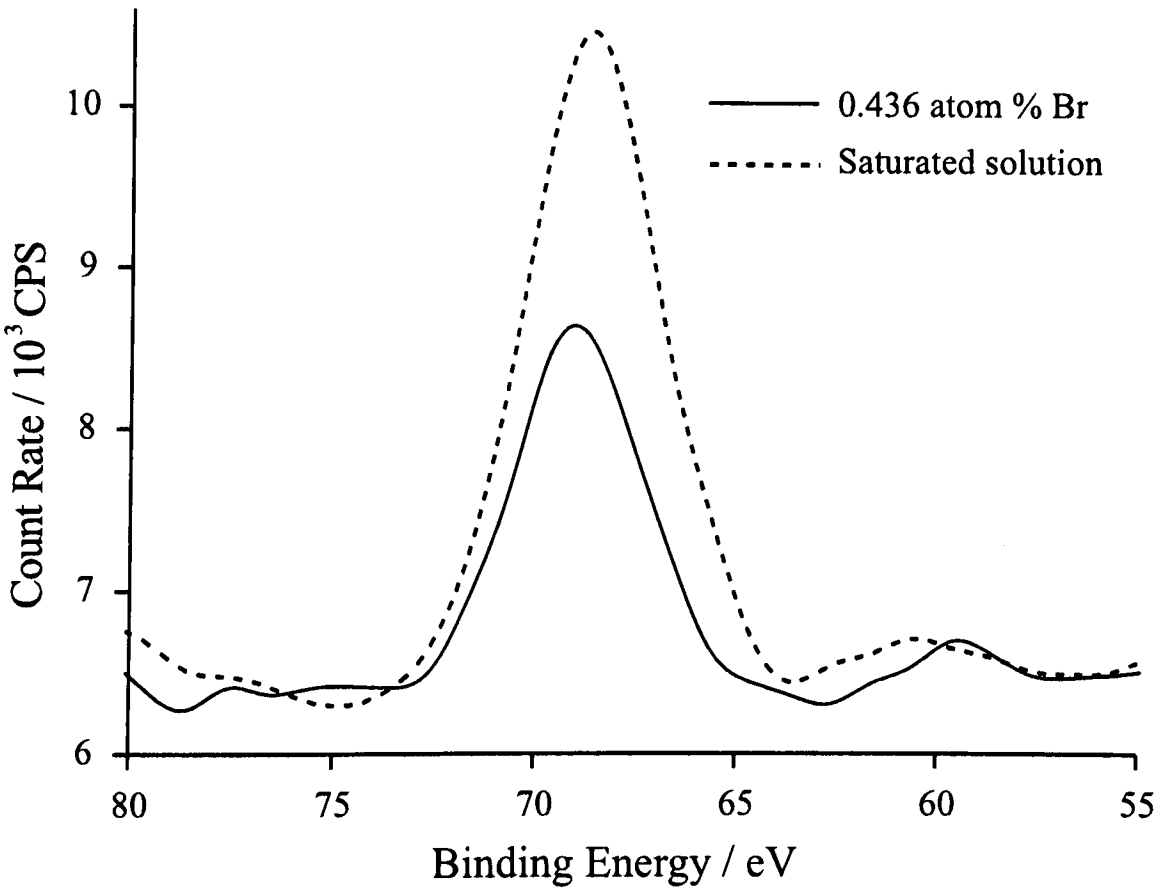

Figure 4.2: XPS spectra of the bromine (3d) photoemission, observed at characteristic binding energy for both the saturated and the 0.436 Br atom % solutions.

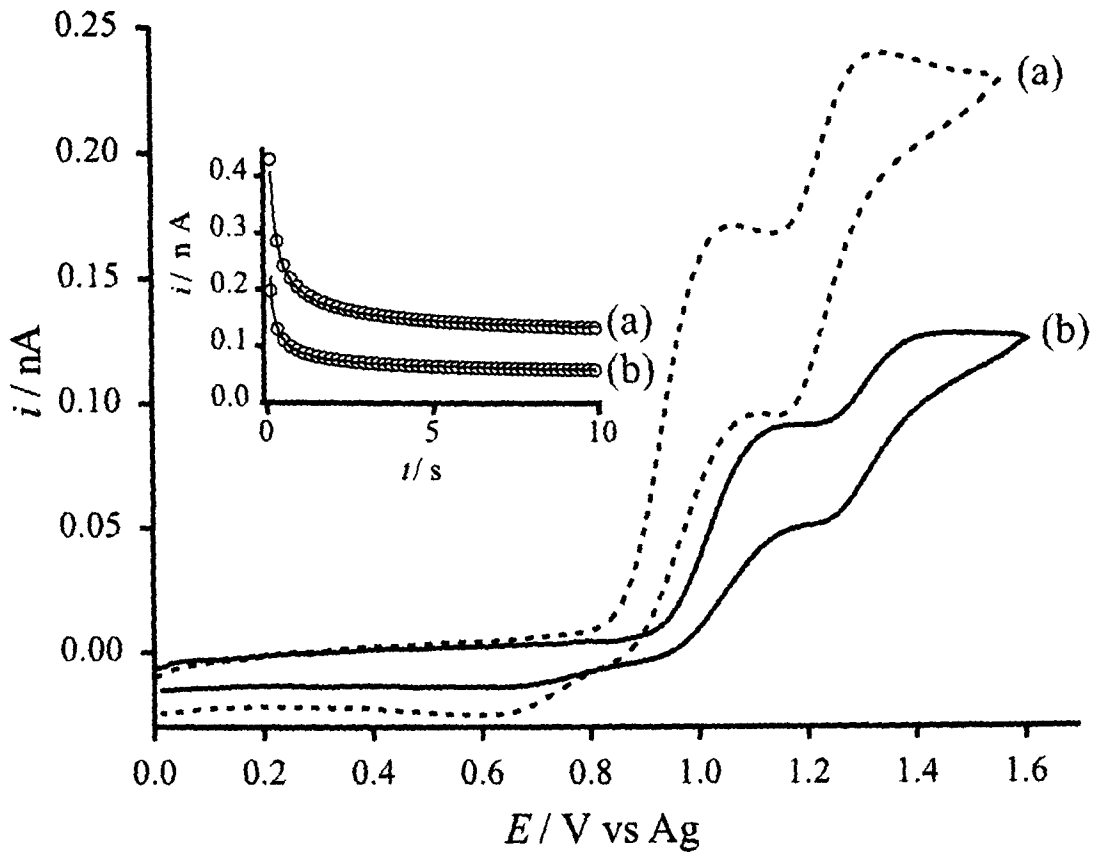

Figure 4.3: Cyclic voltammograms at 298 K for the oxidation of (a) the saturated solution, and (b) the 0.436 Br atom % solution of $[C_4mpyrr]Br$ in $[C_4mpyrr][NTf_2]$ at a Pt microelectrode (diameter 10 μm). Scan rate 100 mV s^{-1}. Note: the solutions were diluted by 42 times to give final concentrations of 17.8 and 8.6 mM respectively, in order for an accurate analysis. Inset shows experimental (–) and fitted theoretical (o) chronoamperometric transients for the oxidation of $[C_4mpyrr]Br$ in $[C_4mpyrr][NTf_2]$ from (a) 0 to +1.17 V, and (b) 0 to +1.22 V.

sis. Figure 4.3 shows cyclic voltammograms for the oxidation of (a) 17.8 mM and (b) 8.6 mM $[C_4mpyrr]Br$ in $[C_4mpyrr][NTf_2]$ on a platinum microdisk electrode (diameter 10 μm) at a scan rate of 100 mV s^{-1}. Two oxidative waves are observed at approximately +1.1 V and +1.4 V *vs* Ag (with some difference in the potential noted due to the shift in the silver wire pseudo-reference electrode). The oxidation of Br^- has been previously investigated by Allen *et al.*[11] in the RTIL $[C_4mim][NTf_2]$, and are thought to occur *via* the following processes:

For the first oxidation:

$$2Br^- - 2e^- \rightarrow Br_2 \tag{4.1}$$

$$Br_2 + Br^- \rightleftharpoons Br_3^- \tag{4.2}$$

and for the second oxidation:

$$Br_3^- \rightleftharpoons Br^- + Br_2 \tag{4.3}$$

$$Br^- - e^- \rightarrow \frac{1}{2}Br_2 \tag{4.4}$$

Since the two waves observed in the present study are similar in shape and position to the previous study,[11] we can conclude that the same mechanism is taking place.

In order to calculate accurate concentrations, chronoamperometry was then performed on the two solutions. The inset to Figure 4.3 shows typical chronoamperometric transients carried out on both the (a) 17.8 mM and (b) 8.6 mM solutions. The potential was stepped from 0.0 V (corresponding to no faradaic current) to a potential after the first oxidative wave, and the experimental data was fitted to the Shoup and Szabo[12] expression. The results from fitting gave a diffusion coefficient of 7.6 ($\pm$ 0.4) $\times$ 10^{-12} m^2 s^{-1} at 298 K, which compares relatively well to the value of 1.4 ($\pm$ 0.2) $\times$ 10^{-11} m^2 s^{-1} obtained in $[C_4mim][NTf_2]$ at 295 K,[11] given the higher viscosity of the liquid used in the present study (89 cP for $[C_4mpyrr][NTf_2]$[13] compared to 52 cP for $[C_4mim][NTf_2]$[14] at 293 K), and concentrations of 9.0 ($\pm$) 0.4 mM and 17.6 ($\pm$) 0.5 mM for the two solutions respectively.

4.4 Conclusions

Two RTIL solutions with different concentrations of dissolved bromide were studied using XPS. By analysing the Br 3d emission peak area, the concentrations of the saturated and 0.436 % Br solutions were calculated. The solutions were then independently studied by cyclic voltammetry and potential-step chronoamperometry to obtain diffusion coefficients and concentrations of bromide. The concentrations were found to be accurate to within experimental error for both solutions, so therefore we can conclude that the assumption of the concentration (from XPS) of the saturated solution was correct, and that XPS is a valuable technique for quantifying the

solubility of bromide in ionic liquids, giving the solubility of Br^- in $[C_4mpyrr][NTf_2]$ as *ca.* 0.90 Br atom %, or 746 mM.

In this chapter, it has been shown that ionic liquids can survive under ultra high-vacuum conditions due to their unique low-volatility. As a result, X-Ray Photoelectron Spectroscopy, a technique usually only applied to solids (and occasionally gases) was performed on an a liquid, and the solubility of bromide was calculated. In the next chapter, we begin to look at the mechanistic and kinetic behaviour or organic solutes in room temperature ionic liquids. In particular, we will compare the reduction mechanisms of nitrobenzene and 4-nitrophenol to that seen in conventional molecular aprotic solvents, in order to try to understand the behaviour of dissolved species in ionic liquid media.

References

[1] Silvester, D. S.; Broder, T. L.; Aldous, L.; Hardacre, C.; Crossley, A. and Compton, R. G., *Analyst*, 2007, **132**, 196–198.

[2] Briggs, D. and Seah, M. P., Eds., *Practical Surface Analysis, Vol 1: Auger and X-Ray Photoelectron Spectroscopy*, John Wiley and Sons: Chichester, UK, 1994.

[3] Caporali, S.; Bardi, U. and Lavacchi, A., *J. Electron Spectrosc. Relat. Phenom.*, 2006, **151**, 4–8.

[4] Fortunato, R.; Afonso, C. A. M.; Benavente, J.; Rodriguez-Castellón, E. and Crespo, J. G., *J. Membr. Sci.*, 2005, **256**, 216–223.

[5] Gottfried, J. M.; Maier, F.; Rossa, J.; Gerhard, D.; Schulz, P. S.; Wasserscheid, P. and Steinrueck, H.-P., *Z. Phys. Chem.*, 2006, **220**, 1439–1453.

[6] Höfft, O.; Bahr, S.; Himmerlich, M.; Krischok, S.; Schaefer, J. A. and Kempter, V., *Langmuir*, 2006, **22**, 7120–7123.

[7] Smith, E. F.; Rutten, F. J. M.; Villar-Garcia, I. J.; Briggs, D. and Licence, P., *Langmuir*, 2006, **22**, 9386–9392.

[8] Smith, E. F.; Villar Garcia, I. J.; Briggs, D. and Licence, P., *Chem. Commun.*, 2005, **45**, 5633–5635.

[9] Shirley, D. A., *Phys. Rev. B: Solid State*, 1972, **5**, 4709–4714.

[10] Note: Although normally it is not usual to quote figures to two decimal places, here it seems necessary given the small expected values for the concentration of bromide. however, there figures merely represent the limit of detection rater than the accuracy, since a 10 % error is possible for the values quoted.

[11] Allen, G. D.; Buzzeo, M. C.; Davies, I. G.; Villagrán, C.; Hardacre, C. and Compton, R. G., *J. Phys. Chem. B*, 2004, **108**, 16322–16327.

[12] Shoup, D. and Szabo, A., *J. Electroanal. Chem. Interfacial Electrochem.*, 1982, **140**, 237–245.

[13] Okoturo, O. O. and VanderNoot, T. J., *J. Electroanal. Chem.*, 2004, **568**, 167–181.

[14] Bonhôte, P.; Dias, A.-P.; Papageorgiou, N.; Kalyanasundaram, K. and Grätzel, M., *Inorg. Chem.*, 1996, **35**, 1168–1178.

Chapter 5

Electrochemical Reduction of Nitrobenzene and 4-Nitrophenol in the RTIL $[C_4dmim][NTf_2]$

In this chapter, the reductions of nitrobenzene and 4-nitrophenol are studied using cyclic voltammetry in the room temperature ionic liquid 1-butyl-2,3-dimethylimidazolium bis(trifluoromethylsulfonyl)imide ($[C_4dmim][NTf_2]$) on a gold microelectrode. Nitrobenzene is reduced reversibly by one electron and further by two electrons in a chemically irreversible step. The more complicated reduction of 4-nitrophenol reveals three reductive peaks (two chemically irreversible and one reversible) which are successfully simulated using the digital simulation program DigiSim® using a mechanism of rapid self-protonation, previously suggested by Amatore *et al.* in DMSO.[1]

Two further anodic peaks are observed and are attributed to the oxidations of 4-hydroxyphenylhydroxylamine and 4-nitrophenolate respectively. For both nitrobenzene and 4-nitrophenol, diffusion coefficients are roughly two orders of magnitude smaller than in conventional solvents. It appears that both species are reduced following the same mechanisms as in conventional aprotic solvents, with differences in the voltammetry primarily due to the viscous nature of the ionic liquid. This work has been published in the Journal of Electroanalytical Chemistry.[2]

5.1 Introduction

In this work, we report the electro-reductions of several aromatic nitro compounds in a room temperature ionic liquid. Nitro compounds are used widely by organic chemists since the nitro group can be easily reduced without affecting other functional groups.[3] A variety of products can be generated, depending on the exact nature of the experimental conditions, and hence these are interesting compounds for electrochemists to study in order to fully understand the reaction mechanisms involved and, in particular, to identify any similarities or differences in behaviour

when different electrochemical solvents are employed.

The electrochemistry of nitrobenzene ($PhNO_2$) has been extensively studied and is known to yield a stable radical anion from the one electron reduction in both aprotic media[4–6] and aqueous alkali solutions.[7,8] In all media, a second, irreversible reduction process has been reported at more negative potentials, which was identified as the three-electron reduction from the radical anion to phenylhydroxylamine (PhNHOH). This reduction is thought to proceed *via* the generation of nitrosobenzene (PhNO), which is electroactive at the nitrobenzene first reduction potential. The formation of azo (PhN=NPh) and azoxy (PhN=NOPh) compounds[9,10] has also been reported for the reduction of nitrosobenzene in acetonitrile, which is thought to result from the coupling of the nitrosobenzene radical anion with a parent molecule. The dianion salt of nitrobenzene has been isolated in liquid ammonia by both Chon and Paik[11] and Smith *et al.*,[12] and by Jensen and Parker[13] in highly purified DMF. A typical reaction scheme showing the formation of these products in aprotic solvents is given in Figure 5.1. In protic media, the predominant reduction product is either 4-aminophenol ($HOPhNH_2$)[14,15] or aniline ($PhNH_2$)[16] (depending upon the strength of the acid medium) *via* the intermediate *N*-phenylhydroxylamine.

The reduction of 4-nitrophenol ($HOPhNO_2$) has been studied previously in aprotic solvents such as DMF[17] and DMSO[1,18] and also in protic solvents.[19,20] Even in so-called 'aprotic' solvents, the radical anion of 4-nitrophenol is unstable, due to the acidic nature of the parent molecule, giving rise to a self-protonation reaction. The reduction to form the radical anion is chemically irreversible, even at very high scan rates[17] suggesting that the protonation step is very rapid. Amatore *et al.*[1] proposed a reaction mechanism for the reduction in DMSO, the initial steps of which are shown in Figure 5.2. The final product of this initial reaction mechanism is nitrosophenol (HOPhNO), which in this environment is thought to undergo further follow-up chemistry to yield ultimately 4-aminophenol ($HOPhNH_2$). Both Farnia *et al.*[18] and Amatore *et al.*[1] showed that, in DMSO, the only final products of the electrode reaction were 4-aminophenol

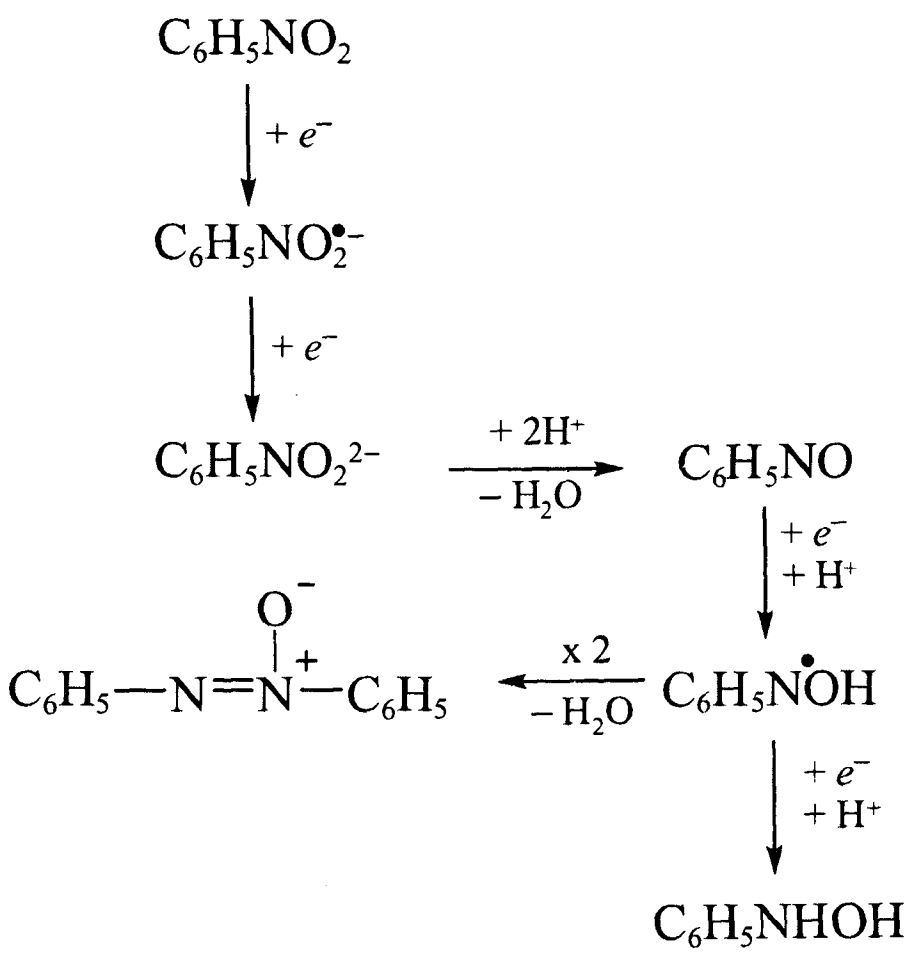

Figure 5.1: Reaction scheme for the reduction of nitrobenzene in aprotic solvents, showing the pathways for formation of nitrosobenzene, phenylhydroxylamine and azoxybenzene.

(6 electron reduction) along with the 4-nitrophenolate anion.

Various nitro- and nitroso- compounds have been explored in this study, specifically nitrobenzene, 4-nitrotoluene, 4-nitroanisole, 4-nitrophenol, nitrosobenzene, 4-nitrosophenol and 4-nitrophenolate, with a view to compare the reduction characteristics (wave shapes, kinetics and mechanism) in an ionic liquid, to that already known in conventional aprotic solvents. Here, we report the reduction of nitrobenzene, and for the first time, the reduction of 4-nitrophenol in the room temperature ionic liquid 1-butyl-2,3-dimethylimidazolium bis(trifluoromethylsulfonyl)imide ($[C_4dmim][NTf_2]$) on a gold electrode, with an interpretation of the mechanism using digital simulation (DigiSim®) of the microdisk voltammetry.

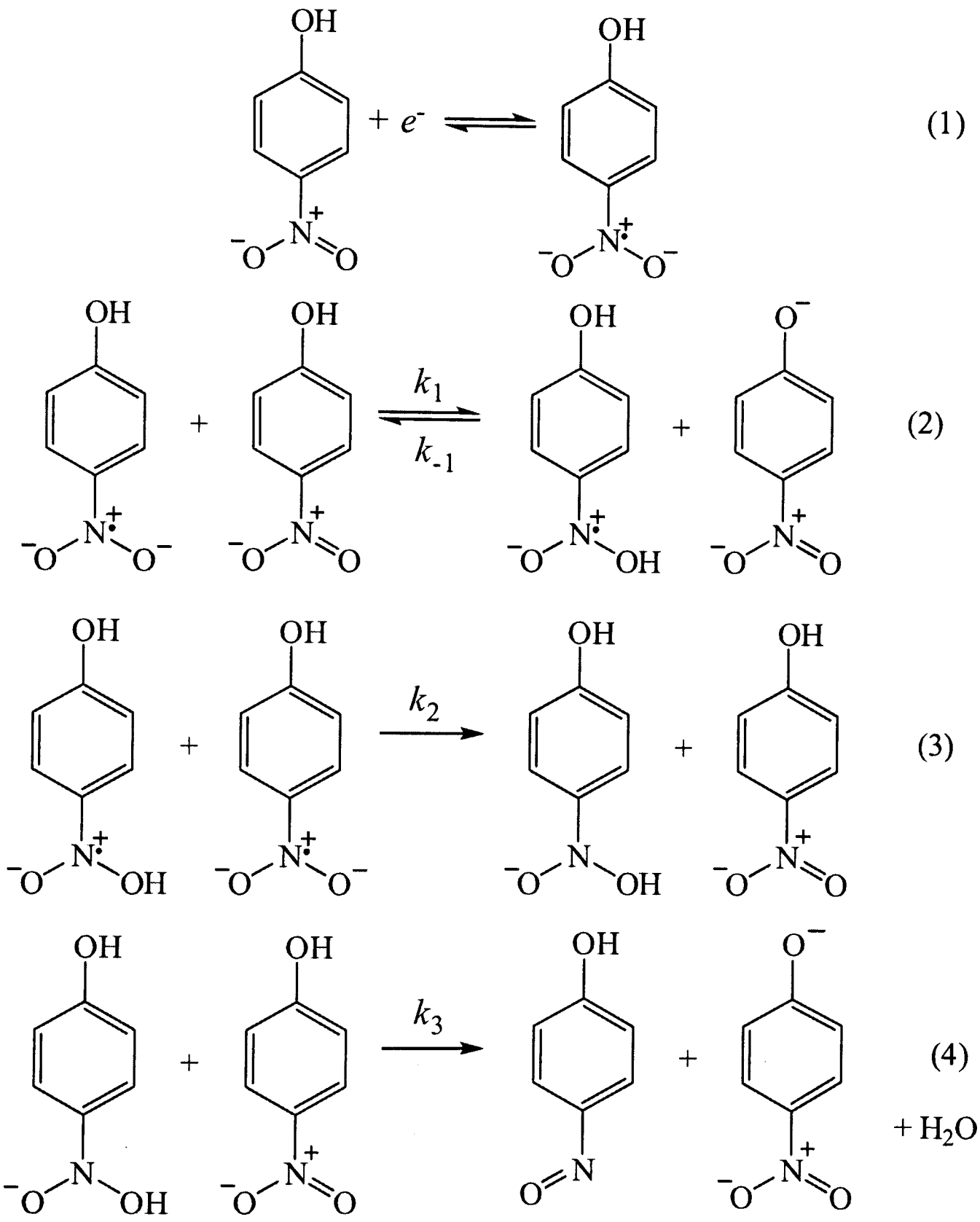

Figure 5.2: Reaction scheme proposed by Amatore[1] for the reduction of 4-nitrophenol.

5.2 Experimental

Throughout this work, experiments were undertaken in $[C_4dmim][NTf_2]$ since this gave a particularly clean baseline in the electrochemical window of interest when purged under vacuum. All experiments were performed inside a T-cell (described in Chapter 3) on a 25 μm diameter Au electrode with a 0.5 mm diameter Ag wire a quasi-reference electrode. The solvent-evaporation based procedure described in Chapter 3 was employed to dissolve known concentrations of each electroactive species in the RTIL.

5.3 Results and Discussion

5.3.1 Reduction of Nitrobenzene in $[C_4dmim][NTf_2]$

Figure 5.3 shows the reduction of 8 mM nitrobenzene in $[C_4dmim][NTf_2]$ on a 25 μm diameter gold microdisk electrode at a scan rate of 100 mV s^{-1}. The voltammetric wave at -1.2 V *vs* Ag (peak i) corresponds to the reversible one-electron reduction to the radical anion which is commonly known in aprotic solvents.[4–6,13–15,21] When scanning to more negative potentials, a second peak is observed at -1.85 V *vs* Ag (peak ii) which is chemically irreversible at all scan rates measured (0.01–4 V s^{-1}). This would suggest that the dianion, formed by further reduction of the radical anion, is unstable in this environment and most likely undergoes rapid protonation[4–6,21] after which the loss of a water molecule yields nitrosobenzene. It is thought that the dianion is a base strong enough to remove protons from species, which, under normal conditions are not regarded as acidic. For example, it has been previously reported that even *t*-butylammonium salts are acidic enough to act as proton donors.[22] It is therefore possible that protons present in the cation of the ionic liquid also behave in the same way. Although $[C_4dmim]^+$ is not likely to be as acidic as for example $[C_4mim]^+$ (1-butyl-3-methylimidazolium) which has an acidic proton at the C(2) position, $[C_4dmim]^+$ still has two acidic ring protons

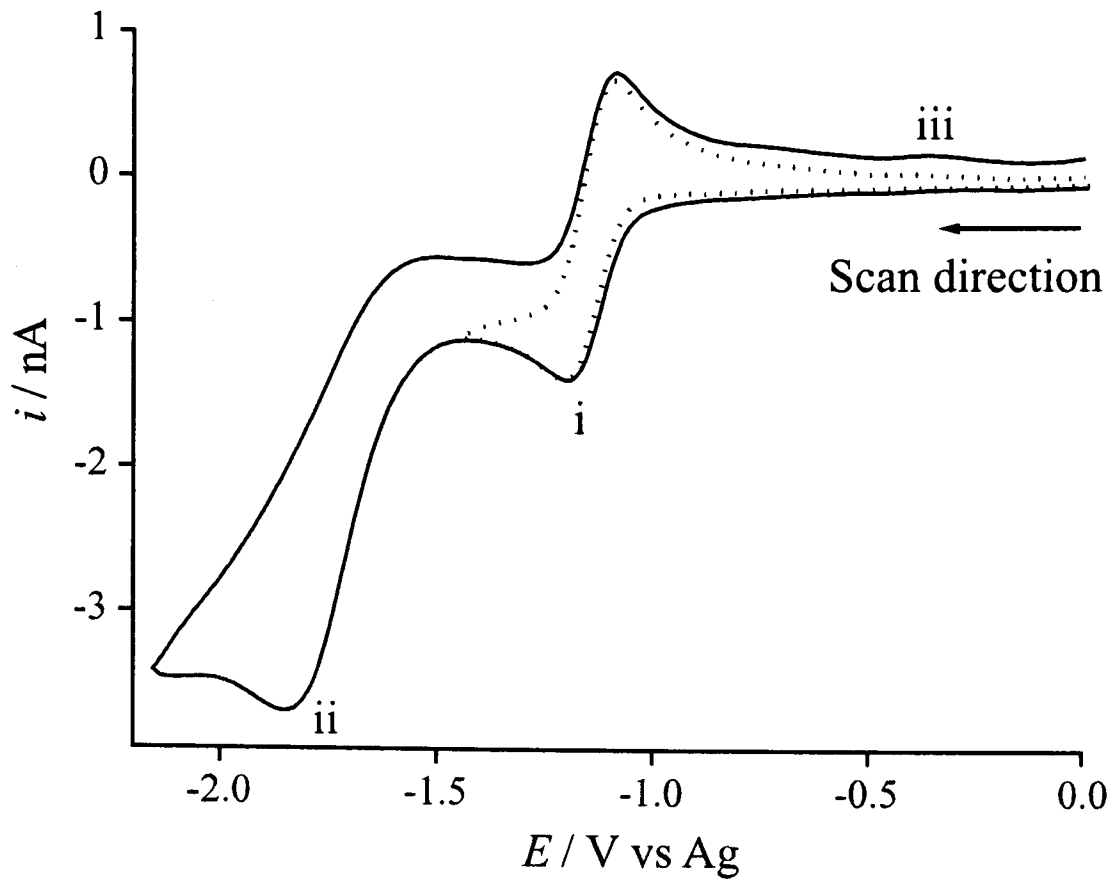

Figure 5.3: Cyclic voltammograms on a Au microelectrode (diameter 25 μm) for the reduction of 8 mM nitrobenzene in $[C_4dmim][NTf_2]$ at a scan rate of 100 mV s^{-1}. (–) reversed at -2.2 V, (dots) reversed at -1.5 V.

which have been shown to be exchangeable with D_2O[23] and these may be involved.

Chronoamperometry revealed that the number of electrons transferred in the first wave is close to one (1.03 ± 0.05) and, for the second wave, a further two electrons (overall 3.05 ± 0.09), which in contrast with conventional aprotic solvents,[4–8] indicates that the 4 electron reduction to phenylhydroxylamine is not achieved. The electron count observed for the second reduction wave might suggest that the product of this step is the nitrosobenzene radical anion. Voltammetry of nitrosobenzene in this ionic liquid demonstrated a reduction peak close to -0.9 V *vs* Ag, a potential less negative than that of peak I, which is not inconsistent with the formation of such a species. However, some authors[9,14,16,24] have postulated that this undergoes a dimerisation process to yield azoxybenzene, which in DMF can be oxidized at approximately -0.4 V *vs* Pt in MeCN[9] and -0.55 V *vs* Pt in DMF.[24] Although the peak positions cannot be directly compared (since the present study takes place in a different medium and on a different electrode) the

occurrence of a small anodic peak at -0.39 V *vs* Ag in Figure 5.3 (peak iii) might suggest that this is the case.[25]

The reduction of 4-nitrotoluene and 4-nitroanisole was also carried out under the same conditions, showing nearly identical behaviour to that of nitrobenzene. The diffusion coefficients obtained from chronoamperometry were, for nitrobenzene: 1.95 ($\pm$ 0.3) $\times$ 10^{-11} m^2 s^{-1}, for 4-nitrotoluene: 1.75 ($\pm$ 0.2) $\times$ 10^{-11} m^2 s^{-1} and for 4-nitroanisole: 2.15 ($\pm$ 0.1) $\times$ 10^{-11} m^2 s^{-1}, which are roughly two orders of magnitude less than the value obtained for nitrobenzene in DMF,[17] consistent with much slower diffusion due to the high viscosity of the ionic liquid (105 cP for $[C_4dmim][NTf_2]$[26] compared 0.92 cP for DMF[27] at 293 K).

5.3.2 Reduction of 4-Nitrophenol in $[C_4dmim][NTf_2]$

The voltammograms for the reduction of 8 mM nitrobenzene and 8 mM 4-nitrophenol in $[C_4dmim][NTf_2]$ at 100 mV s^{-1} on a gold electrode (diameter 25 μm) are overlaid in Figure 5.4. The sizes of the peaks are comparable at the same concentration. It is clear that the presence of the hydroxyl group significantly alters the voltammetric behaviour; for the phenol, a split/double wave (I and II) is observed, close to -1.03 V and -1.31 V *vs* Ag which is irreversible, and a reversible couple (III) at -1.79 V *vs* Ag. The different behaviour of 4-nitrophenol has been attributed to a self-protonation reaction[1,17,18] (see Scheme 5.2) which is preceded by heterogeneous electron transfer.

Previously reported is the reduction of 4-nitrophenol in DMF (+0.2 M TBAP) using a 3 mm diameter gold electrode.[17] Under these conditions, three reductive peaks were observed at (a) -1.02 V, (b) -1.53 V and (c) -1.92 V vs Ag; the first two peaks were chemically irreversible and the third peak was chemically reversible, with a corresponding oxidative peak at -1.77 V *vs* Ag. These features are similar to those shown in Figure 5.4, but clear differences are evident. In the ionic liquid, the relative ratio of the first two peak currents (I and II) is 1 to 1.8 compared

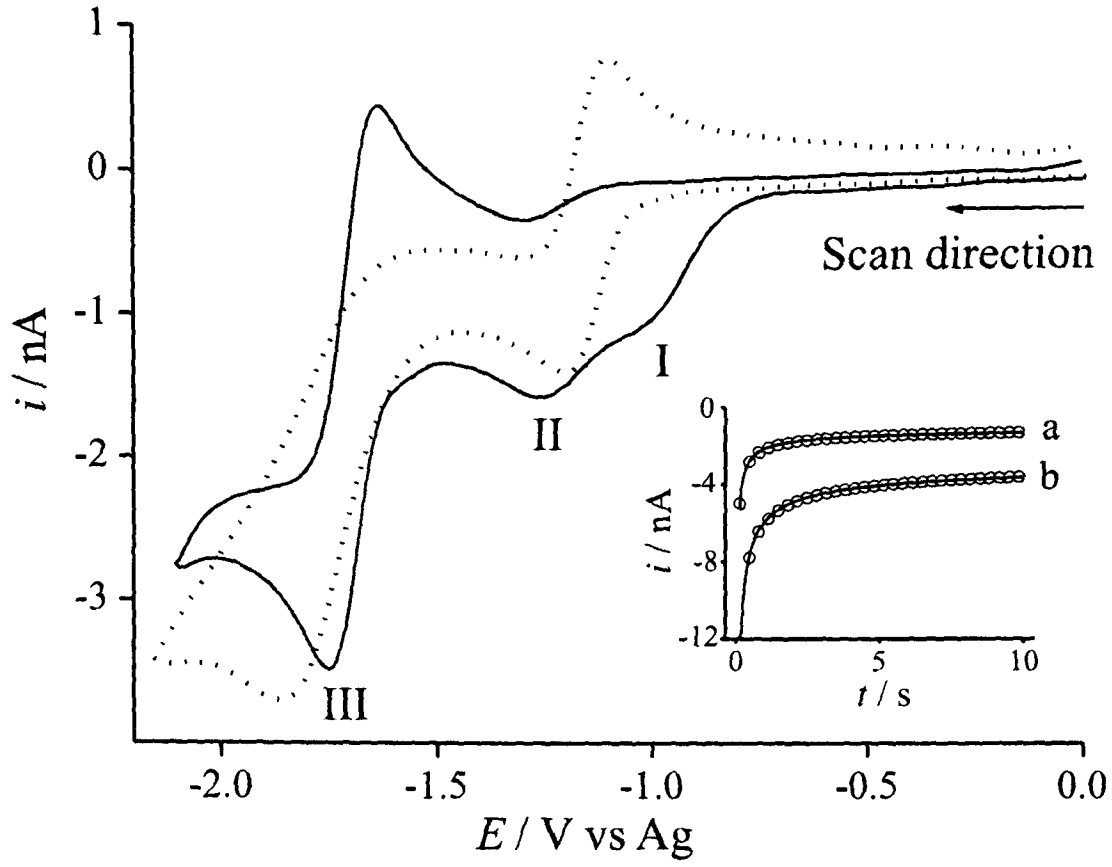

Figure 5.4: Cyclic voltammograms for the reduction of: (dots) 8 mM nitrobenzene; (solid line) 8 mM 4-nitrophenol in $[C_4dmim][NTf_2]$ at a gold microelectrode (diameter 25 μm) at a scan rate of 100 mV s^{-1}. The inset shows the experimental (–) and fitted theoretical (○) chronoamperometric transients for the reduction of 4-nitrophenol in $[C_4dmim][NTf_2]$ from (a) 0 to -1.5 V, (b) 0 to -2.1 V.

to 1 to 0.6 in DMF, and the peaks I and II are separated by only 0.28 V *vs* Ag compared to 0.51 V *vs* Ag in DMF. Such differences are likely to be a result of a higher viscosity and therefore lower diffusion coefficients in RTILs, which has a profound effect on the dynamics of the overall transformation. The fact that wave II is larger than wave I can be explained by either: (a) a possible contribution of current to peak II by the overlapping of peak I (which is relatively broad, and the waves are poorly resolved), or (b) an additional heterogeneous step (see section 5.3.3 below) which coincidently takes place at approximately the same potential as wave II. Chronoamperometric data (Figure 5.4 inset) suggests that the number of electrons involved in the first two peaks of 4-nitrophenol (I and II) combine to give values in the range 0.96–1.01, and the third peak (III) gives a further 1 electron per molecule (combining to give 1.99 ($\pm$ 0.05) electrons overall).

Figure 5.5 shows the reduction of 4-nitrophenol in $[C_4dmim][NTf_2]$ on a gold electrode (di-

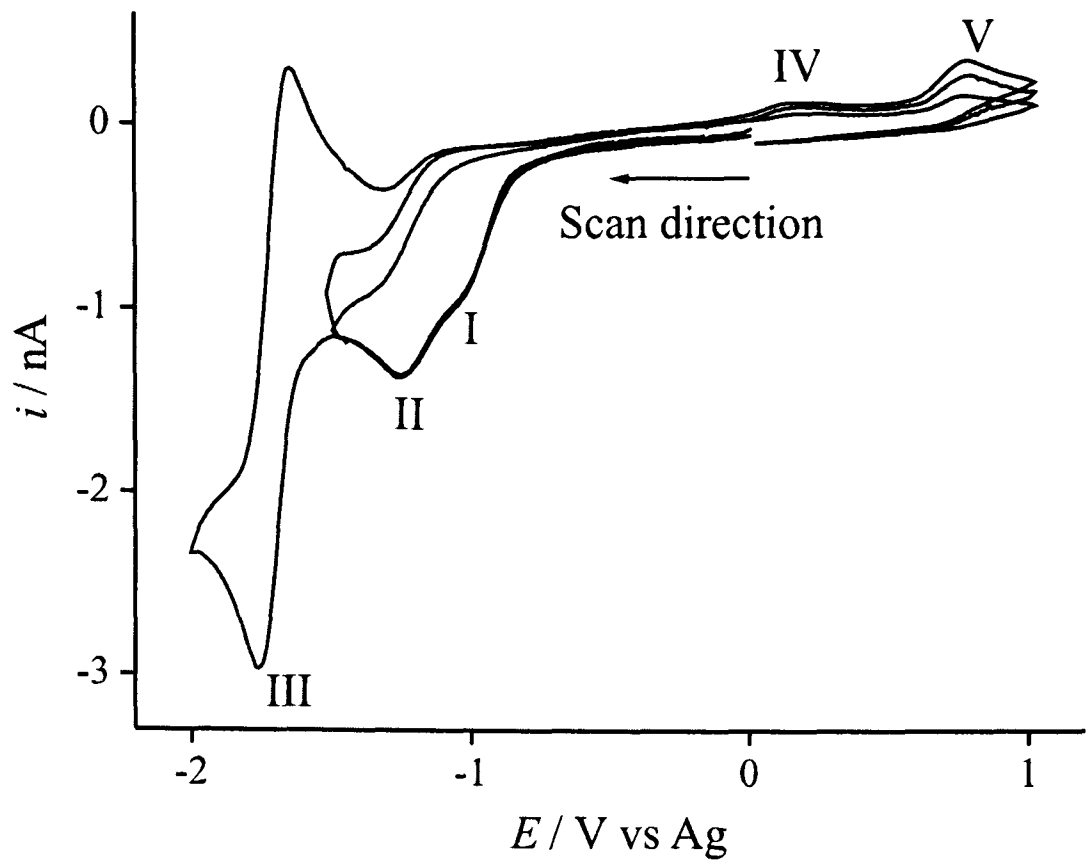

Figure 5.5: Typical cyclic voltammograms for the reduction of 8 mM 4-nitrophenol in $[C_4dmim][NTf_2]$. Graphs shown correspond to the full redox window of 4-nitrophenol, the effect of reversing at -1.5 V, and the effect of reversing and holding the potential for 1 minute at -1.5 V.

ameter 25 μm) at a scan rate of 100 mV s^{-1}. The electrochemical window was extended to +1.0 V *vs* Ag, and two anodic peaks (IV and V) at +0.13 V and +0.81 V *vs* Ag were observed. Overlaid are two further plots: one where the scan is reversed at -1.5 V, and one where the scan is reversed and held for 1 minute at -1.5 V, to allow build-up of products. Peaks IV and V are still evident (although smaller) when the scan is reversed at -1.5 V, and are enhanced when held for 1 minute at -1.5 V indicating that these anodic features correspond to the oxidation of products formed during waves I and II. On the second scan, a small and broad reductive peak was observed at -0.29 V *vs* Ag, which was coupled to peak IV (at +0.13 V *vs* Ag).

Next, the use of digital simulation allows rationalisation of the 'split-wave' feature (peaks I and II combined) on the basis of the reaction scheme shown in Figure 5.2, and the identity of species giving rise to the peaks III, IV and V will be explored.

5.3.3 Modelling the Reduction of 4-Nitrophenol in DigiSim®

The one-dimensional simulation program DigiSim® 3.03 (BAS Technicol)[28] was used to model the cyclic voltammogram for 8 mM 4-nitrophenol shown in Figure 5.5. Scan rates ranging from 10 mV s^{-1} to 4 V s^{-1} were studied experimentally and simulated using the hemispherical diffusion model. Figure 5.6 shows both the experimental and simulated voltammograms at scan rates of 0.1 V s^{-1}, 0.4 V s^{-1} and 1 V s^{-1}.

We considered first the 'split-wave' feature (waves I and II). In previous work in DMF, the first two irreversible waves observed were fully resolved, being separated by 0.51 V, and were attributed to different electrochemical processes[17] (namely the reduction of the phenol and the phenolate). Although it is possible that the same two processes take place in ionic liquid media, with a significantly smaller potential separation, such a notion could not be easily rationalised. An alternative explanation for the double-wave is that it is a feature of the follow-up homogeneous chemistry of the electrogenerated radical anion, and that only a single heterogeneous step is necessary for such a response. Preliminary trials using DigiSim®, on the basis of the scheme in Figure 5.2 showed that this 'split-wave' could indeed be simulated under a given kinetic regime. The generic scheme used in the simulation was:

$$A + e^- = B \tag{5.1}$$

$$B + A = C + D \tag{5.2}$$

$$C + B = E + A \tag{5.3}$$

$$E + A = F + D \tag{5.4}$$

where A is the parent species of 4-nitrophenol and B is the electrochemically reduced radical anion of 4-nitrophenol. The other species can be identified in the scheme in Figure 5.2. The physical rationale for the simulation of the double-wave is that the parent molecule is initially

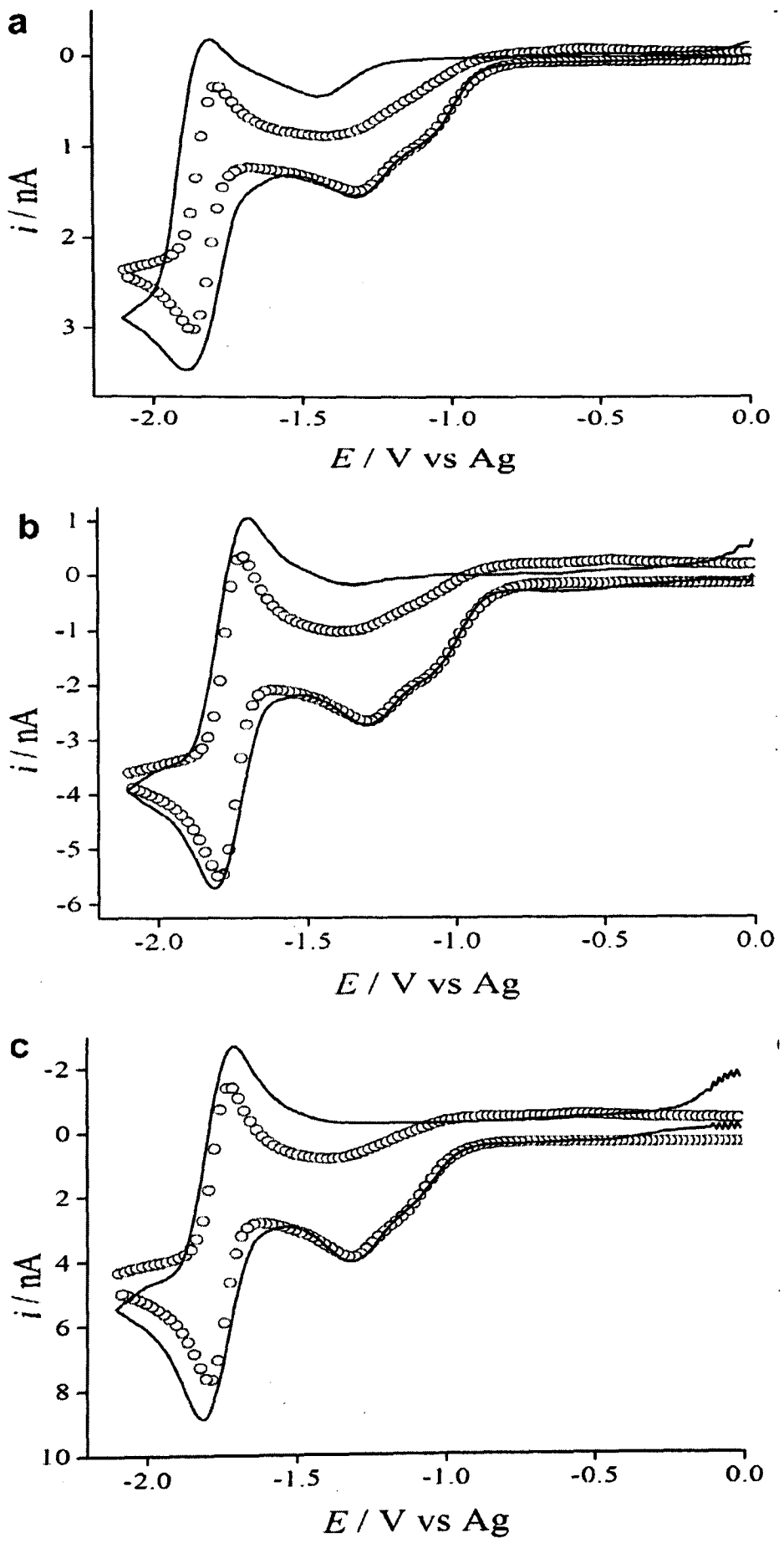

Figure 5.6: A comparison of experimental (–) and simulated (○) voltammograms for the reduction of 8 mM 4-nitrophenol in $[C_4dmim][NTf_2]$ at scan rates of (a) 0.1 V s^{-1}, (b) 0.4 V s^{-1} and (c) 1.0 V s^{-1}. The same parameters were also used for 4 mM and 16 mM 4-np, with similar quality of theoretical fits to experimental voltammograms.

reduced to the radical anion, which then reacts with a second parent molecule in solution. This can be simulated using DigiSim® by entering the following general mechanism: A + e^- → B, and B + A → products. This phenomenon, where a single diffusing species results in two voltammetric waves, has been previously reported by Allen *et al.*[29] for the oxidation of bromide in $[C_4mim][NTf_2]$, and will also be seen in the next chapter.

Attempts to fit waves I and II under the mechanistic scheme posed (Figure 5.2) with equation 5.4 set as the rate limiting step, were successful for the forward scan, but it was found that back peaks associated with waves I and II appeared on the simulation, which were not present on experimental scans when reversed at -1.5 V. It was considered that these simulated reverse waves could explain peaks IV and V, but the potentials of the latter were much too positive for this to be feasible. A number of possibilities were considered in order to remove these simulated back waves, such as additional electrochemical reductions of the other species formed in the scheme in Figure 5.2, but no additional heterogeneous step was of any help. However, it was found that it was possible to render waves I and II irreversible in the simulation if reaction 5.4 was simulated to be fast (hence removing species B from the diffusion layer), and if the following homogeneous reactions for the reduction of the nitroso intermediate were included. Amatore *et al.*[1] proposed the following mechanism for this reduction in DMSO:

$$HOC_6H_4NO + HOC_6H_4NO_2^{\bullet -} \rightarrow HOC_6H_4NO^{\bullet -} + HOC_6H_4NO_2 \quad (5.5)$$

$$HOC_6H_4NO^{\bullet -} + HOC_6H_4NO_2 \rightarrow HOC_6H_4NOH^{\bullet} +^{-} OC_6H_4NO_2 \quad (5.6)$$

$$HOC_6H_4NOH^{\bullet} + HOC_6H_4NO_2^{\bullet -} \rightarrow HOC_6H_4N(O)^{-}H + HOC_6H_4NO_2 \quad (5.7)$$

$$HOC_6H_4NOH^{-} + HOC_6H_4NO_2 \rightarrow HOC_6H_4NHOH +^{-} OC_6H_4NO_2 \quad (5.8)$$

The reduction of 4-nitrosophenol should be thermodynamically feasible, since it was found ex-

perimentally that the nitroso intermediate is readily reducible at the potential of formation (see section 5.3.4 below). Using this set of parameters was sufficient to remove B from the diffusion layer (confirmed by analysing the concentration profile generated by DigiSim®), hence removing the back peaks in the simulation, and matching up well with the experimental results. Further steps were proposed by Amatore *et al.*[1] First, dehydration of the hydroxylamine to benzoquinonimine:

$$HOC_6H_4NHOH \rightarrow OC_6H_4NH + H_2O \tag{5.9}$$

This then undergoes further homogeneous electron and proton transfers, until eventually the amine is formed, the overall reaction being:

$$7HOC_6H_4NO_2 + 6e^- \rightarrow HOC_6H_4NH_2 + 6^-OC_6H_4NO_2 + H_2O \tag{5.10}$$

It was found that the inclusion of reaction 5.9 and the steps which followed had very little effect on the simulated voltammetry, suggesting that this was kinetically insignificant in the set of parameters required for simulation. This is consistent with experiments in the next section which suggest that wave IV can be attributed to the oxidation of phenylhydroxylamine, suggesting its homogeneous consumption cannot be fast on the experimental timescale. This would suggest that, under these voltammetric conditions, the reduction is incomplete and only reaches the hydroxylamine stage.

The above mechanism gave good fits for both the forward and reverse scans of 8 mM 4-nitrophenol (not including wave III), but the same set of parameters were insufficient to fit all scan rates studied. In order to provide enough current for peak II at higher scan rates, an additional heterogeneous step was added at the potential of the second wave, which corresponds to the reduction of the protonated nitrophenol radical. Again, this is not unreasonable given that the homogeneous reduction of this species appears in the scheme in Figure 5.2.

Attempts were also made to fit the reversible wave (III). A number of possibilities were taken into consideration, including the direct reduction to the dianion, to which this wave had been loosely attributed to in DMF.[17] From studying the above equations however, it can be seen that the only species present in the reaction layer at a high enough concentration to produce a reduction wave so large is the 4-nitrophenolate anion; the simulated reversible reduction of any other species in this mechanism led to a wave considerably smaller than that observed experimentally, even when involving two electrons. Although the fits for this wave are not as close as those for waves I and II, the phenolate reduction appears to be the only possible rationalisation for wave III. The one electron reduction of this species to the corresponding dianion (Q) is likely to occur at a more negative potential than that of the neutral parent on the grounds of electrostatic arguments, and so its appearance at this position in the voltammetry is not unexpected. In order to confirm this proposal, the voltammetric reduction of 4-nitrophenolate was attempted. A reductive peak was observed at approximately the same potential (-1.88 V *vs* Ag) as peak III, and showed a similar wave shape (regarding the sharpness and transient behaviour). However, despite prolonged drying under vacuum, this peak remained irreversible, possibly due to the rapid protonation of the dianion by protons from residual water, which outnumber the dianion. It is also possible that the sodium cation plays a role. Although within the mechanism proposed, it is surprising that peak III is reversible (since the dianion is obviously a strong base) it is not unreasonable, since at the potential of wave III, the concentration of proton sources (such as 4-nitrophenol and its reduction products) is significantly depleted in the diffusion layer, the relative concentration of the nitrophenolate at this point is high.[25]

The final parameters used in the simulation are given in Table 5.1. The limiting processes were found to be the equilibrium constant of the first protonation reaction (A + B = C + D) and the rate of reaction (B + C = A + E), as shown in the scheme in Figure 5.2. All other homogeneous processes appear to be relatively fast.

Table 5.1: Parameters employed in the simulation of 4-nitrophenol voltammetry.

Heterogeneous	E_0 / V	α	k_0 / cm s^{-1}
A + e^- = B	-0.89 to -0.94	0.4	0.0001
C + e^- = E	-1.05 to -1.09	0.5	100
D + e^- = Q	-1.76 to -1.83	0.5	1×10^{-5}

Homogeneous	K_{eq}	k_f / M^{-1} s^{-1}
A + B = C + D	100-150	$\geq 1 \times 10^7$
B + C = A + E	Pre-determined[§]	1×10^3 to 1×10^4
A + E = F + D	$\geq 1 \times 10^{10}$	2×10^{10}
All others	$\geq 1 \times 10^7$	$\geq 1 \times 10^7$
Diffusion coefficients	All 3.3×10^{-11} m^2 s^{-1}	

[§] The equilibrium constant for this process is determined by the E_0 for the first two heterogeneous processes.

5.3.4 Analysis of Oxidative Peaks (IV and V) for 4-Nitrophenol

Cyclic voltammograms for: (a) the reduction of 4-nitrosophenol, (b) the oxidation of 4-nitrophenolate (sodium salt) and (c) the oxidation of 4-nitrosophenol on a gold electrode (diameter 25 μm) at a scan rate of 100 mV s^{-1} are shown in Figure 5.7, overlaid on the voltammogram of 8 mM 4-nitrophenol. The inset shows a close-up view of the oxidative window. (It should be noted that the problems encountered in investigating the cathodic behaviour of 4-nitrophenolate did not influence the oxidative window of the ionic liquid, and so the anodic voltammetry could be interpreted). On comparing the potential of the anodic waves, this voltammetry would suggest that the nitrophenolate is responsible for peak V, as opposed to nitrosophenol. This is consistent with the mechanism proposed, in that the concentration of the nitrophenolate is likely to greatly exceed that of nitrosophenol at the surface of the electrode, especially since the nitroso group can be reduced at potentials less negative than -1.5 V *vs* Ag; this fact is evident from the nitrosophenol reduction wave shown in Figure 5.7 (dot-dashed line).

There has been much speculation in the literature as to the identity of peak IV at +0.13 V *vs* Ag (and its corresponding reduction peak at -0.29 V *vs* Ag, which was noted earlier). Hu *et al.*[30] reported a redox couple at approximately +0.2 V *vs* Pt in aqueous NaH_2PO_4 (at pH 4.5)

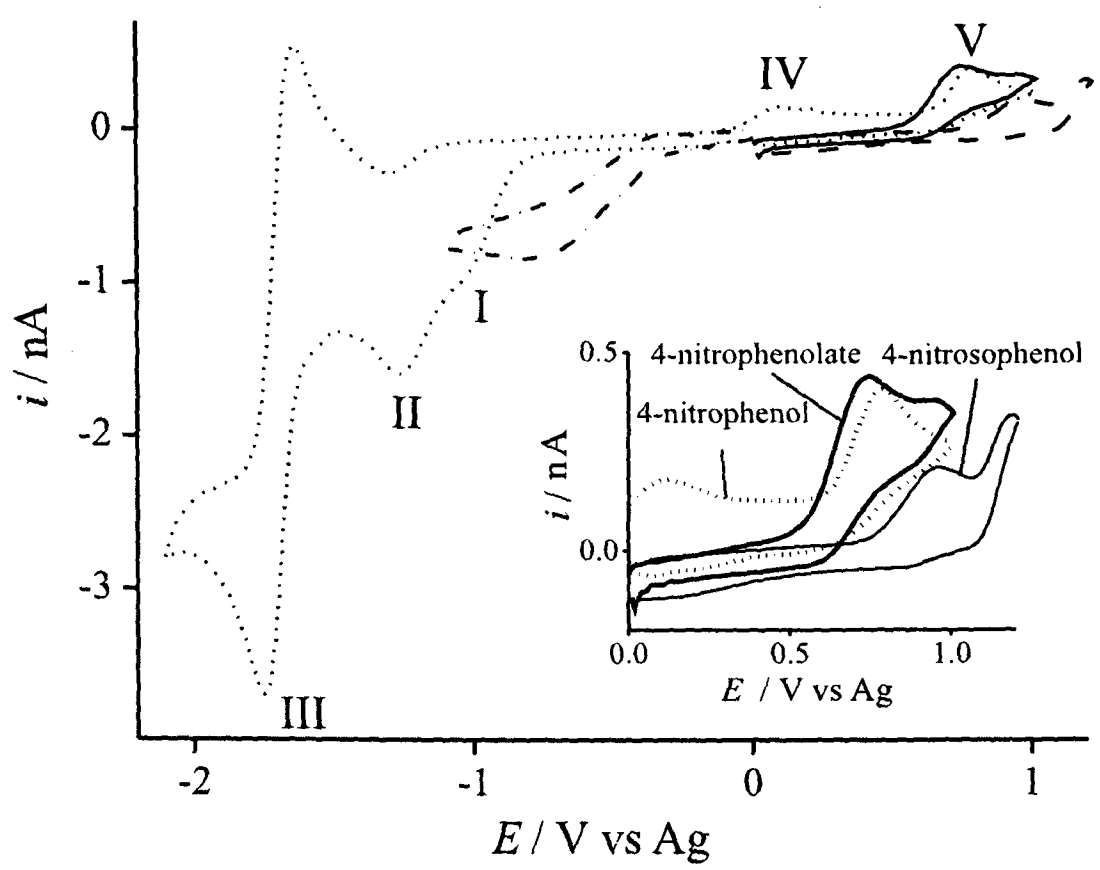

Figure 5.7: Typical cyclic voltammograms showing: the reduction of 4-nitrosophenol (dot dash dot), the full redox window of 4-nitrophenol (dots), the oxidation of 4-nitrophenolate (sodium salt) (solid line), the oxidation of 4-nitrosophenol (dashes) in $[C_4dmim][NTf_2]$. The inset shows the oxidative window in more detail.

on a modified glassy carbon electrode, and assigned this to the reversible two-electron oxidation of 4-hydroxyphenylhydroxylamine to 4-nitrosophenol. Amatore *et al.*[1] mention the appearance of an anodic peak for 2-nitrophenol in DMSO, and suggest this is the oxidation of 2-hydroxyphenylhydroxylamine due to its slow dehydration to benzoquinonimine. A phenylhydroxylamine/nitrosobenzene redox couple has also been widely reported in the literature for the reduction of nitrobenzene in a range of solvents, including molten acetamide,[8] methanol[7] and THF.[31] Several groups attribute a similar peak (close to 0 V *vs* Ag/Pt) for nitrobenzene to the azoxybenzene/azobenzene[10] or the head-to-tail coupled dimer[9] redox couple. This cannot be ruled out entirely, but, in the case of 4-nitrophenol, the latter is unlikely to form due to the presence of the hydroxyl group, and generation of the former requires the presence of an acid (*e.g.* benzoic acid).[9] Furthermore, Elbs[32] reported that contrary to other aromatic nitro compounds, 4-nitrophenol does not give the corresponding azoxy, azo or hydrazo compound,

but instead gives 4-aminophenol. We therefore propose in light of the mechanism suggested by Amatore and the findings of the DigiSim® analysis above, that peak IV corresponds to the oxidation of 4-hydroxyphenylhydroxylamine to 4-nitrosophenol.

5.4 Conclusions

The electrochemical reductions of nitrobenzene and 4-nitrophenol have been studied in the room temperature ionic liquid $[C_4dmim][NTf_2]$. In the case of nitrobenzene, a one-electron reduction to the stable radical anion was observed, followed by another process at more negative potentials. The second process was chemically irreversible, possibly resulting from the formation of azoxybenzene, as suggested by chronoamperometric experiments. This was further supported by the appearance of an oxidative peak close to that reported in the literature for the oxidation of azoxybenzene.[9,24] 4-nitrotoluene and 4-nitroaniline showed similar behaviour to nitrobenzene in $[C_4dmim][NTf_2]$, and owing to the viscous nature of this liquid, all three species had diffusion coefficients two orders of magnitude less than in conventional solvents such as DMF.[17]

The reduction of 4-nitrophenol is more complex. The radical anion is rapidly protonated by an acidic parent molecule, resulting in further chemical reactions, following a scheme proposed by Amatore *et al.*[1] Three reductive waves were observed; the first two were irreversible (with the first wave appearing as a shoulder on the larger second wave), and the third wave was chemically reversible. Two further anodic waves were observed on the oxidative sweep, and were attributed to oxidations of product species (the hydroxylamine and 4-nitrophenolate anion) formed during the first two waves. All three reductive waves were successfully simulated at scan rates of 0.01–4 V s^{-1} in DigiSim® and this allowed the following conclusions: (a) the 'split-wave' feature arises from the initial reduction of a parent molecule, and the reaction of the radical anion with a second parent molecule (b) the reduction is thought to proceed only to the hydroxylamine in this medium (c) the third reversible wave is most likely the one-electron reduction of 4-

nitrophenolate, which is a product species resulting from the initial reaction scheme. Equilibrium and rate constants were determined for each homogeneous reaction. The reduction was found to be kinetically limited by the equilibrium and rate constants of two reactions.

To summarise, the electrochemical behaviour of 4-nitrophenol in an ionic liquid most likely follows the same mechanism as that in DMF[17] and DMSO,[1] but significant differences appear in the voltammetric response due to the much smaller diffusion coefficients in this highly viscous medium.

It has been shown in this chapter that the electrochemical reduction of the organic solutes, nitrobenzene and 4-nitrophenol, likely follow the same mechanism as in conventional solvents such as DMF. The differences in the voltammetry appear to be due to the difference in the kinetics of the heterogeneous and homogeneous steps, mainly due to the higher viscosity of RTIL media. In the next few chapters, we turn to look at the electrochemical mechanisms of several inorganic species dissolved in RTIL media. In chapter 6, we report the electrochemical mechanism of phosphorus trichloride and phosphorus oxychloride. The electrochemical mechanisms of these compounds have not been studied in detail previously, due to the instability of the molecules in conventional media. However, we show that ionic liquids provide a unique environment for the stabilty of such molecules, and allows the detailed study of these compounds for the first time.

References

[1] Amatore, C.; Capobianco, G.; Farnia, G.; Sandonà, G.; Savéant, J. M.; Severin, M. G. and Vianello, E., *J. Am. Chem. Soc*, 1985, **107**, 1815–1824.

[2] Silvester, D. S.; Wain, A. J.; Aldous, L.; Hardacre, C. and Compton, R. G., *J. Electroanal. Chem.*, 2006, **596**, 131–140.

[3] Fry, A. J. and Peters, D. G., *Proc. Electrochem. Soc.*, 2002, **10**, 77–80.

[4] Kemula, W. and Sioda, R., *Bull. Acad. Polonaise Sci.*, 1962, **10**, 507–512.

[5] Pelekourtsa, A.; Missaelidis, N. and Jannakoudakis, D., *Chim. Chron.*, 1997, **26**, 39–48.

[6] Zuman, P. and Fijalek, Z., *J. Electroanal. Chem. Interfacial Electrochem.*, 1990, **296**, 583–588.

[7] Kokkinidis, G.; Karabinas, P. and Jannakoudakis, D., *Chim. Chron.*, 1981, **10**, 193–201.

[8] Saraswathi, R. and Narayan, R., *Bull. Electrochem.*, 1988, **4**, 157–162.

[9] Steudel, E.; Posdorfer, J. and Schindler, R. N., *Electrochim. Acta*, 1995, **40**, 1587–1594.

[10] Asirvatham, M. R. and Hawley, M. D., *J. Electroanal. Chem. Interfacial Electrochem.*, 1974, **57**, 179–190.

[11] Chon, J. K. and Paik, W. K., *Bull. Korean Chem. Soc.*, 1983, **4**, 55–57.

[12] Smith, W. H. and Bard, A. J., *J. Am. Chem. Soc*, 1975, **97**, 5203–5210.

[13] Jensen, B. S. and Parker, V. D., *J. Chem. Soc., Chem. Commun.*, 1974, **10**, 367–368.

[14] Marquez, J. and Pletcher, D., *J. Appl. Electrochem.*, 1980, **10**, 567–573.

[15] Sun, Y.; Xu, W. and Scott, K., *Electrochim. Acta*, 1993, **38**, 1753–1759.

[16] Cyr, A.; Huot, P.; Belot, G. and Lessard, J., *Electrochim. Acta*, 1990, **35**, 147–152.

[17] Forryan, C. L.; Lawrence, N. S.; Rees, N. V. and Compton, R. G., *J. Electroanal. Chem.*, 2004, **561**, 53–65.

[18] Farnia, G.; Roque Da Silva, A. and Vianello, E., *J. Electroanal. Chem. Interfacial Electrochem.*, 1974, **57**, 191–202.

[19] Heras Caballero, A. M.; Avila Manzano, J. L.; Camacho Delgado, L. and Garcia Blanco, F., *Afinidad*, 1986, **43**, 76–79.

[20] Saraswathi, R. and Narayan, R., *J. Electrochem. Soc. India*, 1990, **39**, 129–138.

[21] Kemula, W. and Sioda, R., *J. Electroanal. Chem.*, 1964, **7**, 233–241.

[22] Kemula, W. and Krygowski, T. M., *Encyclopedia of Electrochemistry of the Elements*, ed. Bard, A. J. and Lund, H., Marcel Dekker, New York, USA, 1979.

[23] Dieter, K. M.; Dymek, Chester J., J.; Heimer, N. E.; Rovang, J. W. and Wilkes, J. S., *J. Am. Chem. Soc.*, 1988, **110**, 2722–2726.

[24] Lipsztajn, M.; Krygowski, T. M. and Galus, Z., *J. Electroanal. Chem. Interfacial Electrochem.*, 1977, **81**, 347–356.

[25] Note: The availability of only strictly finite quantities of the ionic liquid solvent precluded detailed exploration.

[26] Okoturo, O. O. and VanderNoot, T. J., *J. Electroanal. Chem.*, 2004, **568**, 167–181.

[27] Lide, D. R., Ed., *Handbook of Chemistry and Physics: 76th Edition*, CRC Press, Boca Raton, USA, 1996.

[28] Rudolph, M.; Reddy, D. P. and Feldberg, S. W., *Anal. Chem.*, 1994, **66**, 589A–600A.

[29] Allen, G. D.; Buzzeo, M. C.; Villagrán, C.; Hardacre, C. and Compton, R. G., *J. Electroanal. Chem.*, 2005, **575**, 311–320.

[30] Hu, S.; Xu, C.; Wang, G. and Cui, D., *Talanta*, 2001, **54**, 115–123.

[31] Gard, J. C.; Lessard, J. and Mugnier, Y., *Electrochim. Acta*, 1993, **38**, 677–680.

[32] Elbs, K., *Z. Elektrochem. Angew. Phys. Chem.*, 1900, **7**, 133–141.

Chapter 6

An Electrochemical Study of PCl_3 and $POCl_3$ in the RTIL $[C_4mpyrr][NTf_2]$

Voltammetric studies of PCl_3 and $POCl_3$ have rarely been reported in the literature to date, probably due to the instability of these molecules in conventional aprotic solvents giving unstable and irreproducible results. From a previous study,[1] it was found that ionic liquids have the ability to offer a uniquely stable solution phase environment for the study of these phosphorus compounds. Consequently, in this chapter, the electrochemistry of PCl_3 and $POCl_3$ is studied on a gold microelectrode in the ionic liquid $[C_4mpyrr][NTf_2]$ (*N*-butyl-*N*-methylpyrrolidinium bis(trifluoromethylsulfonyl)imide). For both compounds, reduction and oxidation waves are observed and a tentative assignment of the waves is given. For PCl_3, the reduction is thought to proceed *via* a mechanism involving a one-electron transfer. For $POCl_3$, the suggested reduction mechanism is analogous to PCl_3. It is found that the diffusion coefficient of PCl_3 is unusually slow (3.1×10^{-12} m^2 s^{-1}), *ca.* one order of magnitude less than that for $POCl_3$ (2.2×10^{-11} m^2 s^{-1}). This work has been published in the Journal of Physical Chemistry B.[2]

6.1 Introduction

In this chapter, the electrochemistry of PCl_3 (phosphorus trichloride) in a $[NTf_2]^-$ based ionic liquid is reported. The world production of PCl_3 exceeds one-third of a million tonnes,[3] making it a useful and important compound to study. PCl_3 is a reducing agent, being readily oxidised to phosphorus pentachloride or phosphorus oxychloride. It reacts rapidly and exothermically with water to form phosphorous acid, H_3PO_3 and HCl.[4] PCl_3 is used directly as a reagent in organic synthesis, for example to convert primary and secondary alcohols into alkyl chlorides, carboxylic acids into acyl chlorides and primary nitro compounds into nitriles.[4]

PCl_3 is an important starting point for the manufacture of many industrial products containing phosphorus. It is used on an industrial scale to make phosphonates,[5] the herbicide glyphosate,[6] triphenylphosphine for the Wittig reaction,[7] and phosphate esters which may be used as industrial intermediates or in the Horner-Wadsworth-Emmons reaction,[8] both important methods for making alkanes. It is also used as the starting material for the manufacture of insecticides such as diazinon,[9] and of organic phosphates such as triphenyl phosphate and tricresyl phosphate, which have applications as flame retardants[10] and plasticisers for PVC.[11]

Literature data on electrochemical studies of phosphorus halogen compounds is scarce. The electroreduction of PCl_3, PBr_3 and PI_3 was reported by Kisil′ *et al.*[12] in thoroughly dehydrated acetonitrile on a dropping mercury electrode, although no cyclic voltammetry was shown. They claimed that the reduction was "controlled by diffusion and was irreversible". They reported an $E_{1/2}$ value of -0.915 V *vs* mercury pool, an electron count of 1, a transfer coefficient, α, of 0.311, and a standard electrochemical rate constant, k_0, of 1.3×10^{-7} cm s^{-1} using an LP-60 polorograph. From these findings, they proposed some simple equations for the reduction of PCl_3, which are shown below:

$$PCl_3 + e^- \rightarrow^{\bullet} PCl_2 + Cl^- \tag{6.1}$$

and further chemical reactions, *e.g.*

$$2^{\bullet}PCl_2 \rightarrow PCl_3 + PCl \tag{6.2}$$

$$3PCl + 3Hg \rightarrow Hg_3P_2{\cdot}PCl_3 \tag{6.3}$$

Berberova[13] reported the *oxidation* of PCl_3 on a platinum disk electrode, but again, no cyclic voltammetry was shown. The oxidation wave of PCl_3 in acetonitrile was extremely unstable and disappeared after applying several voltage pulses. PCl_3 was found to be most stable in methylene chloride with TBAP, or sodium perchlorate with a crown ether (dibenzo-16-crown-6). A single electron oxidation wave was reported on Pt at +1.58 V *vs* Ag/AgCl, which was

partially reversible and diffusion limited. The radical cation of PCl_3 was also confirmed to be present in solution by electrochemical and ESR data in a different study.[14]

In both these studies,[12,13] no voltammetry was shown, and diffusion coefficients for PCl_3 were not calculated. It is a similar story for $POCl_3$ (phosphorus oxychloride); no voltammetry is reported in the literature. Berberova[13] states that reduction waves of phosphorus oxychloride were observed at -0.21 V and -2.06 V *vs* Ag/AgCl, but mentions nothing about the size, shape and/or reversibility of the waves. Various groups[15–17] have attached electrons to gas phase molecules of $POCl_3$ and have proposed equations which ultimately result in the formation of chloride ions, amongst other products.

Amigues *et al.*[1] recently discovered that both PCl_3 and $POCl_3$ were unusually stable in ionic liquid media. Their stability was dependent on mainly upon the identity of the anion, but changing both the anion and cation had some effect. PCl_3 was found to be most hydrolytically stable (> 95%) in the RTIL *N*-butyl-*N*-methylpyrrolidinium bis(trifluoromethylsulfonyl)imide ($[C_4mpyrr][NTf_2]$) for weeks, even when stirred in air and without drying the ionic liquid. Conversely, $POCl_3$ hydrolysed rapidly in wet ILs, even those based on $[NTf_2]^-$ anions, with the exception of $[C_5mim][FAP]$ (1-pentyl-3-methylimidazolium tris(perfluoroalkyl)trifluorophosphate). They reported the formation of various hydrolysis products, resulting either from reaction with the ionic liquids or from reaction with the water naturally present in the solvent (0.1 wt % water even in 'dry' ILs). The products were identified by NMR and included species such as HPOClOH, $PO(OH)_2Cl$, PF_3 (from $[BF_4]^-$ anions), $HPO(OTf)_2$ (from $[OTf]^-$ anions), $POCl_2$ (OMs) (from $[OMs]^-$ (methylsulfonate) anions) and $PO(OH)_2Cl$, amongst others. It is surprising that, given the higher water content of 'dry' ILs (0.01 wt. %) compared to organic solvents (dry THF, 0.005 wt %), ionic liquids have shown to offer a more stable environment than organic solvents for storage of PCl_3 and $POCl_3$. This work reports the electrochemistry of PCl_3 and $POCl_3$ and chloride ($[C_4mpyrr]Cl$) in $[C_4mpyrr][NTf_2]$.

6.2 Experimental

PCl_3 and $POCl_3$ were kept under a constant stream of dried nitrogen whilst handling. A three-electrode arrangement was employed, with a gold microelectrode (diameter 25 μm) as the working electrode, Ag/Ag^+ as the reference electrode, and a platinum coil wire as the counter electrode. The electrodes were placed in a specially designed cell for volumes from 1-5 mL. This consisted of a glass vial topped with a 15 mm thick cylinder of PTFE with four holes of specific diameter (three for the electrodes and one for the nitrogen line), so as to keep a closed system throughout the measurements. The cell was housed in a Faraday cage in order to minimize background noise.

Since the chemicals under study were not stable in conventional solvents such as acetonitrile, the solvent evaporation procedure (see Chapter 3) could not be employed. Instead, solutions of $[C_4mpyrr]Cl$, PCl_3 and $POCl_3$ were made up directly in 2 mL ionic liquid to roughly 15 mM concentrations. The ionic liquid was dried at 343 K under high vacuum for at least 48 hours prior to use, then stored under nitrogen. The solutions were further purged throughout the experiments by bubbling dried nitrogen into the solution. It should be noted that due to the instability of PCl_3 and $POCl_3$ in air, the chemicals were only useful for one experiment before redistilling was required. However, in the ionic liquid, the voltammetry was stable for weeks in the case of PCl_3, but only hours for $POCl_3$. The behaviour of PCl_3 and $POCl_3$ in the ionic liquid changed after a long period of time when exposed to air. This gave rise to extra peaks in the voltammetry, probably due to the reduction and/or oxidation of electroactive hydrolysis products. Interestingly, in a different batch of the same ionic liquid, solutions became opaque/cloudy soon after conducting electrochemical experiments, possibly due to the larger water content in this batch. We also note that the voltammetry of concentrations of PCl_3 above 30 mM was unstable, and accurate data could not be obtained. Concentrations below 15 mM PCl_3 were also not easily achieved, since this required a larger volume of the ionic liquid solvent

(only small amounts were available), and the resulting solutions will contain a larger water to PCl_3 ratio, which will likely affect the stability of PCl_3.

6.3 Theory

The reductions of both PCl_3 and $POCl_3$ (see section 6.4) gave rise to a 'split-wave' phenomenon, where two peaks arise close together, with the first resembling a shoulder on the second, larger wave. This behaviour is approximately similar to that observed in Chapter 5. Chronoamperometry (see later) revealed that, in both cases, the overall electron count was 1. The discussion below describes how the 'split-waves' of PCl_3 and $POCl_3$ (reported in section 6.4) were simulated using the one-dimensional digital simulation program DigiSim® 3.03 (BAS Technicol),[18] applying a single one-electron transfer step with subsequent follow-up chemistry.

6.3.1 Modelling the Reduction of PCl_3 and $POCl_3$ in DigiSim®

It was found that a one-electron 'split-wave' could be successfully simulated using the simple generic reaction scheme:

$$A + e^- = B \tag{6.4}$$

$$B + A = C + D \tag{6.5}$$

Figure 6.1 shows a simulated cyclic voltammogram following this generic reaction scheme over the voltage range studied experimentally. The cathodic wave was simulated to be electrochemically irreversible, in line with experimental voltammograms. The simulation also revealed a significant anodic back peak. Figure 6.1b shows simulated voltammograms at scan rates of 100 mV s^{-1}, employing different values for the standard electrochemical rate constant, k_0, over 5 orders of magnitude (10^{-5}, 10^{-7}, 10^{-9}, and 10^{-10} cm s^{-1}), with an equilibrium constant, K_{eq}, for equation 6.5 of 50 in all cases. It can be seen that the separation between the cathodic and

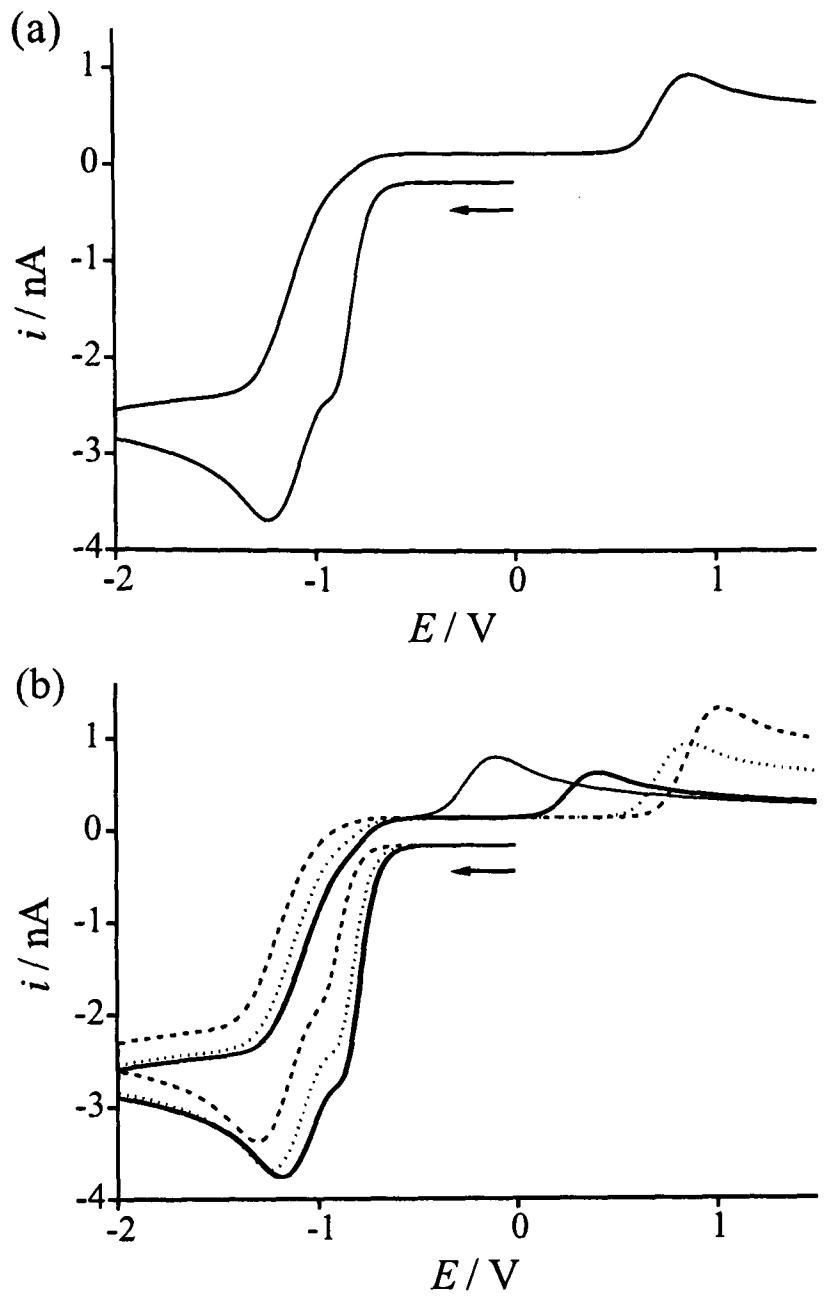

Figure 6.1: Simulated voltammograms of the reductive 'split-wave' of PCl_3, at a scan rate of 100 mV s^{-1}, obtained from the generic scheme given by equations 6.4 and 6.5. (a) The best fit to the experimental data (see section 6.4.1), using a standard electrochemical rate constant, k_0, of 1×10^{-9} cm s^{-1} and a K_{eq} value of 50 (α=0.5, E_0=-0.75 V). (b) The effect of employing various k_0 values: (thin solid line) 10^{-5} cm s^{-1}, (thick solid line) 10^{-7} cm s^{-1}, (dotted line) 10^{-9} cm s^{-1} and (dashed line) 10^{-10} cm s^{-1}, with a K_{eq} value of 50, other parameters adjusted accordingly.

anodic peaks significantly increases when k_0 is decreased. By employing a k_0 value of 10^{-9} cm s^{-1} (Figure 6.1a) and by careful selection of the kinetic parameters, it was possible to simulate the shape of the double wave, and position a back-peak corresponding to that of peak II (see section 6.4.1)

However, this simple reaction scheme was not sufficient enough to simulate the reductive waves of PCl_3 and $POCl_3$ over a wide range of scan rates (0.01–4 V s^{-1}). It was found that

dividing equation 6.5 into two separate equations allowed more manipulation of kinetic parameters which in turn made it easier to simulate the peak potentials and wave shapes for both PCl_3 and $POCl_3$ over this range of scan rates. The generic scheme used in the final simulation of the reductive waves of PCl_3 and $POCl_3$ is shown below:

$$A + e^- = B \tag{6.6}$$

$$B = C + D \tag{6.7}$$

$$C + A = E \tag{6.8}$$

The theoretical simulations fitted the experimental data approximately, even though the shapes of the reductive waves of PCl_3 and $POCl_3$ are quite unusual and complicated (because of irreversibility and slow diffusion). The mechanistic analysis shown above is thought to be the minimum sufficient to explain the appearance of a one electron 'split-wave' feature for both species. The kinetic parameters used in the simulations are discussed in section 6.4.1 for PCl_3 and in section 6.4.2 for $POCl_3$.

Given the second order nature of some of the reactions in the scheme defined by equations 6.6, 6.7 and 6.8, the simulations were performed for variable substrate concentrations and also for different concentrations of added chloride. In each case, the effect was quantified by monitoring the size of the shoulder on the larger wave relative to the size of the latter, as quantified by the fraction f ($0 \leq f \leq 1$), where $f = 0$ corresponds to no shoulder. The results are discussed below.

6.4 Results and Discussion

The ionic liquid $[C_4mpyrr][NTf_2]$ was used as the solvent in all electrochemical experiments throughout this work, since this was shown[1] to be a highly suitable solvent in which to store PCl_3 for long periods of time, and $POCl_3$ for a few hours. It also had a very clean and featureless electrochemical baseline.

6.4.1 Voltammetry of PCl_3 in $[C_4mpyrr][NTf_2]$

Figure 6.2a shows a typical cyclic voltammogram obtained for the reduction of 14.8 mM PCl_3 on a gold microelectrode (diameter 25 μm) in $[C_4mpyrr][NTf_2]$, at a scan rate of 100 mV s^{-1}. A second scan is overlaid (dots), which shows a decrease in the size of the reduction peak, I. It is thought that this is due to the slow diffusion of the electroactive species from the electrode surface. This is exemplified by Figures 6.2b and 6.2c, recorded at scan rates of 10 mV s^{-1} and 1 V s^{-1} respectively, under the same conditions. A scan rate of 10 mV s^{-1} (Figure 6.2b) is slow enough to allow diffusion of reduced material away from the surface, whereas at faster scan rates (1 V s^{-1}, Figure 6.2c) the rate of diffusion is outrun. It is interesting that the reductive peak appears as a 'split-wave' at all scan rates, similar to that reported for the oxidation of bromide in $[C_2mim][NTf_2]$,[19] and for the reduction of 4-nitrophenol in $[C_4dmim][NTf_2]$ (see Chapter 5). In both of these cases, the 'split-wave' was attributed to the initial reduction of a parent molecule, followed by reaction of this reduced species with another parent molecule ($A + e^- \rightarrow B$, and $B + A \rightarrow$ products). It is likely that an analogous process is happening here, according to equations 6.9, 6.10 and 6.11.

$$PCl_3 + e^- \rightleftharpoons PCl_3^- \tag{6.9}$$

$$PCl_3^- \rightleftharpoons Cl^- +^{\bullet} PCl_2 \tag{6.10}$$

$$Cl^- + PCl_3 \rightleftharpoons PCl_4^- \tag{6.11}$$

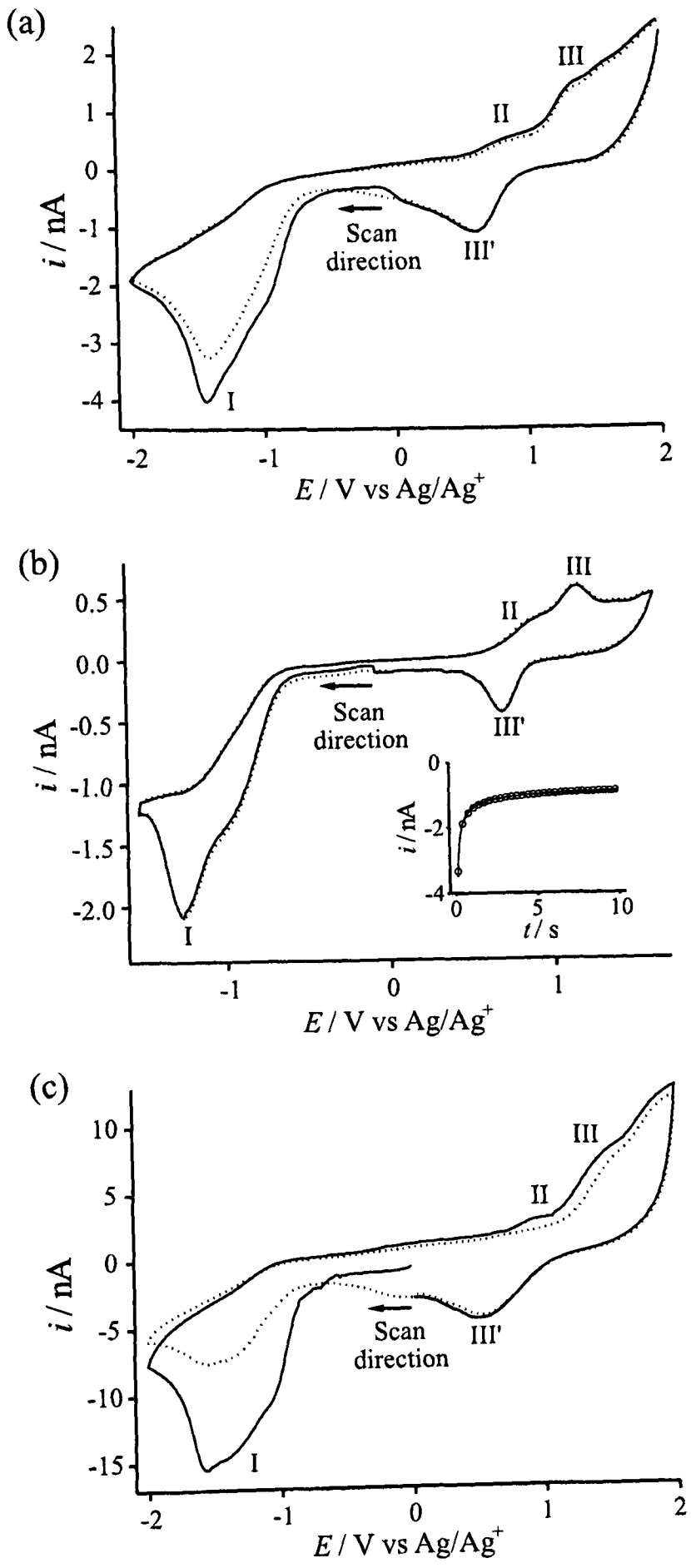

Figure 6.2: Cyclic voltammetry for the reduction of 14.8 mM PCl_3 in $[C_4mpyrr][NTf_2]$ on a gold microelectrode (diameter 25 μm) at scan rates of (a) 100 mV s^{-1}, (b) 10 mV s^{-1} and (c) 1 V s^{-1}. First scan is shown as a solid line; second scan is shown as dots. The inset figure shows the experimental (solid line) and fitted theoretical (circles) chronoamperometric transient obtained under the same conditions. The potential was stepped from 0.0 V to -2.0 V.

In this mechanism, the parent molecule is initially reduced by one electron, followed by chemical dissociation to chloride and a radical species. Chloride then reacts with a second parent molecule to form PCl_4^-. Section 6.3 describes how the reductive wave of PCl_3 can be explained (by digital simulation) to proceed by the proposed reaction scheme (equations 6.9, 6.10 and 6.11). There may also be further reactions which consume the radical $^{\bullet}PCl_2$, although these were not included in the simulation.

The reductive wave, I, is electrochemically irreversible at all scan rates studied (0.01–4 V s^{-1}), and the equilibrium position of reaction 6.11 is shifted towards the product PCl_4^- in accordance with DigiSim® fits. The reduction does not appear to be fully *chemically* irreversible, if the back peak II relates to the re-oxidation of PCl_4^-. The peak potential of wave I occurs at -1.45 V *vs* Ag/Ag^+ (at a scan rate of 100 mV s^{-1}), which is 0.54 V more negative than that observed by Kisil' *et al.*[12] *vs* mercury pool in anhydrous acetonitrile. A distinct one-electron wave was reported for the reduction in acetonitrile,[12] indicating that the 'split-wave' seen here is a feature of the slower diffusion in the ionic liquid, probably *via* promotion of second order follow-up kinetics.

The best theoretical fit to the experimental 'split-wave' was achieved (assuming a transfer coefficient, α, of 0.5) when the following conditions applied: (a) the rate constant for the electrochemical step, k_0, was very slow (*ca.* 1×10^{-9} cm s^{-1}, two orders of magnitude smaller than in MeCN)[12] subject to the assignment of peak II discussed below, (b) the forward rate constant, k_f, for the both the homogeneous reactions (equations 6.10 and 6.11) were made to be fast ($> 1 \times 10^7$ s^{-1}), and (c) when the equilibrium constant, K_{eq}, of equation 6.11 was shifted towards the product PCl_4^- (in the range 50 to 100 mol^{-1} dm^3). It is therefore thought that peak II is either: (a) a back-peak resulting from the reduction scheme (Figure 6.1, following equations 6.9, 6.10 and 6.11) or (b) the oxidation of chloride on a filmed electrode (see section 6.4.4), or a combination of both. If (a) is not the case, then it is possible that the rate constant for the

electrochemical step, k_0, is smaller than 1×10^{-9} cm s^{-1}, which would shift the back peak to an even more positive than the peak potential of wave II (and would appear somewhere under wave III). The electrochemical rate constant is clearly unusually small, raising the possibility that cleavage of the P–Cl bond may be concerted (electron transfer and bond cleavage take place together) in the ionic liquid medium studied. In this case, peak II could be related to the oxidation of PCl_4^-. The identity of peaks III and III′ are thought to be due to the oxidation of $POCl_3$, formed from PCl_3, and will be discussed later in section 6.4.4, based on comparisons in peak potential with that of $POCl_3$.

Steady-state behaviour for the reduction wave of PCl_3 could not be achieved on a 25 μm diameter electrode, even at scan rates as slow as 1 mV s^{-1}, suggesting that diffusion of PCl_3 from the electrode surface is very slow. Chronoamperometry data further supports this observation. The inset to Figure 6.2b shows a chronoamperometric transient obtained for the reduction wave of 14.8 mM PCl_3 on a 25 μm gold microelectrode. The potential was stepped from 0.0 V (corresponding to no faradaic current) to -2.0 V (a potential cathodic of the reductive peak) and the current was measured for 10 s. The fitting of experimental data to the Shoup and Szabo[20] equation gave an approximate diffusion coefficient and electron count as given in Table 6.1. The diffusion coefficient for PCl_3 is very small, even when compared to other species in the same ionic liquid (*cf.* 2.31×10^{-11} m^2 s^{-1} for ferrocene in $[C_4mpyrr][NTf_2]$),[21] suggesting that the diffusion coefficient of PCl_3 is unusually small. The electron count achieved is similar to that reported by Kisil′ *et al.*[12] in dehydrated acetonitrile on a dropping mercury electrode, further supporting the reaction mechanism given by equations 6.9, 6.10 and 6.11.

Interestingly, the diffusion coefficient is similar to that of the self diffusion coefficient of the anion and cation in $[C_4mim][PF_6]$ measured using pulse field gradient NMR.[22] Therein, the anion and cation values were found to be similar between 3 and 6×10^{-12} m^2 s^{-1}. Furthermore preliminary structural data on the dissolution of PCl_3 in 1,3-dimethylimidazolium

Table 6.1: Diffusion coefficients and electron counts obtained from analysis of chronoamperometric potential steps performed on the reductive waves of 14.8 mM PCl_3 and 15.3 mM $POCl_3$ in $[C_4mpyrr][NTf_2]$ at 298 K.

	Diffusion coefficient / $m^2\ s^{-1}$	no. of electrons transferred
Reductive wave of PCl_3	3.1 ($\pm$ 0.2) $\times\ 10^{-12}$	1.05 ($\pm$ 0.04)
Reductive wave of $POCl_3$	2.2 ($\pm$ 0.1) $\times\ 10^{-11}$	1.08 ($\pm$ 0.04)

bis(trifluoromethylsulfonyl)imide ($[C_1mim][NTf_2]$) showed little structural rearrangement of the ionic liquid in the presence of the solute.[23] The combination of the diffusion coefficient and the structural information indicate that the solute dissolves in the interstices of the ionic liquid and that there is a strong interaction with the ionic liquid. For the PCl_3 to move, the interstice must move which requires a motion involving both the anion and cation hence the low diffusion coefficient. This may also contribute to the high stability of the PCl_3 in the $[NTf_2]^-$ based ionic liquids.

Figure 6.3 shows three consecutive scans for the *oxidation* of 14.8 mM PCl_3 on a gold microelectrode (diameter 25 μm) in $[C_4mpyrr][NTf_2]$ at a scan rate of 100 mV s^{-1}, overlaid on that of the first reductive scan (from Figure 6.2a). When the cycle was scanned positively from 0.0 V an additional peak, i, was observed, with a corresponding reductive peak i′. This redox couple was not observed when first scanning reductively, probably due to the consumption of parent molecules in solution (equation 6.11). A potential step could not be performed on the oxidative wave i, since it overlaps with another anodic peak; fitting of chronoamperometric transients would be a combination of wave i and wave II, and data would not be reliable. Peak i can therefore be tentatively assigned to the direct one-electron oxidation of PCl_3, which is partially reversible (peak i′). This is analogous to that observed by Berberova[13] in acetonitrile, and is further supported by an ESR study[14] in acetonitrile which reported the formation of a radical cation of PCl_3.

Next, we considered the possible voltammetric information to be obtained by means of

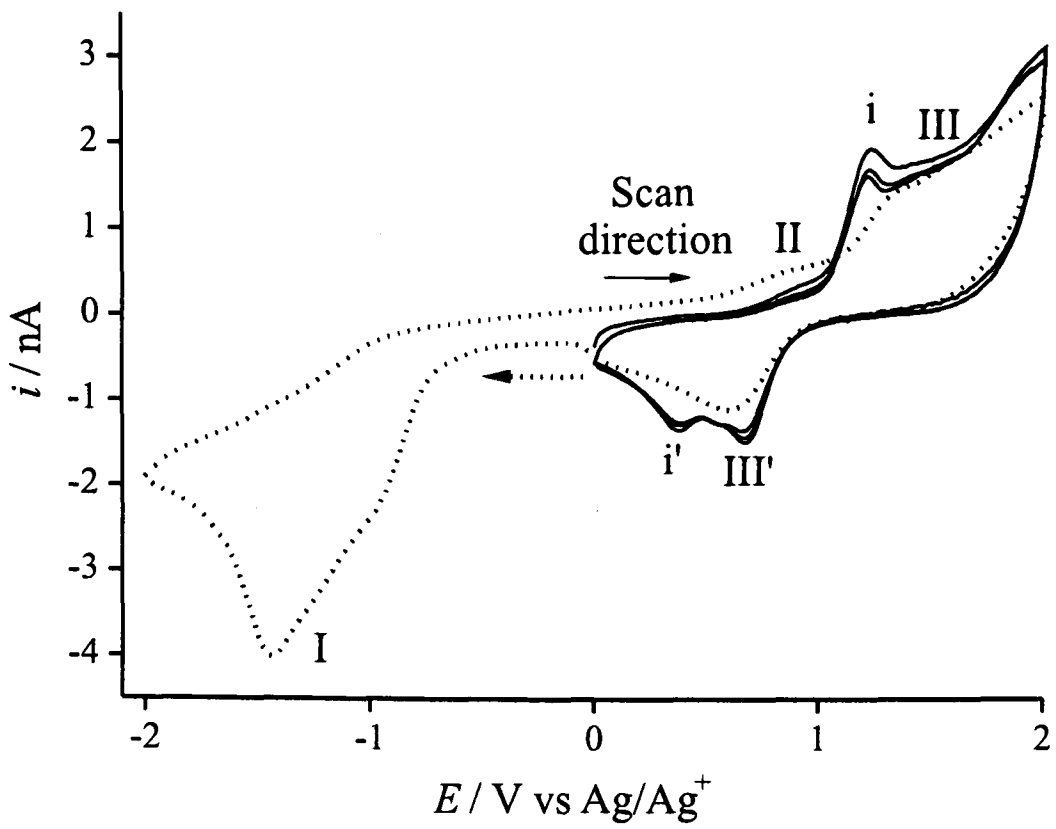

Figure 6.3: Cyclic voltammetry for the oxidation of 14.8 mM PCl_3 in $[C_4mpyrr][NTf_2]$ on a gold microelectrode (diameter 25 μm) at a scan rate of 100 mV s^{-1}. Three repeat scans are shown, overlaid on the reductive cycle from Figure 6.2 (dots).

variable concentration studies as revealed by simulation. First, varying the concentration of PCl_3 over the range 1.5 mM to 150 mM was predicted to change the fraction, f, of current caused by the shoulder (see Theory section 6.3) to vary from 0.55 to 0.51, suggesting that within the likely experimental error, no insights were likely. That said, voltammetric experiments performed using 75 mM, whilst being rather more un-reproducible from scan to scan than those reported above, showed no substantial deviation in the value of f from that obtained using 15 mM, consistent with the predictions of the simulation. Second, simulations were carried out for 15 mM PCl_3 in the presence of 0 to 0.1 M added chloride ions; the value of f varied from 0.55 to 0.49, again suggesting that experiments of this nature would shed little conclusive insight.

6.4.2 Voltammetry of $POCl_3$ in $[C_4mpyrr][NTf_2]$

Partly in order to try to identify whether any of the peaks obtained from the reduction of PCl_3 were due to $POCl_3$, the voltammetry of $POCl_3$ was next studied. Figure 6.4 shows the

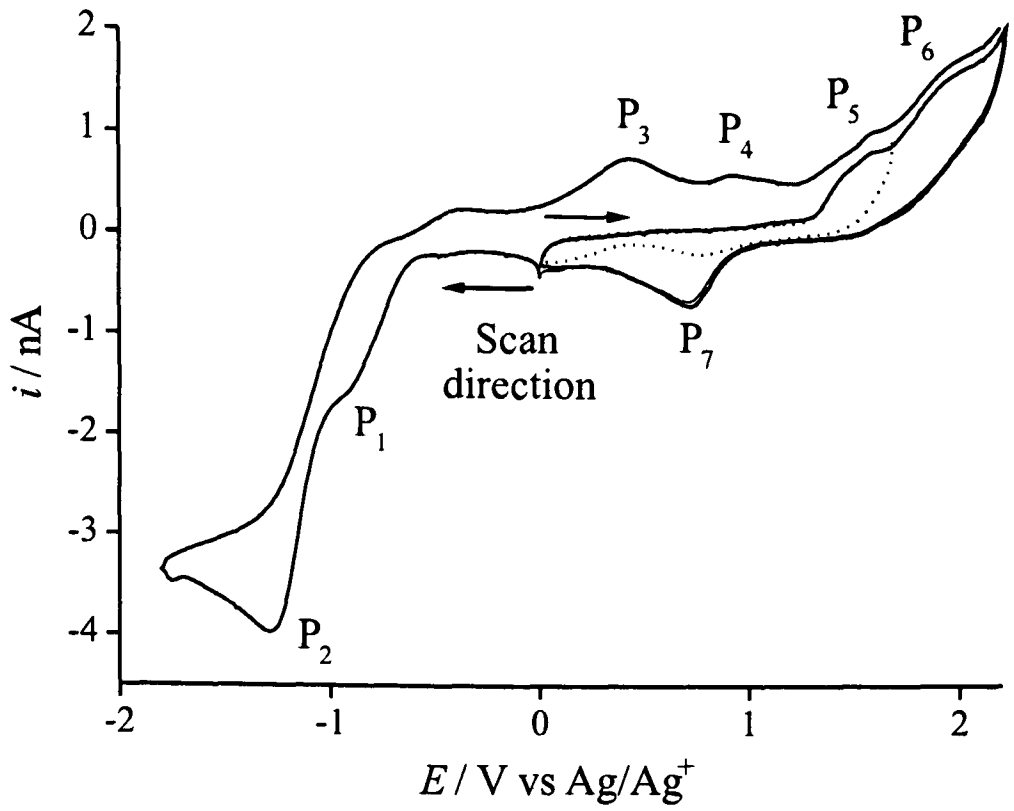

Figure 6.4: Cyclic voltammetry for the reduction of 15.3 mM $POCl_3$ in $[C_4mpyrr][NTf_2]$ on a gold microelectrode (diameter 25 μm) at a scan rate of 100 mV s^{-1}. Two oxidative sweeps are shown with anodic limits of +1.7 V and +2.2 V, respectively.

reduction of 15.3 mM $POCl_3$ on a gold microdisk electrode (diameter 25 μm) in $[C_4mpyrr][NTf_2]$ at a scan rate of 100 mV s^{-1}. The reductive behaviour observed was similar to that of PCl_3 (section 6.4.1) in that a 'split-wave' was seen (waves P_1 and P_2), with a combined electron count of approximately 1 (see Table 6.1). A potential step was performed on the reductive wave from 0.0 V (corresponding to no faradaic current) to -1.8 V (a potential past that of the reductive peak), and fitting to experimental data revealed an electron count of 1, and a diffusion coefficient of 2.2 ($\pm$ 0.1)$\times$ 10^{-11} m^2 s^{-1} for $POCl_3$, which is more comparable in magnitude to other species in ionic liquids (*cf.* 2.31 $\times$ 10^{-11} m^2 s^{-1} for ferrocene in $[C_4mpyrr][NTf_2]$),[21] indicating that diffusion of $POCl_3$ from the electrode surface is not as slow as PCl_3.

The suggested mechanism for the reduction of $POCl_3$ is thought to follow equations 6.12, 6.13 and 6.14, as indicated by digital simulation (see section 6.3).

$$POCl_3 + e^- \rightleftharpoons POCl_3^- \tag{6.12}$$

$$POCl_3^- \rightleftharpoons Cl^- +^\bullet POCl_2 \quad (6.13)$$

$$Cl^- + POCl_3 \rightleftharpoons POCl_4^- \quad (6.14)$$

This is analogous to the reduction scheme proposed for PCl_3 (see section 6.4.1), with the best fit achieved when: (a) the rate constant for the electrochemical step, k_0, was very slow (*ca.* 1×10^{-9} cm s^{-1} or less) assuming peak P_3 in Figure 6.4 relates to the re-oxidation of $POCl_3^-$, and (b) the forward rate constant, k_f, for the both the homogeneous reactions (equations 6.13 and 6.14) were made to be fast ($> 1 \times 10^7$ s^{-1}), and also assuming a value for the transfer coefficient, α, of 0.5. As with PCl_3, it is possible that k_0 for $POCl_3$ is equal to, or smaller than *ca.* 1×10^{-9} cm s^{-1}, which would shift the simulated back-peak to potentials close to that of peaks P_3 and P_4 (Figure 6.4). A k_0 value of *ca.* 1×10^{-9} cm s^{-1} may account for the observation that peak P_3 is larger than peak P_4 (*cf.* chloride oxidation, section 6.4.3), since the back peak from the reduction may add to the current of P_3. The only difference in the parameters used in the simulation was that the equilibrium constant for equation 6.14 was smaller (1–10 mol^{-1} dm^3) than for PCl_3 (50–100 mol^{-1} dm^3), suggesting that $POCl_4^-$ is a less stable species than PCl_4^-. Additionally, the higher diffusion coefficient of $POCl_3$ compared to PCl_3 (see Table 6.1) gives a wave shape closer to steady-state behaviour, but one which is still electrochemically irreversible at all scan rates studied (10 mV s^{-1}–4 V s^{-1}). Peaks P_3 and P_4 are attributed to the oxidation of chloride ions (see section 6.4.3 and 6.4.4) which are formed as a result of the initial reduction of $POCl_3$ from equation 6.13. Peaks P_5, P_6 and P_7 are a result of the oxidation of $POCl_3$. The appearance of these oxidative features were not diminished when first scanning reductively, which further supports the suggestion that the equilibrium of equation 6.14 is not sufficiently shifted towards products (since there will still be a large enough concentration of $POCl_3$ molecules present after reduction to give rise to these oxidative features), or that the diffusion from the electrode surface is much faster than for PCl_3.

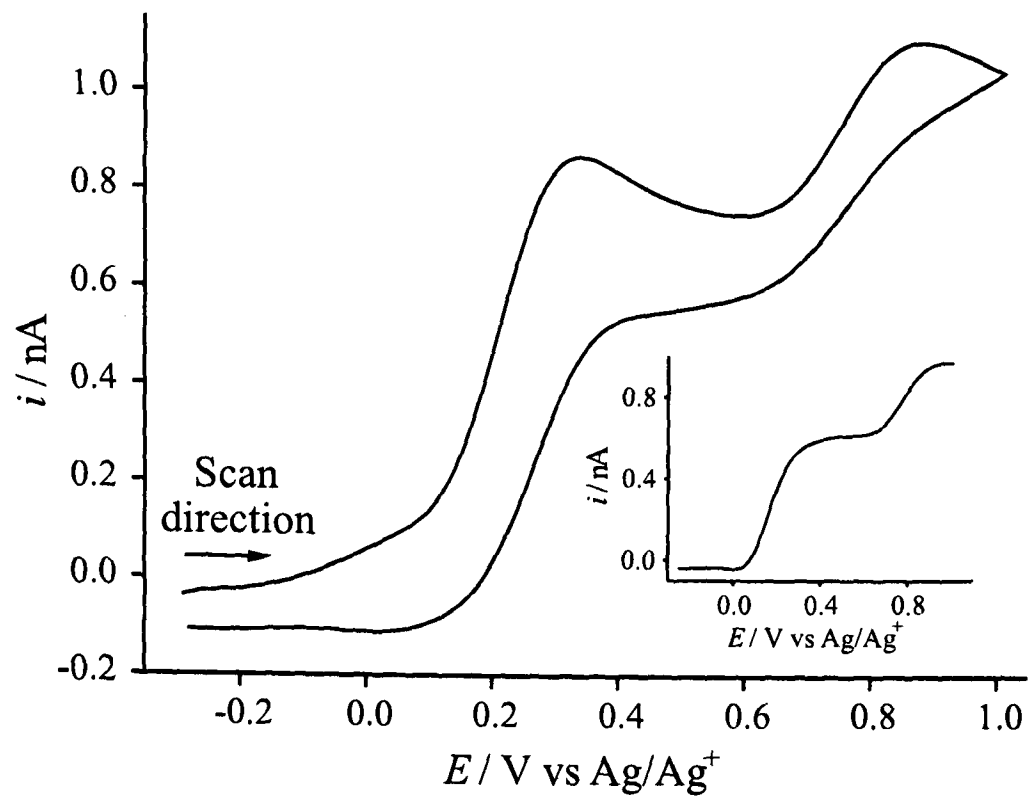

Figure 6.5: Cyclic voltammetry for the oxidation of 15.9 mM chloride (from $[C_4mpyrr]Cl$) in $[C_4mpyrr][NTf_2]$ on a gold microelectrode (diameter 25 μm) at a scan rate of 100 mV s^{-1}. The inset shows a steady-state linear sweep voltammogram under the same conditions, at a scan rate of 5 mV s^{-1}.

6.4.3 Oxidation of Chloride ($[C_4mpyrr]Cl$) in $[C_4mpyrr][NTf_2]$

Figure 6.5 shows the oxidation of 15.9 mM chloride (from $[C_4mpyrr]Cl$) on a gold microdisk electrode (diameter 25 μm) in $[C_4mpyrr][NTf_2]$ at a scan rate of 100 mV s^{-1}. Two oxidative processes were resolved, as previously observed in $[C_4mim][BF_4]$[24] and $[C_4mim][NTf_2]$[25] at gold macroelectrodes, which have been ascribed[25] to:

$$3Cl^- - 2e^- \rightarrow Cl_3^- \tag{6.15}$$

$$Cl_3^- - e^- \rightarrow \frac{3}{2}Cl_2 \tag{6.16}$$

The inset of Figure 6.5 shows a linear-sweep steady-state voltammogram for the oxidation of 15.9 mM $[C_4mpyrr]Cl$ in $[C_4mpyrr][NTf_2]$ on a gold microdisk electrode (diameter 25 μm) at a scan rate of 5 mV s^{-1}. Steady-state behaviour was easily achieved at this scan rate,

and gave a relative peak current ratio of 2:3 between the two waves. Electron counts obtained from fitting to chronoamperometric transients gave values of two thirds of an electron, and a further one third of an electron for the respective processes. These values coincide with the processes presented in equations 6.15 and 6.16. The diffusion coefficient of chloride was found to be 1.02 ($\pm$ 0.05) $\times$ 10^{-11} m^2 s^{-1}, comparable to that previously obtained for chloride (1.1 $\times$ 10^{-11} m^2 s^{-1}) in $[C_4mim][BF_4]$[24] and for bromide (1.4 $\times$ 10^{-11} m^2 s^{-1}) in $[C_4mim][NTf_2]$.[19] This voltammetry will be compared to that of PCl_3 and $POCl_3$ in order to assign the necessary waves to the oxidation of chloride.

6.4.4 Comparison of Peak Positions of PCl_3, $POCl_3$ and Cl^-

It was essential that this study was carried out with a stable reference electrode, since the positions of peaks shifted significantly over the course of an experiment when a silver-wire reference was used. To accurately compare anodic peak positions, a Ag/Ag^+ reference electrode was employed, and this was shown to give stable peak positions over a number of days and in various different solutions of PCl_3 in the IL. Figure 6.6 shows a comparison of the voltammetry of 14.8 mM PCl_3, 15.3 mM $POCl_3$ and 15.9 mM chloride (from $[C_4mpyrr]Cl$) in $[C_4mpyrr][NTf_2]$ on a gold microelectrode (diameter 25 μm) at a scan rate of 100 mV s^{-1}. Although the peaks above +1.0 V are not very well defined for PCl_3, it can be seen that peak III′ occurs at the same potential as peak P_7 of $POCl_3$ (Figure 6.4). From the position of the peaks, it is possible to tentatively assign waves III and III′ from PCl_3 (thick solid line) to the oxidation of $POCl_3$. This oxidation has been shown to occur in molecular solvents in the presence of Cl_2, shown by equation 6.17.[26] This process is possible due to the oxidation of chloride to chlorine *via* equations 6.15 and 6.16. PCl_3 has also been shown to react directly with water[27] (in the absence of chlorine) to form mainly H_3PO_3, but with a number of other by-products including $POCl_3$. It is more likely that the reaction requires the presence of chlorine as no evidence for

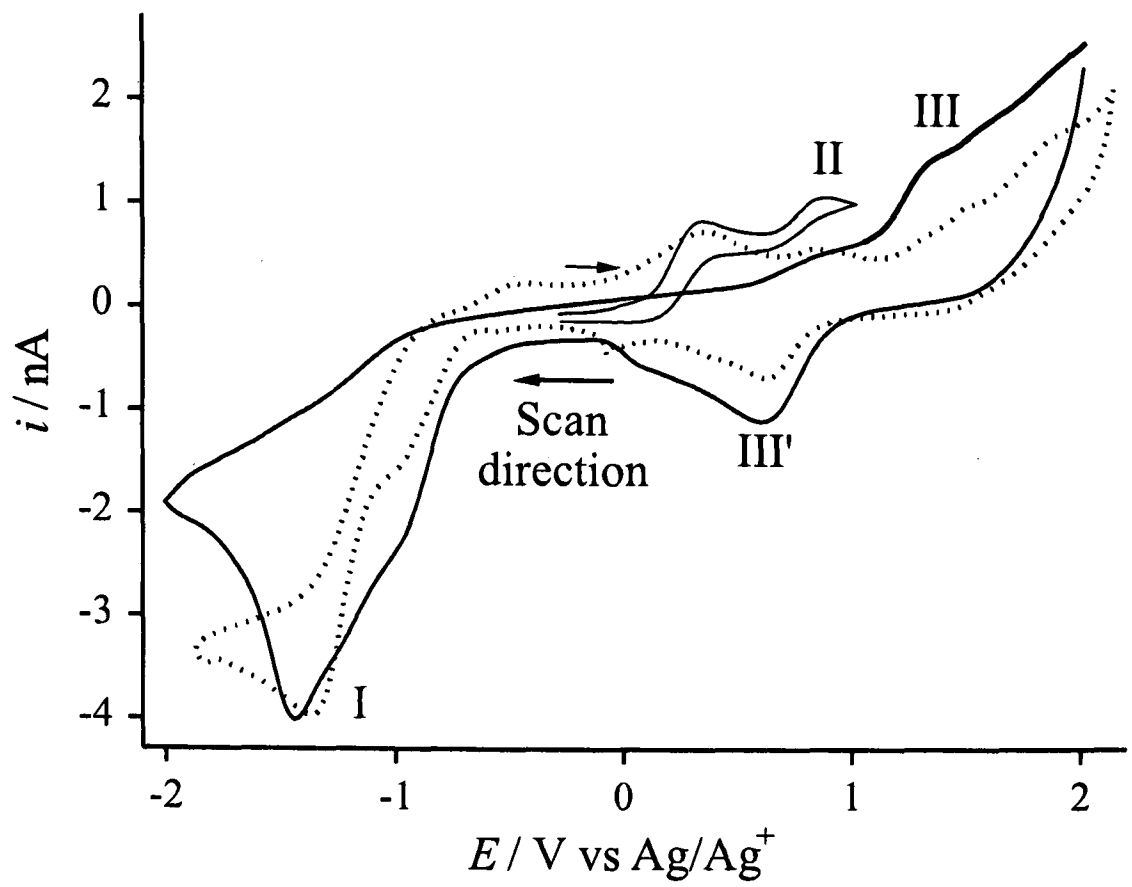

Figure 6.6: A comparison of cyclic voltammetry of: 14.8 mM PCl_3 (thick solid line), 15.3 mM $POCl_3$ (dots) and 15.9 mM chloride (from $[C_4mpyrr]Cl$) (thin solid line) in $[C_4mpyrr][NTf_2]$ on a gold microelectrode (diameter 25 μm) at a scan rate of 100 mV s^{-1}.

$POCl_3$ was found when the PCl_3 was stirred in air in any $[NTf_2]^-$ based ionic liquids, even those where hydrolysis was eventually observed.[1]

$$PCl_3 + H_2O + Cl_2 \rightarrow POCl_3 + 2HCl \tag{6.17}$$

The chloride oxidation peaks overlay well with peaks P_3 and P_4 (which are seen following the reduction of $POCl_3$), and hence P_3 and P_4 are identified according to equations 6.15 and 6.16. P_3 may also have some contribution to the current from a back peak of the initial reduction (see Section 6.3). Surprisingly, PCl_3 does not show the characteristic chloride peaks even though it is likely that chloride ions are released after the reduction. It is possible that either a film of some sort has formed on the surface, such that the electrode no longer displays the characteristic two step oxidation of Cl^- at Au, or the equilibrium of equation 6.10 is sufficiently shifted to the left

so that there is very little free chloride present in the solution.

6.5 Conclusions

For the first time, cyclic voltammetry for the reduction and oxidation of both PCl_3 and $POCl_3$ has been shown. A 'split-wave' was observed for the reduction of PCl_3, and this was shown (by chronoamperometry and digital simulation) to be due to an electrochemical step (involving a one electron transfer) followed by a chemical step. Similar reductive behaviour was observed for $POCl_3$ and an identical reaction scheme was proposed. Two oxidative features were observed for PCl_3 after initially reducing the parent; one wave was thought to be either a back peak from the reduction, or chloride oxidation on a filmed electrode surface. The second peak is most likely the oxidation of $POCl_3$ (formed by reaction of PCl_3 with trace water in the presence or absence of chlorine). An extra redox couple was observed when the scan was swept positively from 0 V, and this is thought to be the partially-reversible one electron oxidation to the radical cation of PCl_3. Several oxidative features were observed on the anodic sweep after reduction of $POCl_3$. Two were due to the oxidation of chloride, confirmed by matching the peak potentials with those of authentic chloride samples, and a further two peaks were due to the oxidation of parent molecules, shown by oxidative sweeps of the same solution. The most interesting finding from this study was the observation that the diffusion coefficient of PCl_3 was very small (3×10^{-12} m^2 s^{-1}) in comparison to $POCl_3$ (2×10^{-11} m^2 s^{-1}) and with other species from previous studies in RTILs (ferrocene; 2.31×10^{-11} m^2 s^{-1})[21] but is comparable with the self-diffusion coefficient of the anion and cation in $[C_4mim][PF_6]$.[22] This suggests that PCl_3 binds with the anion or cation of the ionic liquid, and moves with it. This may be why PCl_3 is so stable in this medium. The slowness ($\leq 1 \times 10^{-9}$ cm s^{-1}) of the electrochemical rate constant, k_0, was also unusual, possibly indicating a concerted cleavage of the phosphorus-chlorine bond during electron transfer. It is clear that this particular ionic liquid shows promise for use as a

solvent in which to store unstable compounds which would otherwise hydrolyse in traditional media.

It has been shown in this chapter that the ionic liquid medium provides a unique environment to stabilise reactive phosphorus compounds, allowing for a mechanistic study to be carried out for the first time. In the next chapter, the mechanisms of some dissolved inorganic solids (nitrates) are studied in ionic liquids, in order to compare their behaviour to that seen in conventional aprotic solvents. Interestingly, in contrast to that reported for organic mechanisms (see Chapter 5), the results show that the ionic liquid behaves more like a 'molten salt' than an aprotic solvent.

References

[1] Amigues, E.; Hardacre, C.; Keane, G.; Migaud, M. and O'Neill, M., *Chem. Commun.*, 2006, **1**, 72–74.

[2] Silvester, D. S.; Aldous, L.; Lagunas, M. C.; Hardacre, C. and Compton, R. G., *J. Phys. Chem. B*, 2006, **110**, 22035–22042.

[3] Greenwood, N. N. and Earnshaw, A., *Chemistry of the Elements, 2nd ed.*, Butterworth-Heinemann: Oxford, UK, 1997.

[4] March, J., *Advanced Organic Chemistry, 3rd ed.*, Wiley-Interscience: New York, 1985.

[5] Griffiths, W. R.; Tebby, J. C. and Coates, H., *Phosphorus and the Related Group V Elements*, 1976, **6**, 223–230.

[6] Wulff, C.; Orsten, S. and Oftring, A., *PCT Int. Appl.: Method for Production of N-phosphonomethylglycine.*, 2001.

[7] Wittig, G. and Schöllkopf, U., *Chem. Ber.*, 1954, **87**, 1318–1330.

[8] Wadsworth, W. S. and Emmons, W. D., *J. Am. Chem. Soc*, 1961, **83**, 1733–1738.

[9] Louloudes, S. J.; Kaplanis, N. J. and Roan, C. C., *J. Org. Chem.*, 1956, **21**, 685–686.

[10] Levchik, S. V. and Weil, E. D., *Polym. Int.*, 2005, **54**, 11–35.

[11] Coleman, G. H. and McCaskey, D. B., *U.S. Patent: N-Alkylcaproanilides.*, 1954.

[12] Kisil', L. M.; Osadchenko, I. M. and Tomilov, A. P., *Russ. J. Electrochem.*, 2000, **36**, 1029–1030.

[13] Berberova, N. T., *Russ. J. Electrochem.*, 2000, **36**, 174–182.

[14] Klimov, E. S.; Vakar, A. A.; Sokolov, V. P. and Okhlobystin, O. Y., *Zh. Obshch. Khim.*, 1987, **57**, 831–835.

[15] Miller, T. M.; Seeley, J. V.; Knighton, W. B.; Meads, R. F.; Viggiano, A. A.; Morris, R. A.; Van Doren, J. M.; Gu, J. and Schaefer, Henry F., I., *J. Chem. Phys.*, 1998, **109**, 578–584.

[16] Van Doren, J. M.; Friedman, J. F.; Miller, T. M.; Viggiano, A. A.; Denifl, S.; Scheier, P.; Märk, T. D. and Troe, J., *J. Chem. Phys.*, 2006, **124**, 124322/1–124322/9.

[17] Williamson, D. H.; Mayhew, C. A.; Knighton, W. B. and Grimsrud, E. P., *J. Chem. Phys.*, 2000, **113**, 11035–11043.

[18] Rudolph, M.; Reddy, D. P. and Feldberg, S. W., *Anal. Chem.*, 1994, **66**, 589A–600A.

[19] Allen, G. D.; Buzzeo, M. C.; Villagrán, C.; Hardacre, C. and Compton, R. G., *J. Electroanal. Chem.*, 2005, **575**, 311–320.

[20] Shoup, D. and Szabo, A., *J. Electroanal. Chem. Interfacial Electrochem.*, 1982, **140**, 237–245.

[21] Rogers, E. I.; Silvester, D. S.; Poole, D. L.; Aldous, L.; Hardacre, C. and Compton, R. G., *J. Phys. Chem. C*, 2008, **112**, 2729–2735.

[22] Umecky, T.; Kanakubo, M. and Ikushima, Y., *Fluid Phase Equilib.*, 2005, **228-229**, 329–333.

[23] Hardacre, C.; Holbrey, J. D.; Ness, K. A. and Youngs, T. A., Unpublished results.

[24] Villagrán, C.; Banks, C. E.; Hardacre, C. and Compton, R. G., *Anal. Chem.*, 2004, **76**, 1998–2003.

[25] Aldous, L.; Silvester, D. S.; Villagrán, C.; Pitner, W. R.; Compton, R. G.; Lagunas, M. C. and Hardacre, C., *New J. Chem.*, 2006, **30**, 1576–1583.

[26] Roberts, H. P. and Kreighbaum, H. S., *U. S. Patent: Method of Making Phosphorus Oxychloride.*, 1935.

[27] Goubeau, J. and Schulz, P., *Anorg. Allg. Chem.*, 1958, **294**, 224–232.

Chapter 7

Electrochemical Oxidation and Reduction of Nitrate Ions in the RTIL $[C_2mim][NTf_2]$; the Latter Behaves as a 'Melt' Rather than an 'Organic Solvent'

The electrochemical oxidation of 1-butyl-3-methylimidazolium nitrate ($[C_4mim][NO_3]$) is studied by cyclic voltammetry in the RTIL 1-ethyl-3-methylimidazolium bis(trifluoromethylsulfonyl)-imide ($[C_2mim][NTf_2]$). A sharp peak is observed on a Pt microelectrode (diameter 10 μm), and a diffusion coefficient at infinite dilution of *ca.* 2.0×10^{-11} m^2 s^{-1} is obtained. The cyclic voltammetry of sodium nitrate ($NaNO_3$) and potassium nitrate (KNO_3) is also studied in $[C_2mim][NTf_2]$. Similar oxidation peaks are observed, revealing diffusion coefficients at 298 K of *ca.* 8.8 and 9.0×10^{-12} m^2 s^{-1} and solubilities of 11.9 and 10.8 mM for $NaNO_3$ and KNO_3 respectively. The smaller diffusion coefficients for $NaNO_3$ and KNO_3 (compared to $[C_4mim][NO_3]$) may indicate that NO_3^- is ion-paired with Na^+ or K^+. This work may have applications in the electroanalytical determination of nitrate in RTIL solutions. Furthermore, a reduction feature is observed for both $NaNO_3$ and KNO_3, with additional anodic peaks indicating the formation of oxides, peroxides, superoxides and nitrites. This behaviour is surprisingly similar to that obtained from melts of $NaNO_3$ and KNO_3 at high temperatures (*ca.* 623–773 K), and this observation could significantly simplify experimental conditions required to investigate these compounds. X-Ray Photoelectron Spectroscopy (XPS) is also used to suggest that disodium (I) oxide (Na_2O), which has found use as a storage compound for hydrogen, was deposited on a Pt electrode surface following the reduction of $NaNO_3$.

The electrochemical experiments described in this chapter were carried out with the assistance of Miss Tessa Broder, and XPS experiments were performed by Dr. Alison Crossley. This work has been published in the New Journal of Chemistry.[1]

7.1 Introduction

Over the past century, many researchers have realized the importance of studying the reduction of nitrate (NO_3^-) ions, due to their potentially damaging effect on the environment. Most nitrates are highly water soluble, and may lead to severe environmental and health hazards if present in ground water at high concentrations.[2–4] This has lead to many studies focussing on the analytical determination of nitrate (and nitrite, NO_2^-) ion concentrations. Various salts of nitrates are also used commercially for many applications, such as in the production of ammonia gas,[5–7] and of hydroxylamine,[5,7] a valuable raw material in the chemical industry.

Many researchers have reported the catalysed electrochemical reduction of nitrate ions in acidic media,[5,8–10] but the mechanisms proposed are complicated by the presence of protons from the solvent. Other reports[11–14] have focussed on the cyclic voltammetry obtained from melts of several nitrate salts. The main advantage of studying a melt is that the solution is not contaminated by any proton donor species, or by any supporting electrolyte, since the solutions are intrinsically conductive (made entirely of ions). However, the need for high temperatures (*ca.* 623–773 K) is a major drawback in the ease and safety of the experimental set-up.

The suggested mechanism[12,13,15,16] for the reduction of nitrate is given by equation 7.1, resulting in the formation of oxide ions (O^{2-}).

$$MNO_3 + 2e^- \rightarrow MNO_2 + O^{2-} \tag{7.1}$$

where M=metal. In acidic solutions,[5,8–10] the reaction occurs in the presence of protons, which catalyse the reaction, and lead to the formation of water, as opposed to the oxide ion. However, when the ions are in a proton deficient environment, such as in a melt, several authors[12–14] have suggested the formation of oxide, peroxide and superoxide species of the corresponding cations (*e.g.* lithium, sodium and potassium), following the reduction. Several of these compounds

are important in the chemical industry, in particular, sodium oxide (Na_2O) has been shown to possess properties suitable for hydrogen storage.[17]

In the present report, we show how the electrochemistry of two nitrate salts, dissolved in a room temperature ionic liquid (RTIL) at ambient temperatures (*ca.* 298 K), compares surprisingly well with that obtained from melts of the same compounds at much higher temperatures (623–773 K). We report the electrochemistry of both sodium nitrate ($NaNO_3$) and potassium nitrate (KNO_3) in the room temperature ionic liquid 1-ethyl-3-methylimidazolium bis(trifluoromethylsulfonyl)imide ($[C_2mim][NTf_2]$), which may prove to be significant in both the analytical determination of nitrate, and in the application of RTILs as electrolytes in batteries.

7.2 Experimental

7.2.1 Instrumental

All experiments were performed on either a 10 μm Pt electrode, or a custom-made 6 mm diameter electrode (see below). The experiments on the 10 μm diameter Pt electrode were performed in a T-cell, as described in Chapter 3, with a 0.5 mm diameter Ag wire quasi-reference electrode. For experiments using the larger platinum-disk working electrode (see below), a three-electrode arrangement was employed, with a 0.5 mm diameter silver wire as a quasi-reference electrode, and a thin platinum coil as a counter electrode. The electrodes were housed in a cell designed for holding 1–3 mL of (previously degassed) solution, and were placed in the solution through a Teflon cap with four holes. A nitrogen line was fed through the fourth hole, and the top of the cell was covered to create an inert atmosphere above the solution.

7.2.2 Preparation of Solutions

Saturated solutions of $NaNO_3$ and KNO_3 were prepared by dissolving approximately 2 mg of solid in 1.5 mL of $[C_2mim][NTf_2]$. The solutions were stirred for approximately 24 hours to allow for full dissolution. Saturated solutions of $NaNO_2$ and KNO_2 were also prepared in the same way. For $NaNO_2$ and KNO_2, 20 μL of the saturated stock solutions were used. For $[C_4mim][NO_3]$, the four solutions with concentrations of 1153, 524, 275 and 141 mM were prepared by adding 5, 2, 2 and 2 μL of $[C_4mim][NO_3]$ to 20, 20, 40 and 80 μL of $[C_2mim][NTf_2]$ respectively.

7.2.3 Electrode Design and XPS

A 6 mm diameter (1 mm thick) Pt disk was contained in an 8 mm cylindrical block of PTFE (4.5 mm thick) and mounted on a metal stub. The stub was made with the correct dimensions to be held easily inside the UHV chamber. Electrical contact to the Pt disk was made through the centre of the stub *via* a copper wire, with a plastic coating. The surface of the electrode was cleaned with a small amount of acetone on tissue paper. After electrochemical experiments were performed, the wire was cut at the base of the stub. The electrode was removed from the ionic liquid, sprayed rapidly with acetone to remove liquid residues and introduced into the instrument *via* a turbo molecular pumped entry lock. The entry lock was pumped for about 30 minutes before the electrode was introduced into the analysis chamber. XPS was performed in an ion pumped UHV chamber equipped with a VG nine channel CLAM4 electron energy analyser (base pressure 5×10^{-10} torr). 250 Watt unmonochromated Mg X-ray excitation was used. The CLAM 4 has variable slits for small area analysis. The largest slit (5 mm) was used in this case with no apertures selected. The analyser was operated at constant pass energy of 100 eV for wide scans. Detailed scans with the analyser operating at 20 eV pass energy were taken over the Pt 4f and the Na 1s peaks. Data was obtained using a VGX900-W operating system. Peak positions were obtained by setting the main C1s peak to BE 284.8 eV to compensate for

charge shifting. Peak areas were measured after background subtraction following methods of Shirley,[18] divided by an empirically derived sensitivity factor,[19] and normalised to give atomic percentages. We note here that a strong stream of acetone was necessary to remove most of the ionic liquid sample on the surface of the electrode, since otherwise the C, N, O, F and S peaks swamped the smaller sodium and platinum peaks.

7.3 Results and Discussion

The RTIL chosen as the solvent for this study was $[C_2mim][NTf_2]$, since this showed a wide electrochemical window in excess of 5.5 V, and no obvious electrochemical features when fully degassed. $[C_4mim][NO_3]$ was then chosen as a source of nitrate ions, as it is liquid at room temperature and less hygroscopic than solid $[C_2mim][NO_3]$. It is thought that the different nature of the cation will have little/no effect on the voltammetry presented below.

7.3.1 Oxidation of $[C_4mim][NO_3]$ in $[C_2mim][NTf_2]$

Figure 7.1 shows the oxidation of nitrate ions (from $[C_4mim][NO_3]$) in the RTIL $[C_2mim][NTf_2]$ on a Pt microelectrode (diameter 10 μm) at concentrations of 141, 275, 524 and 1153 mM. A plot of peak current *vs* concentration (inset of Figure 7.1) was found to be approximately linear, and the relatively large peak currents reflect the high solubility of $[C_4mim][NO_3]$ in $[C_2mim][NTf_2]$. The oxidation occurs at a high positive potential, in excess of +2 V, which is unsurprising given the already high oxidation state of the ion. To the best of our knowledge, there are no reports of any similar voltammetric peaks in the literature, since, in conventional solvents, the peak is obscured by earlier solvent breakdown on platinum electrodes. The wide electrochemical window of this particular ionic liquid allows the observation of this peak, which is not even seen in melts of nitrate salts.[13,15] The shape of this peak appears sharp at 100 mV s^{-1}, even on a small microelectrode, but becomes close to steady-state at scan rates of 10 mV s^{-1} and below

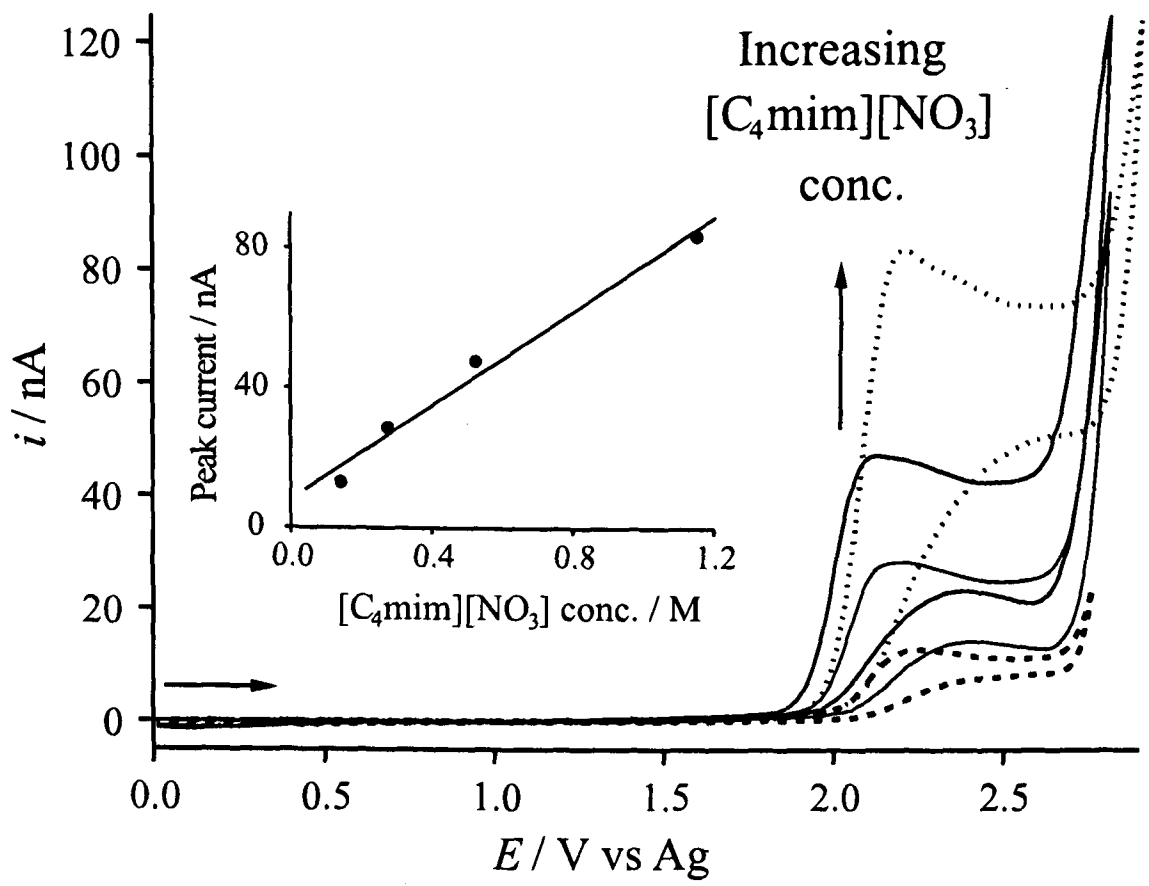

Figure 7.1: Cyclic voltammograms for the oxidation of $[C_4mim][NO_3]$ (concentrations of 141, 275, 524 and 1153 mM) in the RTIL $[C_2mim][NTf_2]$ on a Pt microelectrode (diameter 10 μm). Scan rate: 1 Vs^{-1}. The inset shows a plot of peak current *vs* nitrate concentration (line of best fit: $R^2 = 0.98$).

(not shown here). This is a reflection of the higher viscosity (and hence slower diffusion) of the RTIL compared to conventional solvents, where steady-state behaviour would be expected at 100 mV s^{-1} on such a small microelectrode.

A potential step was carried out on the oxidative peak for all the concentrations studied. The potential was stepped from 0.0 V (corresponding to no faradaic current) to a potential after the nitrate oxidation peak. The chronoamperometric transients were theoretically fit to the Shoup and Szabo[20] expression and in all cases, gave a very good fit ($\pm$ 0.7 %) to the experimental results. The analysis of the transients gives a range of diffusion coefficients at 298 K (1.17 to 1.90 $\times$ 10^{-11} m^2 s^{-1}) for the nitrate ion, which arises due to the different viscosities of the two liquids that make up the mixture (34 cP for $[C_2mim][NTf_2]$,[21] and 266 cP for $[C_4mim][NO_3]$,[22] at 293 K). Figure 7.2 shows a plot of the diffusion coefficients (obtained from the best theoretical fit to the experimental data) *vs* concentration of $[C_4mim][NO_3]$, and will be discussed later.

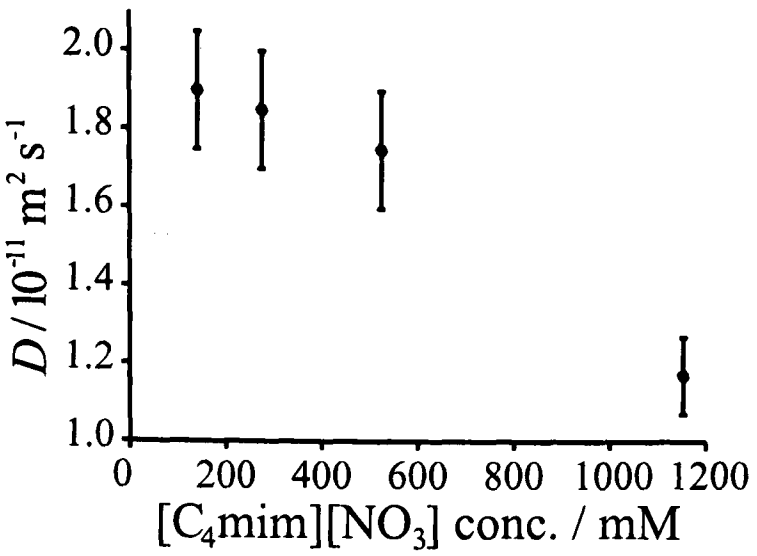

Figure 7.2: Plot of diffusion coefficients, D, against concentration, c, of $[C_4mim][NO_3]$ in $[C_2mim][NTf_2]$. Average D and c values were obtained from fitting to chronoamperometric transients, and error bars were calculated from 3-D contour plots of mean-squared absolute deviation.[23] D = 1.9 (± 0.15), 1.85 (± 0.15), 1.75 (± 0.15) and 1.17 (± 0.10) respectively.

The results from transient analysis also gave a combined value for the number of electrons, n, multiplied by concentration, c. Since c is known, these results indicate a one-electron process, suggesting that the oxidation follows a previously proposed[13] mechanism:

$$NO_3^- \rightarrow NO_2 + \frac{1}{2}O_2 + e^- \qquad (7.2)$$

The highly chemically irreversible shape of the oxidation peak indicates that the electrochemical step must be accompanied by a chemical reaction, further supporting equation 7.2. The gaseous products (nitrogen dioxide and oxygen) must then diffuse from the electrode surface before the scan is swept to the potentials where they are reduced, which explains why no reductive 'back' peaks were observed on the reverse sweep in the potential range +2.0 to -2.0 V (*cf.* reduction potential of oxygen in $[C_2mim][NTf_2]$ is -1.2 V *vs* Ag)[24] at all scan rates studied.

Three-dimensional surface (contour) plots were constructed for the four concentrations, following the mean-scaled absolute deviation, as employed in the reference.[23] The contour plots revealed single minima in all cases, indicating that there is only one set of optimised values for the diffusion coefficient, D, and the concentration, c. As a result of this analysis, error bars have

been added to the plot in Figure 7.2, indicating a small range in D, and a negligible range in c. For the more concentrated solution, the diffusion coefficient was the lowest, as expected from the larger volume of more viscous $[C_4mim][NO_3]$ present in the mixed solution. We can estimate from the graph that the diffusion coefficient of $[C_4mim][NO_3]$ in $[C_4mim][NTf_2]$ at infinite dilution is *ca.* 2×10^{-11} m^2 s^{-1}.

7.3.2 Oxidation of $NaNO_3$ and KNO_3 in $[C_2mim][NTf_2]$

We next looked at the oxidation of both sodium nitrate ($NaNO_3$) and potassium nitrate (KNO_3) separately in $[C_2mim][NTf_2]$. Figure 7.3 shows typical cyclic voltammograms obtained over a range of scan rates (10-400 mVs^{-1}) for the oxidation of a saturated solution $NaNO_3$ in $[C_2mim][NTf_2]$ on a 10 μm diameter Pt electrode. The peak currents observed are much smaller than for $[C_4mim][NO_3]$ in $[C_2mim][NTf_2]$, despite the RTIL solution being saturated with $NaNO_3$. The shapes of the peaks are also more steady-state like, suggesting the possibility of ion pairing (see below), or a result of the lower concentration of $NaNO_3$ compared to $[C_4mim][NO_3]$. The latter effect was observed in Figure 7.1 for the oxidation of $[C_4mim][NO_3]$ in $[C_2mim][NTf_2]$; the oxidation peaks became more transient shaped at higher concentrations.

In order to calculate the concentration (solubility) of sodium nitrate, a potential-step experiment was performed. The potential was stepped from 0.0 V (no faradaic current) to a potential after the peak, and the current was monitored for 10 seconds. The resulting chronoamperometric transient is shown in the inset of Figure 7.3, with the experimental data (–) giving excellent agreement ($\pm$ 0.7 %) with the theoretically derived data (○) from the Shoup and Szabo[20] expression. The diffusion coefficient of $NaNO_3$ in $[C_2mim][NTf_2]$ at 298 K was calculated to be 8.8 ($\pm$ 0.8) $\times$ 10^{-12} m^2 s^{-1} (after analysis of the three-dimensional contour plot) which is approximately 1–2 orders of magnitude smaller than that obtained in aqueous solutions (1.5×10^{-9} m^2 s^{-1} at 298 K),[25,26] and is reasonable considering the higher viscosity of

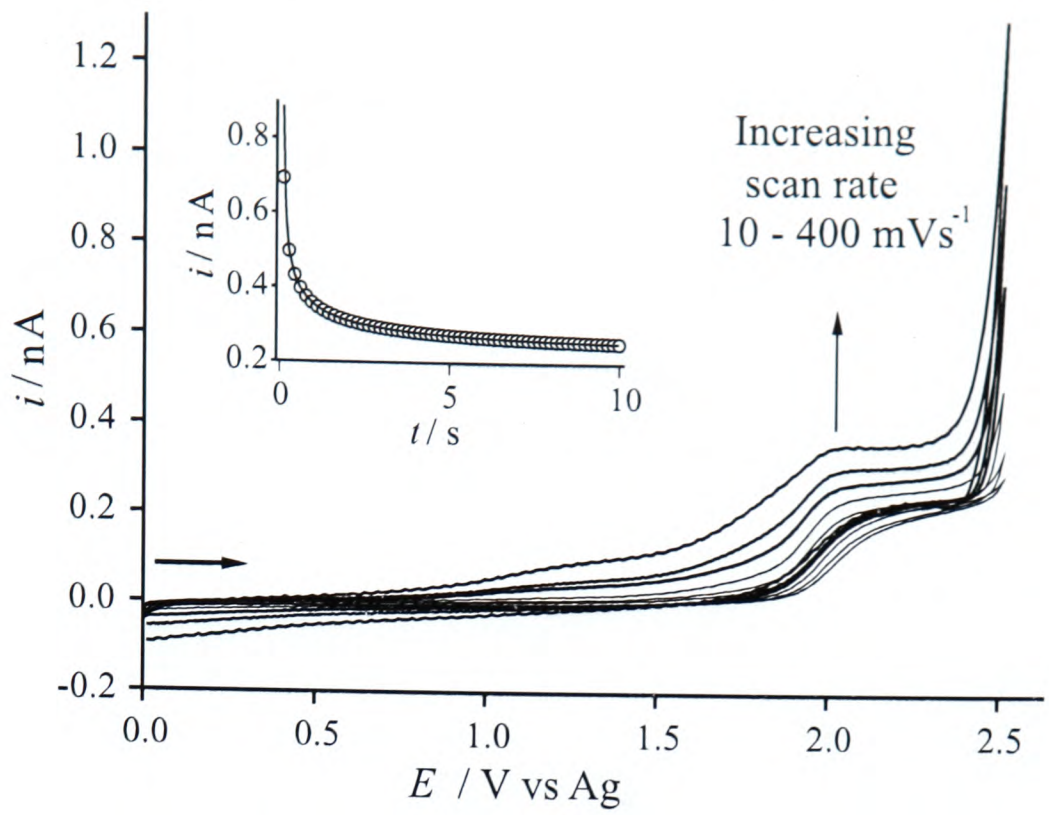

Figure 7.3: Cyclic voltammograms for the oxidation of a saturated solution of $NaNO_3$ in the RTIL $[C_2mim][NTf_2]$ on a Pt microelectrode (diameter 10 μm) at scan rates of 10, 20, 50, 100, 200 and 400 mV s^{-1}. The inset shows the experimental (–) and fitted theoretical (○) chronoamperometric transients for the oxidation of $NaNO_3$ in $[C_2mim][NTf_2]$. The potential was stepped from 0 to +2.3 V.

the RTIL compared to water (34 cP for $[C_2mim][NTf_2]$[21] compared to 1.00 cP for water[27] at 293 K). The results also suggest a concentration (or solubility) of $NaNO_3$ of 11.9 (± 0.5) mM in $[C_2mim][NTf_2]$, and this modest value is consistent with the relatively small peak currents obtained in Figure 7.3.

Analogous experiments were carried out for the oxidation of KNO_3. Figure 7.4 shows cyclic voltammetry for the oxidation of a saturated solution of KNO_3 in $[C_2mim][NTf_2]$ on a Pt electrode (diameter 10 μm) at scan rates of 10-400 mVs^{-1}. The shape and position of the wave is almost identical to that obtained for $NaNO_3$ (Figure 7.3). The results from chronoamperometric fitting (Figure 7.4 inset) and contour analysis gives a diffusion coefficient for KNO_3 of 9.0 (± 0.6) × 10^{-12} m^2 s^{-1} at 298 K (compared to 1.2–1.9 × 10^{-9} m^2 s^{-1} in water at 298 K),[28] and a modest concentration (solubility) of 10.8 (± 0.3) mM. The low solubility of both $NaNO_3$ and KNO_3 in $[C_2mim][NTf_2]$ may be a disadvantage if this technique is to be applied to the an-

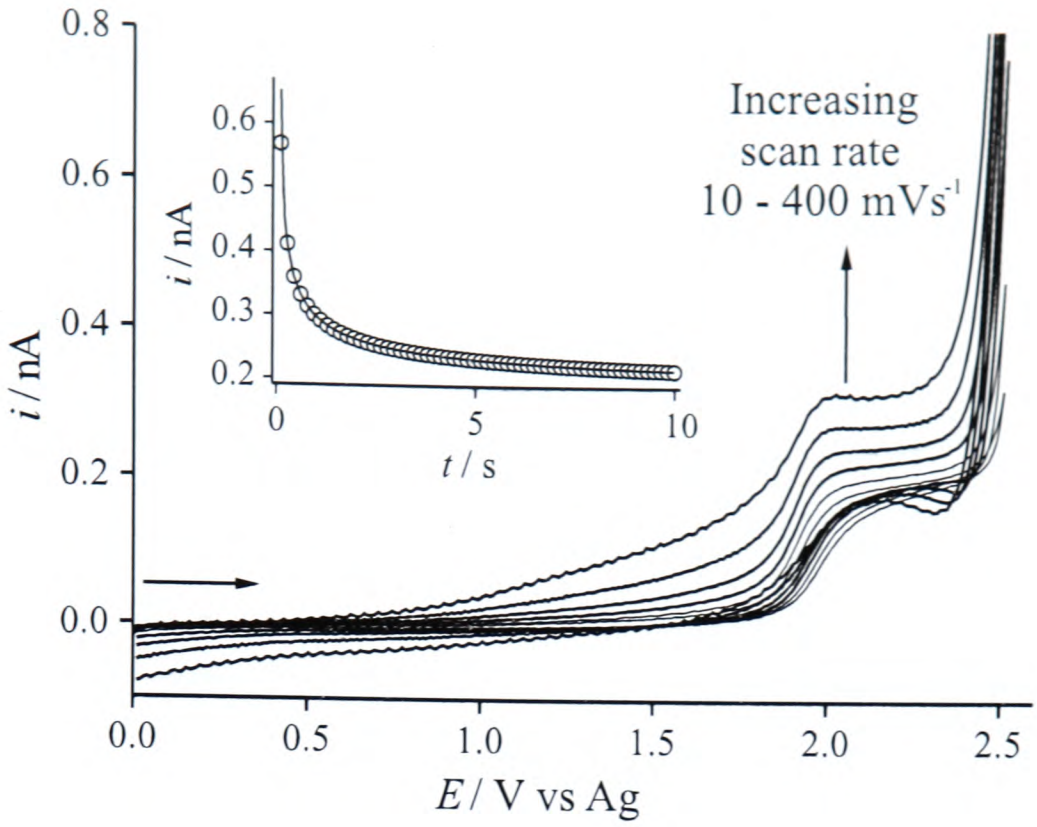

Figure 7.4: Cyclic voltammograms for the oxidation of a saturated solution of KNO_3 in the RTIL $[C_2mim][NTf_2]$ on a Pt microelectrode (diameter 10 μm) at scan rates of 10, 20, 50, 100, 200 and 400 mV s^{-1}. The inset shows the experimental (–) and fitted theoretical (○) chronoamperometric transients for the oxidation of KNO_3 in $[C_2mim][NTf_2]$. The potential was stepped from 0 to +2.2 V.

alytical determination of these compounds in RTILs. When comparing the diffusion coefficients of $NaNO_3$ and KNO_3 to that obtained for $[C_4mim][NO_3]$ (see section 7.3.1), it is obvious that, even with experimental error, the diffusion coefficient for nitrate in the Na^+ and K^+ compounds are much lower than $[C_4mim][NO_3]$. This observation indicates that the nitrate ion may be ion-paired to Na^+ or K^+, leading to slower diffusion of $NaNO_3$ and KNO_3, and supports the suggestion of formation of Na_2O and K_2O as products of the reduction (see section 7.3.4).

7.3.3 Reduction of $NaNO_3$ and KNO_3 in $[C_2mim][NTf_2]$

Next, the reduction of both species was studied. Figure 7.5 shows a typical cyclic voltammogram for the reduction of a saturated solution of $NaNO_3$ in $[C_2mim][NTf_2]$ on a Pt electrode (diameter 10 μm) at a scan rate of 1 V s^{-1}. The reduction is suggested[12–14,16] to follow the mechanism:

$$2Na^+ + NO_3^- + 2e^- \rightarrow Na_2O + NO_2^- \qquad (7.3)$$

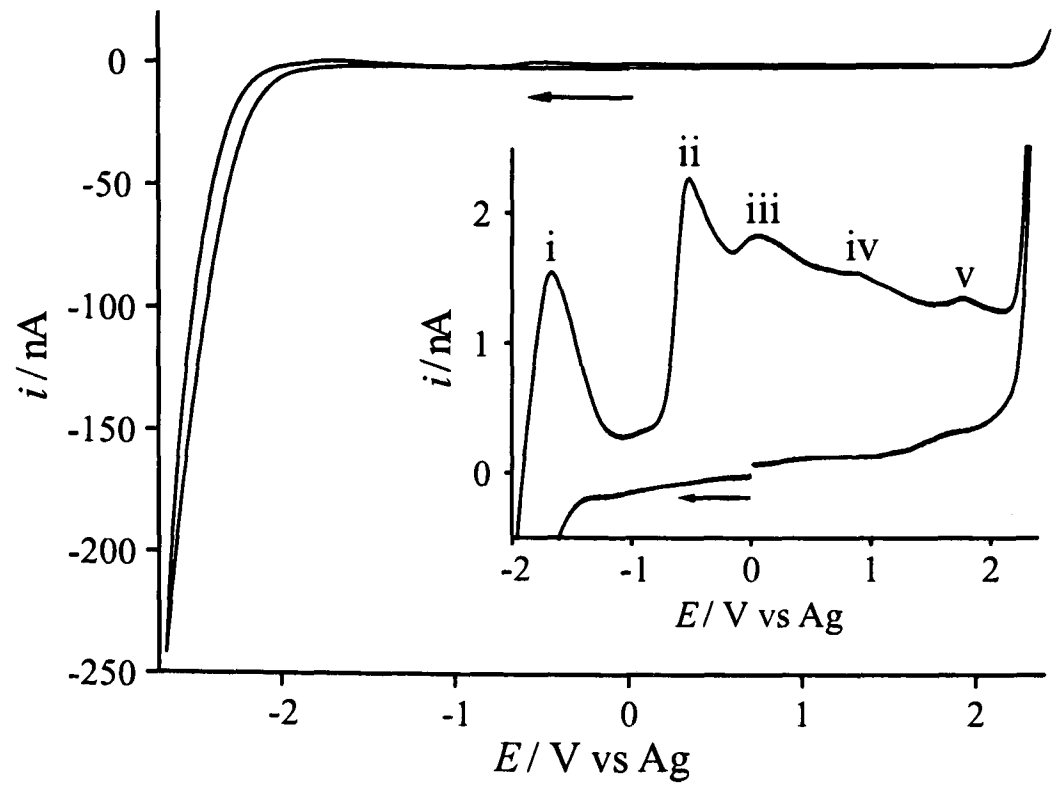

Figure 7.5: Cyclic voltammetry for the reduction of a saturated solution of $NaNO_3$ in $[C_2mim][NTf_2]$ on a Pt microelectrode (diameter 10 μm) at a scan rate of 1 V s^{-1}.

The reduction is not peak-shaped (in contrast with $NaNO_3$ melts)[12–14,16] but the onset of the reduction occurs well before the edge of the RTIL solvent window. A current of approximately -240 nA was chosen as an limiting value for reversal of the voltammetric sweep. On the reverse sweep, several anodic features are observed. The inset to Figure 7.5 shows a close-up view of the voltammetry in a reduced current range. Five distinct peaks are observed, and the identity of peaks i to v is suggested in Table 7.1, based on similar observations in $NaNO_3$ melts.[12–14] We propose that the peak observed at -1.67 V *vs* Ag on Figure 7.5 corresponds to the oxidation of sodium oxide (Na_2O) to sodium peroxide (Na_2O_2), which is followed at -0.52 V by the oxidation of sodium peroxide to sodium superoxide (NaO_2), and further by the oxidation of sodium superoxide to molecular oxygen at +0.06 V. We also suggest that peak iv at +0.87 V *vs* Ag is the oxidation of sodium nitrite ($NaNO_2$), since a separate study of $NaNO_2$ in $[C_2mim][NTf_2]$ (not shown here) showed an oxidation peak in almost the same position *vs* a silver quasi-reference electrode. The identification also seems reasonable, since $NaNO_2$ is formed in the reduction shown by equation 7.1. Peak v at +1.77 V likely corresponds to the oxidation

Table 7.1: Summary of the proposed reactions and peak assignments (Figures 7.5, 7.6 and 7.7) following the reduction of $NaNO_3$ and KNO_3.

$NaNO_3$	KNO_3	Proposed reaction[§]	Equation
i	I	$2M_2O \rightleftharpoons M_2O_2 + 2M^+ + 2e^-$	[7.4]
ii	II	$M_2O_2 \rightleftharpoons MO_2 + M^+ + e^-$	[7.5]
iii	III	$MO_2 \rightleftharpoons O_2 + M^+ + e^-$	[7.6]
iv	IV	$NO_2^- \rightarrow NO_2 + e^-$	[7.7]
v	V	$NO_3^- \rightarrow NO_2 + \frac{1}{2}O_2 + e^-$	[7.2]
iii′		$O_2 + e^- + M^+ \rightleftharpoons MO_2$	[7.8]
ii′		$MO_2 + e^- + M^+ \rightleftharpoons M_2O_2$	[7.9]

[§] $M = Na^+$ or K^+

of $NaNO_3$, initially present in the solution, which has shifted to a slightly more negative value than in Figure 7.3, possibly due to either a slight drift in the Ag quasi-reference, or a catalysing effect due to, for example a Na_2O film/precipitate on the electrode surface, which has been previously reported.[14–16] All equations describing peaks i to v are given in Table 7.1.

The same experiments were repeated for potassium nitrate. Figure 7.6 shows a typical cyclic volammogram for the reduction of a saturated solution of KNO_3 in $[C_2mim][NTf_2]$ on a 10 μm Pt electrode at a scan rate of 1 Vs^{-1}. The onset of the reduction begins at a slightly more negative potential than for $NaNO_3$, but the shape is generally the same. The scan was reversed when the current reached -240 nA, and several features were observed on the anodic sweep. A close up view of these features are shown in the inset of Figure 7.6. As with $NaNO_3$, we propose that peak I at -1.18 V is the oxidation of the oxide (K_2O), peak II at -0.38 V is the oxidation of K_2O_2, peak III at +0.18 V is the oxidation of KO_2, peak IV at +0.82 V is the oxidation of nitrite and peak V at +1.92 V is the oxidation of nitrate. All equations for the peak assignments are given in Table 7.1.

Figure 7.7 shows repeat voltammetric cycles for the reduction of a saturated solution of $NaNO_3$ under the same conditions as in Figure 7.5. Five consecutive scans are shown, with the first scan shown for clarity as dots. As can be clearly seen, on consecutive scans, the onset

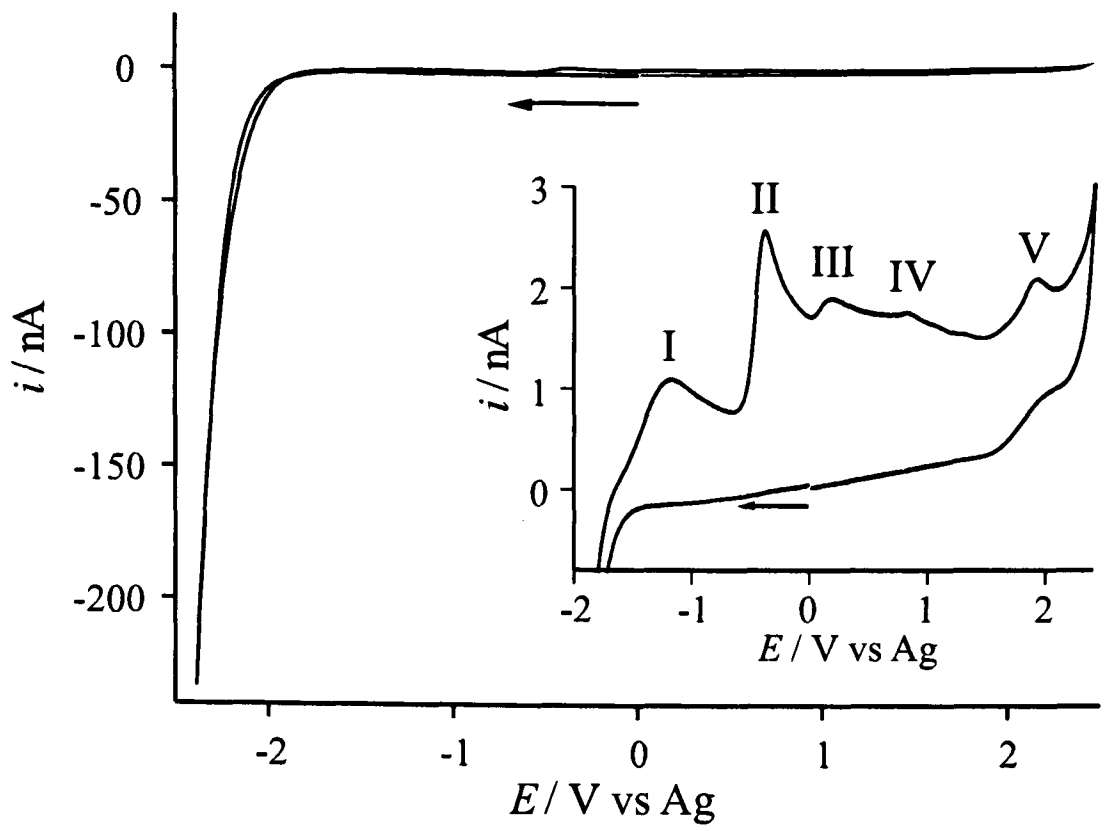

Figure 7.6: Cyclic voltammetry for the reduction of a saturated solution of KNO_3 in $[C_2mim][NTf_2]$ on a Pt microelectrode (diameter 10 μm) at a scan rate of 1 V s^{-1}.

of the reduction shifts to a slightly more negative potential and the heights of all three anodic peaks decrease. The decrease in peak heights is most likely due to the lower current maxima reached on successive scans. We also observe that the height of the peroxide and superoxide peaks (ii and iii) decrease by a greater extent than the oxide peak (i), indicating some build-up of disodium (I) oxide on the electrode surface. The formation of a Na_2O precipitate in a pure $NaNO_3$ melt is well documented in the literature.[14–16] The second observation is the appearance of two new cathodic peaks, ii′ and iii′, labelled with the same numbers as the anodic peaks to which they relate. When the cycles are reversed at -0.25 V, peak iii′ is not observed, but the small peak ii′ is still present (although smaller). We therefore identify peak iii′ as the reduction of oxygen to superoxide (equation 7.8), and peak ii′ as the reduction of superoxide to peroxide (equation 7.9). This effect has also been noted previously.[12,14] We then observed some evidence of fouling/deposition on the electrode after the appearance of the two extra peaks; peaks iii′ and ii′ were present on the first scan, even after the electrode was left for 30 minutes to equilibrate under high vacuum conditions. Polishing of the electrode was required to restore the platinum

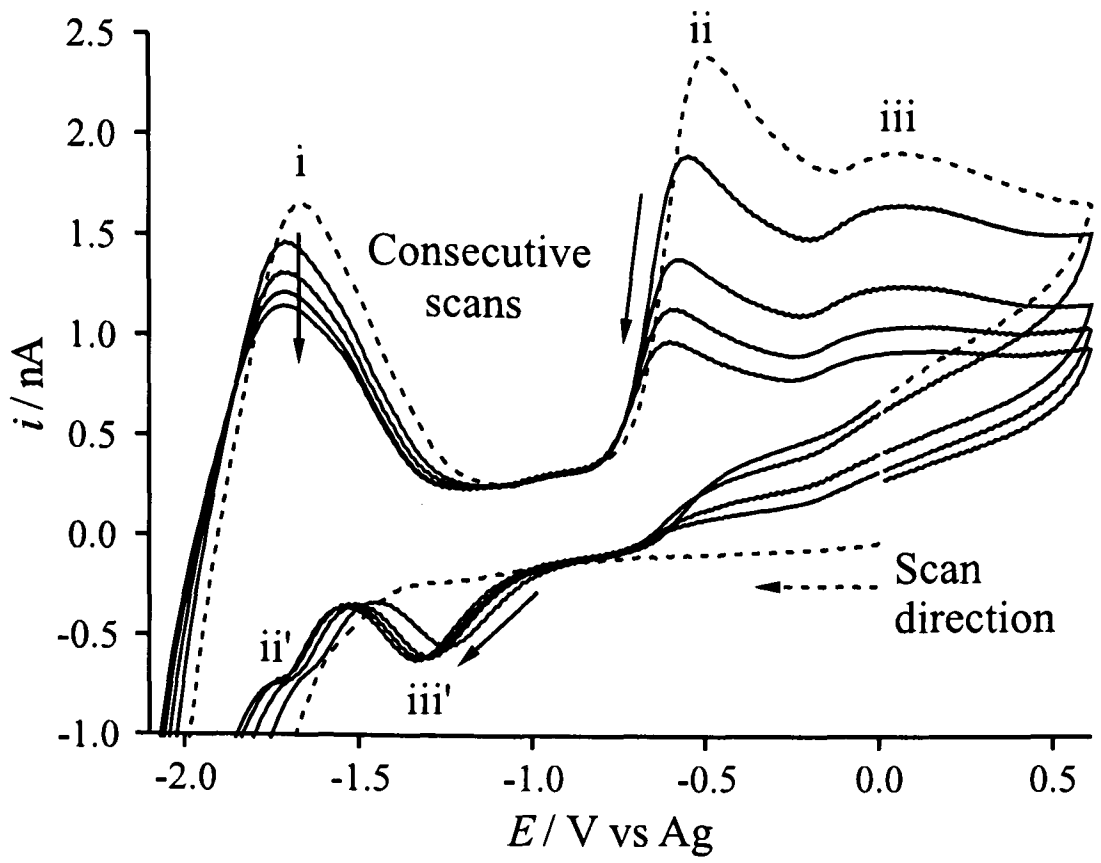

Figure 7.7: Cyclic voltammetry for the reduction of a saturated solution of $NaNO_3$ in $[C_2mim][NTf_2]$ at a Pt microelectrode (diameter 10 μm) with a reduced anodic limit of +0.5 V. The first scan (dots) and 4 subsequent scans (solid lines) are shown at a scan rate of 1 V s^{-1}.

surface to its original state.

7.3.4 X-Ray Photoelectron Spectroscopy (XPS) on the Electrode

Due to the useful hydrogen storage properties of disodium (I) oxide,[17] it would be advantageous to confirm if the reduction of $NaNO_3$ results in the electrodeposition of Na_2O on the electrode surface. Therefore, further studies were performed on the saturated solution of $NaNO_3$. The height of the peaks from the voltammetry (Figure 7.5) suggests that all three species, Na_2O, Na_2O_2 and NaO_2, are present after the reduction, but does not shed light on the identity, if at all, of any deposit. In order to confirm the presence or absence on the electrode surface of any of these species (disodium (I) oxide, sodium peroxide or sodium superoxide) using X-Ray Photoelectron Spectroscopy (XPS), a larger platinum disk electrode was constructed (see experimental). The reduction of the saturated solution of $NaNO_3$ (as in Figure 7.5) was first repeated with this larger electrode, to ensure that the same reactions were taking place. The voltammetry showed similar

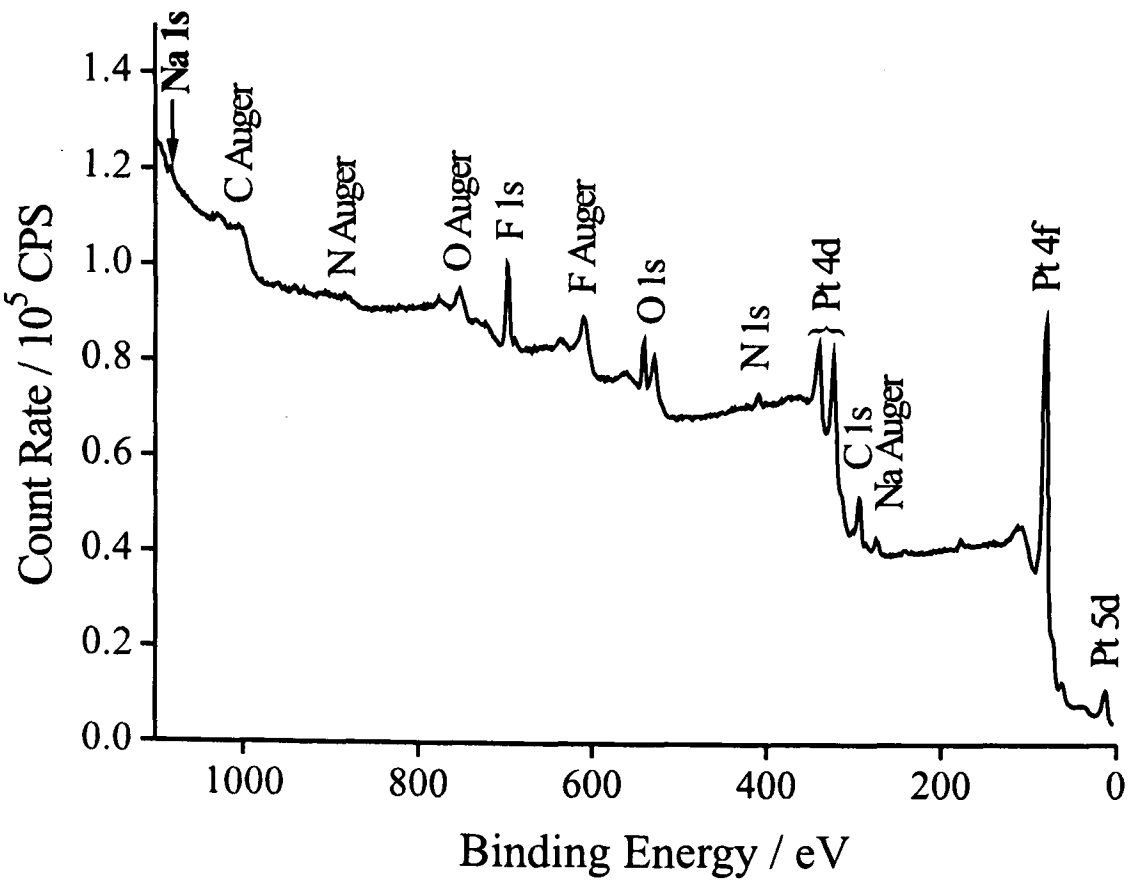

Figure 7.8: Survey Scan XPS spectrum of the surface of a 6 mm diameter Pt electrode (after 10 minutes electrochemical deposition time in a saturated solution of $NaNO_3$ in $[C_2mim][NTf_2]$). The peaks from the constituent atoms that make up the RTIL (C, N, O, F), and the Na (1s) and Pt (4f, 4d and 5d) peaks are all labelled.

features to that obtained with the 10 μm diameter Pt microelectrode, and so was not included here. The potential was then swept from 0 V to -2.8 V, and held for 10 minutes in order to maximise any deposition that may be taking place. We briefly note here that after 10 minutes deposition time, the $NaNO_3$/RTIL solution changed from colourless to a deep yellow-brown colour, and increased the height of all anodic peaks by *ca.* 50 %.

Figure 7.8 shows an XPS spectrum of the electro-deposited electrode. The figure is labelled with the peaks corresponding to the atoms that make up the structure of the RTIL. Initially, the XPS spectra obtained from the electrode was swamped by C, N, O, F and S peaks from the ionic liquid. Once the electrode was vigorously sprayed with acetone, the resultant spectrum showed a clear platinum peak at a binding energy of 71.1 eV (charge compensated and corrected), and a sodium (Na 1s) signal at 1072.6 eV (also labelled on Figure 7.8). In order to identify the sodium deposit, two standards, sodium oxide and sodium peroxide were also studied. The binding energy

of the standards were as follows: sodium oxide 1073.6 eV, and sodium peroxide 1071.6 eV. The small deviation in binding energy from the standards may be due to the deposited species partially oxidising in air during the transfer process. These results indicate that the species present on the platinum surface is sodium oxide, Na_2O.

7.4 Conclusions

By dissolving the solids of sodium nitrate and potassium nitrate in a common room temperature ionic liquid (RTIL) $[C_2mim][NTf_2]$, several observations were made. (1) The wide electrochemical window of $[C_2mim][NTf_2]$ has allowed the observation of a clear oxidation peak, and easy calculation of concentrations and diffusion coefficients of both $NaNO_3$ and KNO_3 at 298 K. This work may have applications in the electrochemical determination of nitrate ions, although the low solubility in RTILs could prove to be a limiting factor. (2) The voltammetric features observed for the reduction of $NaNO_3$ and KNO_3 were almost identical to that obtained in melts at temperatures of 623-773 K. Without the need for such extreme conditions, studies of other melts may be significantly more facile by simply dissolving them in an RTIL. (3) XPS studies have also revealed that sodium oxide is likely electrodeposited on the platinum electrode in a $NaNO_3$/RTIL solution.

In the next chapter, the electrochemistry of some inorganic nitrite (NO_2^-) salts are studied, mainly to determine their reaction mechanisms in ionic liquid media. The oxidation of NO_2^- is thought to lead to the formation of nitrogen dioxide gas (NO_2), and so the electrochemistry of NO_2 gas has also been studied. The ability of RTILs to detect nitrogen dioxide gas may also help to determine if ionic liquids may be potentially useful gas sensing media.

References

[1] Broder, T. L.; Silvester, D. S.; Aldous, L.; Hardacre, C.; Crossley, A. and Compton, R. G., *New J. Chem.*, 2007, **31**, 966–972.

[2] Moorcroft, M. J.; Davis, J. and Compton, R. G., *Talanta*, 2001, **54**, 785–803.

[3] Davis, J.; Moorcroft, M. J.; Wilkins, S. J.; Compton, R. G. and Cardosi, M. F., *Analyst*, 2000, **125**, 737–742.

[4] Pletcher, D. and Poorabedi, Z., *Electrochim. Acta*, 1979, **24**, 1253–1256.

[5] Dima, G. E.; de Vooys, A. C. A. and Koper, M. T. M., *J. Electroanal. Chem.*, 2003, **554-555**, 15–23.

[6] El-Deab, M. S., *Electrochim. Acta*, 2004, **49**, 1639–1645.

[7] Taniguchi, I.; Nakashima, N.; Matsushita, K. and Yasukouchi, K., *J. Electroanal. Chem. Interfacial Electrochem.*, 1987, **224**, 199–209.

[8] de Groot, M. T. and Koper, M. T. M., *J. Electroanal. Chem.*, 2004, **562**, 81–94.

[9] Fedurco, M.; Kedzierzawski, P. and Augustynski, J., *J. Electrochem. Soc.*, 1999, **146**, 2569–2572.

[10] Hsieh, S.-J. and Gewirth, A. A., *Langmuir*, 2000, **16**, 9501–9512.

[11] Fletcher, A. N.; Miles, M. H. and Chan, M. L., *J. Electrochem. Soc.*, 1979, **126**, 1496–1501.

[12] Johnson, K. E. and Zacharias, P. S., *J. Electrochem. Soc.*, 1977, **124**, 448–450.

[13] Miles, M. H. and Fletcher, A. N., *J. Electrochem. Soc.*, 1980, **127**, 1761–1766.

[14] Zambonin, P. G., *J. Electroanal. Chem. Interfacial Electrochem.*, 1970, **24**, 365–377.

[15] Bartlett, H. E. and Johnson, K. E., *J. Electrochem. Soc.*, 1967, **114**, 64–67.

[16] Swofford, H. S., J. and Laitinen, H. A., *J. Electrochem. Soc.*, 1963, **110**, 814–820.

[17] Xu, Q.; Wang, R.; Kiyobayashi, T.; Kuriyama, N. and Kobayashi, T., *J. Power Sources*, 2006, **155**, 167–171.

[18] Shirley, D. A., *Phys. Rev. B: Solid State*, 1972, **5**, 4709–4714.

[19] Briggs, D. and Seah, M. P., Eds., *Practical Surface Analysis, Vol 1: Auger and X-Ray Photoelectron Spectroscopy*, John Wiley and Sons: Chichester, UK, 1994.

[20] Shoup, D. and Szabo, A., *J. Electroanal. Chem. Interfacial Electrochem.*, 1982, **140**, 237–245.

[21] Bonhôte, P.; Dias, A.-P.; Papageorgiou, N.; Kalyanasundaram, K. and Grätzel, M., *Inorg. Chem.*, 1996, **35**, 1168–1178.

[22] Seddon, K. R.; Stark, A. and Torres, M.-J., *ACS Symp. Ser.*, 2002, **819**, 34–39.

[23] Fietkau, N.; Clegg, A. D.; Evans, R. G.; Villagrán, C.; Hardacre, C. and Compton, R. G., *ChemPhysChem*, 2006, **7**, 1041–1045.

[24] Buzzeo, M. C.; Klymenko, O. V.; Wadhawan, J. D.; Hardacre, C.; Seddon, K. R. and Compton, R. G., *J. Phys. Chem. A*, 2003, **107**, 8872–8878.

[25] Harned, H. S. and Shropshire, J. A., *J. Am. Chem. Soc.*, 1958, **80**, 2618–2619.

[26] Yeh, H. S. and Wills, G. B., *J. Chem. Eng. Data*, 1970, **15**, 187–189.

[27] Lide, D. R., Ed., *Handbook of Chemistry and Physics: 76th Edition*, CRC Press, Boca Raton, USA, 1996.

[28] Daniel, V. and Albright, J. G., *J. Solution Chem.*, 1991, **20**, 633–642.

Chapter 8

Electrochemical Oxidation of Nitrite and the Oxidation and Reduction of NO_2 in the RTIL $[C_2mim][NTf_2]$

In this chapter, cyclic voltammetry for the oxidation of potassium nitrite in $[C_2mim][NTf_2]$ at platinum electrodes is reported. A chemically irreversible oxidation peak is observed, and a solubility of 7.5 ($\pm$ 0.5) mM and diffusion coefficient of 2.0 ($\pm$ 0.2) $\times$ 10^{-11} m^2 s^{-1} at 298 K is calculated from potential step chronoamperometry on the microdisk electrode. A second, and sometimes third, oxidation peak is also observed when the anodic limit is extended, and these are provisionally assigned to the oxidation of nitrogen dioxide (NO_2) and nitrate (NO_3^-) respectively. The electrochemical oxidation of nitrogen dioxide gas (NO_2) is also studied by cyclic voltammetry in $[C_2mim][NTf_2]$ on Pt electrodes of various size, giving a solubility of *ca.* 51 ($\pm$ 0.2) mM and diffusion coefficient of 1.6 ($\pm$ 0.05) $\times$ 10^{-10} m^2 s^{-1} at 298 K. It is likely that NO_2 exists predominantly as its dimer, N_2O_4, at room temperature. The oxidation mechanism follows a CE process, which involves the initial dissociation of the dimer to the monomer, followed by a one-electron oxidation. A second, larger oxidation peak is observed at more positive potentials and is thought to be the direct oxidation of N_2O_4. In addition to understanding the mechanisms of NO_2^- and NO_2 oxidations, this work has implications in the electrochemical detection of nitrite ions and of NO_2 gas in RTIL media; the latter which may be of particular use in gas sensing.

The work presented in this chapter was carried out with the assistance of Miss Tessa Broder, and has been published in the Journal of Physical Chemistry B.[1]

8.1 Introduction

Nitrite ions are widely used as an additive in some foods[2] and also as a corrosion inhibitor.[3] The determination of nitrite ions is of huge environmental concern due to the toxicity and potential contribution to environmental release hazards when present in groundwater.[4] As a result, there have been several protocols dealing with the detection of nitrite in water using electrochemical and other methods.[5–7]

The mechanism of nitrite oxidation has been studied in solvents ranging from pure alkali nitrite melts,[8] sodium nitrate-potassium nitrate eutectic melts,[8–12] the aprotic solvent dimethyl sulfoxide (DMSO)[13,14] and water.[15–17] The electro-*reduction* of nitrite has also been reported in protic solvents, the mechanism involving participation of water molecules. However, to the best of our knowledge, no obvious reduction peaks have been found in aprotic solvents or melts.

In all media, the *oxidation* of nitrite is thought to proceed by equation 8.1, resulting in the formation of nitrogen dioxide gas:

$$NO_2^- \rightarrow NO_2(g) + e^- \tag{8.1}$$

Any further reactions appear to depend on the nature of the solvent. In protic media, NO_2 (or its dimer N_2O_4) is believed to undergo a disproportionation reaction to form nitrate ions (NO_3^-) and protons:[15–17]

$$N_2O_4 + H_2O \rightleftharpoons H^+ + NO_3^- + HNO_2 \tag{8.2}$$

However, in nitrate melts (KNO_3-$NaNO_3$), the electro-generated NO_2 reacts with NO_2^- in solution to form nitrate and NO gas:[8,11,12]

$$NO_2 + NO_2^- \rightleftharpoons NO_3^- + NO \tag{8.3}$$

In DMSO, the mechanism is thought to involve oxidation of NO_2^- to form NO_2, then dimerisation to N_2O_4, followed by association with the solvent.[13,14] In pure molten nitrites, it is believed[8,9] that the only species generated from the oxidation reaction is NO_2, which is in equilibrium with its dimer, N_2O_4. Several reports[8,9,14] have also claimed that the platinum electrode surface (formation of platinum oxides) plays a part in the mechanism. Furthermore, Piela and Wrona[16] claim that the formation of an oxide layer on Pt hinders the nitrite oxidation process in water.

In order to identify the products following the oxidation of nitrite, it is helpful to study the voltammetry of nitrogen dioxide, NO_2, gas. NO_2 is a brown toxic gas, which causes damage to respiratory organs and contributes to air pollution. The sensing/determination of nitrogen dioxide in air is of huge importance as the gas is emitted from cars, boilers and other combustion facilities. Several methods have been used to determine NO_2, including those based on electrochemistry.[18,19] Despite the interest in NO_2 detection, there is relatively little reported on the voltammetry and electrochemical mechanism of NO_2 gas dissolved in solvents. Only a few studies[10–12] in KNO_3-$NaNO_3$ melts have reported the addition of NO_2 gas to the solvent, but no voltammetry was shown. However, the electrochemistry of its dimer N_2O_4 (added as a liquid) has been studied in a range of aprotic solvents by several authors.[20–22] In all cases, a single oxidative wave was reported and is assigned to the following CE mechanism:

$$N_2O_4 \rightleftharpoons 2NO_2 \rightleftharpoons 2NO_2^+ + 2e^- \tag{8.4}$$

A detailed kinetic study was described in two of these reports,[20,22] but no reductive features were observed. Contrastingly, Boughriet *et al.*[21] report two reduction steps involving reaction of the dimer with the monomer and suggest that the redox properties are complicated by trace quantities of water, forming N_2O_3, HNO_3 and HNO_2, all electrochemically active species.

The aim of the present study is to explore the oxidation mechanism of nitrite and the

redox properties of NO_2 gas in a room temperature ionic liquid (RTIL). This work reports the electro-oxidation of nitrite ions (from KNO_2) and the oxidation and reduction properties of NO_2 gas dissolved in the RTIL $[C_2mim][NTf_2]$ in order to understand and analyse the reaction mechanisms and kinetics in this media. This work may also have implications in the analytical determination of nitrite ions and in the amperometric sensing of nitrogen dioxide gas.

8.2 Experimental

A saturated solution of KNO_2 was prepared by dissolving *ca.* 2 mg of solid in 1 mL of $[C_2mim][NTf_2]$. The solution was stirred overnight to allow for full dissolution. A 30 mM solution of NO_2BF_4 was prepared by dissolving 10 mg of the solid in 2 mL of $[C_2mim][NTf_2]$ (previously dried under vacuum at 0.05 Torr for 24 hours at 353 K).

Experiments involving KNO_2 and NO_2BF_4 on the 100 μm and 0.5 mm diameter platinum working electrodes were carried out using a three-electrode arrangement in a small cell (described in Chapter 3), with a 0.5 mm diameter silver wire as a quasi-reference electrode and a platinum coil as a counter electrode. The cell was kept under a constant flow of nitrogen throughout measurements. Experiments involving NO_2 gas on a 10 μm Pt working electrode were performed in the T-cell (described in Chapter 3), with 20 μL of 'blank' ionic liquid in the cavity above the electrode. A PTFE tube leading directly from the NO_2 gas cylinder was attached to one arm of the cell, and an outlet PTFE tube to the other. The gas (brown in colour) was allowed to diffuse through the cell, passing over the solution, until equilibrium was achieved (typically after 20 minutes, as evidenced by maximum stable peak currents). The solution turned dark green after *ca.* 2 minutes. For experiments involving NO_2 on the 100 μm and 0.5 mm diameter Pt working electrodes, a sealed five-necked flask was used. A 0.5 mm diameter silver wire was employed as a quasi-reference electrode and a 0.5 mm diameter platinum wire as a counter electrode. 1 mL of blank RTIL was placed under vacuum for 2 hours then transferred to the

five-necked flask. Two large syringe needles were attached to the inlet and outlet PTFE tubing and used to pierce the seals of two necks of the flask. This allowed a constant flow of NO_2 gas over the RTIL throughout the experiments. The three other necks of the flask were used to house the electrodes. The solution showed a light green colour after approximately 10 minutes. All experiments involving NO_2 were performed in a fume cupboard.

8.3 Results and Discussion

The RTIL chosen as the solvent in this study was $[C_2mim][NTf_2]$ due to its wide electrochemical window, clean baseline and relatively low viscosity (34 cP at 293 K),[23] which gives higher current responses at microelectrodes. All results below are reported in this medium.

8.3.1 Oxidation of KNO_2 in $[C_2mim][NTf_2]$

Figure 8.1a shows the oxidation of a saturated solution of KNO_2 in $[C_2mim][NTf_2]$ on a Pt microelectrode (diameter 10 μm) at a range of scan rates from 10 mV s^{-1} to 1 V s^{-1}. A single oxidative peak is observed in the voltage range from +0.4 to +1.3 V *vs* Ag, which is assigned to the following reaction:

$$NO_2^- \rightarrow NO_2(g) + e^- \tag{8.5}$$

This is directly comparable to oxidation peaks observed in protic media,[15–17] in DMSO,[13,14] in KNO_3-$NaNO_3$ melts[8,10,11,24] and in pure nitrite melts.[8] The oxidation peak shown in Figure 8.1a becomes more transient shaped at higher scan rates, and a plot of peak current *vs* square root of scan rate is linear, indicating that the process is diffusion controlled. The peak also appears chemically irreversible, as shown by the absence of any back peak following the oxidation at all scan rates studied.

Several authors[11,12,24] have suggested that the oxidation reaction (equation 8.5) is chemically reversible, whereas others have shown its irreversibility.[13–16] To understand this discrepancy,

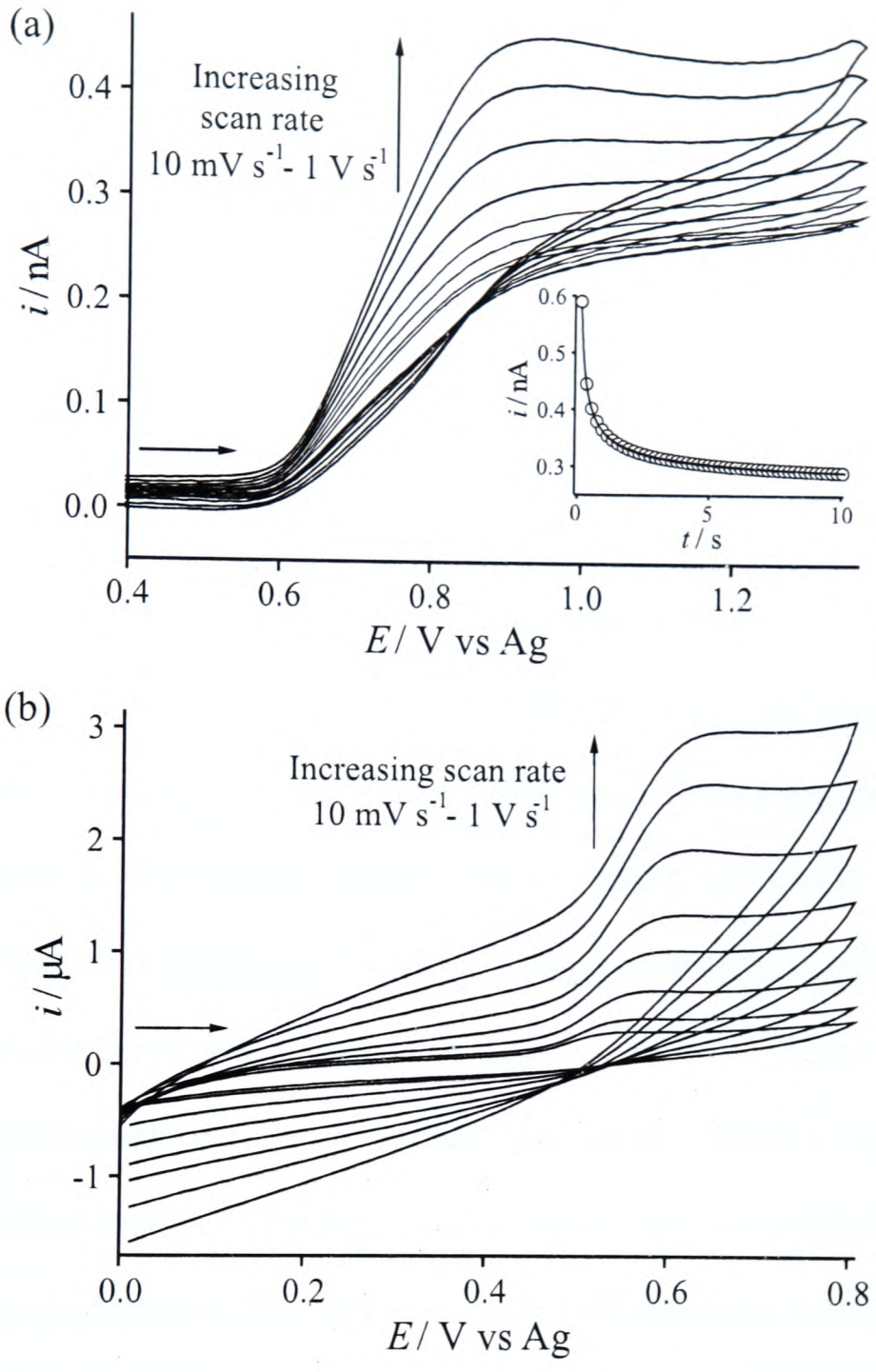

Figure 8.1: Cyclic voltammograms for the oxidation of a saturated solution of KNO_2 in $[C_2mim][NTf_2]$ on (a) a Pt microelectrode (diameter 10 μm) and (b) a Pt macroelectrode (diameter 0.5 mm) at scan rates of 10, 20, 50, 100, 200, 400, 700 and 1000 mV s^{-1}. The inset to (a) shows the experimental (–) and fitted theoretical (○) chronoamperometric transients for the oxidation of KNO_2 in $[C_2mim][NTf_2]$ on a 10 μm diameter Pt electrode. The potential was stepped from +0.4 to +1.2 V.

Desimoni *et al.*[24] showed that the oxidation peak of nitrite was chemically reversible in KNO_3-$NaNO_3$ melts, but became more irreversible with the addition of small amounts of water. The overall catalytic mechanism shown in equation 8.6 was thought to be in competition with the simple electrode process given in equation 8.5.[24]

$$NO_2^- + H_2O \rightleftharpoons NO_3^- + 2H^+ + 2e^- \tag{8.6}$$

To confirm the irreversibility of the oxidation in $[C_2mim][NTf_2]$, the same saturated solution of KNO_2 was studied on a larger Pt disk electrode, demonstrating slower apparent electrode kinetics. Figure 8.1b shows cyclic voltammograms for the oxidation of a saturated solution of KNO_2 on a Pt electrode (diameter 0.5 mm) at scan rates of 10 mV s^{-1} to 1 V s^{-1}. Again, a single oxidative peak is observed which shows no reduction peaks at all scan rates studied, even when the reverse scan was swept to -2.0 V (not shown here). This suggests that reaction (1) is chemically irreversible in RTIL media, possibly due to reaction with trace water present in the ionic liquid, following equation 8.6. We note here that no obvious voltammetry from water was observed when the ionic liquid was further dried under vacuum for 2 hours, suggesting that the amount of water present may be in a small enough quantity not to be detected voltammetrically.

To calculate a concentration (solubility) and diffusion coefficient of KNO_2 in $[C_2mim][NTf_2]$, a potential step was performed on the oxidative wave. The potential was stepped from +0.4 V to +1.2 V on a 10 μm diameter Pt electrode, and the current was measured for 10 seconds. The inset to Figure 8.1a shows the experimental (solid line) and theoretically fitted (dots) chronoamperometric transients. The experimental data were fitted to the Shoup and Szabo[25] expression, and gave a concentration (solubility) of 7.5 ($\pm$ 0.5) mM, and a diffusion coefficient at 298 K of 2.0 ($\pm$ 0.2) $\times$ 10^{-11} m^2 s^{-1}, which is approximately two orders of magnitude less than that in water (1.8 $\times$ 10^{-9} m^2 s^{-1}),[26] and is reasonable given the higher viscosity of the RTIL (34 cP)[23] compared to water (1.00 cP)[27] at 293 K. The modest solubility is also consistent

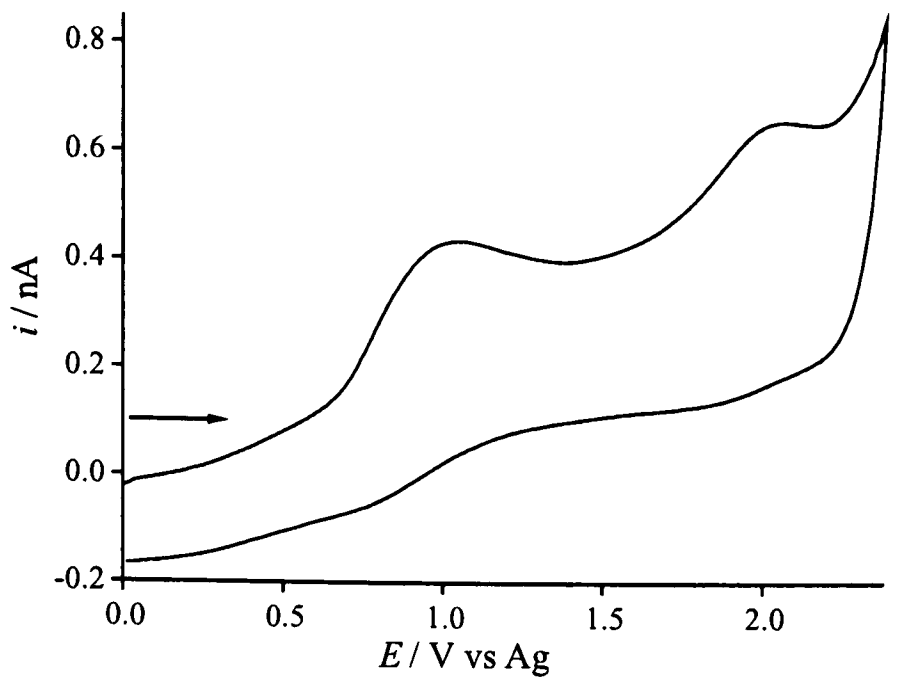

Figure 8.2: Cyclic voltammetry (with an extended anodic limit) for the oxidation of a saturated solution of KNO_2 in $[C_2mim][NTf_2]$ on a Pt microelectrode (diameter 10 μm), at a scan rate of 1 V s^{-1}.

with that observed previously for $NaNO_3$ and KNO_3 in the same RTIL (see Chapter 7).

On sweeping the potential more positive, a further oxidative wave was observed. Figure 8.2 shows the oxidation of a saturated solution of KNO_2 in $[C_2mim][NTf_2]$ on a Pt microelectrode (diameter 10 μm) with an extended anodic limit of +2.4 V. The voltammetry is presented at a scan rate of 1 V s^{-1} in order to show transient shaped peaks more clearly. The initial oxidation peak at +1.05 V *vs* Ag (small shift due to quasi-reference electrode) is consistent with that shown in Figure 8.1a, and there is also a broad second oxidative wave at +1.98 V. This was coupled to a broad reductive wave at *ca.* +1.72 V (not shown), which was quite irreproducible and only observed intermittently. The second oxidative peak is more defined on the microelectrode compared to the macroelectrode due to lower capacitance, so only the microelectrode results are presented. On the 10 μm Pt microelectrode, there was also evidence of a third oxidation peak (not shown here), but this was very broad and un-defined, and also only observed intermittently.

To suggest the identity of the three oxidation peaks, the voltammetry of nitrite was referenced to the ferrocene/ferrocenium (Fc/Fc^+) redox couple in solution. As the peak potentials of nitrite oxidation and Fc/Fc^+ are similar, the voltammetry of nitrite was first referenced to

cobaltocenium/cobaltocene (Cc^+/Cc), and then adjusted to Fc/Fc^+. Ferrocene is recommended by IUPAC[28] as a stable redox couple in aprotic media, and has been used in RTILs for this purpose.[29] The oxidation of ferrocene occurred at a potential of +0.85 V in this solution, which gives the positions of the three oxidation peaks as *ca.* +0.20, +1.13 and + 1.57 V *vs* Fc/Fc^+. The identity of the second peak is thus provisionally thought to be the oxidation of NO_2 (monomer), which was formed in equation 8.5, as the peak potential is similar that of NO_2 oxidation (+1.10 V *vs* Fc/Fc^+, see section 8.3.2). This suggests that if equation 8.6 is occurring, it is either not instantaneous or does not go to completion in this medium. The third peak is likely the oxidation of NO_3^- (produced in equation 8.6), as the peak potential matches that of NO_3^- *vs* Fc/Fc^+ (not shown here).

8.3.2 Oxidation of NO_2 gas in $[C_2mim][NTf_2]$

In order to explore the oxidation/reduction mechanisms and kinetics of NO_2, and to show the possible analytical utility of RTILs as a gas sensor for NO_2, the voltammetry of NO_2 was obtained on three Pt electrodes of diameter 10 μm, 100 μm and 0.5 mm. Figure 8.3 shows the oxidation of NO_2 gas (1 atm.) in $[C_2mim][NTf_2]$ on a 10 μm diameter Pt electrode in the potential range +0.4 V to +1.0 V. Three repeat cycles are overlaid at a scan rate of 1 V s^{-1}. A steady-state oxidation peak at *ca.* +0.86 V (*vs* Ag) is observed, with a corresponding transient-shaped reduction peak at +0.55 V, which is stable on successive cycles. The oxidation peak current is relatively high compared to KNO_2 (Figure 8.1a), suggesting a larger solubility of NO_2 in $[C_2mim][NTf_2]$ (solubility values discussed below).

The experiments were then repeated under the same conditions on two larger Pt electrodes of diameter 100 μm and 0.5 mm, and are shown in Figures 8.4a and 8.4b respectively at a range of scan rates. A plot of peak current *vs* square root scan rate for the oxidation peak on the 100 μm diameter Pt electrode (Figure 8.4a) is linear, indicating that the process is diffusion

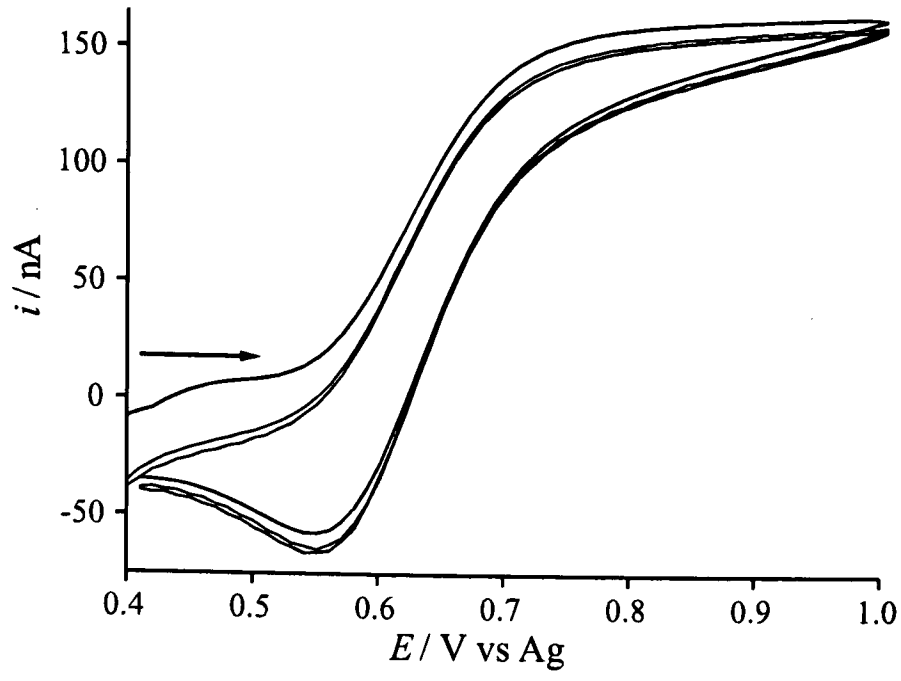

Figure 8.3: Cyclic voltammograms (three repeat scans) for the oxidation of 1 atm. NO_2 gas in $[C_2mim][NTf_2]$ on a Pt microelectrode (diameter 10 μm) at a scan rate of 1 V s^{-1}.

controlled. However, the same plot on the larger (0.5 mm diameter) Pt electrode is curved, suggesting that the process may be controlled by a chemical step preceding the electrochemical step. This suggests that NO_2 probably exists in solution as its more stable dimer, N_2O_4, and undergoes dissociation before the electrochemical step. This is in agreement with that observed by Amatore *et al.*[22] and Wartel *et al.*,[20,21] who propose the following CE mechanism:

$$N_2O_4 \underset{k_{-1}}{\overset{k_1}{\rightleftharpoons}} 2NO_2 \tag{8.7}$$

$$NO_2 \xrightarrow{k_0} NO_2^+ + e^- \tag{8.8}$$

There was also no voltammetric evidence to suggest that heterolytic dissociation occurs in this medium. It is believed that the corresponding reduction peak on Figures 8.3 and 8.4 is thus due to the reduction of the nitronium cation, NO_2^+, back to NO_2. This was further confirmed separately by matching the peak positions of NO_2^+/NO_2 *vs* Fc/Fc^+ (not shown here), using nitronium tetrafluoroborate (NO_2BF_4) as the source of the nitronium cation. We note here that the addition of NO_2 gas shifted the peak potential of ferrocene oxidation very significantly,

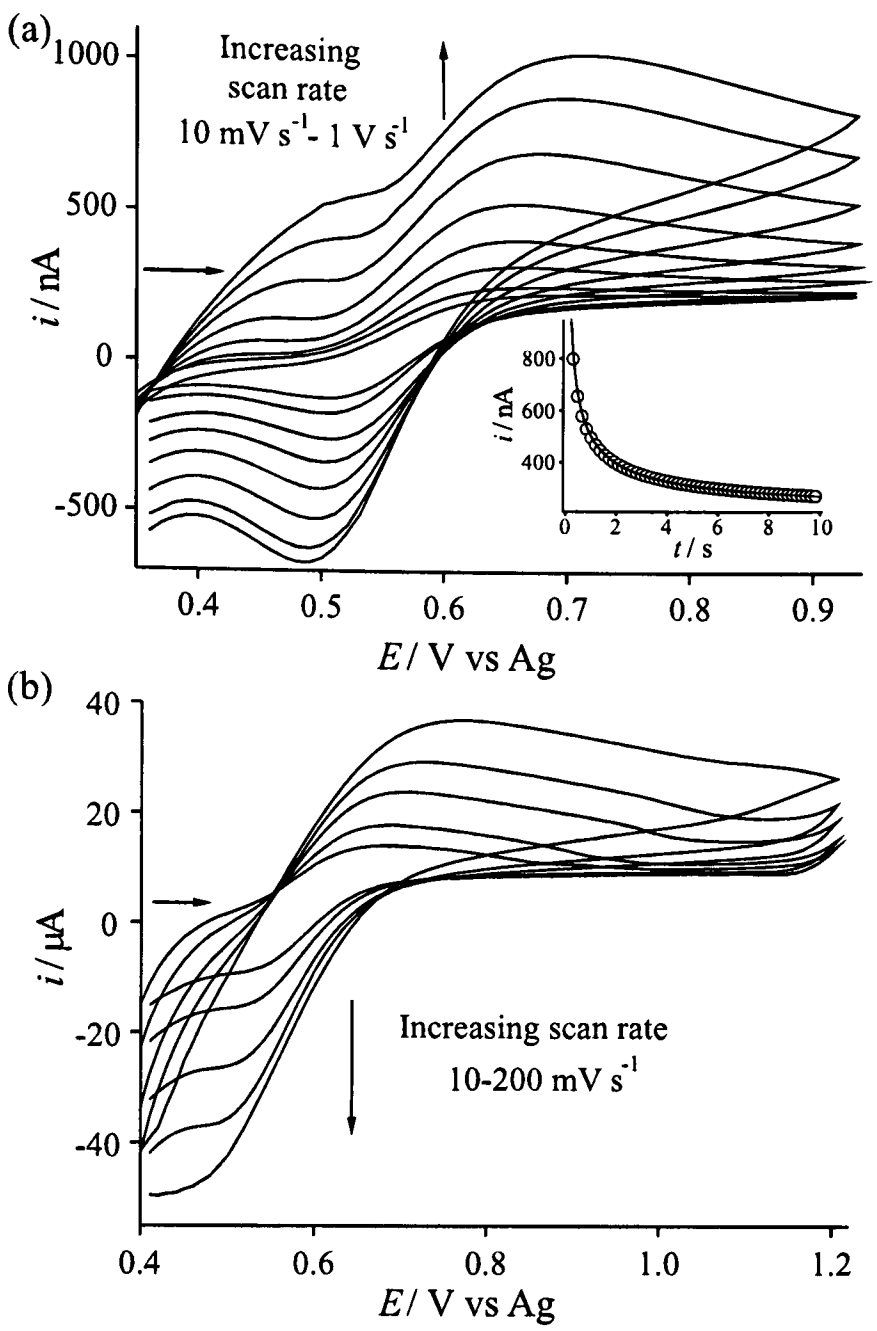

Figure 8.4: Cyclic voltammograms for the oxidation of 1 atm. NO_2 gas in $[C_2mim][NTf_2]$ on (a) a Pt microelectrode (diameter 100 μm) at scan rates of 10, 20, 50, 100, 200, 400, 700 and 1000 mV s^{-1} and (b) a Pt macroelectrode (diameter 0.5 mm) at scan rates of 10, 20, 50, 100 and 200 mV s^{-1}. The inset to (a) shows the experimental (–) and fitted theoretical (o) chronoamperometric transients for the oxidation of NO_2 on a 100 μm diameter Pt electrode. The potential was stepped from +0.4 to +0.9 V.

and that the positions (at 100 mV s^{-1}) of the oxidative and reductive waves on the 10 μm diameter Pt electrode are +1.10 V and +0.84 V *vs* Fc/Fc^+, respectively. The above mechanism is then used to simulate the oxidative peak of NO_2 on a 0.5 mm diameter Pt electrode in the one-dimensional simulation program DigiSim® 3.03 (BAS Technicol)[30] and is discussed later in Section 8.3.2.1.

To calculate the solubility of NO_2 (or N_2O_4) in $[C_2mim][NTf_2]$, a potential step was per-

formed on the oxidative wave of NO_2. The potential was stepped from +0.4 V to +0.9 V on the 100 μm diameter Pt electrode (which gave a better fit (*ca.* ± 0.7 % for both D and nc) to the Shoup and Szabo[25] expression than on the 10 μm diameter Pt electrode) and the current was measured for 10 seconds. The resulting chronoamperometric transient is shown as a solid line (Figure 8.4a inset), together with the theoretical fit (dots). The solubility of NO_2 in $[C_2mim][NTf_2]$ was calculated to be 51.2 (± 0.2) mM, which is more than 10 times greater than that observed in KNO_3-$NaNO_3$ melts (5 mM at 573 K[11] and 2 mM at 523 K),[12] suggesting the possibility of using RTILs as NO_2 potential gas sensing media. The diffusion coefficient of NO_2 (D_{NO_2}) in $[C_2mim][NTf_2]$ was found to be 1.59 (± 0.05) × 10^{-10} m^2 s^{-1} at 298 K, which is of the same order of magnitude as O_2 in $[C_2mim][NTf_2]$ (8.3 × 10^{-10} m^2 s^{-1} at 298 K),[31] and *ca.* one order of magnitude less than D_{NO_2} in the aprotic solvents dichloromethane (DCM), nitromethane (NM), acetonitrile (MeCN) and propylene carbonate (PC) at 296 K (1.4,[22] 1.1,[20] 1.8[22] and 0.28[20] × 10^{-9} m^2 s^{-1} respectively), which is reasonable given the higher viscosity of the RTIL at 293 K (34 cP)[23] compared to DCM (0.44 cP), NM (0.61 cP), MeCN (0.34 cP) and PC (2.5 cP).[27]

8.3.2.1 Simulating the Oxidation of NO_2 gas in $[C_2mim][NTf_2]$ on a 0.5 mm Diameter Pt Electrode

The one-dimensional simulation program DigiSim® 3.03 (BAS Technicol)[30] was used to model the oxidative wave of NO_2 on a 0.5 mm diameter Pt electrode at a range of scan rates. The generic reaction scheme used in the simulation was:

$$A = 2B \tag{8.9}$$

$$C + e^- = B \tag{8.10}$$

Table 8.1: Parameters employed in the simulation of NO_2 oxidation (first wave) following equations 8.7 and 8.8 at 298 K.

$[N_2O_4] = 46\ (\pm\ 5)$ mM	$K_{eq} = 6.0\ (\pm\ 0.5) \times 10^{-4}$ mol dm^{-3}
$[NO_2] = 140\ (\pm\ 10)$ mM	$k_1 = 10\ (\pm\ 0.5)$ s^{-1}
area of disk $= 1.96 \times 10^{-3}$ cm^2	$k_{-1} = 1.67\ (\pm\ 0.2) \times 10^4$ dm^3 mol^{-1} s^{-1}
$E_0 = 0.5$ V	$D_{N_2O_4} = 1.5\ (\pm\ 0.1) \times 10^{-6}$ cm^2 s^{-1}
$\alpha = 0.5$	$D_{NO_2} = 5.0\ (\pm\ 0.4) \times 10^{-6}$ cm^2 s^{-1}
$k_0 = 0.002\ (\pm\ 0.0001)$ cm s^{-1}	$D_{NO_2^-} = 6.0\ (\pm\ 0.5) \times 10^{-6}$ cm^2 s^{-1}

where A = N_2O_4, B = NO_2 and C = NO_2^+. It was found that the oxidative wave could be best simulated under a set of kinetic parameters, given in Table 8.1. The diffusion coefficient of N_2O_4 was 1.5×10^{-10} m^2 s^{-1}, very similar to that obtained from chronoamperometry (see above), and the diffusion coefficients of NO_2 and NO_2^+ were adjusted accordingly to give the best fit. The initial concentration of N_2O_4 was varied close to the value of 51 mM (from chronoamperometry), with the best fit obtained when the concentration was 46 ($\pm$ 5) mM. The remaining kinetic parameters (electrochemical rate constant, k_0, homogeneous equilibrium constant, K_{eq}, rate constants for the forward and backward reactions, k_1 and k_{-1}) were then also iterated to give the best possible fit, and are given in Table 8.1. The experimental (solid line) and simulated voltammograms (dots) for the oxidation of NO_2 on a 0.5 mm diameter Pt electrode are shown in Figure 8.5 at scan rates of (a) 20, (b) 50, (c) 100 and (d) 200 mV s^{-1}. These figures represent the best fit obtained from simulation of the mechanism given by equations 8.9 and 8.10.

It was found that the parameters given in Table 8.1 are comparable to those obtained in dichloromethane (DCM).[22] In DCM, k_0, K_{eq}, k_1 and k_{-1} were found to be 0.017 cm s^{-1}, 6.0×10^{-4} mol dm^{-3}, 10 s^{-1} and 1.8×10^4 dm^3 mol^{-1} s^{-1} respectively.[22] In the RTIL [C_2mim][NTf_2], these numbers are almost exactly the same, with the exception of k_0, which is 0.002 cm s^{-1} in the RTIL, indicating slower kinetics for the electrochemical step. This is not unexpected in a qualitatively different medium (34 cP[23] compared to 0.44 cP[27] at 293

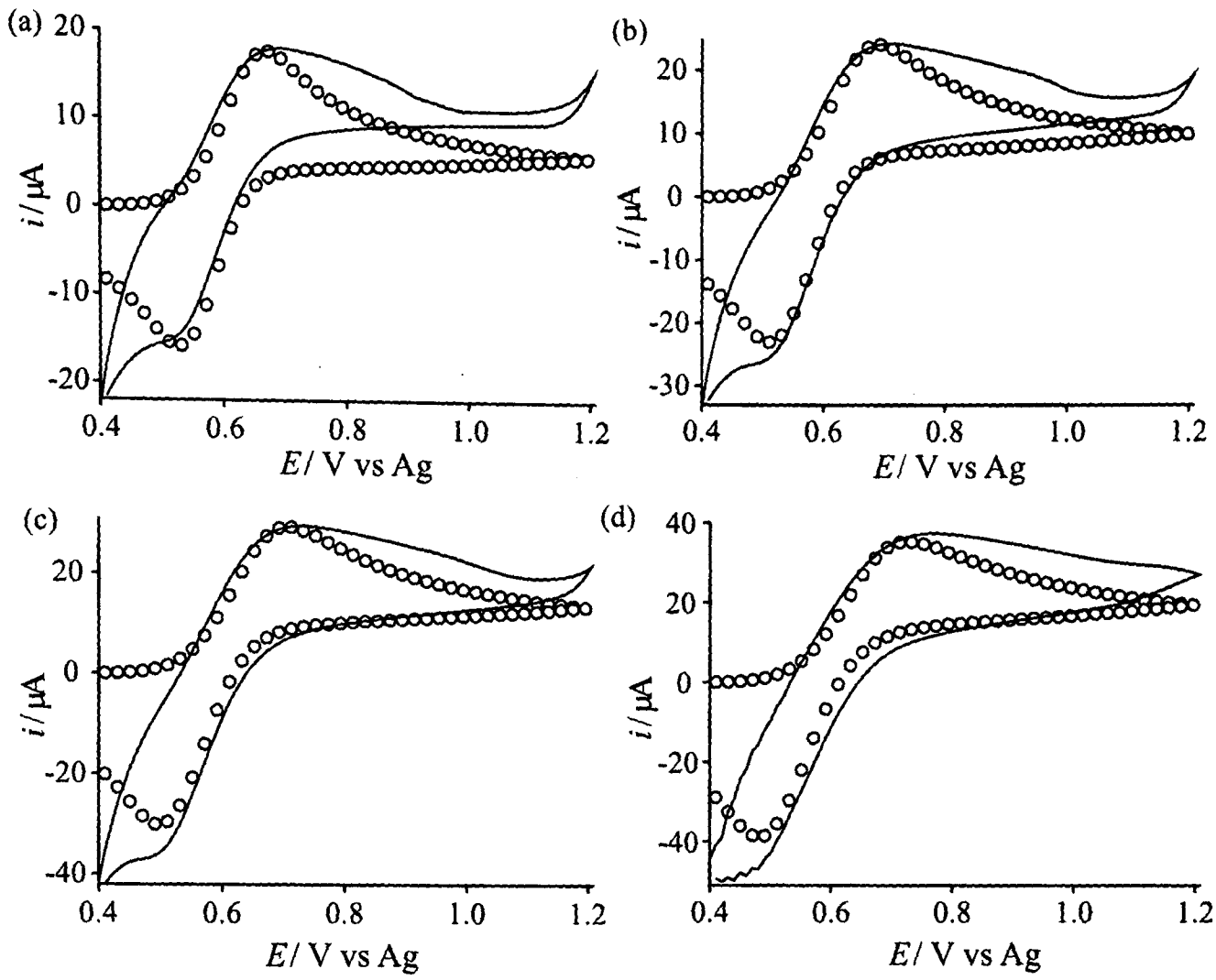

Figure 8.5: A comparison of experimental (–) and simulated (○) cyclic voltammetry for the oxidation of 1 atm. NO_2 in $[C_2mim][NTf_2]$ on a Pt macroelectrode (diameter 0.5 mm) at scan rates of (a) 20 (b) 50 (c) 100 and (d) 200 mV s^{-1}.

K) and also given the smaller electrode size used here in the RTIL study (0.5 mm diameter compared to 1 mm diameter in DCM).[22] These results suggest that the same mechanism for the oxidation of NO_2 (N_2O_4) is taking place inside an RTIL as in conventional solvents such as dichloromethane,[22] nitromethane,[20] acetonitrile,[22] and propylene carbonate.[20]

8.3.2.2 Extension of the Anodic Window

Unlike previous studies for the oxidation of NO_2,[20–22] a second oxidative wave was observed when the anodic window was extended further. This is likely a result of the wider accessible electrochemical window available in RTILs compared to conventional solvents. Figure 8.6 shows the oxidation of NO_2 (or its dimer N_2O_4) in $[C_2mim][NTf_2]$ on (a) a 100 μm diameter Pt electrode and (b) on a 0.5 mm diameter Pt electrode, at a range of scan rates. The second

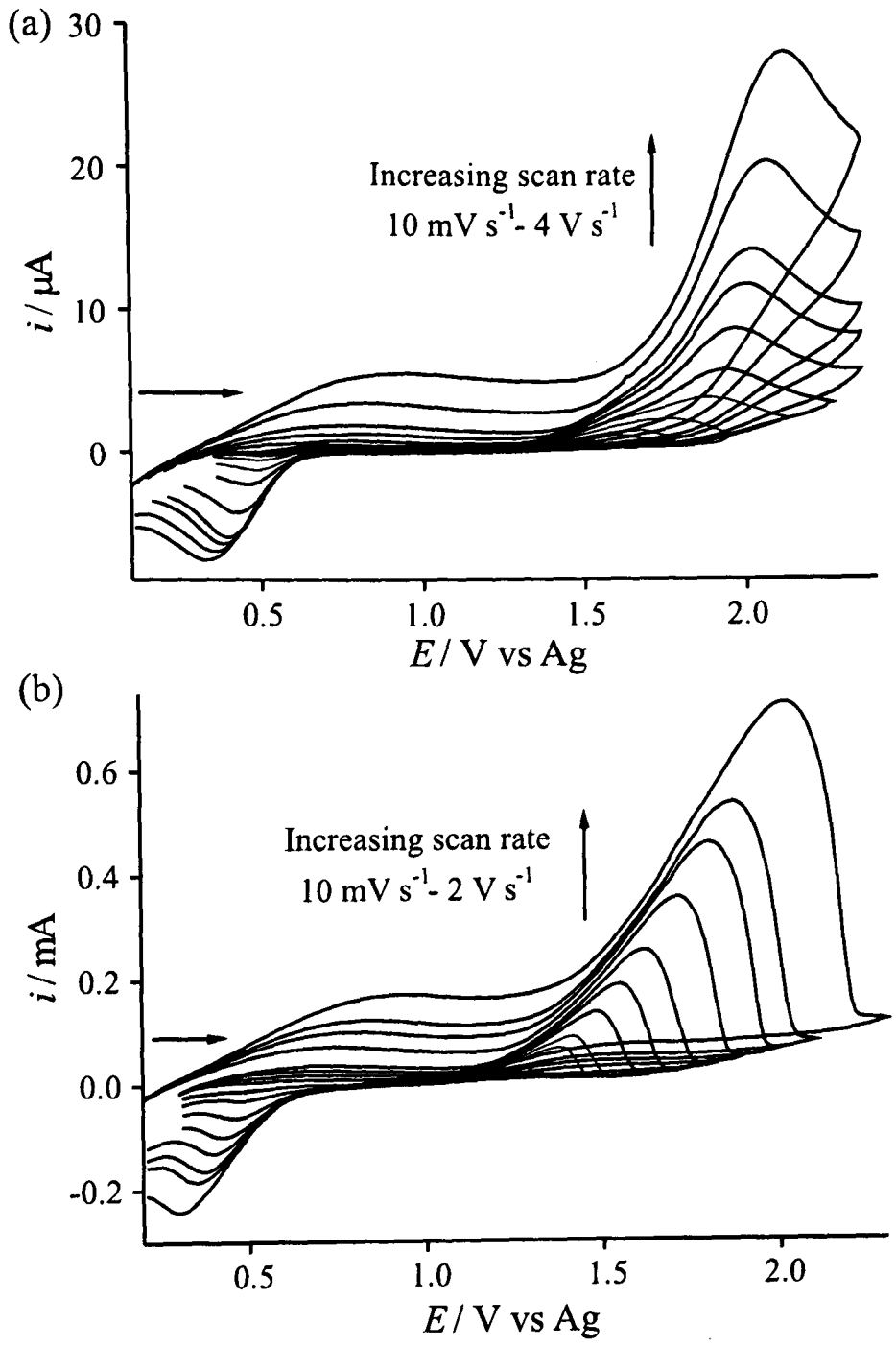

Figure 8.6: Cyclic voltammetry for the oxidation of 1 atm. NO_2 gas in $[C_2mim][NTf_2]$ with an extended anodic window on (a) a Pt microelectrode (diameter 100 μm) at scan rates from 10 to 4000 mV s^{-1}, and (b) a Pt macroelectrode (diameter 0.5 mm) at scan rates from 10 to 2000 mV s^{-1}.

oxidation appeared outside the accessible solvent window on the 10 μm diameter electrode, and hence is not shown. The first oxidation peak shown in Figure 8.4a (100 μm diameter electrode) is present at *ca.* +0.7 V *vs* Ag (+1.10 V *vs* Fc/Fc^+), and there is a second, much larger oxidative peak at +1.89 V (+2.24 V *vs* Fc/Fc^+ at 100 mV s^{-1}). This second oxidation is also observed at +1.54 V (+1.89 V *vs* Fc/Fc^+, 100 mV s^{-1}) on the 0.5 mm diameter electrode. In both cases, the separation between the second oxidation peak and the reduction peak increases

with scan rate (more dramatically on the larger 0.5 mm diameter Pt electrode), indicating that the system is not fully reversible, and complicated by follow-up chemistry in the mechanism. Furthermore, attempts to fit a potential step (chronoamperometric transient) to the Shoup and Szabo[25] expression were unsuccessful for the second wave, supporting this conclusion. In light of these findings, we tentatively suggest that the second oxidation wave corresponds to the direct oxidation of N_2O_4, possibly following an ECE mechanism given below:

$$N_2O_4 \rightarrow N_2O_4^+ + e^- \tag{8.11}$$

$$N_2O_4^+ \rightleftharpoons NO_2 + NO_2^+ \tag{8.12}$$

$$NO_2 \xrightarrow{k_0} NO_2^+ + e^- \tag{8.13}$$

This mechanism is further supported by the observation that the reduction peak at *ca.* +0.4 V (reduction of the nitronium cation) gets larger on repeat cycles, indicating that the nitronium cation (NO_2^+) is a product of the second oxidation. To demonstrate this, Figure 8.7 shows five consecutive cyclic voltammograms for the oxidation of NO_2 in $[C_2mim][NTf_2]$ on a 0.5 mm diameter Pt electrode at a scan rate of 1 V s^{-1}. The peak current of the reduction peak at *ca.* +0.4 V *vs* Ag increases systematically on consecutive cycles, despite the fact that the second oxidation peak at *ca.* +1.89 V decreases. This evidence allows the suggestion of the identity of the second peak as the direct oxidation of N_2O_4, which is not unreasonable given the higher potentials required for its direct oxidation.

8.3.3 Reduction of NO_2 gas in $[C_2mim][NTf_2]$

As a final step in investigating the full electrochemical mechanism of NO_2 in $[C_2mim][NTf_2]$, the reductive window was next studied. Figure 8.8a shows the reduction of NO_2 starting at +1.25 V in $[C_2mim][NTf_2]$ on a 0.5 mm diameter Pt electrode at a scan rate of 100 mV s^{-1}. In starting

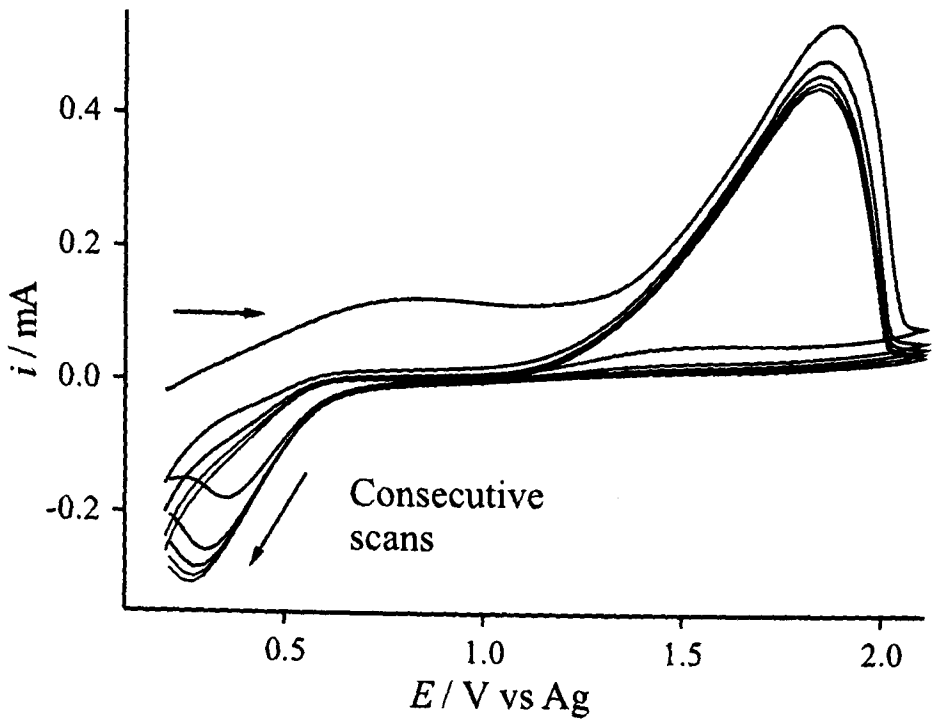

Figure 8.7: Cyclic voltammetry for the oxidation of 1 atm. NO_2 gas in $[C_2mim][NTf_2]$ with an extended anodic window on a Pt macroelectrode (diameter 0.5 mm). Five consecutive scans are shown at a scan rate of 1 V s^{-1}.

at a positive potential, the initial reduction peak as seen in Figure 8.4b (part of the redox couple given in equations 8.7 and 8.8) at *ca.* +0.5 V is clearly evident. At more negative potentials, there is a much larger reduction peak (at -0.62 V, -0.11 V *vs* Fc/Fc^+), with a corresponding broad oxidative wave (at +0.49 V *vs* Ag, +1.0 V *vs* Fc/Fc^+). The peak separation is much too large to be from oxygen (*cf.* ΔE_{pp} $(O_2/O_2^{\bullet -}) = 0.35$ V in $[C_2mim][NTf_2]$)[31] and therefore must be due to the reduction of NO_2 (N_2O_4) in solution. Figure 8.8b shows cyclic voltammograms for the reduction of NO_2 in $[C_2mim][NTf_2]$ on a Pt electrode (diameter 0.5 mm) at a scan rates from 10 to 200 mV s^{-1}. A plot of peak current *vs* square root scan rate for the reductive wave was linear, indicating that the process is diffusion controlled. The peak separations increase dramatically with scan rate, suggesting that the process is strongly electrochemically irreversible.

There are very few literature reports showing the reduction of NO_2; however Boughriet *et al.*[21] state that two reductive waves were observed following the reduction of N_2O_4 in sulfanone. They propose that the first wave corresponds to the reduction:

$$NO_2 + N_2O_4 + e^- \rightleftharpoons N_2O_3 + NO_3^- \qquad (8.14)$$

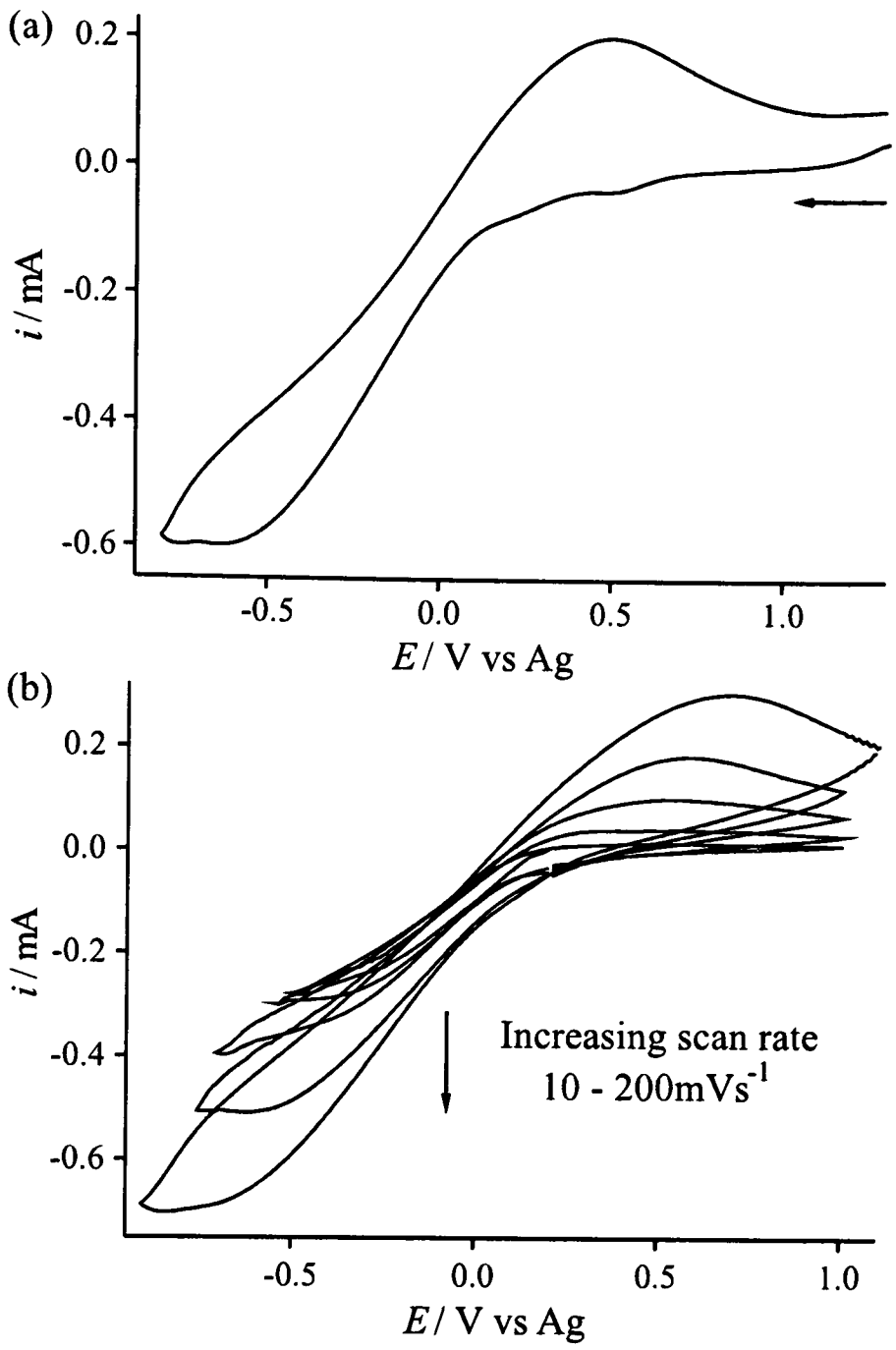

Figure 8.8: Cyclic voltammetry for the reduction of 1 atm. NO_2 gas in $[C_2mim][NTf_2]$ on a Pt macroelectrode (diameter 0.5 mm) starting from (a) +1.25 V (scan rate 100 mV s^{-1}), and (b) +0.2 V at scan rates of 10, 20, 50, 100 and 200 mV s^{-1}.

and the second wave corresponds to either/all of the following equations:

$$3N_2O_4 + 2e^- \rightleftharpoons 2N_2O_3 + 2NO_3^- \tag{8.15}$$

$$N_2O_4^+ + e^- \rightleftharpoons NO + NO_3^- \tag{8.16}$$

$$2N_2O_3 + e^- \rightleftharpoons 3NO + NO_3^- \tag{8.17}$$

It is possible that some or all of these processes operate in the RTIL medium. Furthermore, successful fitting to a chronoamperometric transient was not achieved, suggesting that the reduction is not a simple n-electron transfer step, which is consistent with the above equations. It is difficult to determine the nature of any intermediates, although there was no evidence of any deposit on the electrode surface following the reduction. We note here that two isomers of N_2O_4 are possible (O_2N-NO_2 and ONO-NO_2) which would be likely to exhibit different redox behaviour, although we have seen no voltammetric evidence to distinguish between the two. Since the peaks are relatively broad, it may be possible that they both exist and contribute to the peak shape in Figure 8.8.

8.4 Conclusions

The electrochemical oxidations of the nitrite ion (from KNO_2) and nitrogen dioxide gas (NO_2) in $[C_2mim][NTf_2]$ have been studied by cyclic voltammetry on various Pt electrodes of size 10 μm, 100 μm and 0.5 mm. A one-electron oxidation wave was observed for the oxidation of nitrite, followed by a second (and sometimes third) oxidation peak at more positive potentials. The peak positions were observed at +0.20, +1.13 and + 1.57 V *vs* Fc/Fc^+ (standard internal reference redox couple). These peaks were assigned to the oxidations of nitrite, NO_2 and nitrate (NO_3^-) respectively. From chronoamperometry, a solubility value of 7.5 mM and diffusion coefficient at 298 K of 2.0×10^{-11} m^2 s^{-1} for KNO_2 was calculated. The oxidation of NO_2 gas was then studied. The gas is thought to be in equilibrium with its dimer, N_2O_4 in this medium. Two oxidative waves (+1.10 and +2.24 V *vs* Fc/Fc^+ at 100 mV s^{-1} on the 100 μm diameter electrode) were observed, and are assigned to: (a) the oxidation of N_2O_4 following a CE process given in equations 8.7 and 8.8, and (b) the *direct* oxidation of N_2O_4 following an ECE process given in equations 8.11, 8.12 and 8.13. An electrochemically irreversible reductive wave (at -0.31 V *vs* Fc/Fc^+) was also observed, although its identity is unconfirmed. A diffusion coefficient at 298 K

of 1.6×10^{-10} m^2 s^{-1} and a solubility of *ca.* 51 mM was calculated, suggesting the possibility for using RTILs as potential media for the analytical sensing of NO_2 gas.

Up until now, the work in this thesis has mainly focussed on determining the mechanisms of dissolved organic and inorganic species in one or two chosen ionic liquids. However, the next few chapters will now focus on the behaviour of protons in a range of ionic liquid media, in order to try to understand the nature of acid-base reactions in ionic liquids. For this, several different ionic liquids with varying cations and anions have been utilized. Since we have shown in this chapter that ionic liquids can be used for the detection of nitrogen dioxide gas, the next chapter also expands the understanding of gas sensing in RTILs by describing the oxidation of hydrogen gas in ten different ionic liquids.

References

[1] Broder, T. L.; Silvester, D. S.; Aldous, L.; Hardacre, C. and Compton, R. G., *J. Phys. Chem. B*, 2007, **111**, 7778–7785.

[2] Alonso, A.; Etxaniz, B. and Martinez, M. D., *Food Addit. Contam.*, 1992, **9**, 111–117.

[3] Sanyal, S., *Bull. Electrochem.*, 1990, **6**, 392–394.

[4] Genders, J. D.; Hartsough, D. and Hobbs, D. T., *J. Appl. Electrochem.*, 1996, **26**, 1–9.

[5] Davis, J.; Moorcroft, M. J.; Wilkins, S. J.; Compton, R. G. and Cardosi, M. F., *Analyst*, 2000, **125**, 737–742.

[6] Moorcroft, M. J.; Davis, J. and Compton, R. G., *Talanta*, 2001, **54**, 785–803.

[7] Zhao, G.; Liu, K.; Lin, S.; Liang, J.; Guo, X. and Zhang, Z., *Mikrochim. Acta*, 2004, **144**, 75–80.

[8] Martins, M. E.; Calandra, A. J. and Arvía, A. J., *Electrochim. Acta*, 1970, **15**, 111–126.

[9] Calandra, A. J. and Arviá, A. J., *Electrochim. Acta*, 1966, **11**, 1173–1188.

[10] Swofford, H. S., J. and McCormick, P. G., *Anal. Chem.*, 1965, **37**, 970–974.

[11] Topol, L. E.; Osteryoung, R. A. and Christie, J. H., *J. Phys. Chem.*, 1966, **70**, 2857–2862.

[12] McCormick, P. G. and Swofford, Harold S., J., *Anal. Chem.*, 1969, **41**, 146–152.

[13] Wargon, J. A. and Arvía, A. J., *Electrochim. Acta*, 1971, **16**, 1619–1626.

[14] Wargon, J. A. and Arvía, A. J., *Electrochim. Acta*, 1972, **17**, 649–664.

[15] Caro, C. A.; Bedioui, F. and Zagal, J. H., *Electrochim. Acta*, 2002, **47**, 1489–1494.

[16] Piela, B. and Wrona, P. K., *J. Electrochem. Soc.*, 2002, **149**, E55–E63.

[17] Tanaka, N. and Kato, K., *Bull. Chem. Soc. Japan*, 1956, **29**, 837–842.

[18] Hohercáková, Z. and Opekar, F., *Sens. Act. B*, 2004, **B97**, 379–386.

[19] Mizutani, Y.; Matsuda, H.; Ishiji, T.; Furuya, N. and Takahashi, K., *Sens. Act. B*, 2005, **B108**, 815–819.

[20] Boughriet, A.; Wartel, M.; Fischer, J. C. and Bremard, C., *J. Electroanal. Chem. Interfacial Electrochem.*, 1985, **190**, 103–115.

[21] Boughriet, A.; Wartel, M. and Fischer, J. C., *Talanta*, 1986, **33**, 385–390.

[22] Lee, K. Y.; Amatore, C. and Kochi, J. K., *J. Phys. Chem.*, 1991, **95**, 1285–1294.

[23] Bonhôte, P.; Dias, A.-P.; Papageorgiou, N.; Kalyanasundaram, K. and Grätzel, M., *Inorg. Chem.*, 1996, **35**, 1168–1178.

[24] Desimoni, E.; Palmisano, F. and Zambonin, P. G., *J. Electroanal. Chem. Interfacial Electrochem.*, 1977, **84**, 315–322.

[25] Shoup, D. and Szabo, A., *J. Electroanal. Chem. Interfacial Electrochem.*, 1982, **140**, 237–245.

[26] Daniel, V. and Albright, J. G., *J. Chem. Eng. Data*, 1995, **40**, 519–522.

[27] Lide, D. R., Ed., *Handbook of Chemistry and Physics: 76th Edition*, CRC Press, Boca Raton, USA, 1996.

[28] Grützner, G. and Kuta, J., *Pure Appl. Chem.*, 1984, **56**, 461–466.

[29] Hultgren, V. M.; Mariotti, A. W. A.; Bond, A. M. and Wedd, A. G., *Anal. Chem.*, 2002, **74**, 3151–3156.

[30] Rudolph, M.; Reddy, D. P. and Feldberg, S. W., *Anal. Chem.*, 1994, **66**, 589A–600A.

[31] Buzzeo, M. C.; Klymenko, O. V.; Wadhawan, J. D.; Hardacre, C.; Seddon, K. R. and Compton, R. G., *J. Phys. Chem. A*, 2003, **107**, 8872–8878.

Chapter 9

The Electrochemical Oxidation of Hydrogen at Activated Platinum Electrodes in Several RTILs

This chapter presents the oxidation of hydrogen on a Pt microelectrode (diameter 10 μm) using cyclic voltammetry in the following ionic liquids: $[C_2mim][NTf_2]$, $[C_4mim][NTf_2]$, $[N_{6,2,2,2}][NTf_2]$, $[P_{14,6,6,6}][NTf_2]$, $[C_4mim][OTf]$, $[C_4mim][BF_4]$, $[C_4mim][PF_6]$, $[C_4mim][NO_3]$, $[C_6mim]Cl$ and $[C_6mim][FAP]$ (the full names of which are given in Chapter 3). Activation of the Pt electrode is necessary to obtain reliable and reproducible voltammetry. After activation of the electrode, the H_2 oxidation waves are nearly electrochemically and chemically reversible in $[C_nmim][NTf_2]$ ionic liquids, chemically irreversible in $[C_6mim]Cl$ and $[C_4mim][NO_3]$, and show intermediate characteristics in $[OTf]^-$, $[BF_4]^-$, $[PF_6]^-$, $[FAP]^-$ and other $[NTf_2]^-$-based ionic liquids. These differences reflect the contrasting interactions of protons with the respective RTIL anions. The appearance and position of the reverse (reduction) peak on the voltammograms is thought to depend on three factors: (1) the stability of the proton solvated by the RTIL anion, HA, (2) the position of equilibrium of the protonation reaction $H^+ + A^- \rightleftharpoons HA$, and (3) any follow-up chemistry *e.g.* dissociation or reaction of the solvated proton, HA. The reduction of $H[NTf_2]$ is also studied in two $[NTf_2]^-$ based RTILs, and match well to the oxidation waves from hydrogen. The oxidation peaks of hydrogen are reported relative to the half-wave potential of the cobaltocenium/cobaltocene redox couple in all ionic liquids studied, giving an indication of the relative proton interactions of each ionic liquid. A preliminary temperature study (*ca.* 298–333 K) is also carried out in some of the ionic liquids. Diffusion coefficients and solubilities of hydrogen at 298 K are obtained from potential-step chronoamperometry, and there is no obvious relationship found between the diffusion coefficients and solvent viscosity. RTILs possessing $[NTf_2]^-$ and $[FAP]^-$ anions show the highest microelectrode peak currents for the oxidation in H_2 saturated

solutions, with $[C_4mim][NTf_2]$ being the most sensitive. The large number of available RTIL anion/cation pairs allows scope for the possible electrochemical detection of hydrogen gas for use in gas-sensor technology.

Part of this work was carried out with the assistance of Mr. Kristopher R. Ward, an undergraduate summer project student at Oxford University. The work in this chapter has been published in two parts; in the Journal of Physical Chemistry B[1] and in the Journal of Electroanalytical Chemistry.[2]

9.1 Introduction

It is of general interest to explore the oxidation of hydrogen (H_2) gas due to its major importance in fuel cells[3] among other applications. The oxidation of gaseous hydrogen is (at least in principle) believed to be conceptually one of the simplest processes, involving a simple one-electron transfer per proton. The electrochemical oxidation of hydrogen has been extensively studied on platinum and palladium surfaces in protic solvents[4–7] such as H_2O, but relatively little work has been done in aprotic solvents. Barrette and Sawyer[8] showed chemically reversible oxidation waves for dissolved H_2 in dimethyl sulfoxide (DMSO), pyridine, *N*,*N*-dimethylformamide (DMF) and acetonitrile (MeCN), and observed broad, diffuse anodic peaks whose peak currents were irreproducible and not proportional to the partial pressure of H_2. However, when the electrodes were activated electrochemically (preanodized) at potentials more positive than the initial peaks, the H_2 oxidation peak changed from a shape characteristic of an electrochemically quasi-reversible process to one for a nearly reversible one-electron transfer.[8] In all solvents except MeCN, reversible waves with peak currents proportional to the partial pressure of H_2 were observed, allowing in principle for a quantitative analysis of the solubility of H_2.

Daniele and Bontempelli[9] have also investigated the H^+/H_2 redox couple in a range of organic polar solvents. By the in situ electrogeneration of anhydrous perchloric acid, and assuming its

subsequent quantitative dissociation in line with:

$$HClO_4 + S \rightleftharpoons HS^+ + ClO_4^- \tag{9.1}$$

where S = solvent, the half-wave potential for the reversible H^+/H_2 system could be related to the relative bulk solvent basicity. This system was then expanded to electrochemically evaluate a range of added bases, although both cases relied upon the use of a reference system that was strictly independent of the nature of the solvent.[9]

Concerning ionic liquids, Welton and co-workers[10] have used Kamlet-Taft parameterization to investigate a range of cations and anions, which gave trends in order of their basicity and their relative hydrogen bonding accepting and donating ability. Conventional acid-base indicators have also been used to physically probe the inherent acidity and basicity of ionic liquids; however, such probes are not calibrated towards ionic liquids and all observed colour changes can be the result of hydrogen-bonding interactions in addition to acid-base equilibria.[11–13] In addition, the nature of the solvation of strong acids in ionic liquids (*e.g.* $H_xS_y{}^{y+}$) has still to be conclusively demonstrated, and little is understood about the nature and relative strength of acidity within these ionic systems, despite numerous previous applications of inherently Brønsted acidic ionic liquids.[14–18] Del Popolo and co-workers[19] carried out a first-principles simulation study in order to investigate the solvation structure of a proton, simulating HCl dissolved in the ionic liquid $[C_1mim]Cl$. Rather than dissociation, this revealed the immediate formation of the anion $[HCl_2]^-$. At its most stretched configuration $[HCl_2]^-$ can only be considered as $[Cl\text{-}HCl]^-$, and the breaking of one H-Cl bond resulted in the formation of a new H-Cl bond, highlighting the possibility of proton transport by proton 'hopping', moving from chloride to chloride.

Anomalies relating to protons in ionic liquids have also been observed in catalytic reactions. For Friedel-Craft reactions performed in ionic liquids using both Lewis- and Brønsted-based catalysts, reactions have been observed to only perform well in ionic liquids based upon the

bis(trifluoromethylsulfonyl)imide anion ($[NTf_2]^-$) compared with $[OTf]^-$ and $[BF_4]^-$.[20,21] In addition, in $[NTf_2]^-$ based ionic liquids, the acid catalysts $H[BF_4]$ and H[OTf] demonstrate significantly lower reaction rates than $H[NTf_2]$, despite all three being strong acids in water.

In the present report, the oxidation of hydrogen gas (H_2) has been studied in a range of room temperature ionic liquids (RTILs) incorporating different common cations and anions, namely $[C_2mim][NTf_2]$, $[C_4mim][NTf_2]$, $[N_{6,2,2,2}][NTf_2]$, $[P_{14,6,6,6}][NTf_2]$, $[C_4mim][OTf]$, $[C_4mim][BF_4]$, $[C_4mim][PF_6]$, $[C_4mim][NO_3]$, $[C_6mim]Cl$ and $[C_6mim][FAP]$. A main focus of this work was to ascertain if reversible oxidation waves could be obtained for the oxidation of H_2 in ionic liquids where the product, HA, was stable (or not) on the voltammetric timescale. We anticipate the following reaction for the oxidation of hydrogen in an RTIL solvent (where A^-=solvent anion):

$$H_2 - 2e^- + 2A^- \rightleftharpoons 2HA \tag{9.2}$$

where the product HA is either stable or unstable. If the product is stable, chemically reversible voltammetry is expected, whereas if the product is unstable, a chemically irreversible voltammetric wave will be obtained. We also study the reduction of the acid $H[NTf_2]$ in two $[NTf_2]^-$ based RTILs to give further insight into the H^+/H_2 redox couple. The H_2 oxidation potential is reported *vs* a standard internal redox couple for all ten RTILs, and the effect of temperature on the voltammetry is investigated in four RTILs. It is believed that this may shed light on the nature of acidic proton—ionic liquid interactions, ultimately helping to define a pH scale in RTIL media, and to develop suitable reference electrodes for use in RTILs. This work also has implications in the possible amperometric sensing of H_2 gas.

9.2 Experimental

All experiments involving H_2 gas were performed on a 10 μm Pt (or 5 μm Au) working electrode placed in the T-cell (described in Chapter 3), with 20 μL of 'blank' ionic liquid in the cavity above the electrode. A tube leading directly from the H_2 gas cylinder was attached to one arm of the cell, and an outlet tube led to a fume cupboard. The gas was allowed to diffuse through the cell until equilibrium was achieved (typically after 10 minutes, as evidenced by maximum stable peak currents). Prior to the recording of chronoamperometric transients, the electrode as pre-activated at a chosen potential for 30 seconds. For experiments involving cobaltocenium hexafluorophosphate (Cc^+) as a redox probe, a solution of 20 mM Cc^+ was obtained following the solvent evaporation method described in Chapter 3. For experiments involving $H[NTf_2]$, solutions were first made up in 1 mL RTIL, of which 20 μL was transferred to the T-cell and purged under vacuum. Additional experimental details are given in Chapter 3.

9.3 Results and discussion

The oxidation of hydrogen, H_2, has been studied in a series of room temperature ionic liquids (RTILs) on a platinum microdisk electrode (diameter 10 μm) and a gold microdisk electrode (diameter 5 μm). H_2 gas was allowed to diffuse through 20 μL of the liquid for at least 30 minutes in order to allow complete saturation. There were no noticeable oxidation peaks on the 5 μm diameter gold electrode, so we conclude that H_2 oxidation is voltammetrically inactive on gold. Sizeable, reproducible peaks, however, were seen on the 10 μm diameter platinum electrode. All of the results presented below focus on the voltammetry obtained on the 10 μm diameter platinum electrode in a range of RTILs.

9.3.1 The Oxidation of Hydrogen on Platinum: Preliminary Observations

Figure 9.1 shows cyclic voltammograms obtained for the oxidation of H_2 on a platinum microdisk electrode (diameter 10 μm) in the RTILs $[C_2mim][NTf_2]$ and $[C_4mim][BF_4]$ in the potential range -0.5 V to +2.0 V *vs* Ag. The voltammetry shows a broad oxidation peak at approximately +0.9 V and +0.5 V *vs* Ag for $[C_2mim][NTf_2]$ and $[C_4mim][BF_4]$ respectively. In $[C_2mim][NTf_2]$ (Figure 9.1 solid line), the peak decreases slowly until the potential reaches +1.8 V. When the scan is reversed at +2.0 V, the backward scan measures a lower current than the forward scan until +1.2 V, after which the current rapidly increases to a maximum at +0.9 V. The current then decreases rapidly at +0.5 V, showing a sharp cathodic peak at +0.2 V *vs* Ag. In $[C_4mim][BF_4]$ (dotted line), the anodic peak reaches a maximum at approximately +0.5 V, after which it slowly decreases to almost zero current. On reversal of the scan at +2.0 V *vs* Ag, the current on the backward scan is again less than on the forward scan. At +1.0 V, the current rises sharply to a maximum, then plateaus, after which it then decreases sharply at +0.1 V, and shows the appearance of a small cathodic peak at -0.3 V *vs* Ag. The unusual form of wave shape has also been observed in the aprotic solvent DMSO by Barrette and Sawyer[8] using platinum macroelectrodes, although this phenomena was not fully investigated, and only forward voltammetric scans were shown.

The highly unusual shape of the voltammograms, in which the microelectrode current abruptly falls with increasing potential, might indicate that either (a) the voltammogram has passed through the potential of zero charge (PZC), giving rise to anions on the surface of the electrode rather than cations and hence a change in the electron transfer kinetics, or (b) there is a point of transition where platinum oxides are formed at potentials positive of some threshold. We rule out (a), since the PZC for RTILs is thought to be much more negative than that observed in Figure 9.1. The PZC in $[C_4mim][BF_4]$ was reported[22] to be approximately -0.5 V *vs* Ag, and in $[C_nmim][NTf_2]$ RTILs (n=8, 10), the PZC was -0.254 V and -0.161 V *vs* Ag/Ag^+ respec-

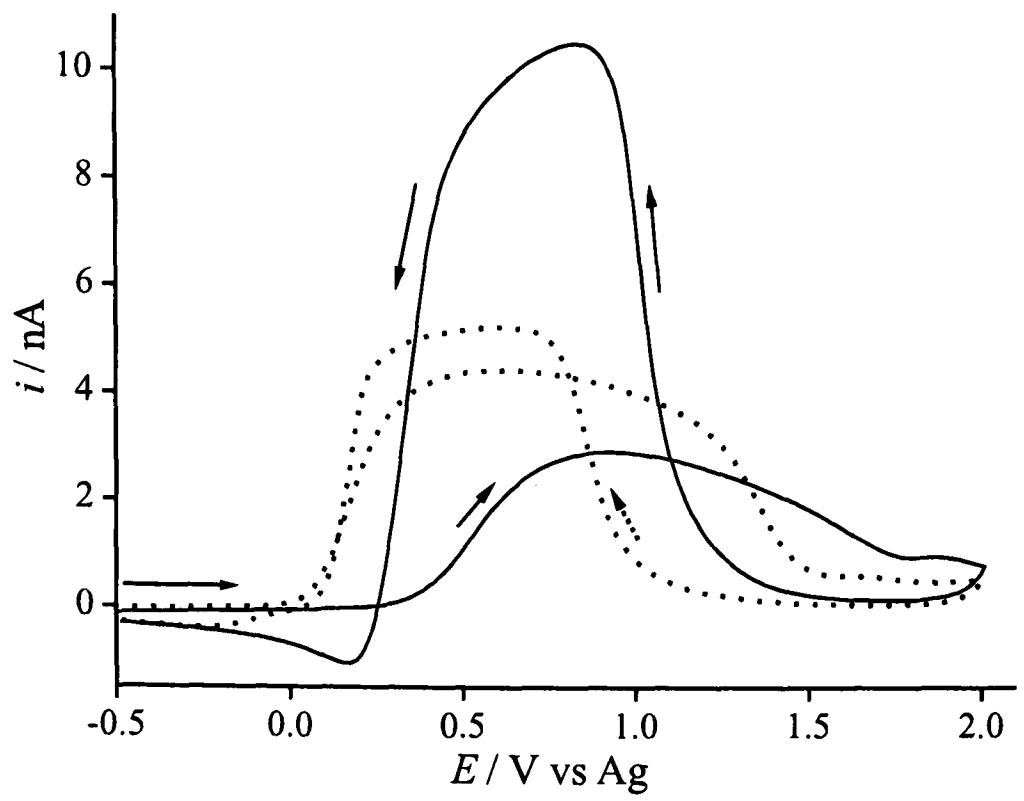

Figure 9.1: Cyclic voltammograms for the oxidation of 1 atm. H_2 on a Pt electrode (diameter 10 μm) in the RTILs [C_2mim][NTf_2] (solid line) and [C_4mim][BF_4] (dotted line) with an anodic limit of +2.0 V. Scan rate 100 mV s^{-1}.

tively.[23] On the other hand, the formation of platinum oxides in the presence of hydrogen has been observed previously in aqueous solutions by Varela and Krischer,[24] and was described by the following equations:

$$Pt + H_2O \rightarrow Pt - OH + H^+ + e^- \tag{9.3}$$

$$Pt - OH \rightarrow Pt - O + H^+ + e^- \tag{9.4}$$

It was suggested[24] that Pt oxide formation sets in close to the upper turning point of the voltammogram, which leads to an inhibition of hydrogen oxidation, noted by the decrease in current and large histeresis in the two scan directions. The formation of Pt oxide was also suggested briefly by Barette and Sawyer[8] for the oxidation of H_2 in aprotic solvents. Based on the shape of the voltammograms in Figure 9.1, it is likely that the same process is happening here. Equation 9.3 suggests that there must be a source of water present in order for platinum oxide formation, and we propose that a small amount of trace water present in the ionic liquid is enough to initiate such a reaction, noting that as little as monolayer oxide formation may

be required to inhibit the H_2 oxidation reaction. We also note here that different RTILs will have different water contents, leading to varying amounts of platinum oxide formation for each system. Although we have previously highlighted[25] that the experimental set-up (employed in this work) is efficient in removing water from the RTIL, it is clearly not possible to obtain completely anhydrous IL samples. The main difference between the voltammograms obtained in aqueous solvents and those presented in Figure 9.1 is noted: in aqueous solutions,[24] the current decreases rapidly after the formation of Pt oxide, and remains close to zero on the reverse scan until the oxide is reduced. In all of the ionic liquids studied (with the exception of $[C_6mim]Cl$ and $[C_4mim][NO_3]$) the current on the reverse scan was *larger* than on the forward scan, resulting in a cross-over of the scans, and the appearance of a reduction peak at all scan rates studied (20 mV s^{-1} to 10 V s^{-1}).

On the second and subsequent scans in all RTILs, the forward peak current increases in comparison with the first scan, indicating that the electrode has been 'activated' after scanning to +2 V. Varela and Krischer[24] report that the peak current on the second and subsequent scans in aqueous solutions remains similar, although the cathodic scans show behaviour which suggests that after an active/passive cycle is formed, the electrode reaches its highest activity that decreases with more cycles, until finally another active/passive cycle occurs. Repeat scans for unactivated electrodes were not discussed for the oxidation of H_2 in aprotic solvents.[8] Figure 9.2 shows the effect of activating the electrode in $[C_4mim][NTf_2]$ on a 10 μm diameter Pt electrode at a scan rate of 100 mV s^{-1}. The peak current of the anodic peak on the first cycle (bold solid line) is 3 nA, which increases to 11 nA on the reverse wide scan (dotted line). The peak current on the third scan (dot dashed line) is 7 nA, more than twice that of the first scan. When the current is held for 30 seconds at +2.0 V *vs* Ag, the peak current on the next scan increased even further to 8 nA (dashed line). Holding the current for 5 minutes (thin solid line), however, did not increase the peak current to a higher value than holding for 30 seconds, indicating that

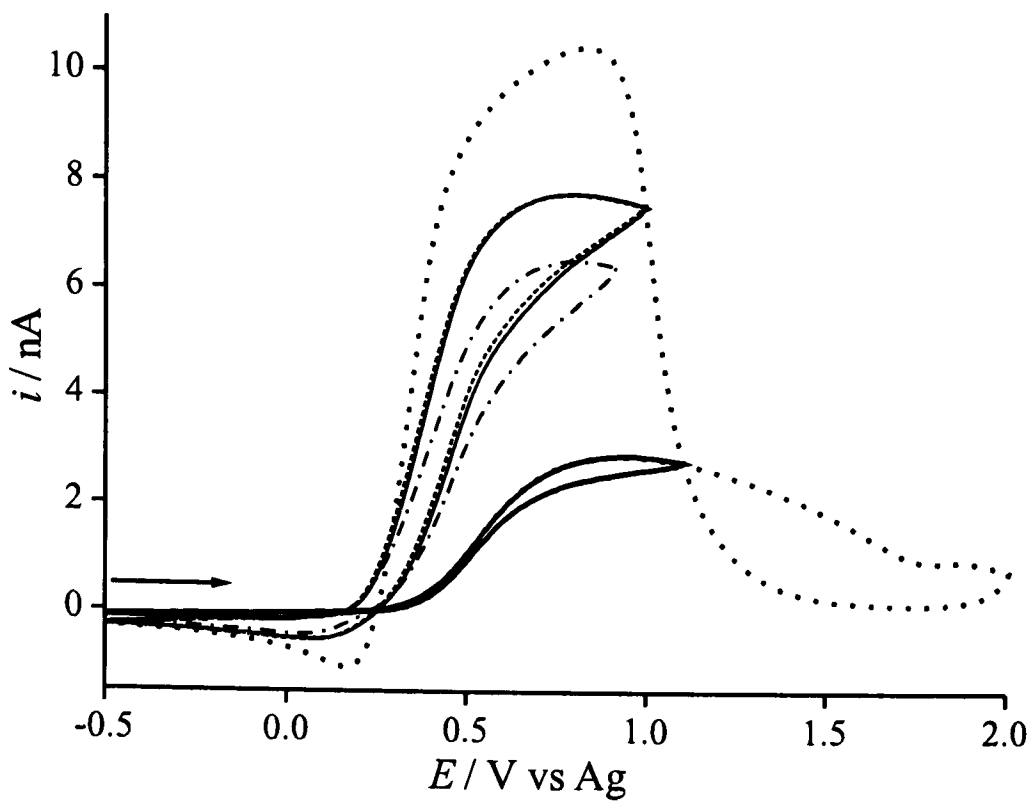

Figure 9.2: Cyclic voltammograms for the oxidation of 1 atm. H_2 in $[C_4mim][NTf_2]$ on a 10 μm diameter Pt electrode, scan rate 100 mV s^{-1}. Bold solid line=first scan, dotted line=second scan (with an extended anodic window), dot-dashed line=third scan, dashed line=scan taken after preanodization for 30 seconds, thin solid line=scan taken after preanodization for 5 minutes.

the 'activation' of the electrode is completed after 30 seconds. Deactivation of activated electrodes appears to occur over a number of minutes unless a second activating cycle is applied. Similar observations have been noted by Barrette and Sawyer[8] in the aprotic solvents MeCN, DMF, DMSO and pyridine, whereas in water, the activation lasted for 20 minutes, probably in each case due to the specific adsorption of trace impurities. It is expected that freshly reduced platinum oxide will give rise to a platinum surface which is free from adsorbed impurities when newly formed, until the adsorption of aprotic solvent molecules which results in the deactivation of the electrode.[8]

9.3.2 The Oxidation of Hydrogen in $[NTf_2]^-$ based RTILs: Activation *vs* Non-Activation

In order to demonstrate the effect of electrode activation on the observed voltammetry, the oxidation of hydrogen was studied on both non-activated and activated electrodes in four RTILs

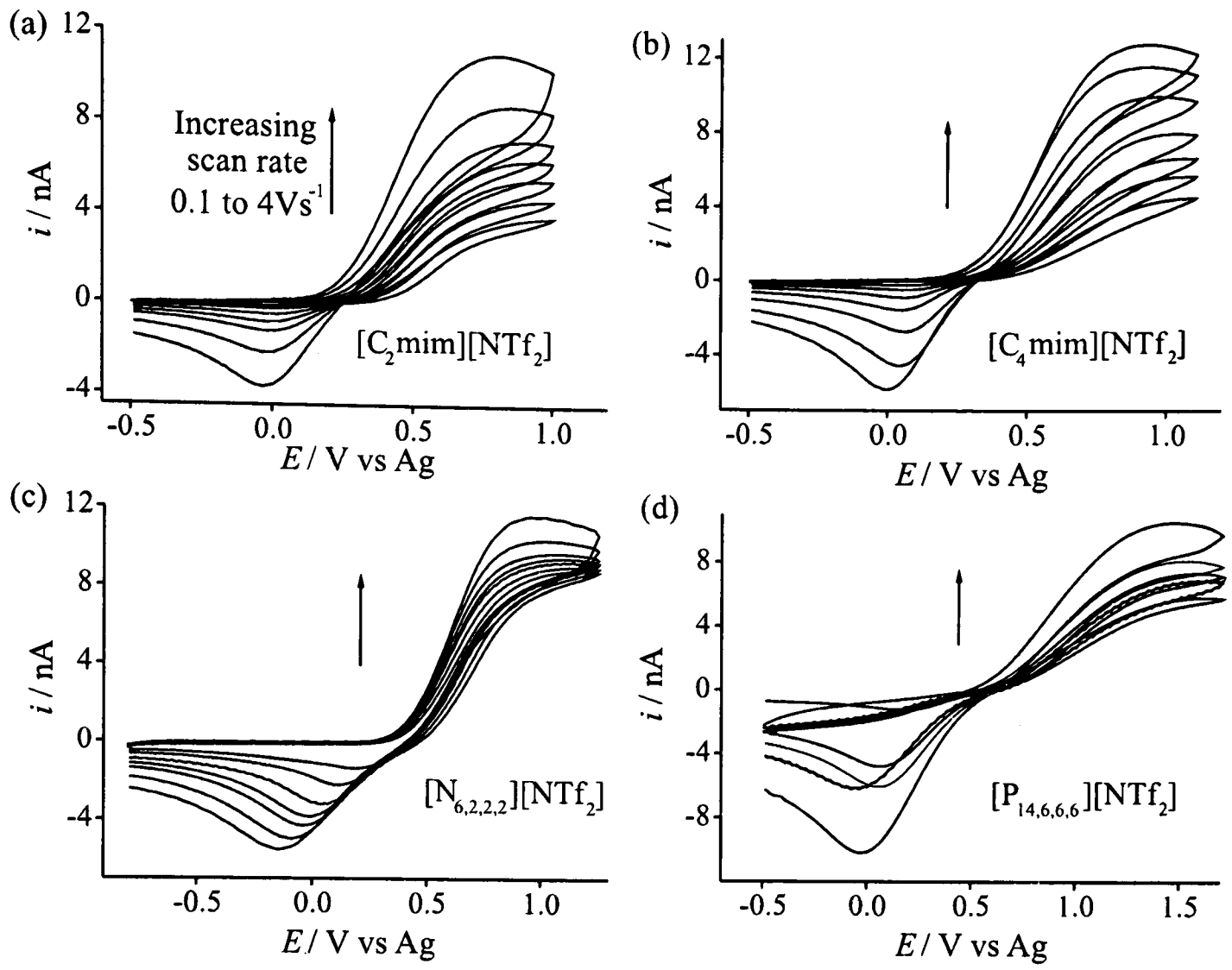

Figure 9.3: Cyclic voltammetry for the oxidation of 1 atm. H_2 on a Pt electrode (diameter 10 μm) at increasing scan rates in the RTILs: (a) $[C_2mim][NTf_2]$, (b) $[C_4mim][NTf_2]$, (c) $[N_{6,2,2,2}][NTf_2]$ and (d) $[P_{14,6,6,6}][NTf_2]$. The electrode was not pre-activated.

with a common anion: $[NTf_2]^-$. Figure 9.3 shows the oxidation of 1 atm. H_2 on a platinum microdisk electrode (diameter 10 μm) in the RTILs (a) $[C_2mim][NTf_2]$, (b) $[C_4mim][NTf_2]$, (c) $[N_{6,2,2,2}][NTf_2]$ and (d) $[P_{14,6,6,6}][NTf_2]$ with no electrode activation. In all four RTILs, the oxidative wave appears broad, and the relatively large separation between anodic and cathodic peak potentials suggests that the process is not fully electrochemically-reversible. All voltammograms show the presence of a reduction peak (particularly at higher scan rates) at *ca.* +0.1 to +0.3 V *vs* Ag, which is likely to be due to the reduction of the electrogenerated proton which has been solvated by the RTIL anion, *i.e.* $H[NTf_2]$. The reduction peak shape is more transient in nature than the oxidation peak in all cases, suggesting that the diffusion coefficient of the solvated proton is much lower than that of hydrogen. In all cases, the peak current for the ox-

idative peak increases systematically with scan rate, however the peak currents were not always stable and reproducible, even if the solution was left to equilibrate for long periods of time (*ca.* 10 minutes) between scans. Similar findings were reported in the aprotic solvents DMSO, DMF, pyridine and MeCN,[8] where the oxidation peaks of H_2 (prior to electrode activation) were found to be broad and diffuse, the peak currents were not reproducible and were not proportional to the partial pressure of H_2.[8] Barrette and Sawyer[8] showed that when the electrode was activated at a potential more positive than the oxidation peak, the peak currents became much more stable and reproducible. For H_2 oxidation in RTILs (current work), similar behaviour is observed and is described below.

Figure 9.4 shows the oxidation of 1 atm. H_2 gas in the RTILs (a) $[C_2mim][NTf_2]$, (b) $[C_4mim][NTf_2]$, (c) $[N_{6,2,2,2}][NTf_2]$ and (d) $[P_{14,6,6,6}][NTf_2]$ on a Pt electrode (diameter 10 μm) which has been electrochemically activated at +2.0 V for 30 seconds prior to the recording of each voltammogram. When compared to the voltammograms obtained on a non-activated Pt electrode (Figure 9.3), the peak currents have increased by *ca.* 20-50 % and the peak separations have become much smaller, particularly in $[C_2mim][NTf_2]$ and $[C_4mim][NTf_2]$. When recording the voltammograms on activated electrodes, almost identical peak currents and wave shapes were observed on subsequent cycles, and only a short equilibration time (*ca.* 1 minute) was required between scans. The separations between the oxidative and reductive peaks shown in Figure 9.4 appear to depend on the nature of the cation (discussed in more detail in section 9.3.7). Although the oxidation peaks have become much less broad compared to the non-activated case, the shape of the reduction peak is still more transient than the oxidative peak, consistent with a lower diffusion coefficient of the solvated proton. The diffusional behaviour of the oxidation peak over a range of scan rates will be discussed later (section 9.3.5). However, first our attention turns to the reduction of the acid, $H[NTf_2]$ in two $[NTf_2]^-$-based RTILs.

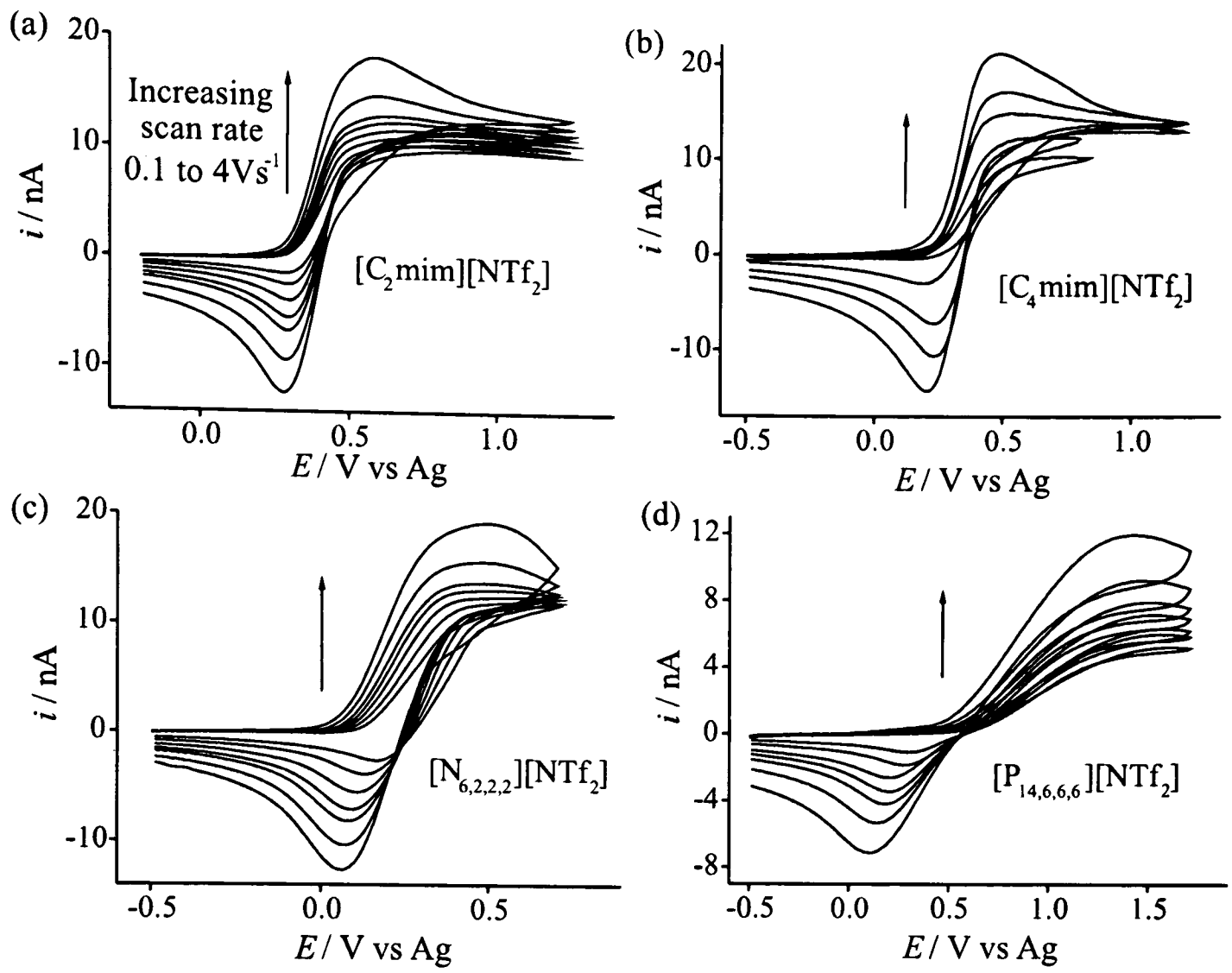

Figure 9.4: Typical cyclic voltammetry for the oxidation of 1 atm. H_2 on a Pt electrode (diameter 10 μm) at increasing scan rates in the RTILs: (a) $[C_2mim][NTf_2]$, (b) $[C_4mim][NTf_2]$, (c) $[N_{6,2,2,2}][NTf_2]$ and (d) $[P_{14,6,6,6}][NTf_2]$. The electrode was pre-activated at +2.0 V for 30 seconds prior to all scans.

9.3.3 The Reduction of the Acid $H[NTf_2]$ in $[C_2mim][NTf_2]$

The oxidation of H_2 in RTILs, as mentioned earlier, is presumed to lead to the formation of protons which are free to associate with the anions of the liquid. In the case of $[NTf_2]^-$ based RTILs, H^+ is likely stabilised and solvated by one or more $[NTf_2]^-$ anions. The exact nature and constitution of solvated protons in ILs are still not presently known. However, we will refer to the solvated proton as HA_x or HA (where A^-=RTIL anion), both for simplicity and in deference to the observed changes in the nature of the proton upon changing the RTIL anion.

In order to try to fingerprint the corresponding reduction peak following the oxidation of hydrogen, the reduction of $H[NTf_2]$ was studied in $[C_2mim][NTf_2]$. The full redox range is first

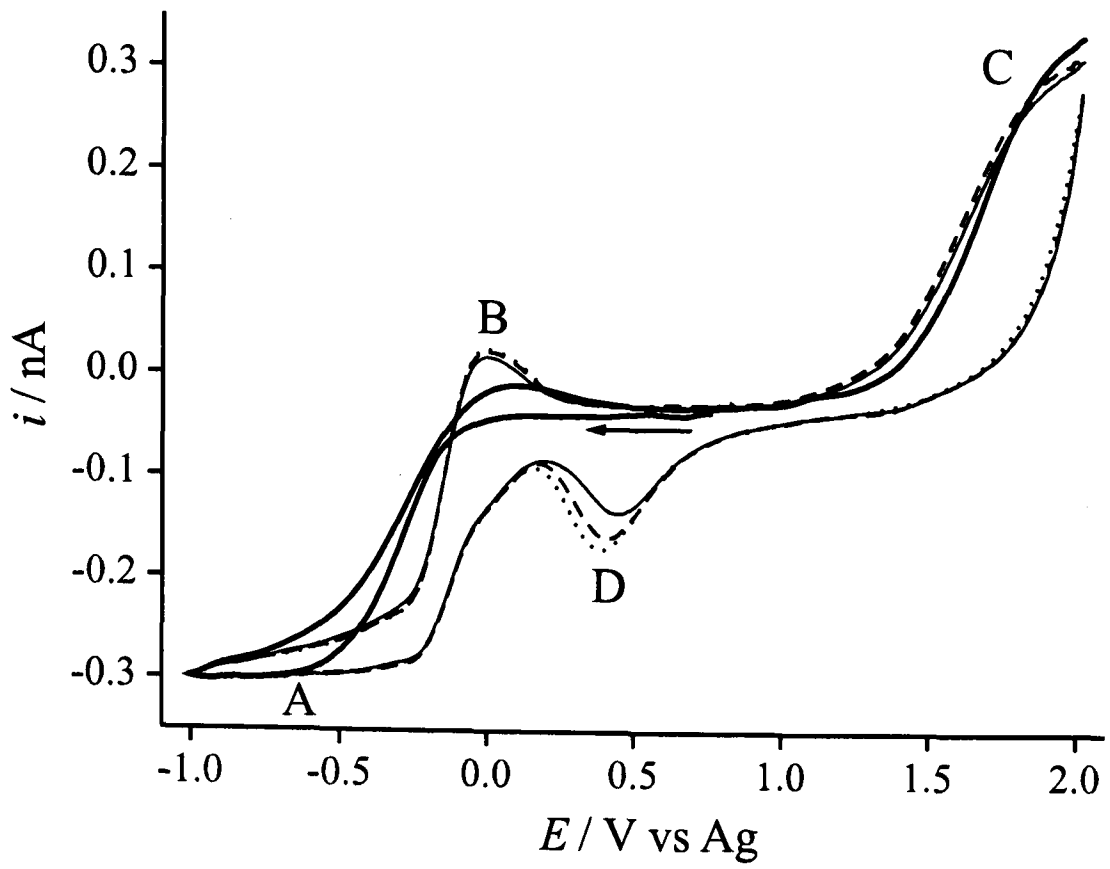

Figure 9.5: Cyclic voltammetry obtained for the reduction of *ca.* 4 mM $H[NTf_2]$ in $[C_2mim][NTf_2]$ on a Pt electrode (diameter 10 μm) with an extended anodic limit of +2.0 V. 4 scans are shown: first (bold solid), second (solid), third (dashed) and forth (dots), scan rate 100 mV s^{-1}.

presented. Figure 9.5 shows the voltammetry obtained for four successive scans over the full redox window of *ca.* 4 mM $H[NTf_2]$ at 100 mV s^{-1} on an unactivated Pt electrode (diameter=10 μm) in $[C_2mim][NTf_2]$. On the first scan, a relatively broad reduction peak, A, was seen, with a small anodic peak, B, presumed to correspond to the H^+(or HA)/H_2 redox couple. When the anodic limit was extended, a further oxidation peak was seen, C, with a corresponding reduction peak, D. The charge under peak D was calculated to be 2.4 $\times 10^{-9}$ moles cm^{-2}, which gives a surface coverage of 1.45 $\times 10^{15}$ hydrogen atoms cm^{-2}, corresponding well to two reports[31,32] which give the number of hydrogen atoms in a monolayer as 1.5 $\times 10^{15}$ atoms cm^{-2} and 2 $\times 10^{-9}$ moles cm^{-2} respectively. It is tentatively therefore thought that peak C corresponding to the oxidation of $H[NTf_2]$, leads to the formation of products. The reduction of these products then leads to the formation of a monolayer of hydrogen atoms on the surface of the electrode. On the second and subsequent scans (solid, dashed and dotted lines in Figure 9.5), a

sharper reduction peak was obtained for the acid, consistent with the activating effect that was seen for the hydrogen.

As a result of this activation step, and in accordance with the work presented so far for the oxidation of hydrogen, all subsequent experiments were performed on 'activated' electrodes. Figure 9.6a shows the reduction of *ca.* 130 mM $H[NTf_2]$ in $[C_2mim][NTf_2]$ on an activated Pt electrode at a range of scan rates from 0.1 to 1 V s^{-1}. The peak currents for both peaks increase linearly with the square root of scan rate, but do not pass through the origin as the behaviour is likely intermediate of pure microelectrode and pure macroelectrode behaviour. The peak potentials *vs* Ag do not match exactly with those for H_2 oxidation in the same ionic liquid (Figure 9.4a), possibly due to a shift in the quasi-reference electrode, so the voltammetry of the acid was studied in the presence of hydrogen. A higher concentration of acid was chosen for these experiments (130 mM), since the peak currents are expected to be similar to that of those from hydrogen gas oxidation presented in the previous section. Figure 9.6b shows the reduction of 130 mM $H[NTf_2]$ in $[C_2mim][NTf_2]$ at 1 V s^{-1} on an activated Pt electrode in the absence (dotted line) and presence (solid line) of 1 atm. hydrogen gas. As can be seen, the currents of both the oxidation and reduction peaks are increased significantly, indicating that the redox couple corresponds to the H^+(or HA)/H_2 system *i.e.* the reverse of that seen in the previous section.

In order to calculate diffusion coefficients and the number of electrons transferred, a potential step was carried out on the reductive wave of the acid $H[NTf_2]$ (130 mM) in $[C_2mim][NTf_2]$. The potential was stepped from +0.2 V (corresponding to no faradaic current) to -0.8 V *vs* Ag and the current was measured for 10 seconds. The inset to Figure 9.6b shows the experimental data (solid line) and theoretical fit (dots) to the Shoup and Szabo[26] expression. The diffusion coefficient obtained for $H[NTf_2]$ in $[C_2mim][NTf_2]$ was calculated to be 3.2 ($\pm$0.1) $\times$ 10^{-11} m^2 s^{-1} and the *nc* value (number of electrons $\times$ concentration) indicated a one electron process. This

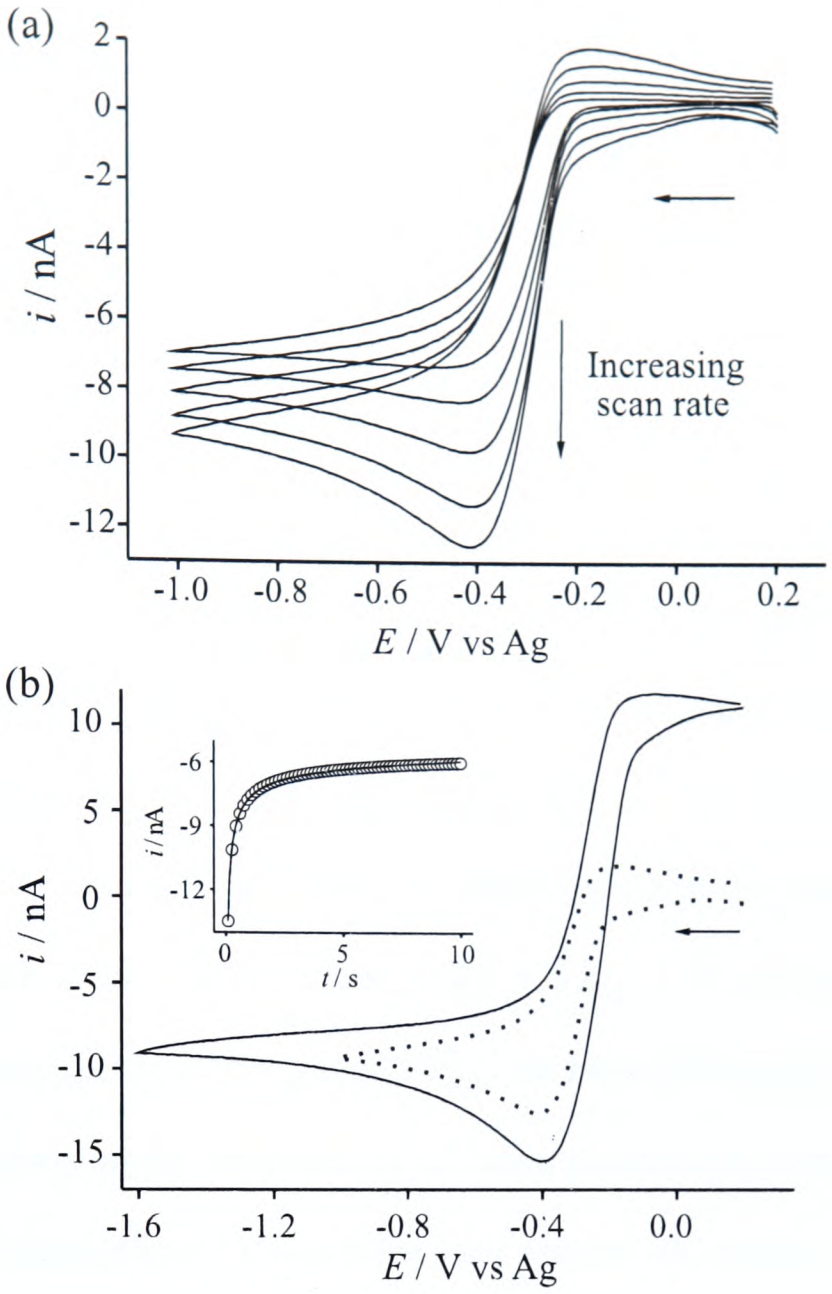

Figure 9.6: (a) Cyclic voltammetry for the reduction of *ca.* 130 mM $H[NTf_2]$ on a Pt electrode (diameter 10 μm) in $[C_2mim][NTf_2]$ at scan rates of 0.1, 0.2, 0.4, 0.7, and 1 V s^{-1}. (b) Cyclic voltammetry obtained under the same conditions as (a) in the absence (dotted line) and presence (solid line) of 1 atm. hydrogen gas at 1 V s^{-1}. The electrode was pre-activated at +1.5 V for 30 seconds prior to all scans. The inset to (b) is a chronoamperometric transient obtained for the reduction of 130 mM $H[NTf_2]$ under the same conditions, showing the experimental data (solid line) and fitted theoretical data (dots) following the Shoup and Szabo[26] expression.

result also implies for:

$$H[NTf_2] \rightleftharpoons H^+ + [NTf_2]^- \tag{9.5}$$

$$H^+ + e^- \rightarrow \frac{1}{2}H_2 \tag{9.6}$$

the pre-equilibrium is rapid, and $H[NTf_2]$ is fully reduced, otherwise agreement with the Shoup and Szabo[26] expression would not be seen.

9.3.4 The Oxidation of Hydrogen in RTILs with different anions on Activated Pt Electrodes

The effect of activation was also studied in ionic liquids with a common imidazolium cation, (either $[C_4mim]^+$ or $[C_6mim]^+$), and a range of different anions (A^-), namely $[OTf]^-$, $[PF_6]^-$, $[BF_4]^-$, $[FAP]^-$, $[NO_3]^-$ and Cl^-. The voltammograms obtained over a range of scan rates for the oxidation of H_2 on an *activated* platinum electrode (diameter 10 μm) for these six RTILs are shown in Figure 9.7. In $[C_4mim][FAP]$, $[C_4mim][OTf]$ and $[C_4mim][PF_6]$ (Figures 9.7a, b and e), quasi-reversible voltammetry is observed, which indicates that the protons formed from the oxidation of H_2 combine with the anions of these RTILs, and the product, HA, is stable-enough to be detected voltammetrically. $H[OTf]$, $H[PF_6]$ and H[FAP] (solvated in water) are all stable known molecules, so chemically reversible voltammetry is not unexpected. It is noted that the acid catalysed decomposition of $[C_4mim][PF_6]$, has been previously reported by Swatloski *et al.*[33] They report the possible formation of the toxic product HF, and note the evolution of acidic HF fumes, and formation of a colourless solid around the reaction vessel containing the RTIL. The degradation of RTILs containing fluorine atoms is also briefly mentioned in a recent review paper.[34] Despite these findings, this process is not expected to feature heavily on the time scale of the experiment in $[C_4mim][PF_6]$ such that quasi-reversibility is maintained.

For $[C_4mim][BF_4]$, $[C_4mim][NO_3]$ and $[C_6mim]Cl$ (Figures 9.7c, d and f), the voltammetric behaviour is clearly different from the $[NTf_2]^-$ based RTILs, in that the reduction peak following the oxidation is much reduced in $[C_4mim][BF_4]$, and is barely seen in $[C_4mim][NO_3]$ and $[C_6mim]Cl$. Little work has been reported concerning degradation of the $[BF_4]^-$ anion, despite various papers reporting this for $[PF_6]^-$.[33,34] Villagran *et al.*[35] appear to be the first to show that, in the presence of varying amounts of water, the decomposition of $[C_4mim][BF_4]$ is much faster and more substantial than the decomposition of $[C_4mim][PF_6]$. It is predicted that for $[C_4mim][BF_4]$, the product $H[BF_4]$ will dissociate according to the following (acid catalysed)

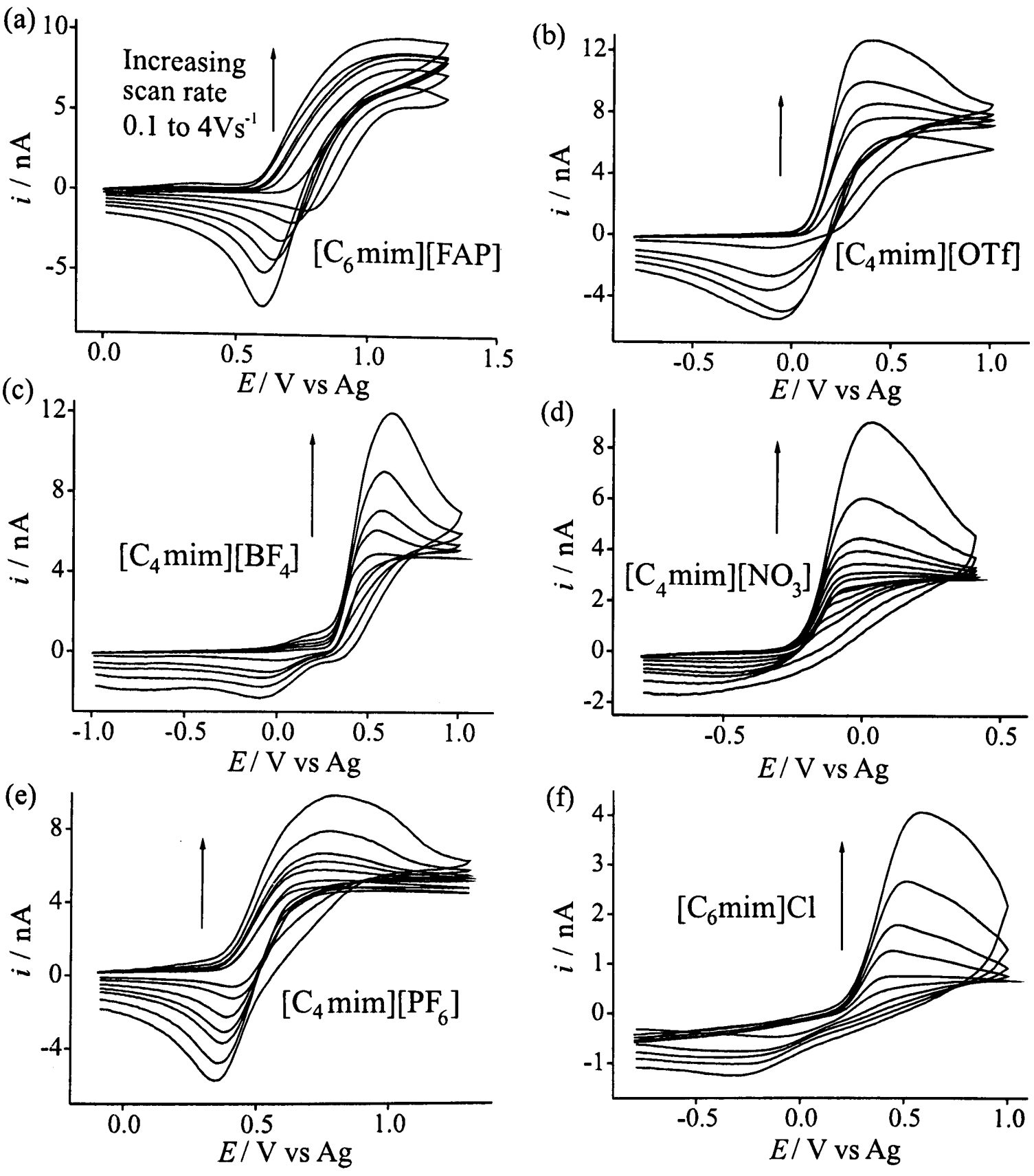

Figure 9.7: Cyclic voltammetry for the oxidation of 1 atm. H_2 on a Pt electrode (diameter 10 μm) at increasing scan rates in the RTILs: (a) [C_6mim][FAP], (b) [C_4mim][OTf], (c) [C_4mim][BF_4] and (d) [C_4mim][NO_3], (e) [C_4mim][PF_6] and (f) [C_6mim]Cl. The electrode was pre-activated at (a) +2.0 V, (b) +2.0 V, (c) +1.8 V, (d) +1.2 V, (e) +2.0 V and (f) +1.2 V for 30 seconds prior to all scans.

equation:[35]

$$H[BF_4] \rightarrow HF + BF_3 \tag{9.7}$$

The voltammograms shown in Figures 9.7c and 9.7e seem to agree well with these findings, and this should be taken into account when handling $[BF_4]^-$ based ionic liquids (particularly in the presence of proton sources) and applying them to green synthesis and indeed any application.

For the oxidation of hydrogen in $[C_4mim][NO_3]$ (Figure 9.7d), the absence of a reductive back-peak suggests that $H[NO_3]$ or $H[NO_3]_2^-$ are likely formed in a chemical step following the reaction, according to:

$$\frac{1}{2}H_2 - e^- \rightleftharpoons H^+ \tag{9.8}$$

and either/both of the following equations:

$$H^+ + NO_3^- \rightarrow H[NO_3] \tag{9.9}$$

$$H^+ + 2NO_3^- \rightarrow H[NO_3]_2^- \tag{9.10}$$

Clear physical evidence of the formation of the hydrogen dinitrate ion has been reported previously.[36] Similarly for $[C_6mim]Cl$ (Figure 9.7e), it is possible that HCl or, more likely $[HCl_2]^-$ (where H^+ is stabilized more in Cl^- media: see Introduction) is formed following the oxidation of hydrogen. The formation of $[HCl_2]^-$ has been previously postulated by Del Popolo *et al.*[19] for HCl in $[C_1mim]Cl$ and observed experimentally by Aldous *et al.*[37] The high viscosity of both $[C_4mim][NO_3]$ and $[C_6mim]Cl$ (266 and 7453 cP at 293 K)[38,39] also indicates that the products of the reaction will diffuse very slowly from the electrode surface, suggesting that $H[NO_3]_2^-$ and $[HCl_2]^-$ are the most likely reaction products.

9.3.5 Comparison of Voltammetric Characteristics for H_2 Oxidation in Ten RTILs

Now that the voltammetry in ten RTILs has been presented, the diffusional behaviour of the oxidation peak over a range of scan rates is discussed. Plots of peak current *vs* square root scan rate (see Figure 9.8) were approximately linear for all ten RTILs studied (least-squares correlation coefficient, R^2, greater than 0.950) but typically do not pass through the origin because the magnitude of the diffusion coefficients have characteristics which lead to voltammetry intermediate of micro/macro-electrode behaviour. This can be explained by considering the following inequality:

$$\nu << \frac{RTD}{nFr_d{}^2} \tag{9.11}$$

where ν represents scan rate, R is the universal gas constant, T is the absolute temperature, D is the diffusion coefficient, F is the Faraday constant and r_d the radius of the disk. For true steady-state behaviour on a disk electrode, equation 9.11 must apply. Therefore, taking a typical diffusion coefficient of 1×10^{-10} m^2 s^{-1} for hydrogen gas diffusing in an RTIL (see next section), a scan rate of less than *ca.* 50 mV s^{-1} is necessary for true microelectrode behaviour. For most of the scan rates studied in this report, the anticipated voltammetric behaviour is intermediate between cases of pure micro- and macro-electrode. Accordingly, although the peak currents increase with scan rate, they do not show a direct proportionality of the peak current *vs* square root scan rate, as is commonly used to fingerprint diffusion controlled processes in macro-electrode voltammetry. However, in the case of H_2 oxidation in $[C_6mim]Cl$, a plot of peak current *vs* square root scan rate *does* pass through the origin (see Figure 9.8) suggesting a smaller diffusion coefficient, which is consistent with the results presented in the next section.

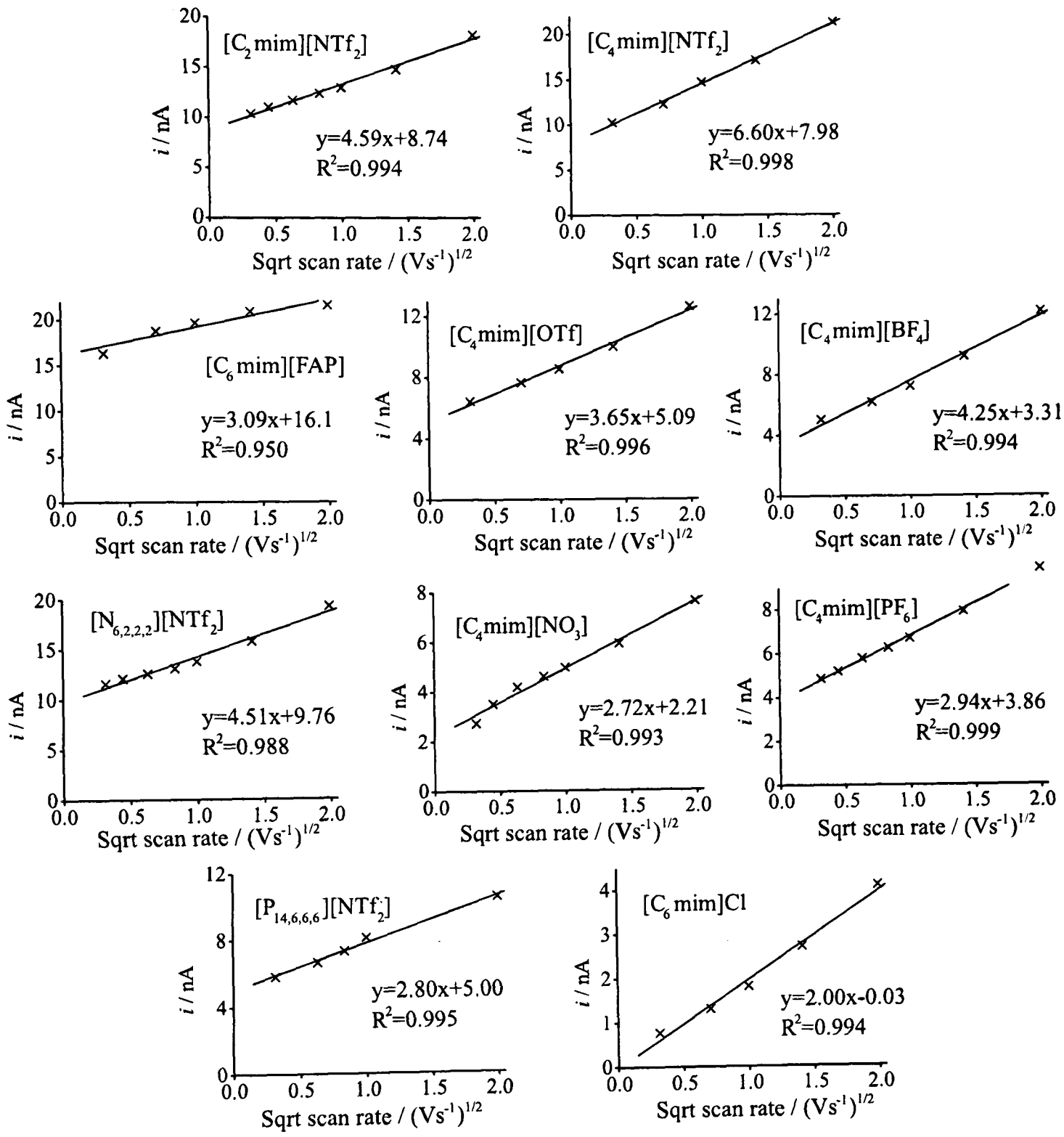

Figure 9.8: Plots of peak current *vs* square root scan rate for the oxidation of 1 atm. H_2 on a Pt electrode (diameter 10 μm) in a range of ionic liquids. The equations of the line of best fit, and least-squares correlation coefficient (R^2) are shown on each graph.

Table 9.1: Summary of the chronoamperometric data obtained from the electrochemical oxidation of hydrogen in different ionic liquids at 298 K.

Ionic Liquid	η at 293 K/cP	$D_{H_2}/\times 10^{-10}$ m^{2}s^{-1}	c/mM	$Dc/\times 10^{-13}$ Mm^{2}s^{-1}
$[C_2mim][NTf_2]$	34[27]	5.5 ($\pm$0.3)	4.2 ($\pm$0.2)	23.1
$[C_4mim][NTf_2]$	52[27]	8.8 ($\pm$0.4)	3.3 ($\pm$0.1)	29.0
$[C_6mim][FAP]$	74[39]	3.6 ($\pm$0.2)	6.6 ($\pm$0.4)	23.8
$[C_4mim][OTf]$	90[27]	3.6 ($\pm$0.2)	4.3 ($\pm$0.2)	15.5
$[C_4mim][BF_4]$	112[42]	2.2 ($\pm$0.1)	5.2 ($\pm$0.1)	11.4
$[N_{6,2,2,2}][NTf_2]$	167[43]	3.2 ($\pm$0.3)	7.2 ($\pm$0.4)	23.0
$[C_4mim][NO_3]$	266[38]	1.0 ($\pm$0.1)	4.8 ($\pm$0.3)	4.80
$[C_4mim][PF_6]$	371[38]	1.5 ($\pm$0.3)	5.1 ($\pm$0.2)	7.65
$[P_{14,6,6,6}][NTf_2]$	450[44]	2.9 ($\pm$0.3)	7.9 ($\pm$0.5)	22.9
$[C_6mim]Cl$	7453[39]	0.13 ($\pm$0.02)	9.7 ($\pm$0.5)	1.26

9.3.6 Potential Step Chronoamperometry

In addition to studying the cyclic voltammetry of H_2 oxidation, a potential step was performed on the oxidative wave in order to try to calculate diffusion coefficients and solubilities of hydrogen in each RTIL. Figure 9.9 shows experimental chronoamperometric transients (solid lines) and fitted theoretical transients following the Shoup and Szabo expression (dots) for the oxidation of 1 atm. H_2 on a Pt microelectrode of diameter 10 μm in ten ionic liquids. Assuming the following 2-electron process applies:

$$H_2 - 2e^- + 2A^- \rightarrow 2HA \tag{9.12}$$

(where A^-=solvent anion), diffusion coefficients and concentrations/solubilities in all ten RTILs were obtained. The data obtained from this analysis is shown in Table 9.1, along with the dynamic viscosities (η) of each RTIL. The diffusion coefficients are approximately of the order 1×10^{-10} m^2 s^{-1}, which is comparable in magnitude to that of oxygen in several RTILs,[40] and *ca.* 1 order of magnitude larger than solid diffusing species in RTILs (*c.f.* 3.35×10^{-11} m^2 s^{-1} for ferrocene in $[C_2mim][NTf_2]$).[41]

According to the Stokes-Einstein relation[30] in equation 9.13, for a simple diffusing species, a

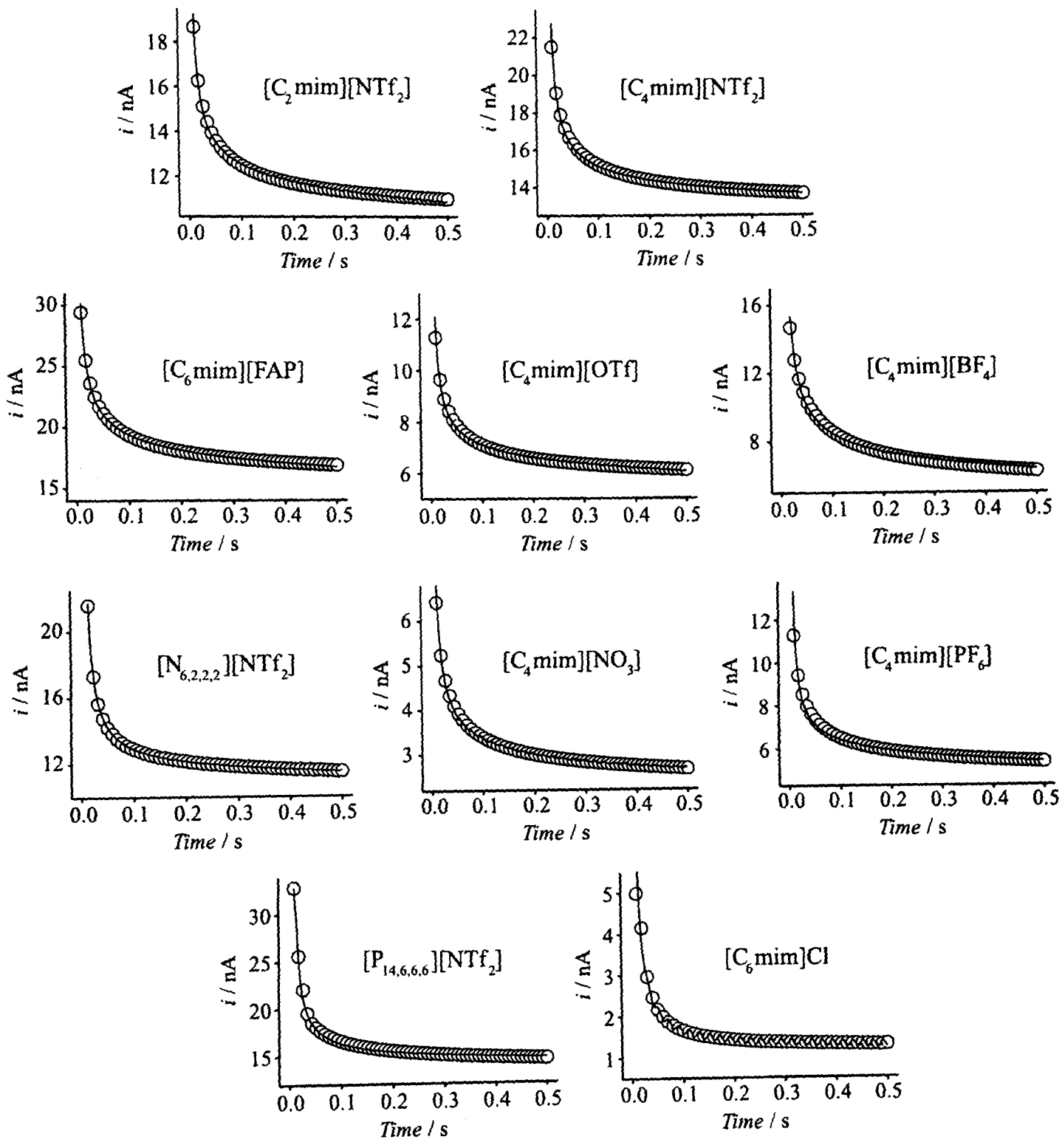

Figure 9.9: Experimental (solid line) and fitted theoretical (dots) chronoamperometric transients following the Shoup and Szabo[26] expression for the oxidation of 1 atm. H_2 on a 10 μm diameter Pt electrode in a range of RTILs. The electrode was activated at a positive potential (typically +2.0 V, but lower for those with a smaller anodic window) for 30 seconds prior to each transient.

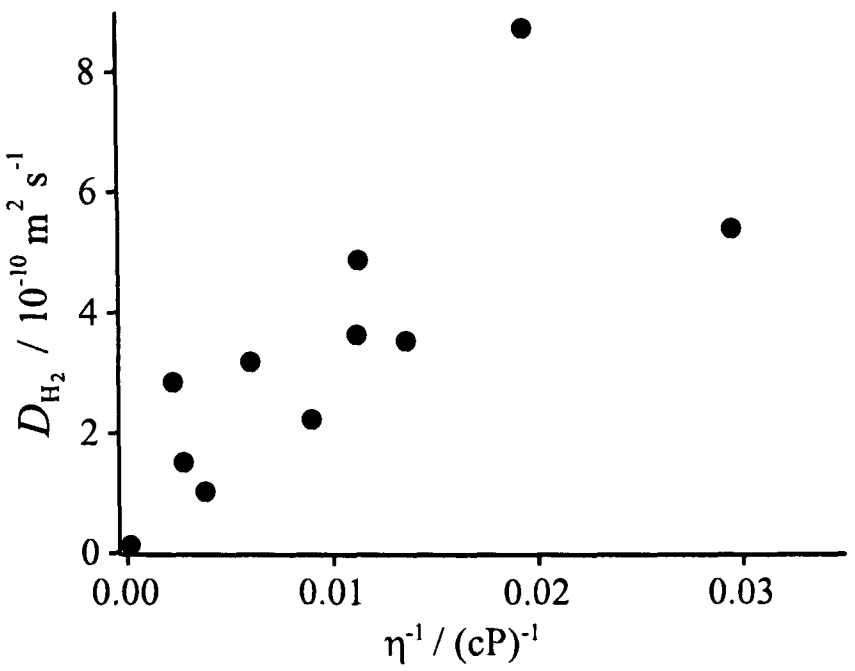

Figure 9.10: Plot of diffusion coefficient (D) at 298 K against the inverse of viscosity (at 293 K) for the ten RTILs studied. D values were obtained from theoretical fitting of chronoamperometric transients to the Shoup and Szabo expression.[26]

linear relationship is expected between the diffusion coefficients (D) and the inverse of viscosity:[30]

$$D = \frac{k_B T}{6\eta\pi\alpha} \tag{9.13}$$

where k_B is the Boltzmann constant, T is the temperature and α is the hydrodynamic radius of the diffusing species. This relationship is commonly followed in conventional molecular solvents, and also for organic molecules in RTILs.[45] However, it has been shown not to apply in the case of small gaseous molecules such as oxygen,[46] sulfur dioxide[47] and hydrogen sulfide[48] in RTILs. A plot of D *vs* $1/\eta$ using the values in Table 9.1 is presented in Figure 9.10, and although a general increase in D is observed with a decrease in viscosity, there is no apparent linear relationship, suggesting that H_2 is far too small a molecule for equation 9.13 to apply. The diffusion coefficients of hydrogen in RTILs are approximately 1-2 orders of magnitude smaller than that obtained in conventional protic and aprotic solvents (*ca.* 1×10^{-9} m^2 s^{-1}, see Table 9.2) which is not unreasonable, considering the higher viscosity of the RTILs (34-7453 cP) compared to that of water (1.00 cP), dimethyl sulfoxide (2.20 cP), dimethylformamide (0.92 cP) and pyridine (0.95 cP) at 293 K.[49]

Table 9.2: Summary of literature data for the solubilities (at 1 atm.) and diffusion coefficients of H_2 in several different solvents. All data taken from Barrette and Sawyer[8] and Dyson *et al.*[50]

Solvent	Solubility H_2/mM	Diffusion coefficient of H_2/m^2 s^{-1}
Water	0.78	2.4×10^{-9}
Dimethyl sulfoxide	1.12	3.0×10^{-9}
Dimethylformamide	1.96	5.2×10^{-9}
Pyridine	2.00	1.0×10^{-9}
Methanol	3.75	-
Ethanol	2.98	-
Toluene	3.50	-
Benzene	2.54	-
Cyclohexane	3.63	-
$[C_4mim][NTf_2]$	0.77	-
$[C_4mim][OTf]$	0.97	-
$[C_4mim][BF_4]$	0.86	-
$[C_4mim][PF_6]$	0.73	-

The concentrations (solubilities) of hydrogen in all ten RTILs studied are relatively moderate (*ca.* 3-10 mM), and are approximately comparable to that of oxygen in RTILs (*cf.* 3.9 mM in $[C_2mim][NTf_2]$ and 11.6 mM in $[N_{6,2,2,2}][NTf_2]$).[40] However, they are much higher than solubilities of hydrogen obtained by other researchers in RTILs using other methods. Several researchers[51–53] report the non-detectable hydrogen concentration at ambient temperatures and pressures due to high viscosity and low gas solubility, and resort to the use of higher temperatures[51] and higher pressures[53] to detect low amounts of H_2. Dyson *et al.*[50] report solubilities at 293 K and 1 atm. of *ca.* 0.7 to 0.9 mM. These have been included in Table 9.2, together with solubilities reported in water and other aprotic solvents.[8] As can clearly be seen by comparing the solubilities in Table 9.2 to Table 9.1 (from this work), the electrochemical method is shown to be much more sensitive, and may be used to detect lower concentrations of hydrogen. Therefore, this method shows great promise for the analytical determination of hydrogen concentrations in Clark-cell type gas sensors.[54]

Since the D and c values vary somewhat with the solvent, the product of the two variables was then calculated in each ionic liquid, and the numbers are included in Table 9.1. The ionic liquid with the highest Dc will give the highest current response (since the steady-state current at a microdisk is proportional to Dc)[26,54] and will therefore be the most suitable medium for sensing *via* the Clark-cell approach. By comparing the numbers in Table 9.1, it is evident that some ionic liquids will give higher attainable currents than others. In particular, all four $[NTf_2]^-$ ionic liquids and $[C_6mim][FAP]$ have Dc values greater than 20, suggesting that they are the most suitable media for hydrogen sensing, with $[C_4mim][NTf_2]$ being the most sensitive. $[C_4mim][OTf]$, $[C_4mim][BF_4]$, $[C_4mim][NO_3]$ and $[C_4mim][PF_6]$ give intermediate current responses, and the ionic liquid which gives the lowest current response for H_2 oxidation is $[C_6mim]Cl$. This is not unexpected given the highly viscous nature of this liquid and the expected slow rate of mass transport.

9.3.7 H_2 Oxidation Potential *vs* Internal Reference Couple

For all ten ionic liquids studied, the oxidation of 1 atm. H_2 was next studied in the presence of *ca.* 20 mM cobaltocenium hexafluorophosphate ($CcPF_6$, where $Cc^+=(C_5H_5)_2Co^+$) as an internal reference. The Cc^+/Cc redox couple has been recommended by the International Union of Pure and Applied Chemistry (IUPAC) as one of several stable reference couples in aprotic solvents and has been used by Bond *et al.*[55] in RTILs this context. By obtaining peak potentials of H_2 oxidation *vs* Cc^+/Cc, it is thought that this may indicate (if formal potentials can be inferred) the relative acid/base properties of the solvent, which at present are relatively unknown in ionic liquids.

Figure 9.11 shows the oxidation of 1 atm. H_2 in the presence of *ca.* 20 mM Cc^+ on a 10 μm diameter Pt electrode at a range of scan rates in (a) $[C_2mim][NTf_2]$, (b) $[C_4mim][NTf_2]$, (c) $[C_4mim][OTf]$ and (d) $[C_4mim][BF_4]$. Similar voltammetry was obtained for the remaining six

Table 9.3: Peak potentials and separations at 298 K for the oxidation of H_2 and the reduction of the solvated proton, 'HA'[§].

Ionic Liquid	Ox H_2*/V	Red 'HA'*[§]/V	ΔE_{pp} /V	E_f^0 of H^+/'HA'*[§]/V
$[C_2mim][NTf_2]$	1.53	1.18	0.35	1.36
$[C_4mim][NTf_2]$	1.52	1.19	0.33	1.36
$[C_6mim][FAP]$	2.45	1.94	0.51	-
$[C_4mim][OTf]$	1.27	0.68	0.59	0.98
$[C_4mim][BF_4]$	1.36	0.36	1.00	-
$[N_{6,2,2,2}][NTf_2]$	1.52	1.08	0.44	1.30
$[C_4mim][NO_3]$	0.82	-	-	-
$[C_4mim][PF_6]$	1.82	1.24	0.58	1.53
$[P_{14,6,6,6}][NTf_2]$	2.02	0.73	1.29	1.38
$[C_6mim]Cl$	0.87	-	-	-

[§]where A^-=solvent anion ($[NTf_2]^-$, $[FAP]^-$, $[OTf]^-$, $[BF_4]^-$, $[NO_3]^-$, $[PF_6]^-$ or Cl^-)
*vs Cc^+/Cc at 4 V s^{-1}.

ionic liquids, but has not been included here. As can clearly be seen in Figure 9.11, the oxidation peaks of H_2 are well separated from the Cc^+/Cc redox couple, allowing for the measurement of H_2 peak potentials relative to the Cc^+/Cc redox couple. However, it is noted that the peak currents for H_2 oxidation decreased slightly (by *ca.* 5-30 %) compared to the peak currents of H_2 alone, suggesting a possible reaction of hydrogen with cobaltocenium hexafluorophosphate or its reduction product.[56] However, this is not expected to influence the calculation of peak potentials. A similar reaction with hydrogen in RTILs was also observed in the presence of N,N,N',N'-tetramethylphenylenediamine, TMPD.[57] Table 9.3 shows the peak potentials for the oxidation of H_2 relative to the Cc^+/Cc redox couple in all ten RTILs studied. A large variation in H_2 oxidation potential is observed. This reflects both kinetics (ΔE_{pp}) and thermodynamics (E_f^0); these will be discussed separately below.

In an attempt to obtain thermodynamic data from the voltammetry, we have analysed those cases in which the back-peak is likely directly related to the H_2 oxidation product (but not those in which there is a suggestion of follow-up chemistry) to give the mid peak potential of the

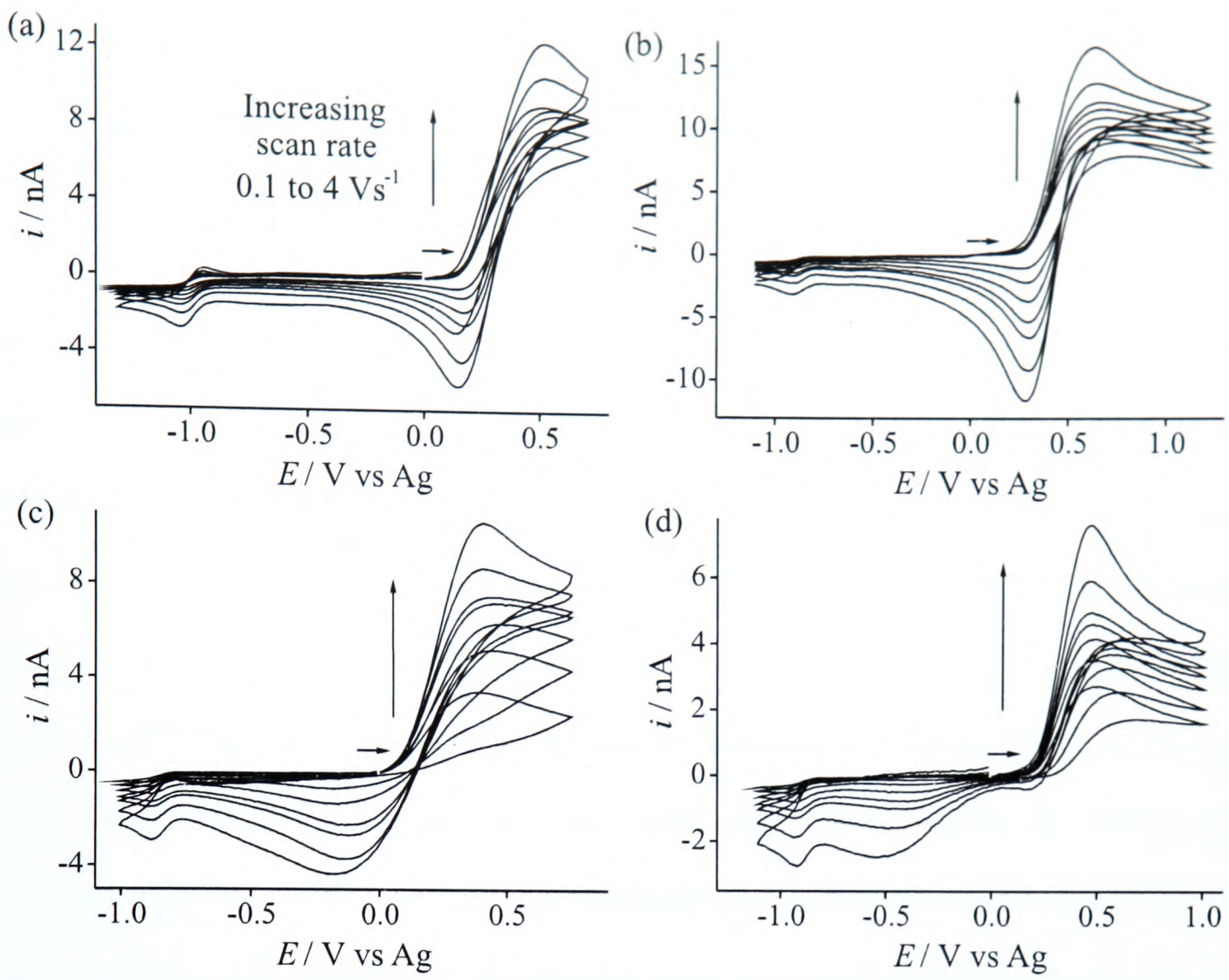

Figure 9.11: Cyclic voltammograms for the oxidation of 1 atm. H_2 on a Pt electrode (diameter=10 μm) in the presence of *ca.* 20 mM Cc^+ in the RTILs: (a) $[C_2mim][NTf_2]$, (b) $[C_4mim][NTf_2]$, (c) $[C_4mim][OTf]$ and (d) $[C_4mim][BF_4]$ at scan rates of 0.1, 0.2, 0.4, 0.7, 1, 2 and 4 V s^{-1}. The electrode was activated at +2 V (+1.8 V in $[C_4mim][BF_4]$) for 30 seconds prior to each scan.

H^+/'HA' couple. Note however that since the voltammograms show characteristics intermediate between those of macro/micro electrodes, this procedure is approximate, and on the basis of full simulations in the RTIL $[C_4mim][PF_6]$; we estimate the likely error being no more than $\pm$0.15 mV. The formal potentials, $E_f{}^0$, are reported in the final column of Table 9.3. The values for the four $[NTf_2]^-$ ionic liquids are relatively consistent at *ca.* 1.30–1.38 V, and are significantly larger than the value of 0.98 V in $[C_4mim][OTf]$, and smaller than that obtained in $[C_4mim][PF_6]$ (1.53 V). This suggests that there is a stronger interaction of the electrogenerated proton with $[OTf]^-$ compared to $[NTf_2]^-$, which is not unexpected as $H[NTf_2]$ is as a stronger acid than H[OTf]. The larger peak separation in $[C_4mim][PF_6]$ is unexpected, but is consistent

with results presented in the next chapter, reporting the oxidation of ammonia in RTILs.[58] where the oxidation potential of NH_3 *vs* Cc^+/Cc is found to be larger than in $[NTf_2]^-$, $[OTf]^-$ and $[BF_4]^-$ based ionic liquids.

Table 9.3 also shows the peak potentials of the 'HA' (where A^-=solvent anion) reduction peak *vs* Cc^+/Cc, and the resulting peak separations of the H_2/'HA' couple (ΔE_{pp}). The ionic liquids giving the smallest peak separations suggest that the H_2/H^+ couple is the least electrochemically irreversible in these media, or that the solvated proton, HA, is easiest to reduce. Therefore, it is seen that the process is more electrochemically reversible (but not fully reversible) in $[C_2mim][NTf_2]$ and $[C_4mim][NTf_2]$, followed by $[C_6mim][FAP]$, $[C_4mim][PF_6]$, $[C_4mim][OTf]$ and $[N_{6,2,2,2}][NTf_2]$, and the largest separations are observed in $[C_4mim][BF_4]$ and $[P_{14,6,6,6}]$-$[NTf_2]$. For $[C_4mim][BF_4]$, the large separation may suggest the possibility for dissociation of the oxidation product, $H[BF_4]$, which is an observation which has been noted before.[59] The very large separation in $[P_{14,6,6,6}][NTf_2]$ may suggest slower electrode kinetics; it is speculated that the slowness may arise for solvent structural reasons. One possibility is that the protons may be locally bound to the $[NTf_2]^-$ anions in a solvation shell, which is then surrounded by large $[P_{14,6,6,6}]^+$ cations, making the reduction of protons back to H_2 more difficult. This may occur to a lesser extent in $[N_{6,2,2,2}][NTf_2]$, where an intermediate peak separation was observed, as the carbon chain lengths are smaller than in $[P_{14,6,6,6}][NTf_2]$. Another reason is that there may be strong adsorption of the large $[P_{14,6,6,6}]^+$ and $[N_{6,2,2,2}]^+$ cations on the electrode surface, particularly if the potential is more negative than the potential of zero charge (PZC). This would also give the appearance of slower electrode kinetics. For the remaining ionic liquids with different anions, the intermediate values of ΔE_{pp} may indicate intermediate electrode kinetics.

9.3.8 Exploratory Temperature study for H_2 Oxidation

Due to the high thermal stability and near-zero volatility of RTIL solvents, they have several advantages over conventional protic and aprotic solvents, particularly when used as solvents in gas sensors at high temperatures, where conventional solvents may evaporate. The ability to perform voltammetric measurements at higher temperature is quantitatively useful, since voltammetric measurements at higher temperatures are more sensitive, and the attainable limiting current is increased. For this reason, a preliminary temperature study (*ca.* 298-333 K) has been carried out in some of the ionic liquids mentioned above.

Figure 9.12 shows the oxidation of 1 atm. H_2 at a range of temperatures at 1 V s^{-1} on a Pt microelectrode (diameter 10 μm) in (a) $[C_4mim][NO_3]$, (b) $[C_2mim][NTf_2]$, (c) $[C_4mim][NTf_2]$ and (d) $[C_4mim][OTf]$. In all cases, the peak current for H_2 oxidation increases systematically with temperature. This is because the viscosity of the RTIL decreases with increasing temperature, and hence the rate of mass transport to the electrode surface is faster, resulting in larger peak currents. The peak separations of the forward and reverse peak appear to decrease very slightly as the temperature is increased, suggesting that HA (where A^-=solvent anion) is more rapidly reduced to H_2 at higher temperatures. The peak shapes become more steady-state in nature as the temperature increases. Steady-state behaviour is typically observed on microelectrodes in conventional molecular solvents, but the much higher viscosity of ionic liquids (1–3 orders of magnitude) means that diffusion coefficients are much smaller, and transient voltrammetric behaviour is common.[60] This is represented in Figure 9.12; as the temperature increases and the viscosity decreases, the peaks become more steady-state in nature. The reduction peak, however, is very sharp, and gets even sharper when the temperature is increased (particularly for the $[NTf_2]^-$-based RTILs), suggesting that the diffusion coefficient of the solvated proton in RTILs is much lower than that of H_2. This leads to voltammetry exhibiting both steady-state and transient behaviour in the same cycle, as observed for the oxygen/superoxide couple in

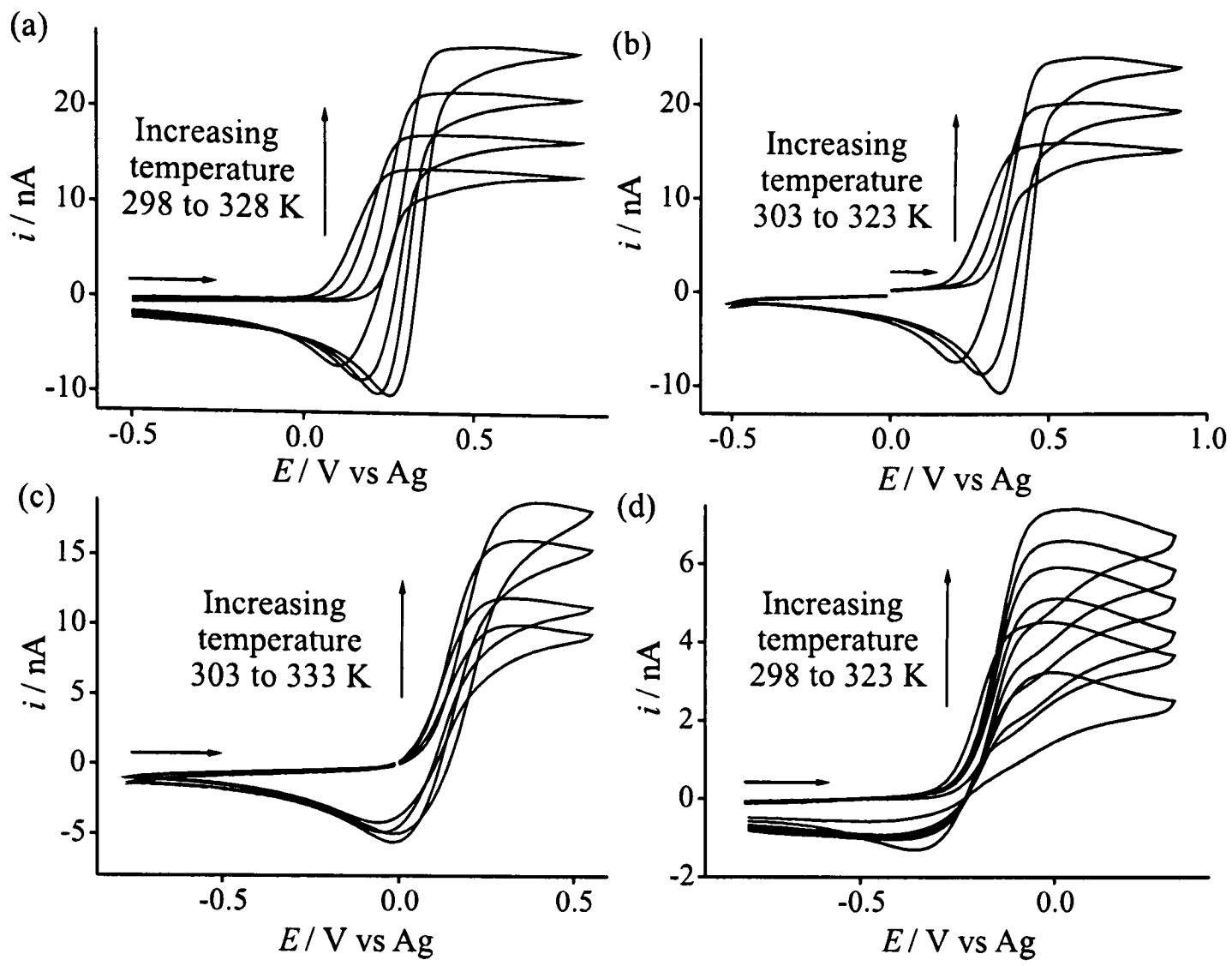

Figure 9.12: Cyclic voltammograms for the oxidation of 1 atm. H_2 on a Pt electrode (diameter=10 μm) at various temperatures in: (a) $[C_2mim][NTf_2]$ at 298, 308, 318 and 328 K, (b) $[C_4mim][NTf_2]$ at 303, 313 and 323 K and (c) $[C_4mim][OTf]$ at 303, 313, 323 and 333 K, (d) $[C_4mim][NO_3]$ at 298, 303, 308, 313, 318 and 323 K. Scan rate 1 V s^{-1}. The electrode was activated at (a) +2 V, (b) +2 V, (c) +2 V and (d) +1.8 V for 30 seconds prior to each scan.

RTILs.[40]

In order to determine if the solubilities and diffusion coefficients change with temperature, potential-step chronoamperometry was then performed on the hydrogen oxidation peak at all temperatures studied. However, the quality of fitting of the experimental data to the Shoup and Szabo[26] expression became systematically poor as the temperature was increased, and the data was deemed unreliable. Qualitatively, though, it can be seen from Figure 9.12 that the limiting currents are higher at increased temperatures. This increased sensitivity may prove to be an advantage when detecting hydrogen gas concentrations at higher temperatures.

9.4 Conclusions

The oxidation of hydrogen has been studied by cyclic voltammetry in a range of RTILs with different cations and anions. The appearance and position of the reverse (reduction) peak on the voltammograms is thought to depend on three factors: (1) the stability of the solvated proton, (2) the position of equilibrium of the protonation reaction (related to the pH) and (3) any unusual follow-up chemistry *e.g.* dissociation or reaction of the solvated proton. In particular, $H[NTf_2]$ is easily reduced to H_2 so that the impression of quasi-electrochemically reversible kinetics is gained from voltammograms such as that in Figure 9.4. On the other hand, the absence of a back-peak for $[C_4mim][NO_3]$ and $[C_6mim]Cl$ may indicate the formation of $H[NO_3]_2^-$ or $[HCl_2]^-$. In the case of $[OTf]^-$, $[PF_6]^-$, $[FAP]^-$ and $[BF_4]^-$, intermediate characteristics are seen, perhaps indicating the scope for dissociation of the anion, especially for $[BF_4]^-$. Diffusion coefficients and solubilities of hydrogen in each ionic liquid were calculated, and there was no obvious linear relationship found between D and viscosity, suggesting that H_2 is too small a molecule for the Stokes-Einstein relation to apply. A voltammetric study at increasing temperatures showed that the peak currents of H_2 oxidation increased with temperature. In addition, the oxidation potential of hydrogen has been reported against a standard internal reference couple, and a large variation in peak potentials was observed, which is thought to be mainly dependent on the nature of the anion and its interaction with the electrogenerated proton.

Having shown the hugely contrasting behaviour of the hydrogen oxidation wave in different ionic liquid media, the focus now turns to the behaviour of ammonia gas in five ionic liquids. Since the mechanism for the oxidation of ammonia is more complicated than for hydrogen, the next chapter first describes ammonia oxidation in one ionic liquid, followed by a comparison of the behaviour in several ionic liquids, in order to further understand the nature of protons in ionic liquid media.

References

[1] Silvester, D. S.; Aldous, L.; Hardacre, C. and Compton, R. G., *J. Phys. Chem. B*, 2007, **111**, 5000–5007.

[2] Silvester, D. S.; Ward, K. R.; Aldous, L.; Hardacre, C. and Compton, R. G., *J. Electroanal. Chem.*, 2008, **818**, 53–60.

[3] O'Hayre, R.; Cha, S.-W.; Colella, W. and Prinz, F. B., *Fuel Cell Fundamentals*, John Wiley and Sons: New York, USA, 2005.

[4] Belokopytov, V. P. and Aladzhalova, N. A., *Elektrokhimiya*, 1966, **2**, 1255–1262.

[5] Jaworski, A.; Donten, M.; Stojek, Z. and Osteryoung, J. G., *Anal. Chem.*, 1999, **71**, 243–246.

[6] Will, F. G., *J. Electrochem. Soc.*, 1963, **110**, 145–151.

[7] Conway, B. E. and Novak, D. M., *J. Phys. Chem.*, 1977, **81**, 1459–1468.

[8] Barrette Jr., W. C. and Sawyer, D. T., *Anal. Chem.*, 1984, **56**, 653–657.

[9] Daniele, S.; Ugo, P.; Mazzocchin, G. A. and Bontempelli, G., *Anal. Chim. Acta*, 1985, **173**, 141–148.

[10] Crowhurst, L.; Mawdsley, P. R.; Perez-Arlandis, J. M.; Salter, P. A. and Welton, T., *PhysChemChemPhys*, 2003, **5**, 2790–2794.

[11] MacFarlane, D. R. and Forsyth, S. A., *ACS Symp. Ser.*, 2003, **856**, 264–276.

[12] MacFarlane, D. R.; Pringle, J. M.; Johansson, K. M.; Forsyth, S. A. and Forsyth, M., *Chem. Commun.*, 2006, **18**, 1905–1917.

[13] Thomazeau, C.; Olivier-Bourbigou, H.; Magna, L.; Luts, S. and Gilbert, B., *J. Am. Chem. Soc.*, 2003, **125**, 5264–5265.

[14] Cole, A. C.; Jensen, J. L.; Ntai, I.; Tran, K. L. T.; Weaver, K. J.; Forbes, D. C. and Davis, James H., J., *J. Am. Chem. Soc*, 2002, **124**, 5962–5963.

[15] Du, Y. and Tian, F., *Synth. Commun.*, 2005, **35**, 2703–2708.

[16] Du, Z.; Li, Z.; Guo, S.; Zhang, J.; Zhu, L. and Deng, Y., *J. Phys. Chem. B*, 2005, **109**, 19542–19546.

[17] Susan, M. A. B. H.; Noda, A.; Mitsushima, S. and Watanabe, M., *Chem. Commun.*, 2003, **8**, 938–939.

[18] Zhao, C.; Burrell, G.; Torriero, A. A. J.; Separovic, F.; Dunlop, N. F.; MacFarlane, D. R. and Bond, A. M., *J. Phys. Chem. B*, 2008, **112**, 6923–6936.

[19] Del Pópolo, M. G.; Kohanoff, J. and Lynden-Bell, R. M., *J. Phys. Chem. B*, 2006, **110**, 8798–8803.

[20] Earle, M. J.; Hakala, U.; Hardacre, C.; Karkkainen, J.; McAuley, B. J.; Rooney, D. W.; Seddon, K. R.; Thompson, J. M. and Wähälä, K., *Chem. Commun.*, 2005, **7**, 903–905.

[21] Hardacre, C.; Katdare, S. P.; Milroy, D.; Nancarrow, P.; Rooney, D. W. and Thompson, J. M., *J. Catal.*, 2004, **227**, 44–52.

[22] Baldelli, S., *J. Phys. Chem. B*, 2005, **109**, 13049–13051.

[23] Fitchett, B. D.; Rollins, J. B. and Conboy, J. C., *Langmuir*, 2005, **21**, 12179–12186.

[24] Varela, H. and Krischer, K., *Catal. Today*, 2001, **70**, 411–425.

[25] Silvester, D. S. and Compton, R. G., *Z. Phys. Chem.*, 2006, **220**, 1247–1274.

[26] Shoup, D. and Szabo, A., *J. Electroanal. Chem. Interfacial Electrochem.*, 1982, **140**, 237–245.

[27] Bonhôte, P.; Dias, A.-P.; Papageorgiou, N.; Kalyanasundaram, K. and Grätzel, M., *Inorg. Chem.*, 1996, **35**, 1168–1178.

[28] Rieger, P. H., *Electrochemistry, 2nd ed.*, Chapman and Hall, Inc.: New York, USA, 1994.

[29] Trasatti, S., *J. Electroanal. Chem. Interfacial Electrochem.*, 1972, **39**, 163–184.

[30] Compton, R. G. and Banks, C. E., *Understanding Voltammetry*, World Scientific, Singapore, 2007.

[31] Mostany, J.; Herrero, E.; Feliu, J. M. and Lipkowski, J., *J. Electroanal. Chem.*, 2003, **558**, 19–24.

[32] Treimer, S. E. and Evans, D. H., *J. Electroanal. Chem.*, 1998, **449**, 39–48.

[33] Swatloski, R. P.; Holbrey, J. D. and Rogers, R. D., *Green Chem.*, 2003, **5**, 361–363.

[34] Xue, H.; Verma, R. and Shreeve, J. M., *J. Fluorine Chem.*, 2006, **127**, 159–176.

[35] Villagrán, C.; Banks, C. E.; Hardacre, C. and Compton, R. G., *Anal. Chem.*, 2004, **76**, 1998–2003.

[36] Roziere, J.; Roziere-Bories, M. T. and Williams, J. M., *Inorg. Chem.*, 1976, **15**, 2490–2494.

[37] Aldous, L.; Silvester, D. S.; Pitner, W. R.; Compton, R. G.; Lagunas, M. C. and Hardacre, C., *J. Phys. Chem. C*, 2007, **111**, 8496–8503.

[38] Seddon, K. R.; Stark, A. and Torres, M.-J., *ACS Symp. Ser.*, 2002, **819**, 34–39.

[39] Ignat'ev, N.; Welz-Biermann, U.; Kucheryna, A.; Bissky, G. and Willner, H., *J. Fluorine Chem.*, 2005, **126**, 1150–1159.

[40] Buzzeo, M. C.; Klymenko, O. V.; Wadhawan, J. D.; Hardacre, C.; Seddon, K. R. and Compton, R. G., *J. Phys. Chem. A*, 2003, **107**, 8872–8878.

[41] Fietkau, N.; Clegg, A. D.; Evans, R. G.; Villagrán, C.; Hardacre, C. and Compton, R. G., *ChemPhysChem*, 2006, **7**, 1041–1045.

[42] Okoturo, O. O. and VanderNoot, T. J., *J. Electroanal. Chem.*, 2004, **568**, 167–181.

[43] Sun, J.; Forsyth, M. and MacFarlane, D. R., *J. Phys. Chem. B*, 1998, **102**, 8858–8864.

[44] Del Sesto, R. E.; Corley, C.; Robertson, A. and Wilkes, J. S., *J. Organometallic Chem.*, 2005, **690**, 2536–2542.

[45] Evans, R. G.; Klymenko, O. V.; Price, P. D.; Davies, S. G.; Hardacre, C. and Compton, R. G., *ChemPhysChem*, 2005, **6**, 526–533.

[46] Evans, R. G.; Klymenko, O. V.; Saddoughi, S. A.; Hardacre, C. and Compton, R. G., *J. Phys. Chem. B*, 2004, **108**, 7878–7886.

[47] Barrosse-Antle, L.; Silvester, D. S.; Aldous, L.; Hardacre, C. and Compton, R. G., *J. Phys. Chem. B*, 2008, **112**, 3398–3404.

[48] O'Mahony, A. M.; Silvester, D. S.; Aldous, L.; Hardacre, C. and Compton, R. G., *J. Phys. Chem. C*, 2008, **112**, 7725–7730.

[49] Lide, D. R., Ed., *Handbook of Chemistry and Physics: 76th Edition*, CRC Press, Boca Raton, USA, 1996.

[50] Dyson, P. J.; Laurenczy, G.; Ohlin, C. A.; Vallance, J. and Welton, T., *Chem. Commun.*, 2003, **19**, 2418–2419.

[51] Kumelan, J.; Pérez-Salado Kamps, A.; Tuma, D. and Maurer, G., *J. Chem. Eng. Data*, 2006, **51**, 11–14.

[52] Anthony, J. L.; Maginn, E. J. and Brennecke, J. F., *J. Phys. Chem. B*, 2002, **106**, 7315–7320.

[53] Berger, A.; de Souza, R. F.; Delgado, M. R. and Dupont, J., *Tetrahedron*, 2001, **12**, 1825–1828.

[54] Buzzeo, M. C.; Hardacre, C. and Compton, R. G., *Anal. Chem.*, 2004, **76**, 4583–4588.

[55] Hultgren, V. M.; Mariotti, A. W. A.; Bond, A. M. and Wedd, A. G., *Anal. Chem.*, 2002, **74**, 3151–3156.

[56] Kaplin, Y. A.; Chernyshova, L, S.; Belysheva, G. V. and Solov'ev, I. F., *Khymiya i Khimicheskaya Tekhnologiya*, 1977, **20**, 944–945.

[57] Silvester, D. S.; Rogers, E. I. and Compton, R. G., *'Reference Electrodes for use in RTILs' in Electrodeposition from Ionic Liquids*, ed. Endres, F, MacFarlane, D. R. and Abbot, A., Wiley, Weinheim Germany, 2008.

[58] Ji, X.; Silvester, D. S.; Aldous, L.; Hardacre, C. and Compton, R. G., *J. Phys. Chem. C*, 2007, **111**, 9562–9572.

[59] Villagrán, C.; Deetlefs, M.; Pitner, W. R. and Hardacre, C., *Anal. Chem.*, 2004, **76**, 2118–2123.

[60] Buzzeo, M. C.; Evans, R. G. and Compton, R. G., *ChemPhysChem*, 2004, **5**, 1106–1120.

Chapter 10

A Mechanistic Study of the Electro-oxidation Pathway of Ammonia in Several RTILs

This chapter reports the direct oxidation of ammonia in five RTILs, namely $[C_4mim][BF_4]$, $[C_4mim][OTf]$, $[C_2mim][NTf_2]$, $[C_4mim][NTf_2]$ and $[C_4mim][PF_6]$ (full names given in Chapter 3) on a 10 μm diameter Pt microdisk electrode. In four of the RTILs studied, the cyclic voltammetric analysis suggests that ammonia is initially oxidised to nitrogen, N_2, and protons. The protons are then transferred to an ammonia molecule, forming NH_4^+ *via* the solvated proton, HA (where A^- is the anion of the RTIL). In contrast, NH_4^+ is formed first in $[C_4mim][PF_6]$, followed by the solvated proton, HA. In all five RTILs, both HA and NH_4^+ are reduced at the electrode surface, forming hydrogen gas, which is then oxidised. The effect of changing the RTIL anion is discussed. This work may have implications in the possible amperometric sensing of ammonia gas.

All experiments described in this chapter were carried out collaboratively with Dr. Xiaobo Ji, a former DPhil student at Oxford University. This work has been published in the Journal of Physical Chemistry C.[1]

10.1 Introduction

Given its high toxicity, the determination of ammonia is essential to a number of applications including environmental protection, clinical diagnosis, industrial processes, food processing and power plants.[2,3] Ammonia detection is also important for the diagnosis of diseases such as renal inadequacy and diabetes.[4] Another important arena for ammonia determination is in water samples where it indicates organic material decomposition, which can be harmful to human health, whilst higher ammonia levels are of analytical interest in industrial operations such as

refrigeration or fertilizer manufacture.[5,6] The electrochemical oxidation of ammonia has been studied in alkaline solutions and has been the subject of continuous investigations.[7–15] As a result, several protocols based on its determination *via* its direct oxidation have been developed. However, to our knowledge, only a few studies[16–18] have been reported in aprotic or RTIL solvents and with relatively little mechanistic detail.

Buzzeo *et al.*[17] have examined the electrochemical oxidation of ammonia in dimethylformamide (DMF) and the RTIL 1-ethyl-3-methylimidazolium bis(trifluoromethylsulfonyl)imide ($[C_2mim][NTf_2]$) and observed similar voltammetric responses in each solvent, with a large oxidative wave seen initially and the appearance of a new reductive wave after the oxidation. It was shown that the ammonium cation was formed after oxidation of ammonia, followed by deprotonation of ammonium to form ammonia and protons, which can then be oxidised at the electrode surface. The mechanism was suggested as follows:

$$4NH_3(g) \rightarrow 3NH_4^+ + \frac{1}{2}N_2(g) + 3e^- \tag{10.1}$$

$$NH_4^+ \rightleftharpoons NH_3(g) + H^+ \tag{10.2}$$

$$H^+ + e^- \rightarrow \frac{1}{2}H_2(g) \tag{10.3}$$

Very recently, Ji *et al.*[18] investigated the electrochemical oxidation of ammonia at a glassy carbon electrode in propylene carbonate (PC) and the electrochemical behaviour of ammonia observed was similar to those reported above.

A substantial part of the work presented here will focus on the mechanistic studies of the electro-oxidation pathway of ammonia in a series of ionic liquids and the subsequent elucidation of the reaction pathway. As a result, the reduction of the ammonium ion will also be studied in order to 'fingerprint' any peaks following the oxidation of ammonia. Martinez *et al.*[19] have studied the electrochemical reduction of the ammonium ion in the aprotic solvent dimethylsulfoxide

(DMSO) on platinum electrodes, and shown that the ion can be electrochemically reduced to produce ammonia and hydrogen. They then proposed that these products could be oxidised at different potentials. Two of the possible mechanisms were suggested[19] as follows:

$$Pt + NH_4^+ + e^- \rightleftharpoons NH_3 + Pt(H) \tag{10.4}$$

$$Pt(H) + NH_4^+ + e^- \rightleftharpoons NH_3 + H_2 + Pt \tag{10.5}$$

or

$$Pt + NH_4^+ + e^- \rightleftharpoons NH_3 + Pt(H) \tag{10.6}$$

$$Pt(H) + Pt(H) \rightleftharpoons 2Pt + H_2 \tag{10.7}$$

The reduction of NH_4^+ was also studied by Buzzeo *et al.*[17] in the RTIL $[C_2mim][NTf_2]$ and in the aprotic solvent DMF, and it was found that the reduction peak of NH_4^+ was at the same potential as the reduction peak following the oxidation of ammonia.

In this report, we have carried out a detailed study of the mechanism of the oxidation of ammonia in several room temperature ionic liquids with different anions, namely $[C_4mim][BF_4]$, $[C_4mim][OTf]$, $[C_2mim][NTf_2]$, $[C_4mim][NTf_2]$ and $[C_4mim][PF_6]$. The cyclic voltammetry obtained has allowed the proposal of a revised mechanism for ammonia oxidation in RTILs. This work has implications in helping to define a pH scale in ionic liquids, and in the possible analytical sensing of ammonia gas.

10.2 Experimental

All experiments were performed in a T-cell (described in Chapter 3), with a 10 μm diameter Pt working electrode and 0.5 mm diameter Ag quasi-reference electrode. Ammonia/hydrogen gas was introduced through one arm of the T-cell, and an outlet line led to a fume cupboard. The gas was then allowed to diffuse through the sample of ionic liquid until equilibration was reached (typically after 30 min for ammonia and 10 min for hydrogen). Signals were monitored over a

period of time to ensure true equilibration was obtained. For experiments involving NH_4NO_3, saturated stock solutions were first made up in *ca.* 100 μL of the corresponding RTIL. The solutions were stirred for at least 4 hours to allow for full dissolution. 20 μL of this solution was then pipetted into the plastic collar above the working electrode, transferred into the T-cell and placed under vacuum. 10 mM cobaltocenium hexafluorophospate ($CcPF_6$) was added to the RTIL inside the T-cell by pipetting 10 μL of a 20 mM $CcPF_6$ solution in MeCN, following the solvent evaporation method. This, and all other experimental details are given in Chapter 3.

10.3 Results and Discussion

The electrochemistry of ammonia has been studied in a range of common RTILs with different anions, namely $[C_4mim][BF_4]$, $[C_4mim][OTf]$, $[C_2mim][NTf_2]$, $[C_4mim][NTf_2]$ and $[C_4mim][PF_6]$, all of which showed a clean voltammetric baseline when fully vacuum purged. Initially, we will first describe the results obtained in one ionic liquid in detail, ($[C_4mim][BF_4]$), and then second report similar findings in the other four RTILs.

10.3.1 Mechanistic Electrochemical Study of NH_3 in $[C_4mim][BF_4]$

10.3.1.1 Voltammetry of Ammonia in $[C_4mim][BF_4]$

The electrochemical oxidation of ammonia was first investigated by passing a positive pressure of ammonia gas (10%; 90% N_2) over a blank solution of $[C_4mim][BF_4]$. Maximum peak currents were obtained after *ca.* 30 minutes of gas diffusing into the liquid. The voltammetric responses of a saturated ammonia solution on a 10 μm platinum electrode are shown in Figure 10.1 at a range of scan rates from 100 mV s^{-1} to 10 V s^{-1} (solid lines), together with a blank cyclic voltammogram at 10 V s^{-1} (dotted line) for comparison. A single oxidative wave, peak I at *ca.* +1.36 V *vs* Ag (at 10 V s^{-1}) is observed, and is attributed to the direct oxidation of ammonia at the electrode surface, as previously reported by Buzzeo *et al.*[17] in the RTIL $[C_2mim][NTf_2]$

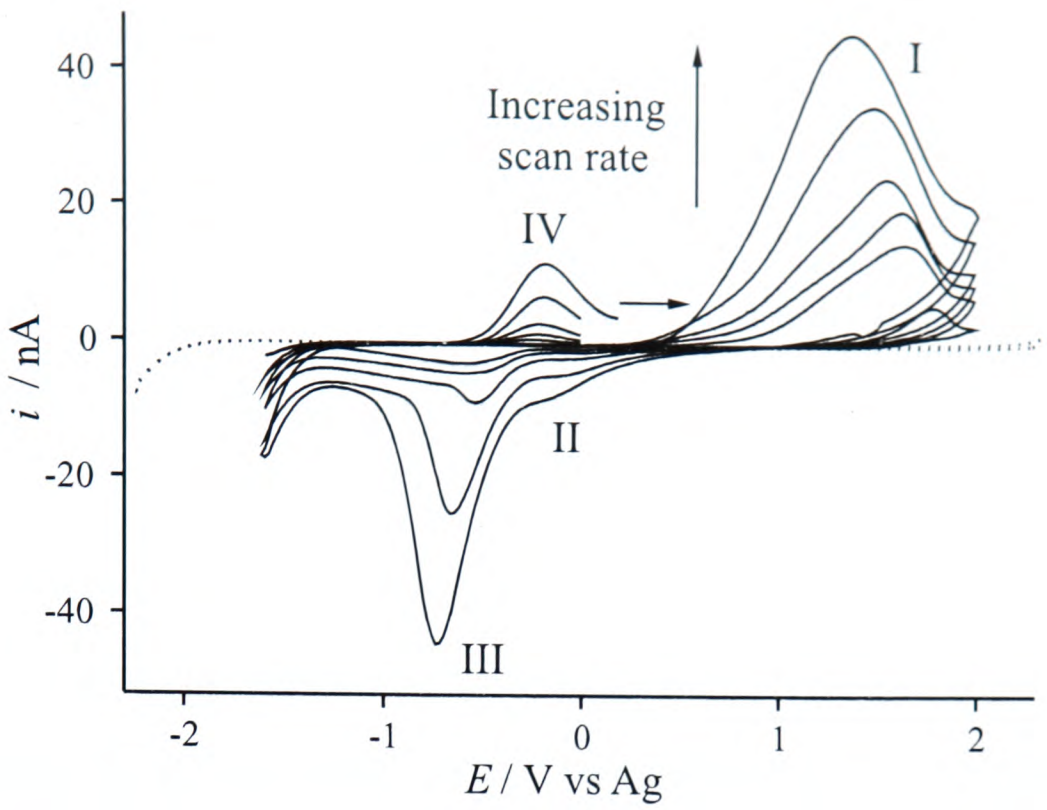

Figure 10.1: Cyclic voltammetric responses of $[C_4mim][BF_4]$ saturated with 10 vol % ammonia on a 10 μm diameter platinum electrode, at scan rates from 0.1 to 10 V s^{-1}. Dotted line = 0 vol % ammonia.

and by Ji *et al.*[18] in propylene carbonate (PC). The peak potential of this wave becomes more negative when the scan rate is increased, indicating electrochemical irreversibility, as confirmed by tafel analysis of the linear region of the current peak, which gave a transfer coefficient, α, of 0.08. It can also be seen that a reductive wave emerges at ca. -0.75 V *vs* Ag (peak III) on the reverse scan, and a corresponding oxidative wave at -0.35 V (peak IV). It is believed that peak III is the reduction of NH_4^+, as indicated by the investigation of the voltammetry of NH_4NO_3, (shown in section 10.3.1.2) and by Buzzeo *et al.*[17] in $[C_2mim][NTf_2]$, and Ji *et al.*[18] in PC. Since the appearance of peak IV has been reported previously,[17,18] but its identity is unconfirmed, a further experiment was then performed. A sample of $[C_4mim][BF_4]$ was saturated with ammonia for *ca.* 30 minutes and a typical voltammogram was obtained. Hydrogen gas was then introduced to the cell for *ca.* 10 minutes, and the resulting voltammogram (not shown here) showed a large increase in the size of peak IV, which allows us to confidently suggest that peak IV corresponds to the oxidation of bulk hydrogen.

As seen in Figure 10.1, there is also evidence of a small 'pre-wave' emerging at -0.20 V

(peak II) on the reductive sweep. It is believed that after the reduction of NH_3, the H^+ is stabilized and solvated by the numerous anions of the RTIL. We believe that peak II is the reduction of the solvated proton, *i.e.* $H[BF_4]$, and this will be discussed later in section 10.3.1.3. Analysis of the oxidative peak current (for all peaks) as a function of scan rate showed a linear dependence with the square root of scan rate, suggesting that all electrochemical processes are diffusion-controlled.

The relative sizes of peaks II and III with increasing scan rate can shed light on the possible mechanism occurring in this system. At lower scan rates (100 mV s^{-1}), peak III is clearly evident, but peak II is not seen. As the scan rate increases (up to 10 V s^{-1}), the relative size of peak II increases. This indicates that the species giving rise to peak II ($H[BF_4]$) is formed first, and can only be seen when the scan rate is sufficiently fast enough to outrun the kinetics of the follow-up chemistry. We therefore propose, in light of these findings, the following general reaction mechanism:

$$NH_3(g) + 3A^- \rightarrow \frac{1}{2}N_2(g) + 3HA + 3e^- \tag{10.8}$$

$$HA + NH_3(g) \rightleftharpoons NH_4^+ + A^- \tag{10.9}$$

$$HA + e^- \xrightarrow{rds} A^- + Pt(H) \rightarrow A^- + \frac{1}{2}H_2(g) \tag{10.10}$$

$$NH_4^+ + e^- \xrightarrow{rds} NH_3(g) + Pt(H) \rightarrow NH_3 + \frac{1}{2}H_2(g) \tag{10.11}$$

where A^- = the RTIL anion, $[BF_4]^-$, and HA is the solvated proton, $H[BF_4]$. Note HA may in fact represent the interaction of H^+ with one or more anions, *e.g.* homoconjugation. In the mechanism, ammonia is initially oxidised (with net three-quarters of a mole of electrons per mole of NH_3),[17,18] producing nitrogen gas and three protons, which readily (probably instantaneously) are solvated by the anion(s). The solvated proton, HA, then reacts with another ammonia molecule to form an ammonium ion, which is in equilibrium with HA. There are now two possible

reduction steps; one is the reduction of HA (equation 10.10, corresponding to peak II) and the second is the reduction of the ammonium ion (equation 10.11, corresponding to peak III). Both equations 10.10 and 10.11 produce hydrogen gas, further supporting the identity of peak IV as the oxidation of hydrogen. Depending on the position of equilibrium of equation 10.9, the relative sizes of peaks II and III are likely to change. It is believed that the position of equilibrium is determined by the thermodynamics of formation of HA, and will vary if the anion is changed. This is explored further in section 10.3.3.

Attempts to obtain a diffusion coefficient (and solubility) of ammonia in $[C_4mim][BF_4]$ by fitting the experimental data to the Shoup and Szabo[20] expression proved inadequate due to the complicated follow-up chemistry in the mechanism. However, the diffusion coefficient is expected to be one or two orders of magnitude less than in conventional aprotic solvents such as acetonitrile and DMF, due to the higher viscosity of the RTIL (112 cP for $[C_4mim][BF_4]$[21] compared to 0.92 cP in DMF[22] at 293 K).

10.3.1.2 Reduction of Ammonium Nitrate in $[C_4mim][BF_4]$

In order to further explore the electrochemical reaction mechanisms of ammonia, we next studied the reduction of NH_4^+ ion (present in this study as ammonium nitrate, NH_4NO_3). Figure 10.2 shows a typical cyclic voltammetric response of saturated NH_4NO_3 obtained at a 10 μm diameter platinum electrode in $[C_4mim][BF_4]$ at a scan rate of 1 V s^{-1}. A large reductive wave, peak ii at -0.75 V *vs* Ag, due to the electrochemical reduction of ammonium ion is observed, followed by two resulting oxidative waves at -0.51 V (peak iii) and +0.06 V (peak iv). A shoulder wave, i, also appears on the voltammogram when the potential is sewpt positively past +1.5 V (*i.e.* electochemically activated). This will be explained in more detail in section 10.3.3. The oxidative wave, peak v, at +2.06 V, corresponds to the oxidation of nitrate, as described in Chapter 7.[23]

A potential step was performed on the reductive wave (peak ii) of NH_4NO_3 in $[C_4mim][BF_4]$

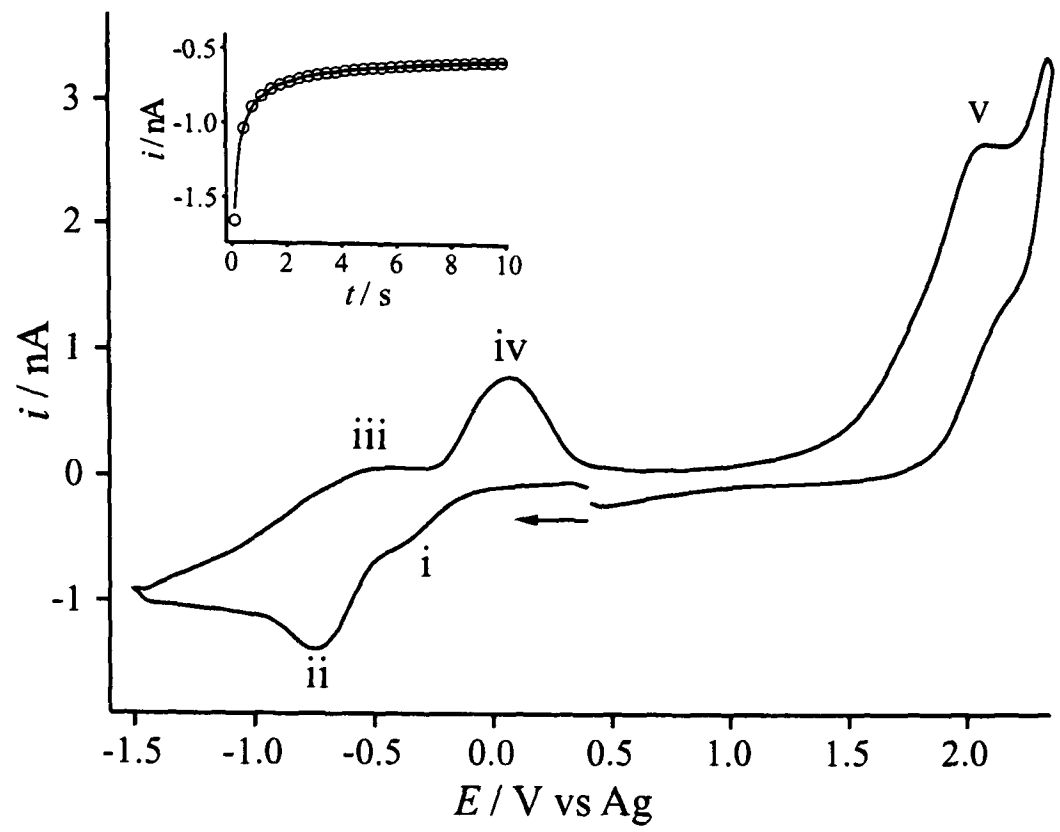

Figure 10.2: Cyclic voltammogram obtained at a platinum microdisk electrode (diameter 10 μm) for a saturated solution of NH_4NO_3 in $[C_4mim][BF_4]$ at a scan rate of 1 V s^{-1}. The electrode was activated for 1 minute at +1.5 V prior to the scan. The inset shows experimental (–) and fitted theoretical (o) chronoamperometric transient obtained for the reduction of a saturated solution of NH_4NO_3 in $[C_4mim][BF_4]$ on a 10 μm Pt electrode. The potential was stepped from 0.0 to -1.0 V.

on a freshly polished electrode and without first sweeping oxidatively, allowing analysis of peak ii without the added complication of peak i. The potential was stepped from a region of no current flow at 0 V to a potential after the peak (-1.0 V) and the current response monitored as a function of time. The diffusion coefficient of ammonium in $[C_4mim][BF_4]$ was found to be 6.2 ($\pm$0.3) $\times$ 10^{-12} m^2 s^{-1} at 298 K (*cf.* 2.14 $\times$ 10^{-9} m^2 s^{-1} and 1.65 $\times$ 10^{-9} m^2 s^{-1} in water at 298 K,[24,25] consistent with much slower diffusion in the RTIL due to the higher viscosity; 112 cP in $[C_4mim][BF_4]$[21] *vs* 1.0 cP in water[22] at 293 K).

It is interesting to note that the reductive peak at -0.37 V (peak i, Figure 10.2) appears only under certain conditions; it is absent on the first reductive sweep, but after the scan is swept to positive potentials (*i.e.* above peak v), it is clearly evident. We believe that this is due to the reduction of the solvated proton, as shown by the addition of hydrogen gas to the solution (see next section). It is thought that the solvated proton is formed in an equilibrium reaction

with NH_4^+, and scanning to a positive potential may cause a small number of ammonium ions to exchange a proton with the anion(s) of the ionic liquid. This phenomenon is also explored in more detail in Section 10.3.3.

The appearance of peaks iii and iv in Figure 10.2 have been observed previously in $[C_2mim][NTf_2]$[17] and in the aprotic solvents DMF[17] and DMSO,[19] and were tentatively attributed to the oxidation of adsorbed hydrogen in two different oxidation states, or to the oxidation of hydrogen to protons and then the direct oxidation of ammonia. In the next section, we show that the second oxidation peak (iv) is due to the oxidation of bulk hydrogen, and we propose that the first oxidation peak (iii) is probably the oxidation of *adsorbed* hydrogen, which is unsurprising given the relatively broad shape of the peak. This is further supported by the observations made by Martinez *et al.*,[19] who reported the disappearance of the two oxidative peaks on gold electrodes. As hydrogen was found to be inactive on gold in Chapter 9, it suggests that both oxidative peaks (iii and iv) are probably due to hydrogen.

10.3.1.3 Addition of Hydrogen Gas and Electrode 'Activation'

In order to try to 'fingerprint' the peaks observed in Figure 10.2, the voltammetry of NH_4NO_3 in the presence of hydrogen gas was studied. In Chapter 9, a quasi-reversible peak was observed for the oxidation of hydrogen in a range of RTILs. This peak was enhanced and became more electrochemically reversible when the electrode was pre-anodized (activated) at a positive potential of +2.0 V, and was thought to be due to the formation of platinum oxides on the surface of the electrode as a result of the oxidation of trace water. Before activation, the oxidation wave of hydrogen was relatively broad and widely separated from the corresponding reduction peak, even at relatively fast scan rates (4 V s^{-1}).[26] A similar activation effect is observed here for the reduction of NH_4^+. The inset to Figure 10.3 shows two voltammograms observed for the reduction of NH_4NO_3 on a Pt microelectrode (diameter 10 μm) at a scan rate of 10 V s^{-1}.

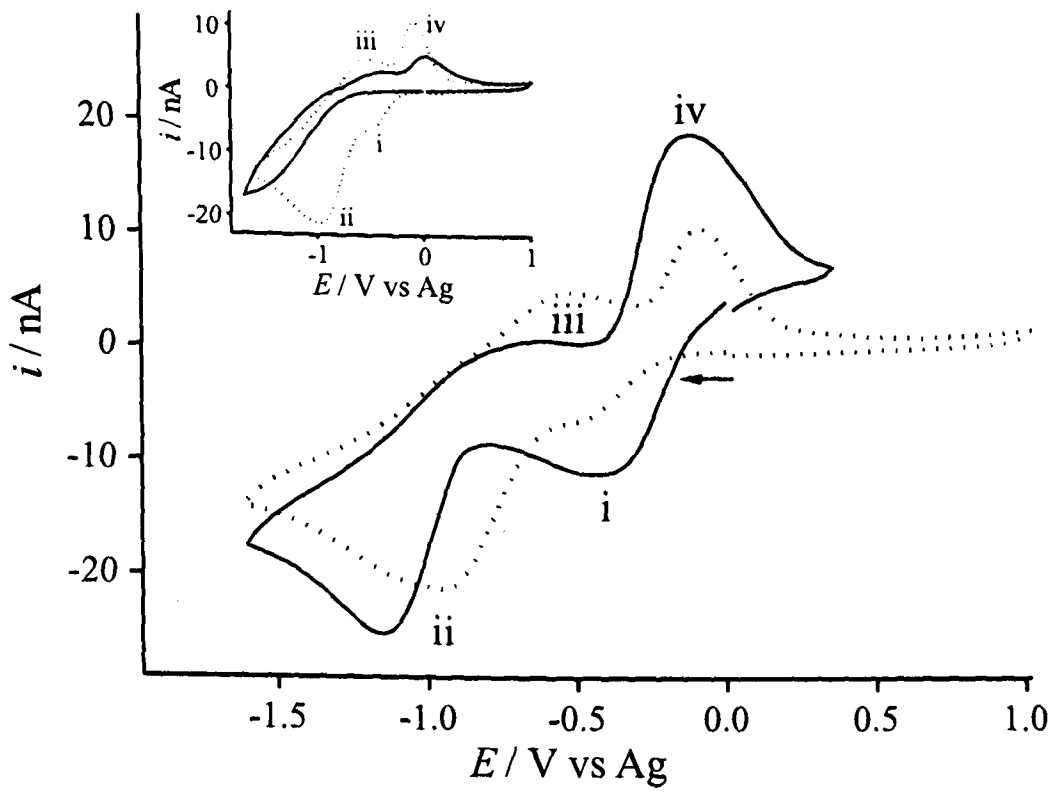

Figure 10.3: Cyclic voltammetry for the reduction of a saturated solution of NH_4NO_3 in the absence (dotted line) and presence (solid line) of 1 atm. H_2 in $[C_4mim][BF_4]$ at a scan rate of 10 V s^{-1} on a 10 μm diameter Pt electrode. The electrode was electrochemically activated for 1 minute at +1.5 V (*vs* Ag) before each scan. The inset shows the reduction of saturated NH_4NO_3 on a 10μm diameter Pt electrode in $[C_4mim][BF_4]$, at a scan rate of 10 V s^{-1}: (a) without activation (solid line), (b) with activation for 1 minute at +1.5 V (dotted line).

The solid line shows the voltammetry obtained before the electrode is activated, and the dotted line shows the voltammetry after activating the electrode at +1.5 V *vs* Ag for 1 minute. It is clearly seen that the shape of all voltammetric peaks became more defined, and the peak separations (between peaks ii and iii) are reduced upon activation, consistent with the electrode activation effect seen for hydrogen (Chapter 9). Figure 10.3 shows the reduction of NH_4NO_3 in the absence (dotted line) and presence (solid line) of hydrogen gas on a 10 μm diameter Pt electrode at a scan rate of 10 V s^{-1}. The electrode was activated at +1.5 V for 1 minute in both cases. It is evident from the overlaid voltammetry that peaks i and iv are enhanced on addition of hydrogen gas, and therefore correspond to the oxidation of hydrogen (peak iv) and the subsequent reduction of the solvated proton, $H[BF_4]$ (peak i).

10.3.1.4 Using Cobaltocenium Hexafluorophosphate as an Internal Reference Couple

As a final test to 'fingerprint' further the peaks resulting from the oxidation of ammonia (Figure 10.1), an internal reference couple, cobaltocenium hexafluorophosphate ($Co(C_5H_5)_2PF_6$ or Cc^+), was added to both the ammonia and ammonium ion solutions. It is expected that some shift in the peak potentials may be observed in these systems due to the Ag quasi-reference electrode used, as this can change its potential in the presence of certain species. The Cc^+/Cc couple has been recommended by IUPAC as one of several stable reference couples in aprotic solvents, and has been used by Bond *et al.*[27] in RTILs in this context. Consequently, the voltammetry for the oxidation of ammonia and the reduction of NH_4NO_3 was studied on a 10 μm diameter Pt electrode in the presence of 10 mM Cc^+ and is shown in Figures 10.4a and 10.4b at a scan rate of 10 V s^{-1}. The inset to Figure 10.4a shows the voltammetry of Cc^+ before the addition of gas. For clarity, the reduction peaks corresponding to the reduction of cobaltocenium hexafluorophosphate:

$$[Co(C_5H_5)_2]^+ + e^- \rightleftharpoons [Co(C_5H_5)_2] \tag{10.12}$$

$$[Co(C_5H_5)_2] + e^- \rightleftharpoons [Co(C_5H_5)_2]^- \tag{10.13}$$

have been labelled as Cc(1) and Cc(2) respectively on all subsequent figures, and as Cc(1)′ and Cc(2)′ for the back peaks corresponding to the reverse of equations 10.12 and 10.13.

Figure 10.4a shows two repeat cyclic voltammograms obtained for the oxidation of ammonia in the presence of Cc^+ at a Pt electrode (10 μm diameter) at a scan rate of 10 Vs^{-1}. The first scan was swept negatively to show the first Cc^+ reduction peak clearly, and was then swept oxidatively over the ammonia oxidation peak. The second scan showed two reductive peaks (II and III) on the cathodic sweep, and peaks Cc(1)′ and IV on the anodic sweep. The same experiment was repeated with NH_4NO_3 in the presence of Cc^+, and the peaks are labelled on

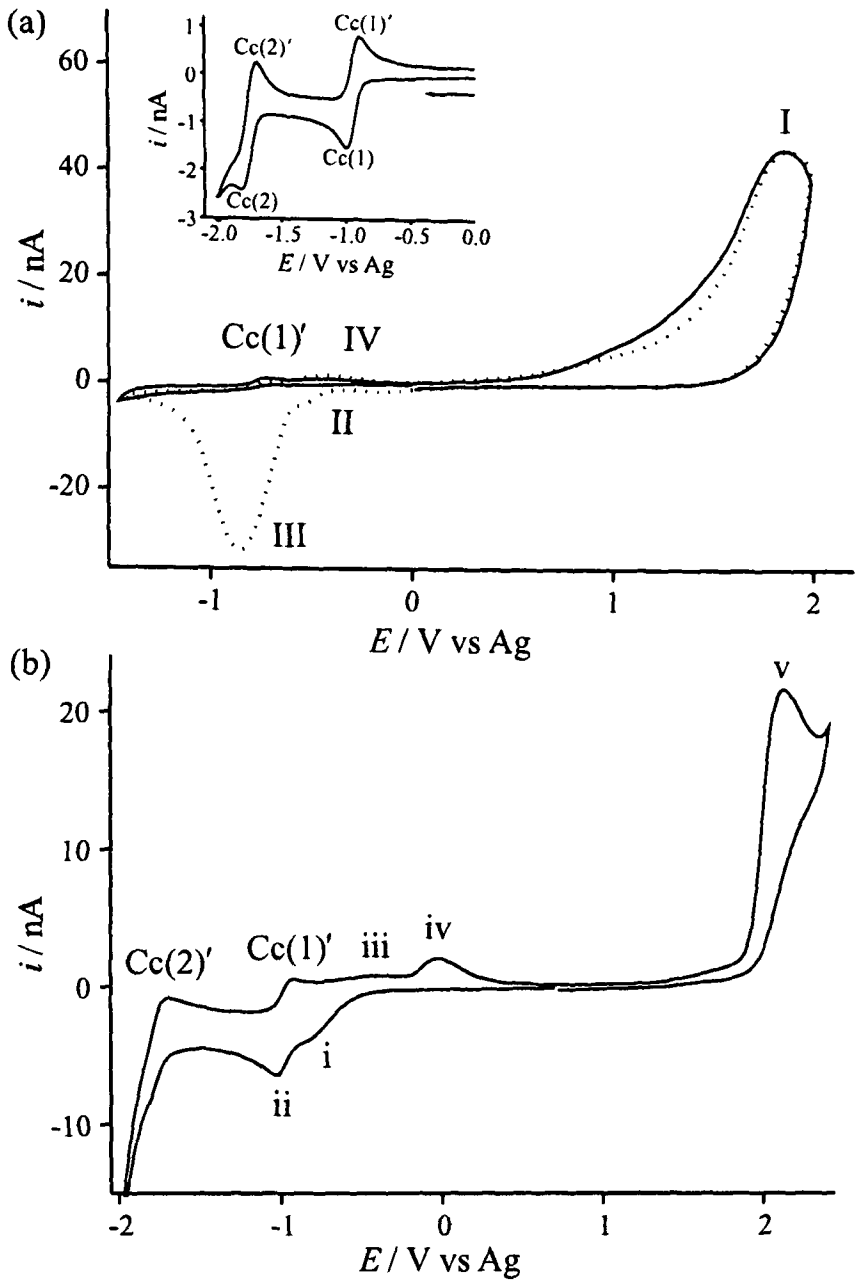

Figure 10.4: (a) Cyclic voltammetric responses of $[C_4mim][BF_4]$ saturated with 10 vol % ammonia obtained at a 10 μm diameter Pt electrode at a scan rate of 10 V s^{-1} with 10 mM Cc^+ added as an internal reference. The first (solid line) and second (dotted line) reductive scans are shown. The inset shows the voltammetry of Cc^+ before the addition of ammonia gas. (b) Cyclic voltammetry obtained at a Pt microdisk electrode (diameter 10 μm) for a saturated solution of NH_4NO_3 in $[C_4mim][BF_4]$ containing 10 mM Cc^+ at a scan rate of 10 V s^{-1}.

the voltammogram (Figure 10.4b). The peak positions relative to Cc(1)′ can now be used to try to 'fingerprint' peaks II, III and IV.

All peak potentials relative to Cc(1)′ for the oxidation of ammonia in $[C_4mim][BF_4]$ are given in Table 10.1, and in Table 10.2 for the reduction of the ammonium ion. Relative to Cc(1)′, peaks III (Figure 10.4a) and ii (Figure 10.4b) are both *ca.* -100 mV, suggesting that peak III can be identified as the reduction of the solvated proton (see section 10.3.1.3). Peaks II (Figure 10.4a)

Table 10.1: Comparison of peak positions[§] of all peaks resulting from ammonia oxidation.

RTIL	I	II	III	IV
$[C_4mim][BF_4]$	+2.59 V	200 mV	-100 mV	300 mV
$[C_4mim][OTf]$	+2.79 V	500 mV	-150 mV	250 mV
$[C_2mim][NTf_2]$	+2.90 V	600 mV	150 mV	400 mV
$[C_4mim][NTf_2]$	+2.87 V	650 mV	100 mV	400 mV
$[C_4mim][PF_6]$	+2.88 V	700 mV	200 mV	450 mV

§ *vs* Cc(1)′. Positions of all peaks are given to the nearest 50 mV.

Table 10.2: Comparison of peak positions* of all peaks resulting from NH_4^+ reduction.

RTIL	i	ii	iii	iv	A	B
$[C_4mim][BF_4]$	200 mV†	-100 mV	450 mV	900 mV		
$[C_4mim][OTf]$	500 mV†	-150 mV	550 mV	1000 mV		
$[C_2mim][NTf_2]$		150 mV	650 mV	1150 mV	1.60 V§	1.05 V§
$[C_4mim][NTf_2]$	600 mV†	100 mV	650 mV	1200 mV	1.50 V§	1.05 V§
$[C_4mim][PF_6]$	750 mV†	200 mV	700 mV	1900 mV		

* *vs* Cc(1)′. Positions of all peaks are given to the nearest 50 mV.
† Obtained from voltammetry of NH_4^+ with 1 min activation at 10 V s^{-1} (see Figure 10.8).
§ Obtained from voltammetry of NH_4^+ with H_2 at 10 V s^{-1} (see Figure 10.7).

and i (Figure 10.4b) are both *ca.* +200 mV *vs* Cc(1)′, allowing the identification of peak III as the reduction of the solvated proton. Peak IV is *ca.* +300 mV, peak iii is *ca.* +450 mV, peak iv is *ca.* +900 mV (all *vs* Cc(1)′), which initially suggests that they are all due to different species. However, as stated earlier, peaks IV and iv were identified as the oxidation of bulk hydrogen, so the 600 mV difference in their positions may be the result of a shift due to platinum oxide on the electrode surface. Peak iii (as suggested earlier) is most likely the oxidation of adsorbed hydrogen.

10.3.2 Electrochemical Study of Ammonia in Different RTILs

In order to investigate any difference in behaviour due to the solvent, the oxidation of ammonia and reduction of the ammonium ion was studied in a range of room temperature ionic liquids with different common anions, namely $[C_4mim][OTf]$, $[C_2mim][NTf_2]$, $[C_4mim][NTf_2]$ and $[C_4mim][PF_6]$.

10.3.2.1 Oxidation of Ammonia

Typical cyclic voltammograms obtained for the oxidation of NH_3 on a non-activated platinum microdisk electrode (10 μm diameter) in these four RTILs are shown in Figure 10.5 at various scan rates from 100 mV s^{-1} to 10 V s^{-1}. In all four RTILs, the voltammetry is similar to that observed in $[C_4mim][BF_4]$, and therefore the peaks can be identified as follows: peak I is the oxidation of ammonia, peak II is the reduction of the solvated proton (HA), peak III is the reduction of the ammonium ion and peak IV is the oxidation of bulk hydrogen (as confirmed by an increase in peak height in the presence of hydrogen in all four RTILs). In three of the four RTILs, peak II increases relative to peak III with increasing scan rate, and therefore is thought to follow the reaction scheme given by equations 10.8 to 10.11, where the solvated proton is formed first, followed by proton transfer to the ammonia. However, in $[C_4mim][PF_6]$, in contrast to all others studied, peak III increases with increasing scan rate to a greater extent than peak II. This suggests that the ammonium ion is formed first, followed by proton transfer to the RTIL anion. We therefore propose a revised mechanism for the oxidation of ammonia in $[C_4mim][PF_6]$:

$$NH_3(g) \rightarrow 3NH_4^+ + \frac{1}{2}N_2(g) + 3e^- \tag{10.14}$$

$$NH_4^+ + A^- + \rightleftharpoons NH_3(g) + HA \tag{10.15}$$

$$HA + e^- \xrightarrow{rds} A^- + Pt(H) \rightarrow A^- + \frac{1}{2}H_2(g) \tag{10.16}$$

$$NH_4^+ + e^- \xrightarrow{rds} NH_3(g) + Pt(H) \rightarrow NH_3 + \frac{1}{2}H_2(g) \tag{10.17}$$

where A^- = the RTIL anion, $[PF_6]^-$, and HA is the solvated proton, $H[PF_6]$. It is also interesting to note that in $[C_4mim][PF_6]$, the peak potentials for the oxidation of ammonia (peak I) do not significantly shift with increasing scan rate (in contrast to all other RTILs studied), further suggesting that a different mechanism is taking place.

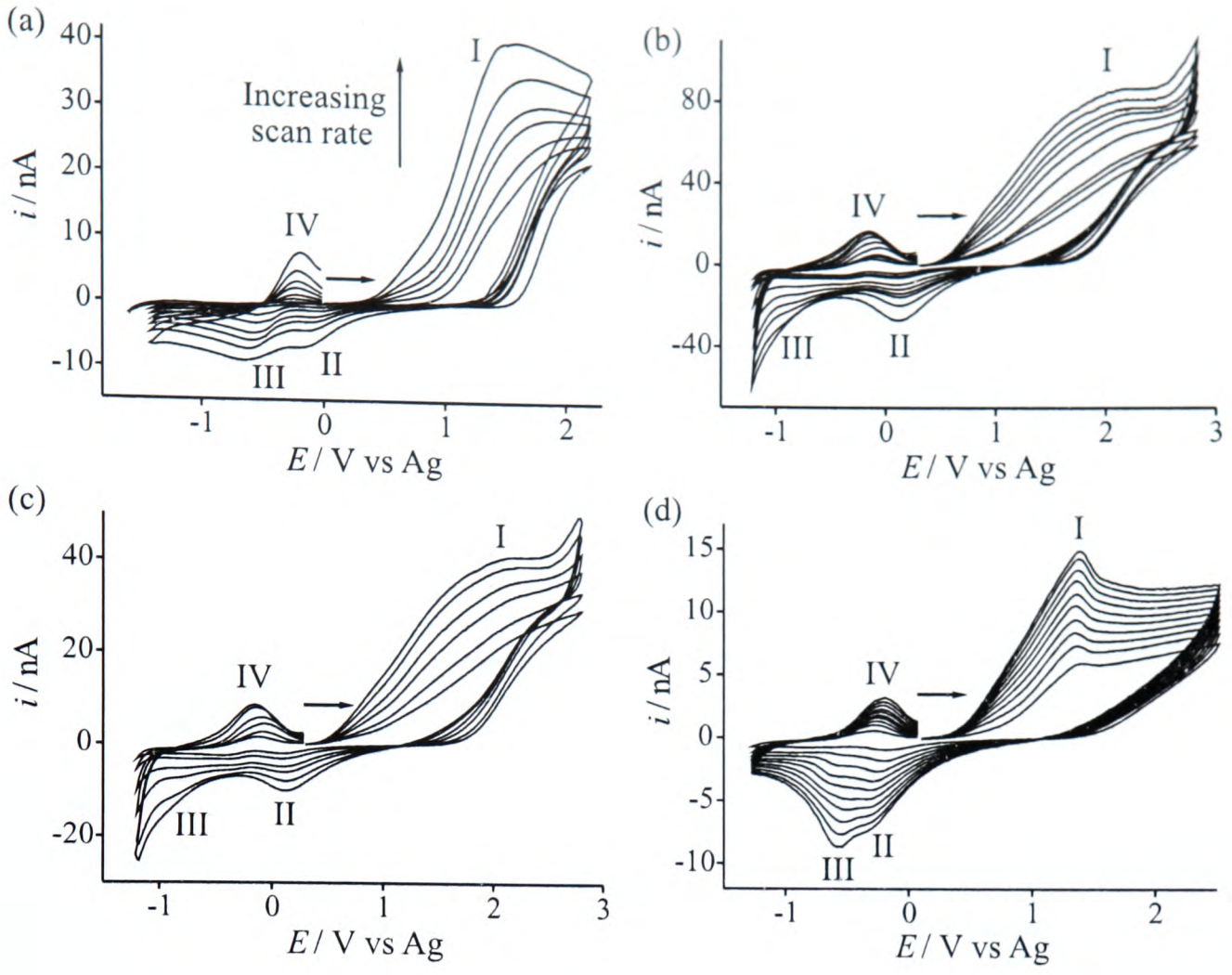

Figure 10.5: Cyclic voltammetry for the oxidation of 10 vol % ammonia on a non-activated 10 μm diameter Pt electrode in: (a) [C_4mim][OTf], (b) [C_2mim][NTf_2], (c) [C_4mim][NTf_2] and (d) [C_4mim][PF_6] at various scan rates from 100 mV s^{-1} to 10 V s^{-1}.

10.3.2.2 Reduction of the Ammonium Ion

Typical voltammetry obtained for the reduction of NH_4NO_3 (or NH_4PF_6 where NH_4NO_3 was sparingly soluble) in [C_4mim][OTf], [C_2mim][NTf_2], [C_4mim][NTf_2] and [C_4mim][PF_6] at a non-activated Pt electrode (diameter 10 μm) at scan rates of 0.1 to 10 V s^{-1} is shown in Figure 10.6. As with [C_4mim][BF_4], in all four RTILs, a reduction peak, ii, was observed and assigned to the direct reduction of the ammonium ion. On the reverse sweep, two oxidation peaks, iii and iv, likely corresponding to the oxidation of 'adsorbed' and 'bulk' hydrogen were seen. In order to calculate diffusion coefficients and solubilities of NH_4^+ in the four RTILs, a potential step was performed on the reductive wave, and the experimental chronoamperometric transients were theoretically fit to the Soup and Szabo[20] expression. The diffusion coefficients of NH_4^+ were

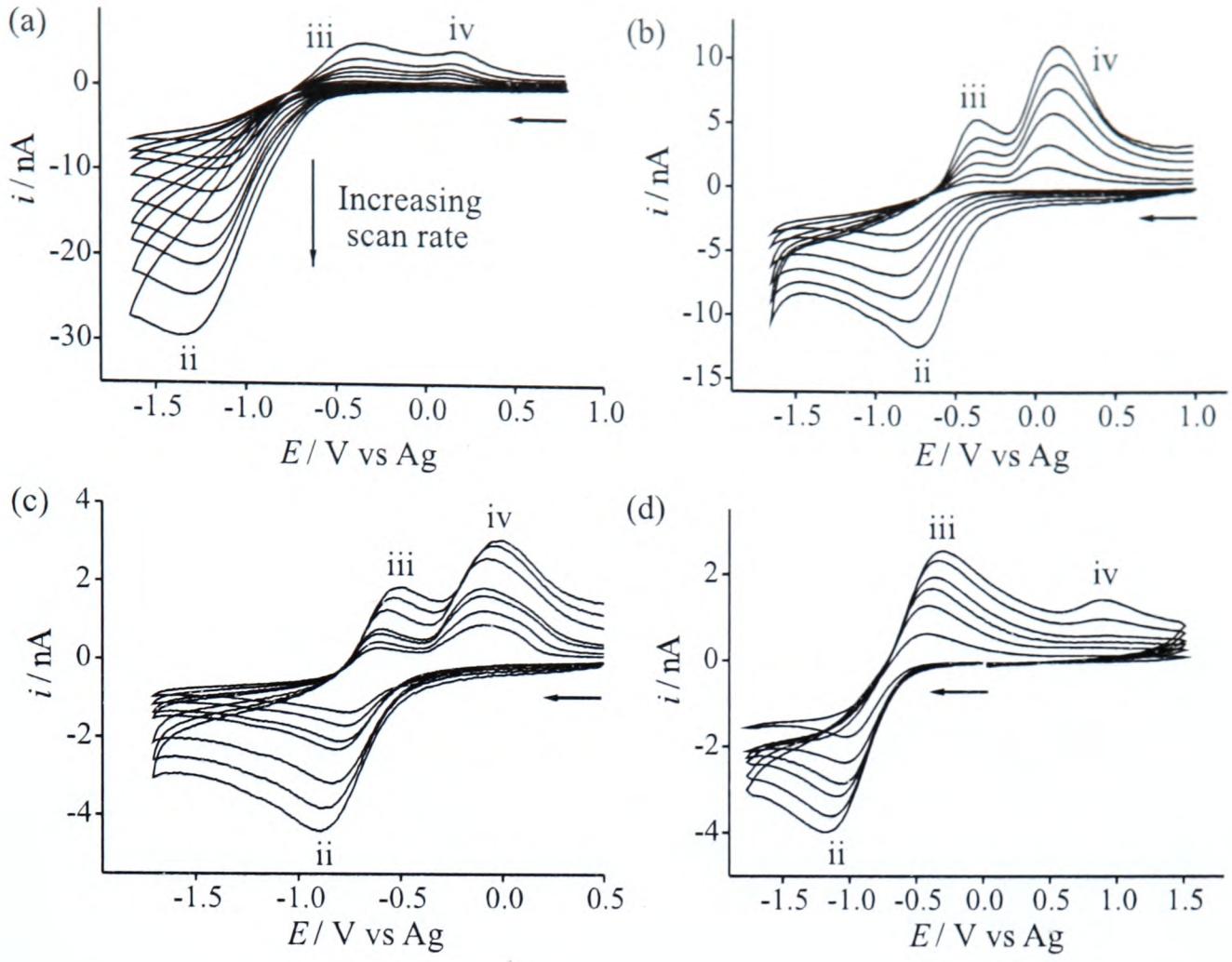

Figure 10.6: Cyclic voltammetry for the reduction of a saturated solution of NH_4NO_3 on a non-activated 10 μm diameter Pt electrode in: (a) [C_4mim][OTf], (b) [C_2mim][NTf_2], (c) [C_4mim][NTf_2] and (d) [C_4mim][PF_6] at a range of scan rates from 100 mV s^{-1} to 10 V s^{-1}.

found to be 7.1, 13.0, 9.8 and 2.5 $\times$ 10^{-12} m^2 s^{-1} at 298 K, and the solubilities were 520, 12.2, 13.7 and 122 mM in [C_4mim][OTf], [C_2mim][NTf_2], [C_4mim][NTf_2] and [C_4mim][PF_6], respectively. A comparison of diffusion coefficients and solubilities in all five studied RTILs is given in Table 10.3, and the values are discussed in more detail section 10.3.4.

Table 10.3: Comparison of calculated diffusion coefficients and solubilities (from potential-step chronoamperometry) at 298 K for NH_4^+ in five different ionic liquids.

RTIL	Viscosity*/ cP	$D_{NH_4^+}$/ $\times$ 10^{-12} m^2 s^{-1}	Solubility NH_4^+/ mM
[C_4mim][BF_4]	112[21]	6.2 ($\pm$ 0.3)	38.5 ($\pm$ 1.5)§
[C_4mim][OTf]	90[28]	7.1 ($\pm$ 0.5)	520 ($\pm$ 30)§
[C_2mim][NTf_2]	34[28]	13.0 ($\pm$ 0.2)	12.2 ($\pm$ 1.0)§
[C_4mim][NTf_2]	52[28]	9.8 ($\pm$ 0.6)	13.7 ($\pm$ 0.5)§
[C_4mim][PF_6]	371[29]	2.5 ($\pm$ 0.1)	122 ($\pm$ 1.0)†

*at 293 K § Present in solution as NH_4NO_3. † Present in solution as NH_4PF_6.

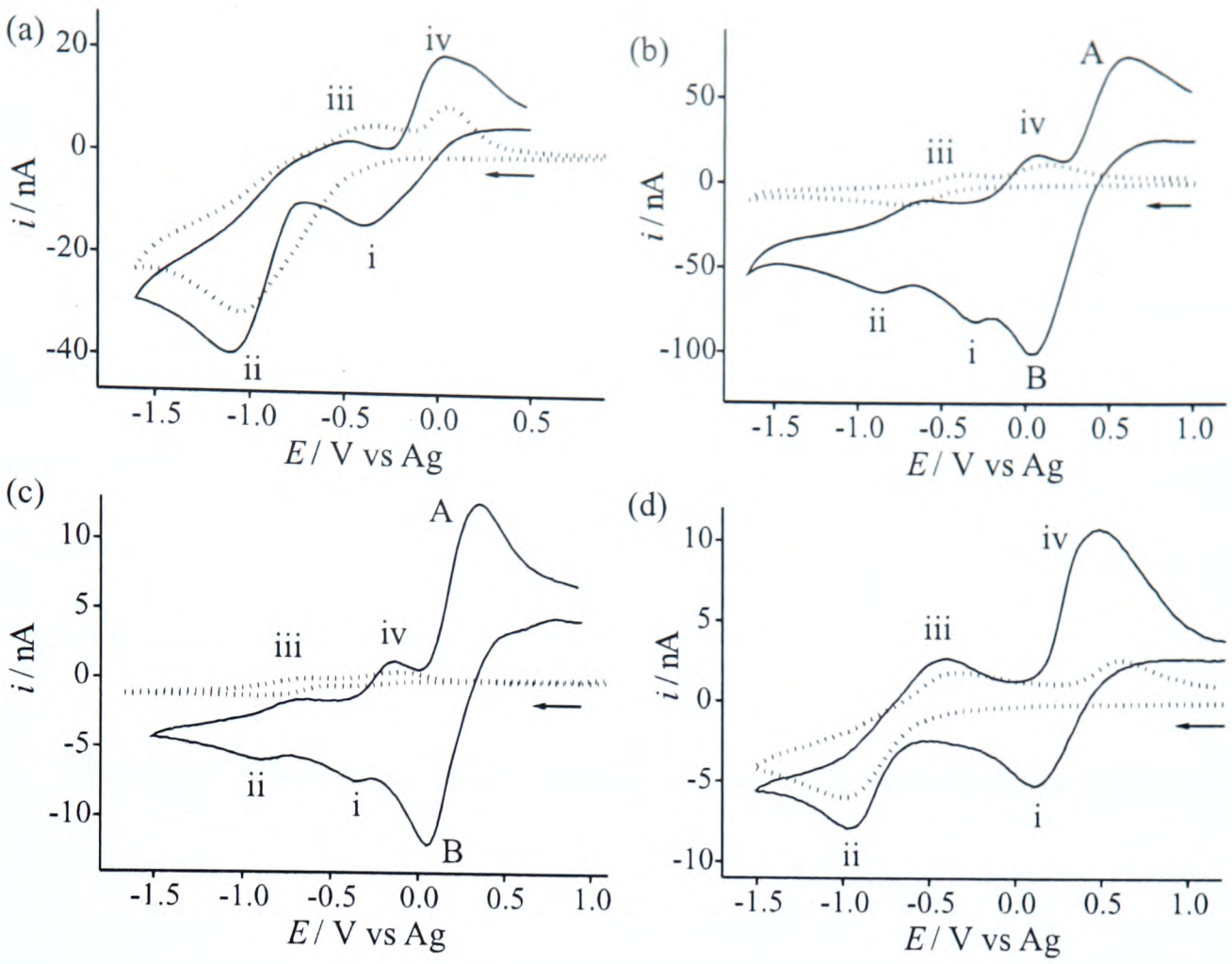

Figure 10.7: Cyclic voltammetry for the reduction of saturated NH_4NO_3 (dotted lines), and NH_4NO_3 in the presence of 1 atm. H_2 (solid lines) at a scan rate of 10 V s^{-1} on a 10 μm diameter Pt electrode in: (a) [C_4mim][OTf], (b) [C_2mim][NTf_2], (c) [C_4mim][NTf_2] and (d) [C_4mim][PF_6]. The electrode was activated at +1.5 V for 1 minute prior to the scans containing NH_4NO_3 and H_2.

10.3.2.3 Reduction of Ammonium Ion in the Presence of Hydrogen Gas

The voltammetry of NH_4NO_3 (or NH_4PF_6) in [C_4mim][OTf], [C_2mim][NTf_2], [C_4mim][NTf_2] and [C_4mim][PF_6] at an activated Pt electrode (diameter 10 μm) in the presence of 1 atm. H_2 is shown in Figure 10.7 at a scan rate of 10 V s^{-1} (solid lines). The voltammograms are overlaid on the voltammograms for the reduction of NH_4^+ on non-activated electrodes (dotted lines). In [C_4mim][OTf], and [C_4mim][PF_6] (Figures 10.7a and 10.7d), the size peak iv increases significantly with the addition of hydrogen gas, suggesting that peak iv is the oxidation of bulk hydrogen (*cf.* [C_4mim][BF_4]). In addition, peak i appears, which likely corresponds to the reduction of the solvated proton, as discussed previously in Chapter 9. However, the voltammetry for the reduction of the ammonium ion in the presence of hydrogen in [C_2mim][NTf_2]

and $[C_4mim][NTf_2]$ is different, and gives rise to an extra redox couple (three in total) on Figures 10.7b and 10.7c. The shapes of the redox couple A and B closely resembles that seen for the oxidation of hydrogen in the same ionic liquids in Chapter 9, so we attribute peaks A and B to the oxidation of bulk hydrogen and the reduction of the solvated proton, respectively. Since peak iii is likely the oxidation of hydrogen adsorbed on the Pt surface (as in all ionic liquids), it is possible that the additional redox couple (peaks i and iv, which are only seen in the $[NTf_2]^-$ ionic liquids) may be due to the oxidation of adsorbed hydrogen and reduction of adsorbed protons stabilised on the Pt electrode by the $[NTf_2]^-$ anion.

10.3.3 Effect of Electrode Activation on the Relative Ratios of Peaks i and ii

As mentioned previously in this study, the peak shapes and relative sizes of all peaks (i to iv) following the reduction of NH_4^+ were altered by electrochemically 'activating' the surface of the Pt electrode prior to the voltammetric scan. This was also seen for the oxidation of hydrogen in several RTILs on a Pt electrode (Chapter 9) and was attributed to the formation of Pt oxides on the electrode surface. As a result, the peak shape for the oxidation of hydrogen became sharper and more electrochemically reversible.[26] This is now demonstrated for the reduction of the ammonium ion. Figure 10.8 shows the effect of activating the surface of the electrode prior to the reduction of NH_4^+ in four RTILs with different anions: (a) $[C_4mim][BF_4]$, (b) $[C_4mim][OTf]$, (c) $[C_4mim][NTf_2]$ and (d) $[C_4mim][PF_6]$, on a Pt electrode (d=10 μm) at a scan rate of 10 V s^{-1}.

In the RTILs $[C_4mim][BF_4]$, $[C_4mim][OTf]$ and $[C_4mim][PF_6]$ (Figures 10.8a, 10.8b and 10.8d), the voltammetry shown in Figure 10.8 represents 'activating' the electrode from 0 (dotted line) to 240 seconds, which was necessary to show the appearance of the reduction of the solvated proton, peak i. In $[C_4mim][NTf_2]$ (Figure 10.8c) and $[C_2mim][NTf_2]$ (not shown), the maximum

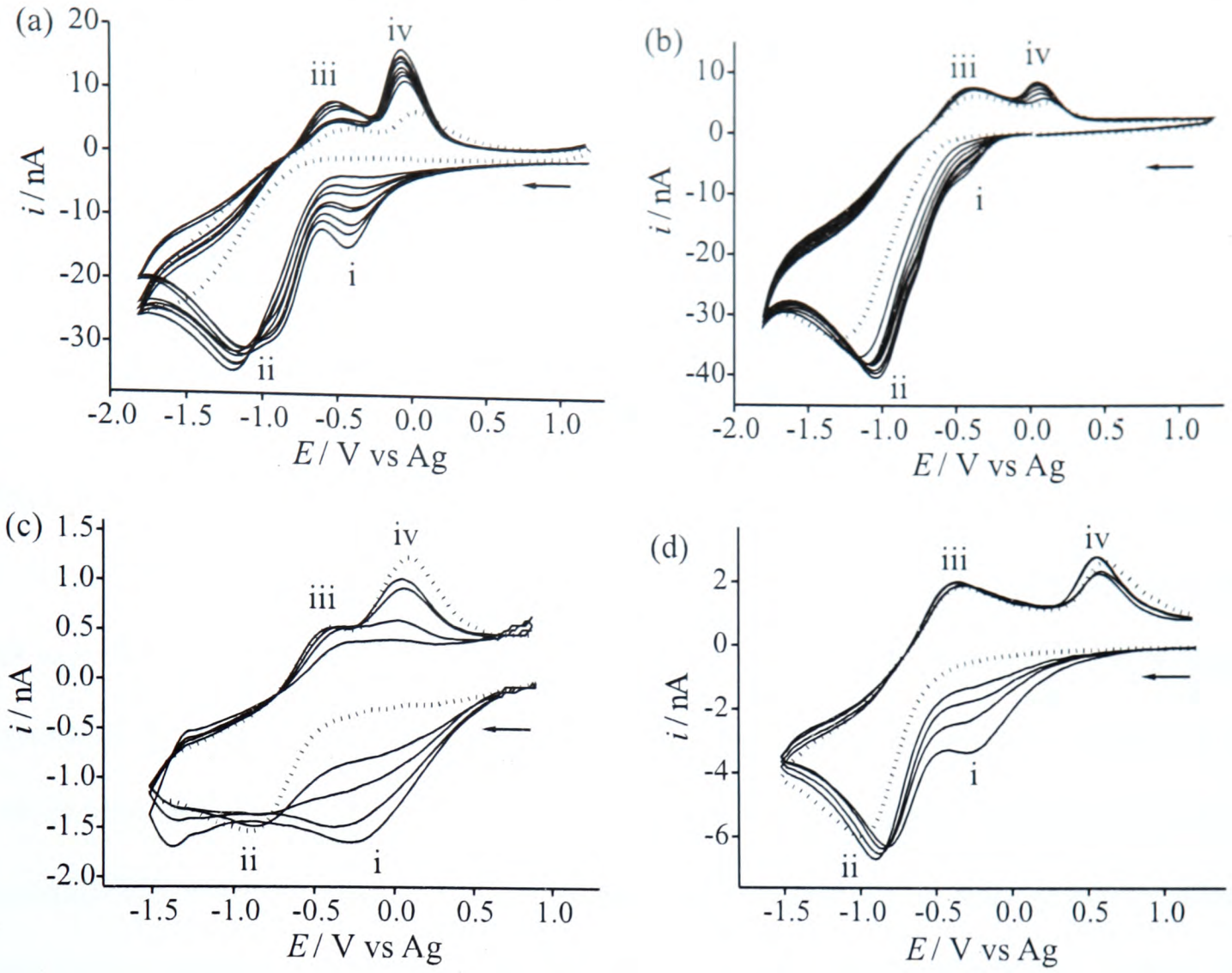

Figure 10.8: Cyclic voltammograms for the reduction of a saturated solution of NH_4^+ on a 10 μm diameter Pt electrode at a scan rate of 10 V s^{-1} in: (a) [C_4mim][BF_4], (b) [C_4mim][OTf], (c) [C_4mim][NTf_2] and (d) [C_4mim][PF_6]. The electrode was activated electrochemically at +1.5 V for the following times: (a) 0 (dotted line), 2, 5, 10, 30, 60, 120 and 240 seconds, (b) 0 (dotted line), 2, 5, 10, 30, 60, 120 and 240 seconds, (c) 0 (dotted line), 1, 2, 5 and 10 seconds, (d) 0 (dotted line), 30, 60, 120 and 240 seconds.

activation time was reduced to 10 seconds, since the size of peak i was already larger than the reduction of the ammonium ion, peak ii. As can clearly be seen in Figure 10.8, the relative size of peak i to peak ii is hugely affected by the nature of the anion. This is not unexpected, since it is thought that the relative sizes of peaks i and ii are dependent on the position of equilibrium of the following equation:

$$NH_4^+ + A^- + \rightleftharpoons NH_3(g) + HA \tag{10.18}$$

where A^- is the RTIL anion, and HA is the solvated proton. It appears that the position of equilibrium is most shifted towards the right hand side in [C_4mim][NTf_2], suggesting that HA is

formed quickly in $[NTf_2]^-$ based RTILs, hence giving rise to a large peak i. On the other hand, peak i remains relatively small after 240 seconds activation in $[C_4mim][OTf]$, suggesting that the position of the equilibrium remains in favour of NH_4^+, *i.e.* only a small amount of H[OTf] is formed in this system. In $[C_4mim][BF_4]$ and $[C_4mim][PF_6]$, the position of equilibrium is somewhere in-between, reflecting a balance between the formation of HA and NH_4^+. The findings compare quite well to a study on the reactivity in zeolite catalysed Friedel-Crafts reactions,[30] where cation exchange with the zeolite produces free acid, which catalyses the reaction. Reactivity for $H[NTf_2]$ was higher than either H[OTf] or $H[BF_4]$ where poor reactions were seen. This may indicate that there is more acid produced in the case of $H[NTf_2]$ due to an increased solvation of H^+ with $[NTf_2]^-$ anions, as seen here. These results also seem to correspond well to those obtained for the oxidation of H_2 in the same RTILs (Chapter 9), with the exception of $[C_4mim][OTf]$, which in contrast to the present results, showed almost fully reversible voltammetry for H_2, suggesting in this case that H^+ is more readily solvated with $[OTf]^-$ anions. This interesting difference suggests the need for further exploration into the pH properties of room temperature ionic liquids with different anions.

10.3.4 Comparison of Results Obtained in all Five RTILs

In order to fully 'fingerprint' the peaks resulting from the oxidation of ammonia and the reduction of NH_4^+, Cc^+ was added as an internal reference. As with $[C_4mim][BF_4]$ above, the voltammetry of NH_3 and NH_4^+ in the other four RTILs was obtained in the presence of Cc^+, and the resultant voltammetry is not shown here. A comparison of peak positions relative to the peak Cc(1)′ are given in Table 10.1 for the all peaks related to the oxidation of ammonia, and in Table 10.2 for all the peaks related to the reduction of NH_4^+. In all RTILs, peak II and i are at approximately the same potential, suggesting that these are both due to the reduction of the solvated proton (as confirmed by addition of H_2 gas, shown earlier in Figure 10.7). Furthermore, the potentials

of peak III and peak ii are the same, indicating that these peaks are both due to the reduction of NH_4^+. In all RTILs, the potential of peaks III and IV do not match up with either peak iii or peak iv. However, the addition of H_2 gas to the solutions in all RTILs suggest that peaks IV and iv are due to the oxidation of bulk hydrogen and the shift is likely due to the formation of platinum oxide on the electrode surface (noted earlier). Peak iii is most likely the oxidation of adsorbed hydrogen (also noted earlier).

There appears to be only a small difference in the peak potentials for ammonia oxidation (peak I) over all RTILs studied, suggesting that this system is relatively insensitive to the identity of the RTIL. This is not surprising, since the mechanism was shown to be highly electrochemically irreversible, and will likely be dependent on the energetics of the solvation of ammonia. For all other peaks reported in Tables 10.1 and 10.2, a small shift is observed in different RTILs, indicating that there may be some RTIL dependence, but is not significantly large, probably due to the highly irreversible nature of the electron transfer. The gradient obtained from Tafel plots for peaks II, III, i and ii was -787, -615, -291 and -556 mV dec^{-1} respectively. These relative large values further suggest that all the peaks are electrochemically very irreversible.

The diffusion coefficients for NH_4^+ obtained in the five RTILs at 298 K are compared in Table 10.3. The diffusion coefficient, D, is expected to be approximately inversely proportional to the viscosity, η, according to the Stokes-Einstein relation[31] given in equation 10.19, and should pass through the origin.

$$D = \frac{k_B T}{6\pi\eta a} \tag{10.19}$$

Here, k_B is the Boltzmann constant, T is the temperature, and a is the hydrodynamic radius of the diffusing species. A plot of D vs $1/\eta$ for the five RTILs is shown in Figure 10.9. The diffusion coefficients appear to be approximately proportional to the inverse of viscosity. The solubility of NH_4^+ in the five RTILs was obtained from chronoamperometry and is also reported

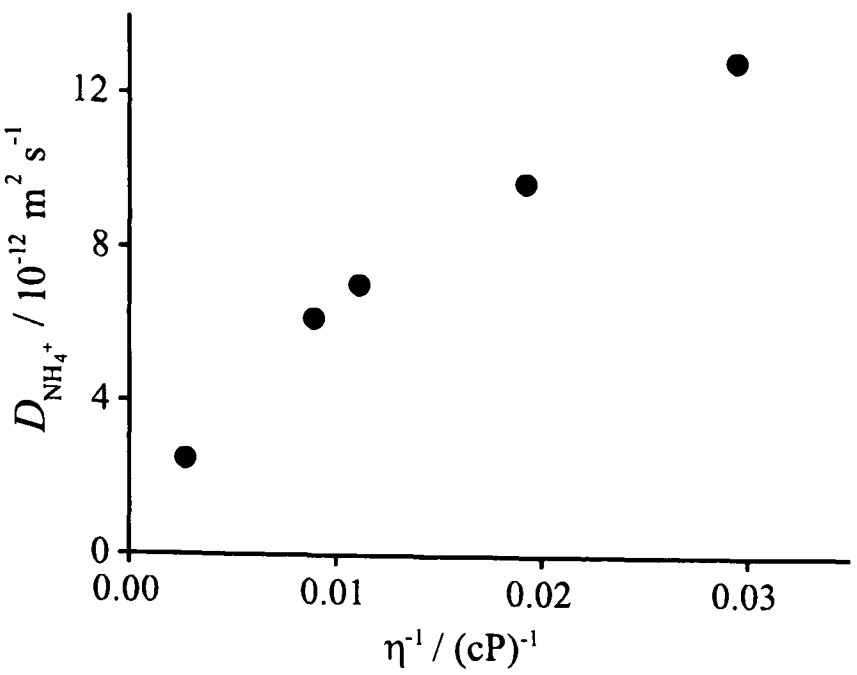

Figure 10.9: Plot of the diffusion coefficient, D, at 293 K of NH_4^+ (calculated from potential step chronoamperometry) against the inverse of viscosity, η^{-1}, for the five RTILs studied.

in Table 10.3. The values are relatively modest in $[C_4mim][BF_4]$, $[C_2mim][NTf_2]$, $[C_4mim][NTf_2]$, relatively large in $[C_4mim][PF_6]$ (perhaps due to fact that the counter anion of NH_4^+ was $[PF_6]^-$ in this case), and high in $[C_4mim][OTf]$ (520 mM), reflecting the solubility differences due to the nature of the RTIL anion.

10.4 Conclusions

The oxidation of ammonia has been studied in a range of RTILs with different anions. In all RTILs studied, the cyclic voltammetry shows a broad oxidative peak, with two cathodic peaks and one anodic peak following the oxidation. The two cathodic peaks were identified as: (1) the reduction of the solvated proton, HA, and (2) the reduction of NH_4^+. The resultant anodic peak is likely the oxidation of bulk hydrogen. In four of the five RTILs studied, the mechanism is thought to follow the scheme given in equations 10.8 to 10.11; HA is formed first, followed by NH_4^+. In $[C_4mim][PF_6]$, NH_4^+ is formed prior to the formation of $H[PF_6]$. In all cases, the solvated proton, HA, and ammonium ion, NH_4^+, are thought to be in equilibrium, and the

position of equilibrium can be altered by changing the nature of the RTIL anion. In all RTILs, the formation of HA is enhanced by 'activating' (pre-anodising) the Pt electrode at positive potentials. This work may have implications in defining pH in RTIL media, and in the possible amperometric sensing of ammonia gas.

The last two chapters have described the behaviour of hydrogen gas and ammonia gas in several ionic liquids, revealing contrasting interactions of the RTIL anion with the electrogenerated proton. The next chapter builds on the understanding of dissolved protons in ionic liquid media, by studying the reduction of a weak acid (namely benzoic acid) in a range of RTIL media.

References

[1] Ji, X.; Silvester, D. S.; Aldous, L.; Hardacre, C. and Compton, R. G., *J. Phys. Chem. C*, 2007, **111**, 9562–9572.

[2] Sazhin, S. G.; Soborover, E. I. and Tokarev, S. V., *Russ. J. Nondestr. Test.*, 2003, **39**, 791–806.

[3] Timmer, B.; Olthuis, W. and van den Berg, A., *Sens. Act. B*, 2005, **B107**, 666–677.

[4] Marcovici, E., *Wiener Klinische Wochenschrift*, 1911, **23**, 1037–1038.

[5] Gallagher, J. T. and Tayler, F. M., *Educ. Chem.*, 1967, **4**, 30–38.

[6] Wöbst, E.; Homman, G. and Friedrich, H., *Brauindustrie*, 1993, **78**, 608–610.

[7] de Vooys, A. C. A.; Koper, M. T. M.; van Santen, R. A. and van Veen, J. A. R., *J. Electroanal. Chem.*, 2001, **506**, 127–137.

[8] Despić, A. R.; Dražić, D. M. and Rakin, P. M., *Electrochim. Acta*, 1966, **11**, 997–1005.

[9] Gerischer, H. and Mauerer, A., *J. Electroanal. Chem. Interfacial Electrochem.*, 1970, **25**, 421–433.

[10] Katan, T. and Galiotto, R. J., *J. Electrochem. Soc.*, 1963, **110**, 1022–1023.

[11] López de Mishima, B. A.; Lescano, D.; Molina Holgado, T. and Mishima, H. T., *Electrochim. Acta*, 1997, **43**, 395–404.

[12] McKee, D. W.; Scarpellino, A. J., J.; Danzig, I. F. and Pak, M. S., *J. Electrochem. Soc.*, 1969, **116**, 562–568.

[13] Pignet, T. and Schmidt, L. D., *J. Catal.*, 1975, **40**, 212–225.

[14] Sasaki, K. and Hisatomi, Y., *J. Electrochem. Soc.*, 1970, **11**, 758–762.

[15] Spetz, A.; Armgarth, M. and Lundström, I., *J. Appl. Phys.*, 1988, **64**, 1274–1283.

[16] Barnes, K. K. and Mann, C. K., *J. Org. Chem.*, 1967, **32**, 1474–1479.

[17] Buzzeo, M. C.; Giovanelli, D.; Lawrence, N. S.; Hardacre, C.; Seddon, K. R. and Compton, R. G., *Electroanalysis*, 2004, **16**, 888–896.

[18] Ji, X.; Banks, C. E. and Compton, R. G., *Electroanalysis*, 2006, **18**, 449–455.

[19] Martínez, C.; Arvía, A. J. and Wargon, J. A., *Electrochim. Acta*, 1973, **18**, 485–499.

[20] Shoup, D. and Szabo, A., *J. Electroanal. Chem. Interfacial Electrochem.*, 1982, **140**, 237–245.

[21] Okoturo, O. O. and VanderNoot, T. J., *J. Electroanal. Chem.*, 2004, **568**, 167–181.

[22] Lide, D. R., Ed., *Handbook of Chemistry and Physics: 76th Edition*, CRC Press, 1996.

[23] Broder, T. L.; Silvester, D. S.; Aldous, L.; Hardacre, C.; Crossley, A. and Compton, R. G., *New J. Chem.*, 2007, **31**, 966–972.

[24] Hall, J. R.; Wishaw, B. F. and Stokes, R. H., *J. Am. Chem. Soc.*, 1953, **75**, 1556–1560.

[25] Lutz, J. L. and Mendenhall, G. D., *J. Cryst. Growth*, 2000, **217**, 183–188.

[26] Silvester, D. S.; Aldous, L.; Hardacre, C. and Compton, R. G., *J. Phys. Chem. B*, 2007, **111**, 5000–5007.

[27] Hultgren, V. M.; Mariotti, A. W. A.; Bond, A. M. and Wedd, A. G., *Anal. Chem.*, 2002, **74**, 3151–3156.

[28] Bonhôte, P.; Dias, A.-P.; Papageorgiou, N.; Kalyanasundaram, K. and Grätzel, M., *Inorg. Chem.*, 1996, **35**, 1168–1178.

[29] Seddon, K. R.; Stark, A. and Torres, M.-J., *ACS Symp. Ser.*, 2002, **819**, 34–39.

[30] Hardacre, C.; Katdare, S. P.; Milroy, D.; Nancarrow, P.; Rooney, D. W. and Thompson, J. M., *J. Catal.*, 2004, **227**, 44–52.

[31] Compton, R. G. and Banks, C. E., *Understanding Voltammetry*, World Scientific, Singapore, 2007.

Chapter 11

The Electrochemical Reduction of Benzoic Acid and Substituted Benzoic Acids in Several RTILs

In this chapter, the electrochemical reduction of benzoic acid (BZA) is studied at Pt microelectrodes (10 μm and 2 μm diameter) in six RTILs, namely $[C_2mim][NTf_2]$, $[C_4mim][NTf_2]$, $[C_4mpyrr][NTf_2]$, $[C_4mim][OTf]$, $[C_4mim][NO_3]$ and $[C_4mim][PF_6]$ (full names given in Chapter 3). In all cases, a main reduction peak is observed, assigned to the reduction of the BZA proton in a CE mechanism, where dissociation of the acid takes place before electron transfer to the dissociated proton. One anodic peak is observed on the reverse sweep, assigned to the oxidation of adsorbed hydrogen, and a reductive 'pre-peak' (assigned to the reduction of protons forming adsorbed hydrogen, H•(ads)) is observed prior to the main reduction peak. On extending the cathodic window, an electrochemically reversible peak is observed in $[C_4mpyrr][NTf_2]$ and $[C_4mim][BF_4]$, assigned to the reduction of the radical anion of BZA forming the di-anion $(C_6H_5{}^{\bullet}C(O^-)_2)$, believed to be stable in RTIL media. The voltammetry of 4-methoxy, 4-chloro, 4-bromo and 4-dialkylamino substituted BZAs is also studied, yielding a main reduction peak, with two anodic peaks on the reverse sweep, (assigned to the oxidation of adsorbed hydrogen H•(ads) and the oxidation of $C_6H_5CO_2{}^-$ to form (C_6H_5)• and CO_2). At more negative potentials, the electrochemically reversible radical anion reduction peak is also observed. Potential-step chronoamperometry reveals diffusion coefficients of *ca.* 2×10^{-11} m^2 s^{-1} for all BZA derivatives studied in $[C_4mpyrr][NTf_2]$, with a slight tendency to decrease with increasing size of substituent. The solubilities of the substituted BZAs are much lower than that of the non-substituted form. In addition, the oxidation of 4-dimethylamino and 4-diethylamino benzoic acid yields a sharp anodic peak, suggesting the possible formation of substituted polyaniline on the Pt electrode surface.

Some of the work described in this chapter was carried out with the assistance of Miss Weisi He, a fourth year undergraduate student at Oxford University, under the supervision of this author. The results reported in this chapter have been published in two parts, in the Journal of Physical Organic Chemistry[1] and in the Journal of Physical Chemistry C.[2]

11.1 Introduction

In order to further investigate the nature of dissolved protons in RTIL media, the reduction of benzoic acid (BZA) and some substituted BZAs is reported six common RTILs: $[C_2mim][NTf_2]$, $[C_4mim][NTf_2]$, $[C_4mpyrr][NTf_2]$, $[C_4mim][OTf]$, $[C_4mim][NO_3]$ and $[C_4mim][PF_6]$. It is well known[3–7] that the electrochemical reduction of weak acids (HA) proceeds by the following generic CE mechanism in water and aprotic solvents such as acetonitrile, where dissociation of the acid takes place before the reduction step:

$$HA \underset{k_{-1}}{\overset{k_1}{\rightleftharpoons}} H^+ + A^- \tag{11.1}$$

$$H^+ + e^- \xrightarrow{k_0} \frac{1}{2}H_2 \tag{11.2}$$

Focussing in particular on the reduction of the benzoic acid proton, cyclic voltammetry has previously been reported in acidic media,[3,6,7] and in the aprotic solvents dimethylformamide (DMF)[8] and dimethylsulfoxide (DMSO).[5] In all cases, the voltammetry was relatively broad and electrochemically quasi-reversible/irreversible and was found to follow a CE reaction mechanism.

The kinetics of the homogeneous step (equation 11.1) can in principle be studied by observing how the limiting current responds to changes in electrode size and concentration of BZA.[9–12] In this work, the findings from this type of kinetic analysis are discussed, and the results may help to understand the electrode kinetics of CE reactions in RTILs. A detailed mechanistic study is also performed for the reduction of BZA and some substituted BZAs in RTILs.

11.2 Experimental

All electrochemical experiments were performed on either a Pt (10 μm diameter), Au (5 μm diameter) or Pt (2 μm diameter) working electrode, and a 0.5 mm diameter silver wire quasi-reference electrode. The electrodes were housed in a glass cell T-cell as described in Chapter 3. 20 μL of ionic liquid (containing dissolved acid) was placed in the cavity above the electrode, and was purged under vacuum for *ca.* 90 minutes. For experiments with hydrogen, the gas was introduced through one arm of the cell, as described in Chapter 9. For most experiments, before each voltammetric scan, the electrode was preanodized/activated for 30 seconds at +1.5 V, in order to obtain reproducible peak currents, and for the reasons described in Chapters 9 and 10. For experiments involving ferrocene (Fc) as a redox probe, a solution of 10 mM Fc was obtained following the solvent evaporation method described in Chapter 3. Additional experimental details are given in Chapter 3.

11.3 Results and discussion

The electrochemical reduction of benzoic acid (BZA) has been examined in detail at various scan rates in six different ionic liquids, namely $[C_2mim][NTf_2]$, $[C_4mim][NTf_2]$, $[C_4mpyrr][NTf_2]$, $[C_4mim][BF_4]$, $[C_4mim][NO_3]$ and $[C_4mim][PF_6]$ to gain an insight into the reduction mechanism. The six ionic liquids showed wide, featureless baselines when purged under a vacuum for 90 minutes, and hence were chosen as suitable solvents for electrochemical experiments. First, the voltammetry of the BZA proton reduction in the six RTILs will be presented, followed by the voltammetry of some substituted benzoic acids in $[C_4mpyrr][NTf_2]$.

11.3.1 The Reduction of Benzoic Acid in Various RTILs

11.3.1.1 Activation of the Pt electrode

Before presenting the voltammetry for BZA reduction in several RTILs, it is important to introduce the topic of 'electrode activation', in light of the results presented in Chapters 9 and 10. In particular, the Pt electrode had to be pre-activated/anodized at a positive potential (*ca.* 2 V) for a period of time (30 seconds) prior to the scan in order to obtain reliable and reproducible voltammetry for hydrogen oxidation in RTILs (Chapter 9). The voltammetry was broad and irreproducible until the activation step took place, and similar observations were made for hydrogen oxidation on Pt in aprotic solvents.[8] In Chapter 10, an activation step prior to the reduction of the ammonium ion (NH_4^+) in RTILs resulted in the formation of a pre-peak prior to the main reduction peak. This pre-peak was assigned to the reduction of a proton solvated by the anion of the RTIL, *i.e.* HA, where A^-=RTIL anion.[13] In the case of BZA reduction in this work, a similar activation step had to be applied to obtain more reliable and reproducible voltammetry. Figure 11.1 shows the reduction of a saturated solution of BZA in the RTIL $[C_4mim][BF_4]$ without electrode activation (dotted line) and with electrode activation at +1.5 V for 30 s (solid line). The voltammetry is much more well-defined at the activated Pt electrode, and the peak separation between the reduction and oxidation peaks is smaller. A similar effect was observed in all six RTILs used in this study. As a result, all of the voltammetry presented for BZA reduction in this work has been obtained at Pt electrodes which have been activated at +1.5 V for 30 seconds, and the results are presented below.

11.3.1.2 Cyclic Voltammetry of BZA Reduction in Six RTILs

Typical cyclic voltammetry for the reduction of saturated solutions of benzoic acid (BZA) in six RTILs on a 10 μm diameter *activated* Pt electrode is shown in Figure 11.2. In general, the voltammetric behaviour is similar in all RTILs, with a main reduction peak at *ca.* -1 to -1.5 V,

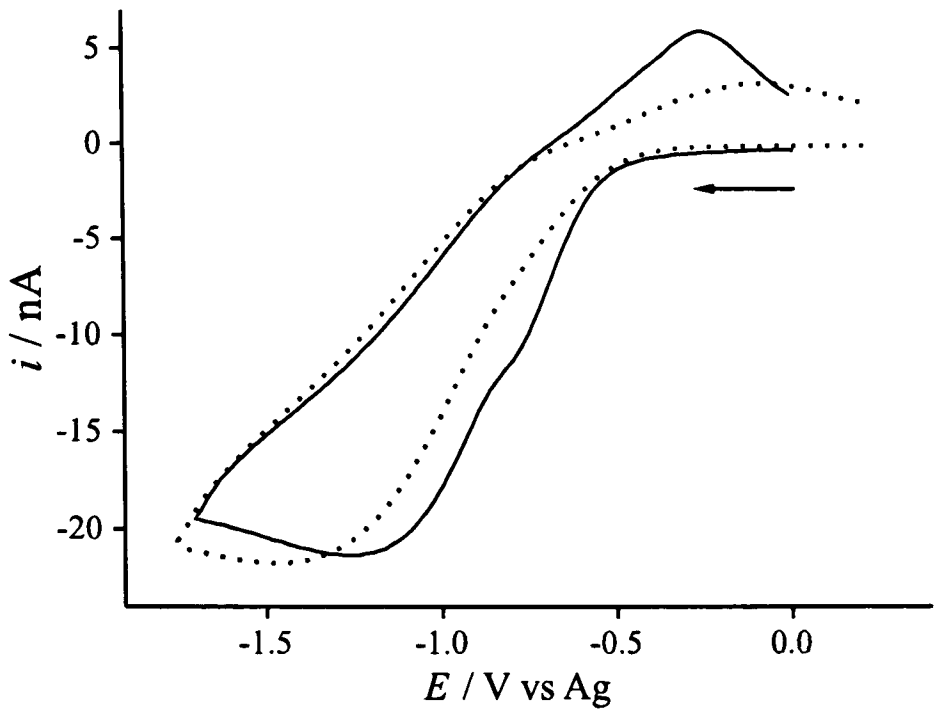

Figure 11.1: Cyclic voltammetry for the reduction of a saturated solution of BZA in $[C_4mim][BF_4]$ at 298 K on a 10 μm diameter Pt electrode at a scan rate of 4 V s^{-1}. The electrode was pre-activated at +1.5 V for 0 seconds (dotted line) and 30 seconds (solid line).

and a corresponding oxidation peak at *ca.* -0.5 to 0 V. No anodic peaks were observed when the scan was swept oxidatively from -0.5 V to solvent breakdown. It is believed that the main reduction peak can be assigned to the reduction of the BZA proton following a CE mechanism, where chemical dissociation of the acid precedes the electron-transfer step:[5,8]

$$C_6H_5COOH \underset{k_{-1}}{\overset{k_1}{\rightleftharpoons}} C_6H_5COO^- + H^+ \tag{11.3}$$

$$H^+ + e^- \xrightarrow{k_0} \frac{1}{2}H_2 \tag{11.4}$$

As can be seen from the voltammetry in Figure 11.2, there is also a reductive 'pre-peak' and an anodic 'back-peak' present in all ionic liquids. The identity of these peaks will be explained later in section 11.3.2.1, but for now, we will focus on the behaviour of the main reductive peak over a range of scan-rates.

The voltammetry presented in Figure 11.2 shows characteristics intermediate to that of pure micro- and pure macro-electrode behaviour. In general, the voltammetry in all six RTILs appears

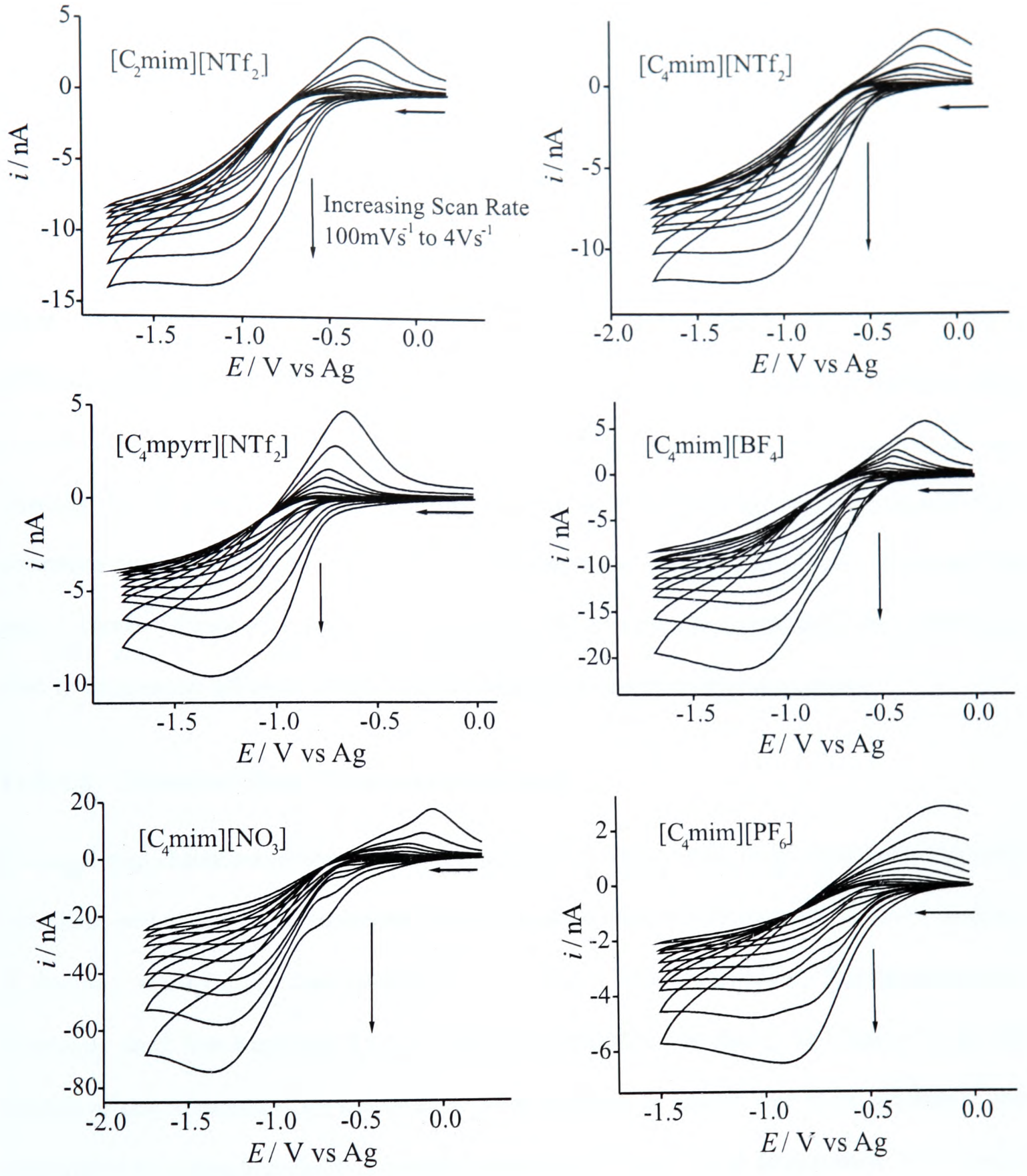

Figure 11.2: Cyclic voltammetry over a range of scanrates (0.1, 0.2, 0.4, 0.7, 1, 2 and 4 V s^{-1}) for the reduction of saturated solutions of BZA in six RTILs on a 10 μm diameter Pt electrode at 298 K. The electrode was pre-activated at +1.5 V for 30 seconds prior to all scans.

to be steady-state in nature at lower scan rates *e.g.* 100 mV s^{-1}, and becomes more 'transient' at higher scan rates (up to 4000 mV s^{-1}). The inequality[14] given in equation 11.5 states that pure micro-electrode behaviour can only be achieved at scan rates of much less than 47 mV s^{-1}, taking a typical diffusion coefficient of 4.6×10^{-11} m^2 s^{-1} (in $[C_2mim][NTf_2]$, see later).

$$\nu << \frac{RTD}{nFr_d{}^2} \tag{11.5}$$

where ν is the scan rate, R is the universal gas constant, T is the absolute temperature, D is the diffusion coefficient, F is the Faraday constant and r_d the radius of the disk. In addition, plots of peak current *vs* square root scan rate were approximately linear for all six RTILs studied, but typically do not pass through the origin because (as mentioned above) the voltammetric characteristics are intermediate of pure micro- and pure macro-electrode behaviour. Although the peak currents increase with scan rate, they do not show a direct proportionality as is commonly used to fingerprint diffusion controlled processes in macro-electrode voltammetry.

11.3.1.3 Potential Step Chronoamperometry

Potential-step chronoamperometry at a microdisk electrode is a commonly used electrochemical technique, and allows the independent calculation of diffusion coefficients and *nc* values (number of electrons multiplied by concentration) with a known microdisk radius. The approximation commonly used (see equations 3.1, 3.2 and 3.3) is described by Shoup and Szabo,[15] and the validity of this approximation has recently been reported in aprotic and RTIL solvents,[16] but only applies for a simple n electron-transfer process *i.e.* $A \pm ne^- \rightleftharpoons B$. In this work, it is believed that if the chemical step (equation 11.3, dissociation of BZA) is rate limiting, the experimental chronoamperometric transients will *not* fit the Shoup and Szabo approximation, and the limiting currents will *not* scale linearly with concentration.

To investigate this, chronoamperometric transients at were obtained for the reduction of

saturated solutions of BZA in six ionic liquids. The potential was stepped from a position of zero current (typically 0 V) to a potential after the reductive peak, and the current was measured for 10 seconds. In all cases, the theoretical fitting of experimental transients to the Shoup and Szabo expression[15] was excellent (± 0.7 %) on a 10 μm diameter Pt electrode, implying that the C step is very fast, giving the response of a simple E step. The diffusion coefficients obtained were of the same order of magnitude (10^{-11} m^2 s^{-1}) as other solid species in RTILs (*cf.* 5.34×10^{-11} m^2 s^{-1} for ferrocene in [C_2mim][NTf_2]),[17] and *ca.* 1-3 orders of magnitude less than that reported for BZA in water (9.0×10^{-10} m^2 s^{-1})[18] and in near critical carbon dioxide (1.3×10^{-8} m^2 s^{-1}).[19]

The calculated diffusion coefficients obtained from this method are given in Table 11.1, and appear to decrease with increasing viscosity. The Stokes-Einstein relation[14] given below (equation 11.6) predicts a linear relationship between the diffusion coefficients (D) and the inverse of viscosity (η^{-1}) of simple diffusing species. This relationship is commonly followed in conventional molecular solvents, and also for large organic molecules,[20] the ammonium ion (Chapter 10), ferrocene[17] and cobaltocenium hexafluorophosphate,[17] but not for small molecules *eg.* O_2,[21] H_2 (Chapter 9), SO_2[22] and H_2S[23] in RTILs.

$$D = \frac{k_B T}{6\eta\pi\alpha} \tag{11.6}$$

where k_B is the Boltzmann constant, T is the temperature and α is the hydrodynamic radius of the diffusing species. A plot of the diffusion coefficient of the BZA proton *vs* the inverse of viscosity is shown in Figure 11.3. An approximate linear relationship is observed (with [C_4mim][NO_3] an outlier at 0.26×10^{-11} m^2 s^{-1}), suggesting that equation 11.6 approximately holds for BZA in most RTILs.

Also included in Table 11.1 are the calculated solubilities of BZA in the six RTILs. The solubilities in the three $[NTf_2]^-$ ionic liquids are almost exactly the same, and a slightly lower

Table 11.1: Summary of peak potentials* obtained for the reduction of the acid (peak i on Figure 11.9) and the radical anion (peak ii on Figure 11.9) at a scan rate of 4 V s^{-1} in various RTILs on a 10 μm diameter Pt electrode at 298 K. Also included are diffusion coefficients and solubilities obtained from theoretical fitting of chronoamperometric data (main reduction peak) to the Shoup and Szabo[15] expression.

RTIL	Compound	E_i* /V	E_{ii}* /V	$D^\dagger/\times10^{-11}$ m^2s^{-1}	Solubility†/mM
$[C_2mim][NTf_2]$	BZA	-1.33	-	4.6 (±0.3)	75 (±2)
$[C_4mim][NTf_2]$	BZA	-1.34	-	3.2 (±0.2)	78 (±4)
$[C_4mpyrr][NTf_2]$	BZA	-1.29 (-1.93)§	-2.69 (-2.69)§	2.7 (±0.3)	74 (±3)
$[C_4mim][BF_4]$	BZA	-1.77	-2.66	1.8 (±0.1)	220 (±10)
$[C_4mim][NO_3]$	BZA	-1.74	-	0.26 (±0.03)	2850 (±200)
$[C_4mim][PF_6]$	BZA	-1.48	-	0.96 (±0.05)	48 (±3)
$[C_4mpyrr][NTf_2]$	MeO-BZA	-1.25	-2.68	2.0 (±0.05)	10 (±1)
$[C_4mpyrr][NTf_2]$	Cl-BZA	-1.15	-2.68	2.3 (±0.3)	4.4 (±0.4)
$[C_4mpyrr][NTf_2]$	Br-BZA	-1.15	-2.66	1.9 (±0.2)	3.7 (±0.3)
$[C_4mpyrr][NTf_2]$	DMA-BZA	-1.45	-2.87	1.8 (±0.3)	7.2 (±0.5)
$[C_4mpyrr][NTf_2]$	DEA-BZA	-1.46	-2.89	1.5 (±0.3)	10 (±1)

*vs Fc/Fc^+

§ ( ) Potential obtained on a 5 μm diameter Au electrode.

† Error bars calculated from the standard deviation of the best theoretical fits from several repeat potential step chronoamperograms.

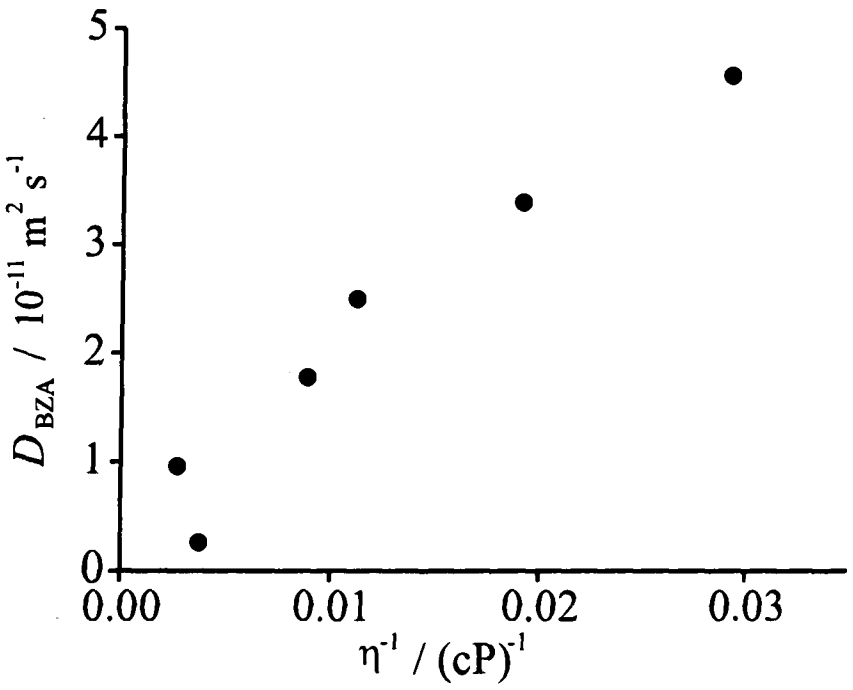

Figure 11.3: Plot of diffusion coefficient, D, (298 K) of BZA against the inverse of viscosity (293 K) for the six RTILs studied. D values were obtained from theoretical fitting of chronoamperometric transients to the Shoup and Szabo expression.[15]

solubility is observed in $[C_4mim][PF_6]$. Interestingly, the solubility is higher in $[C_4mim][BF_4]$, and significantly higher in $[C_4mim][NO_3]$, suggesting a possible interaction of the dissociated proton with the anion of the RTIL. A strong interaction of protons with the nitrate anion might suggest the formation of $H[NO_3]$ or $H[NO_3]_2^-$ (the hydrogen dinitrate ion). The existance of $H[NO_3]_2^-$ is well-known,[24–27] and its formation in RTILs has been suggested in Chapter 9. In general, the solubilities in RTILs are relatively high compared to that reported in water (28 mM),[28] but typically similar to those in MeCN (850 mM).[28]

11.3.2 Different Concentrations of BZA in $[C_4mpyrr][NTf_2]$

Since the chronoamperometric transients fit well in all RTILs for high concentrations (saturated solutions) of BZA, the transients were studied at different concentrations of BZA in the RTIL $[C_4mpyrr][NTf_2]$. It is expected that the steady-state (or chronoamperometric) limiting currents will not scale linearly with concentration for a CE process, except in the case of fast kinetics of the homogeneous step.[10,11] Figure 11.4 shows typical experimental (solid lines) and fitted theoretical (dots) chronoamperometric transients for the reduction of BZA in $[C_4mpyrr][NTf_2]$ at concentrations of 66, 55, 24 and 15 mM on a 10 μm diameter Pt electrode. Good fitting was observed at all concentrations, and the limiting current was found to increase linearly with concentration of BZA (see Figure 11.5), suggesting that the homogeneous kinetics of equation 11.3 are indeed fast in RTILs.

Since it is also known that the kinetics of the homogeneous step can be studied by observing how the limiting current changes as a function of size,[9–11] chronoamperometric transients were recorded at different concentrations of BZA on a smaller micro-electrode of diameter 2 μm. Figure 11.6 shows typical experimental (solid lines) and fitted theoretical (dots) chronoamperometric transients for the reduction of the BZA proton in $[C_4mpyrr][NTf_2]$ at concentrations of 41, 29, 17 and 5 mM. Consistent with the results obtained on the 10 μm diameter Pt electrode,

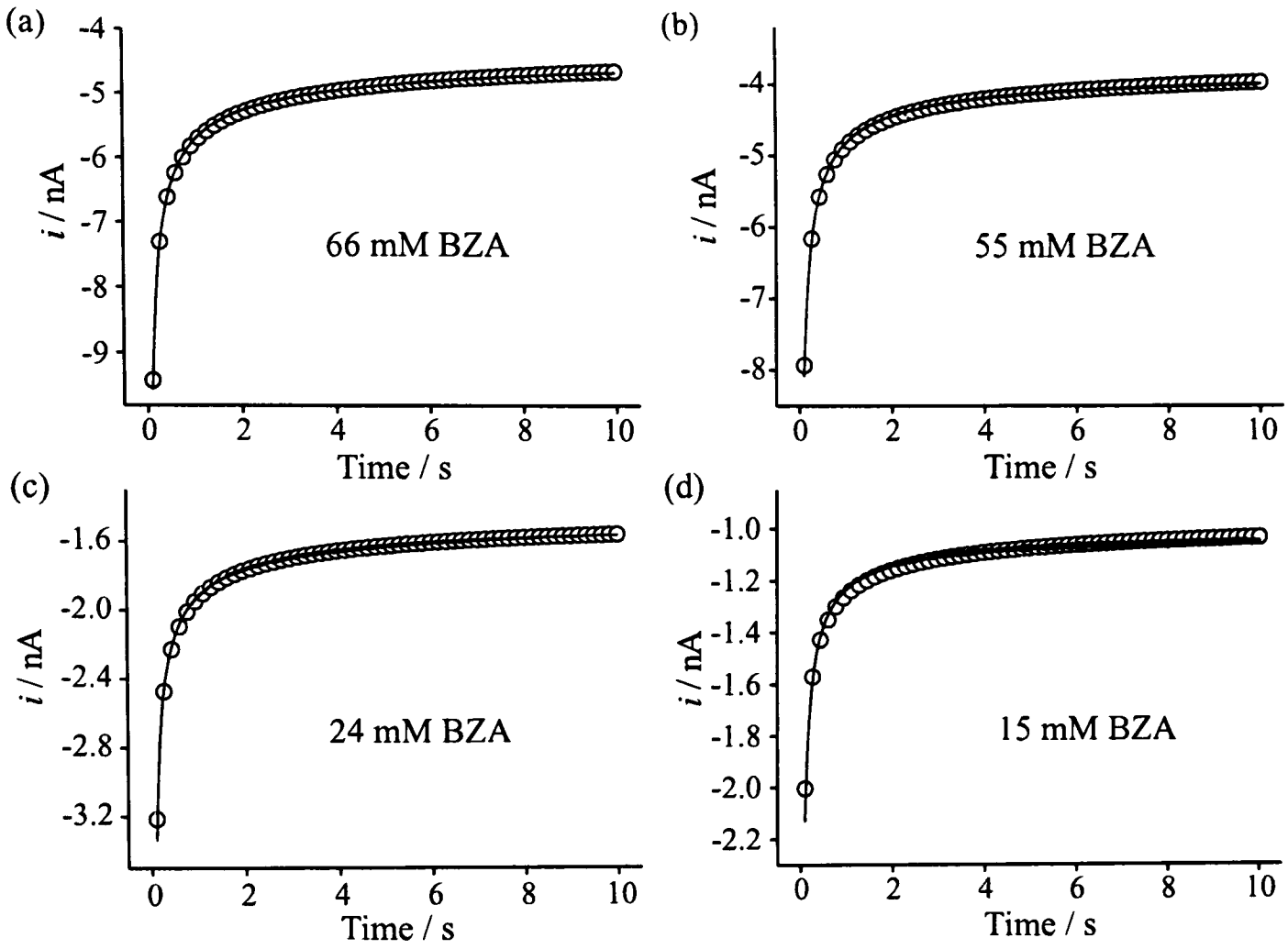

Figure 11.4: Experimental (solid lines) and fitted theoretical (dots) chronoamperometric transients for the reduction of BZA in $[C_4mpyrr][NTf_2]$ on a 10 μm diameter Pt electrode at concentrations of (a) 66, (b) 55, (c) 24 and (d) 15 mM. The experimental data was theoretically fitted to the Shoup and Szabo[15] expression.

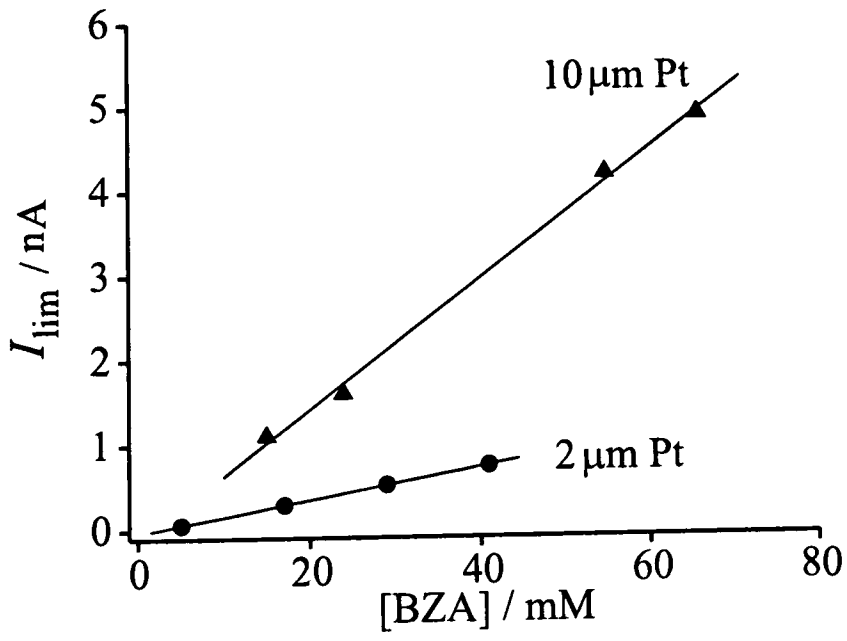

Figure 11.5: Plot of the chronoamperometric limiting current *vs* concentration for the reduction of BZA on a 10 μm and 2 μm diameter Pt electrode in $[C_4mpyrr][NTf_2]$ at 298 K.

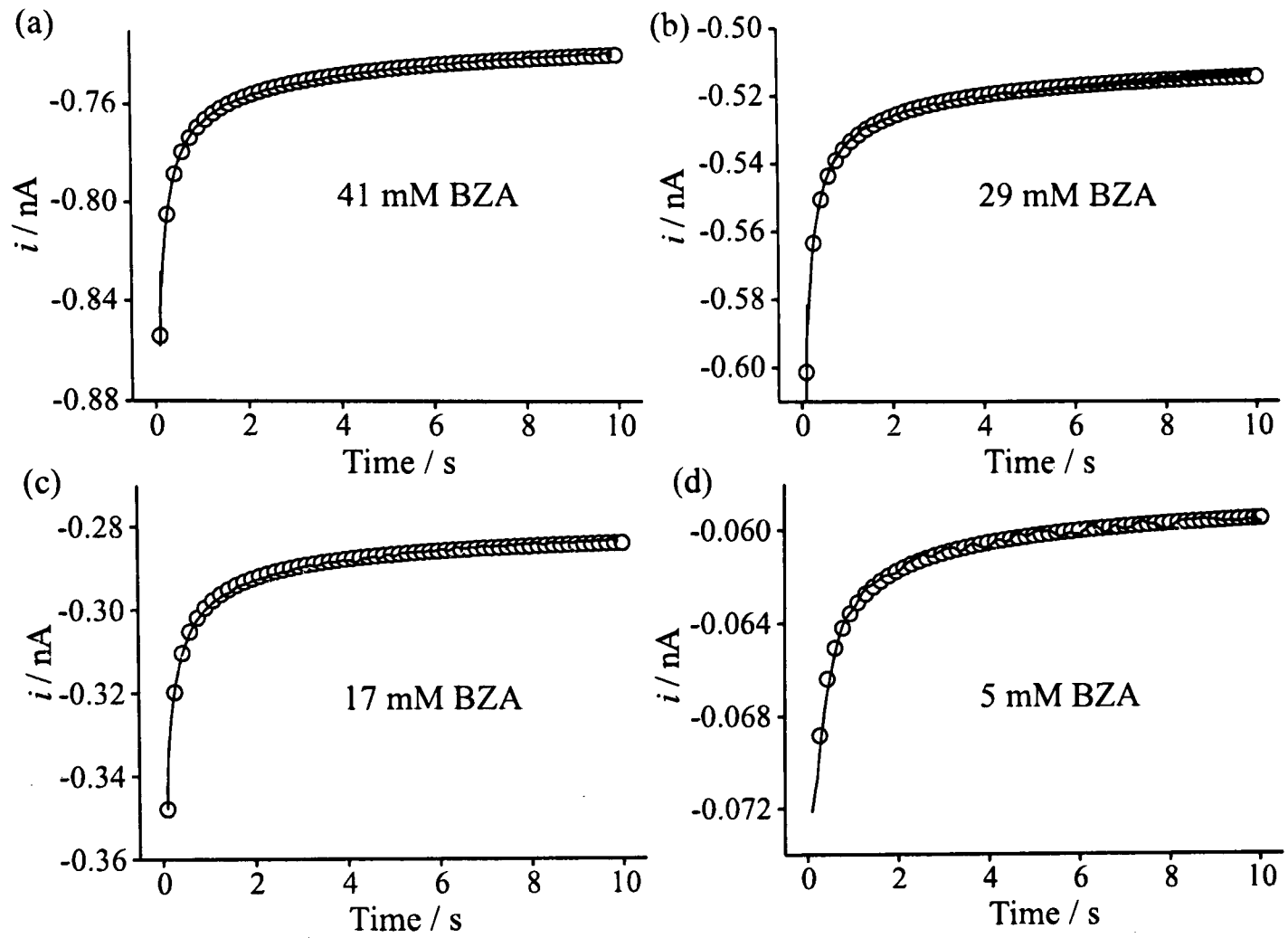

Figure 11.6: Experimental (solid lines) and fitted theoretical (dots) chronoamperometric transients for the reduction of BZA in $[C_4mpyrr][NTf_2]$ on a 2 μm diameter Pt electrode at concentrations of (a) 41, (b) 29, (c) 17 and (d) 5 mM. The experimental data was theoretically fitted to the Shoup and Szabo[15] expression.

good fitting was observed at all concentrations. A plot of the limiting current *vs* concentration of BZA on the 2 μm diameter Pt electrode is also included in Figure 11.5. The gradient of the line on the 10 μm diameter electrode is *ca.* five times that on the 2 μm diameter electrode, suggesting that the limiting current is scaling with electrode size, supporting the suggestion of fast kinetics of the homogeneous reaction given in equation 11.3, at least in $[C_4mpyrr][NTf_2]$.

11.3.2.1 Identification of Voltammetric Peaks for BZA Reduction

In order to try to identity the nature of the reductive 'pre-peak' and the oxidative 'back-peak', the voltammetry of BZA reduction was also studied on a gold microelectrode. The dotted lines on Figures 11.7a and 11.7b show typical voltammetry obtained for the reduction of a saturated solution of BZA in $[C_2mim][NTf_2]$ at a scan rate of 4 V s^{-1} on Pt (10 μm diameter) and Au

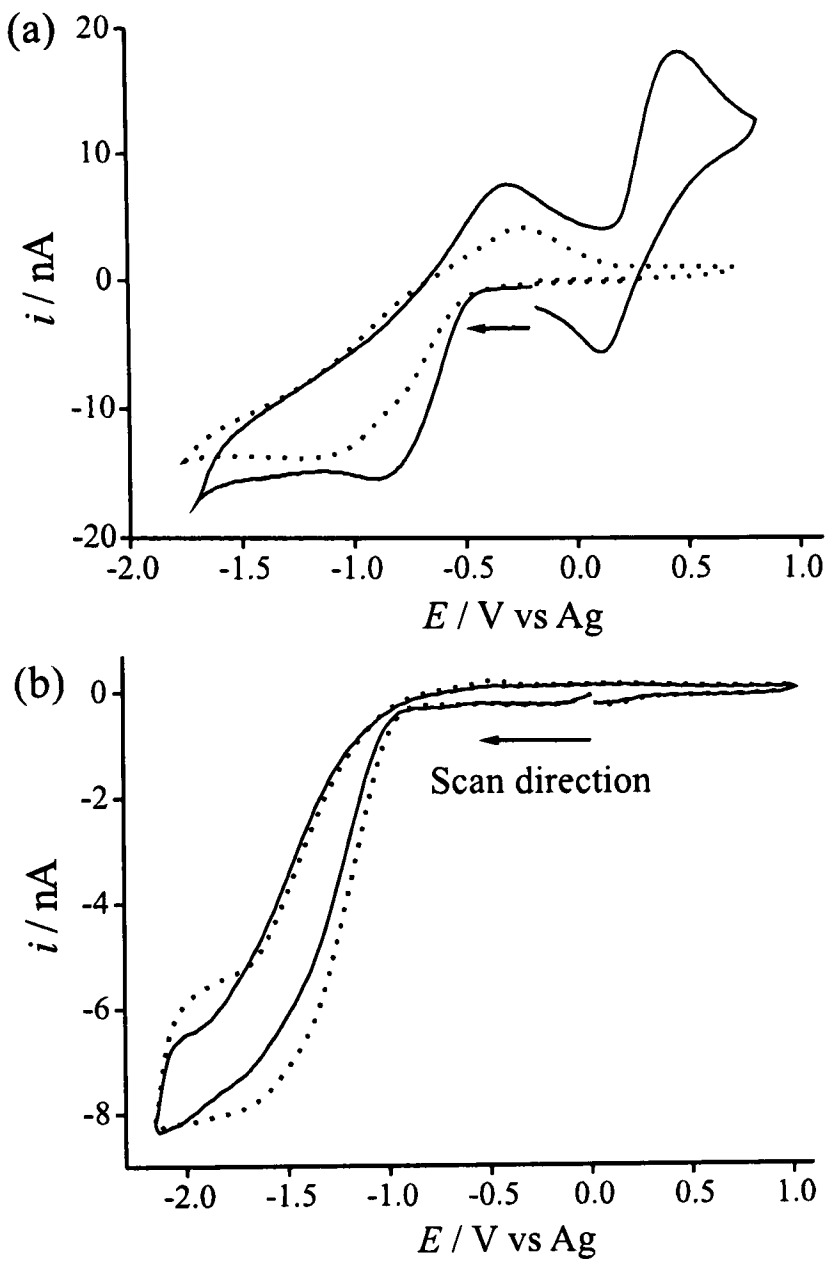

Figure 11.7: Typical cyclic voltammetry obtained for the reduction of a saturated solution of BZA in $[C_2mim][NTf_2]$ at 4 V s^{-1} on (a) a 10 μm diameter Pt electrode and (b) a 5 μm diameter Au electrode in the absence (dotted line) and presence (solid line) of 1 atm. hydrogen gas. The electrode was pre-activated at +1.5 V for 30 seconds prior to all scans.

(5 μm diameter) electrodes. On platinum, the reductive 'pre-peak' and the oxidative 'back-peak' are clearly present, however they are absent on gold (Figure 11.7b). Since it has been shown in Chapter 9 that hydrogen is not electrochemically active on gold electrodes in these media, it is very likely that both of these peaks are due to hydrogen.

To suggest if these peaks are due to either adsorbed or bulk hydrogen, the reduction of BZA was studied in the presence of hydrogen gas under the same conditions. The solid lines of Figures 11.7a and 11.7b show the voltammetry for the reduction of BZA in $[C_2mim][NTf_2]$ in the

presence of 1 atm. H_2 gas, overlaid on the same solutions in the absence of H_2 (dotted lines). On the Pt electrode, the oxidation of bulk hydrogen occurs at a much more positive potential than the oxidative back-peak of BZA proton reduction (in all six RTILs), suggesting that this peak is not due to bulk hydrogen. However, the size of the peak is increased slightly in the presence of hydrogen, and therefore this peak is likely to be the oxidation of adsorbed hydrogen. A similar peak was assigned to the oxidation of adsorbed H_2 on the reverse scan following the reduction of the ammonium ion (NH_4^+) in RTILs (Chapter 10). On the gold electrode, no peaks due to adsorbed or bulk hydrogen are observed, consistent with hydrogen being electrochemically inactive on gold (Chapter 9).

Next, the identity of the BZA reductive 'pre-peak' is discussed. This peak is likely to be either the reduction of protons forming H•(ads) on the platinum electrode surface, or the reduction of the proton solvated by the anion of the RTIL (HA, as seen previously for the reduction of the ammonium ion in Chapter 10). It is unlikely to be the latter, since the position of the reduction peak of the solvated proton (back peak following the oxidation of hydrogen) is at a much more positive potential (Figure 11.7a), and such a peak would not be present in $[C_4mim][NO_3]$, since no reduction peak was seen following the oxidation of hydrogen in this RTIL.[29] Therefore, it is believed that the 'pre-peak' is due the reduction of protons forming adsorbed hydrogen, H•(ads), on the platinum electrode surface. It is noted that the relative size of this peak was changeable, depending on the conditions of the electrode, and was much enhanced by pre-activation of the electrode surface.

11.3.2.2 Calculation of Peak Potentials *vs* Internal Reference Couple

As mentioned in the previous two chapters, it is important to report peak potentials *vs* an internal reference couple in order to compare the behaviour of different species and in different media, to indicate the thermodynamics of the reduction or oxidation process, and ultimately the

pH properties of the solvent. The reference electrode used in this work is a silver wire, which is known to shift over the course of an experiment, or on subsequent days.[30,31] Therefore, the ferrocene/ferrocenium redox couple (recommended by IUPAC,[32] used in RTILs,[33] and recently fully characterised in a range of RTIL media)[17] has been added to all solutions as an internal marker. Figure 11.8 shows the reduction of a saturated solution of BZA in $[C_2mim][NTf_2]$ with *ca.* 20 mM added ferrocene on a 10 μm diameter Pt electrode at a scan rate of 4 V s^{-1}. The reduction peak of the BZA proton is separated from the ferrocene/ferrocenium redox couple, and the potential of the reduction peak *vs* Fc/Fc^+ was found to be -1.33 V. This process was repeated in the remaining five RTILs, and the peak potentials are reported in the third column of Table 11.1. The potentials in the three $[NTf_2]^-$-based RTILs are approximately equal (-1.29–1.34 V), suggesting that the cation has little/no effect on the reduction thermodynamics. However, the potential for BZA proton reduction is lower in $[C_4mim][PF_6]$ (-1.48 V), and significantly lower in $[C_4mim][BF_4]$ (-1.77 V) and $[C_4mim][NO_3]$ (-1.74 V), suggesting that it is the nature of the anion which may influence the thermodynamics (formal potential). This has been observed previously for the formal potential of hydrogen oxidation *vs* the cobaltocenium/cobaltocene redox couple in several RTILs with different anions (Chapter 9). As may be expected, in this work, the lowest peak potentials are observed in RTILs which may show the strongest interaction with the acid ($[C_4mim][BF_4]$ and $[C_4mim][NO_3]$), and are consistent with the solubility being much higher in these media (see Table 11.1).

11.3.3 Extension of the Cathodic window

When the voltammetry was scanned to a more negative potential in $[C_4mpyrr][NTf_2]$, a second, chemically reversible reduction peak was observed. Figure 11.9 shows the reduction of a saturated solution of BZA in $[C_4mpyrr][NTf_2]$ with an extended cathodic window on both (a) Au and (b) Pt electrodes. An electrochemically reversible wave was observed on both electrodes

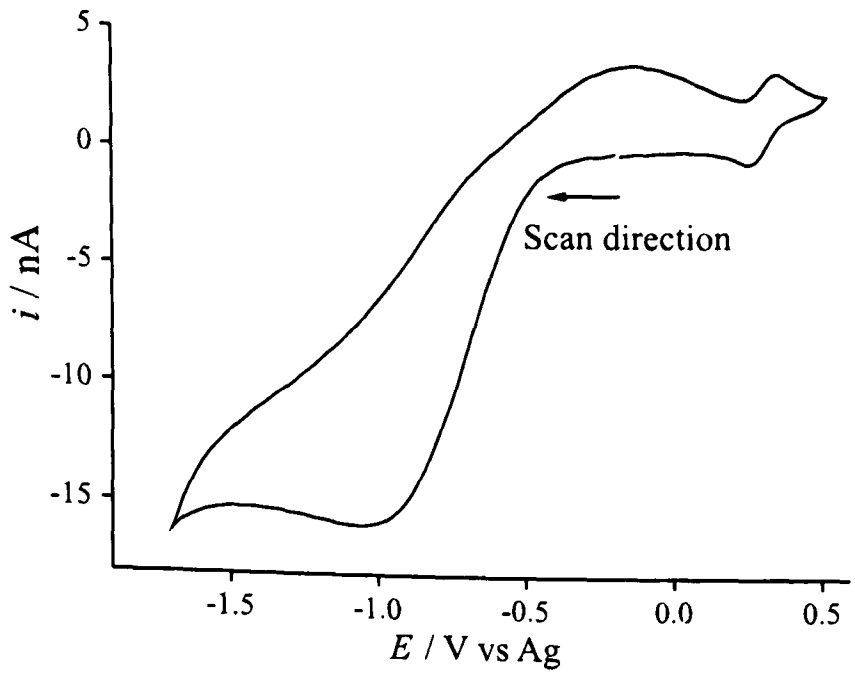

Figure 11.8: Typical cyclic voltammetry for the reduction of a saturated solution of BZA in $[C_2mim][NTf_2]$ in the presence of *ca.* 20 mM ferrocene on a 10 μm diameter Pt electrode at 298K at a scan rate of 4 V s^{-1}. The electrode was pre-activated at +1.5 V for 30 s.

at a potential of *ca.* -2.5 V *vs* Ag, corresponding to a potential of -2.69 V *vs* Fc/Fc^+ (Fc/Fc^+ redox couple at *ca.* +0.2 V *vs* Ag on Figure 11.9). This peak was also observed following the reduction of BZA in $[C_4mim][BF_4]$ at -2.69 V *vs* Fc/Fc^+, but was not seen in the remaining four RTILs. This could be due to the slightly smaller electrochemical window in these solvents, leading to the peak being obscured by solvent breakdown. We speculate that this peak is due to the one-electron reduction of benzoate ($C_6H_5COO^-$) to the radical anion ($C_6H_5{}^{\bullet}C(O^-)_2$), shown below.

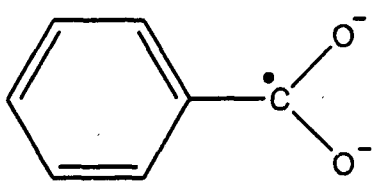

The formation of this species following benzoic acid reduction in liquid ammonia has been proven by ESR experiments.[34] It is possible that the RTIL medium is suitable for the formation of this radical species, and the presence of an oxidative back-peak suggests that the radical anion is stable under these conditions. It can also be seen from Figure 11.9 that the potential for the first reduction peak of BZA is much more negative on the gold electrode (-1.93 V) than on

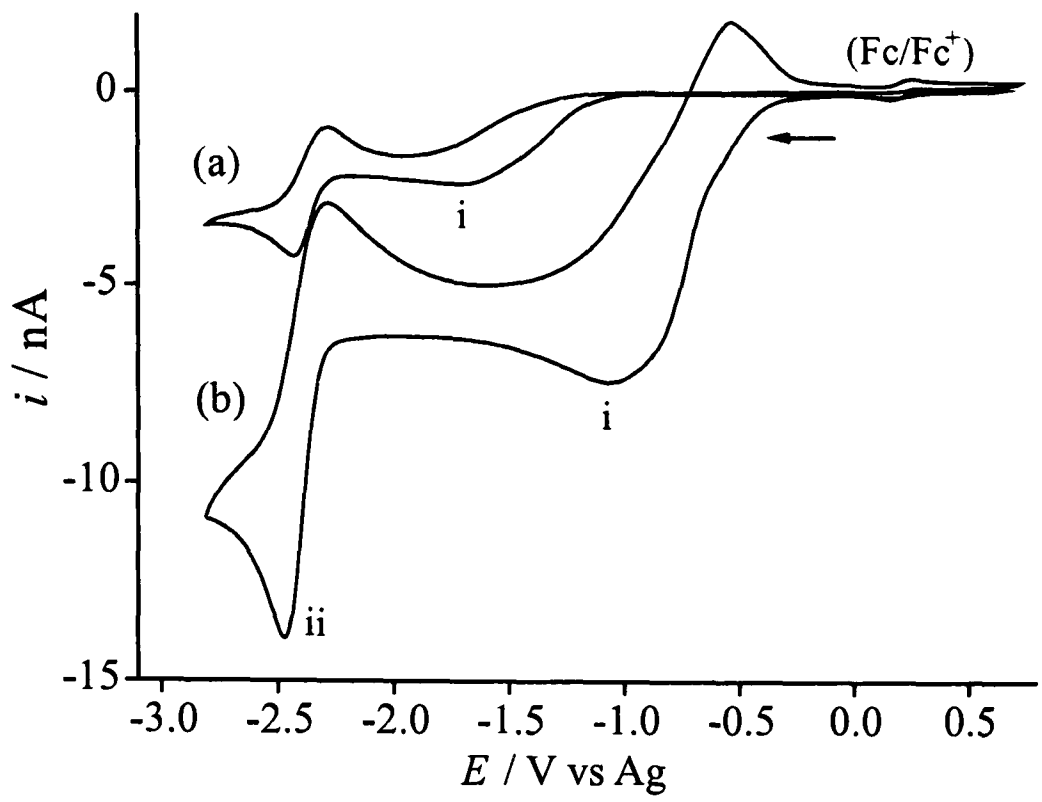

Figure 11.9: Cyclic voltammograms obtained at 4 V s^{-1} for the reduction of a saturated solution of BZA in $[C_4mpyrr][NTf_2]$ at 298 K on (a) a 5 μm diameter Au electrode and (b) a 10 μm diameter Pt electrode with an extended cathodic limit. Ferrocene was added as an internal reference, and the electrodes were pre-activated at +1.5 V for 30 seconds.

platinum (-1.29 V), suggesting that the electrode kinetics are faster on Pt than Au. However, the radical anion is reduced at the same potential (-2.69 V) on both platinum and gold electrodes.

11.3.4 Cyclic Voltammetry for the Reduction of Substituted Benzoic Acids in $[C_4mpyrr][NTf_2]$

In addition to the voltammetry of BZA reduction in several RTILs, the voltammetry of several substituted benzoic acid species was also studied. The RTIL chosen for these experiments was $[C_4mpyrr][NTf_2]$, since this has the widest reductive electrochemical window of all the RTILs studied, and may allow the observation of the radical anion peak (see section 11.3.3) if it is present.

Figure 11.10 shows the reduction of saturated solutions of (a) 4-methoxy BZA, (b) 4-chloro BZA, (c) 4-bromo BZA and (d) 4-dimethylamino BZA in $[C_4mpyrr][NTf_2]$ at a range of scan rates on a 10 μm diameter Pt electrode. The peak currents for the reduction peak are smaller

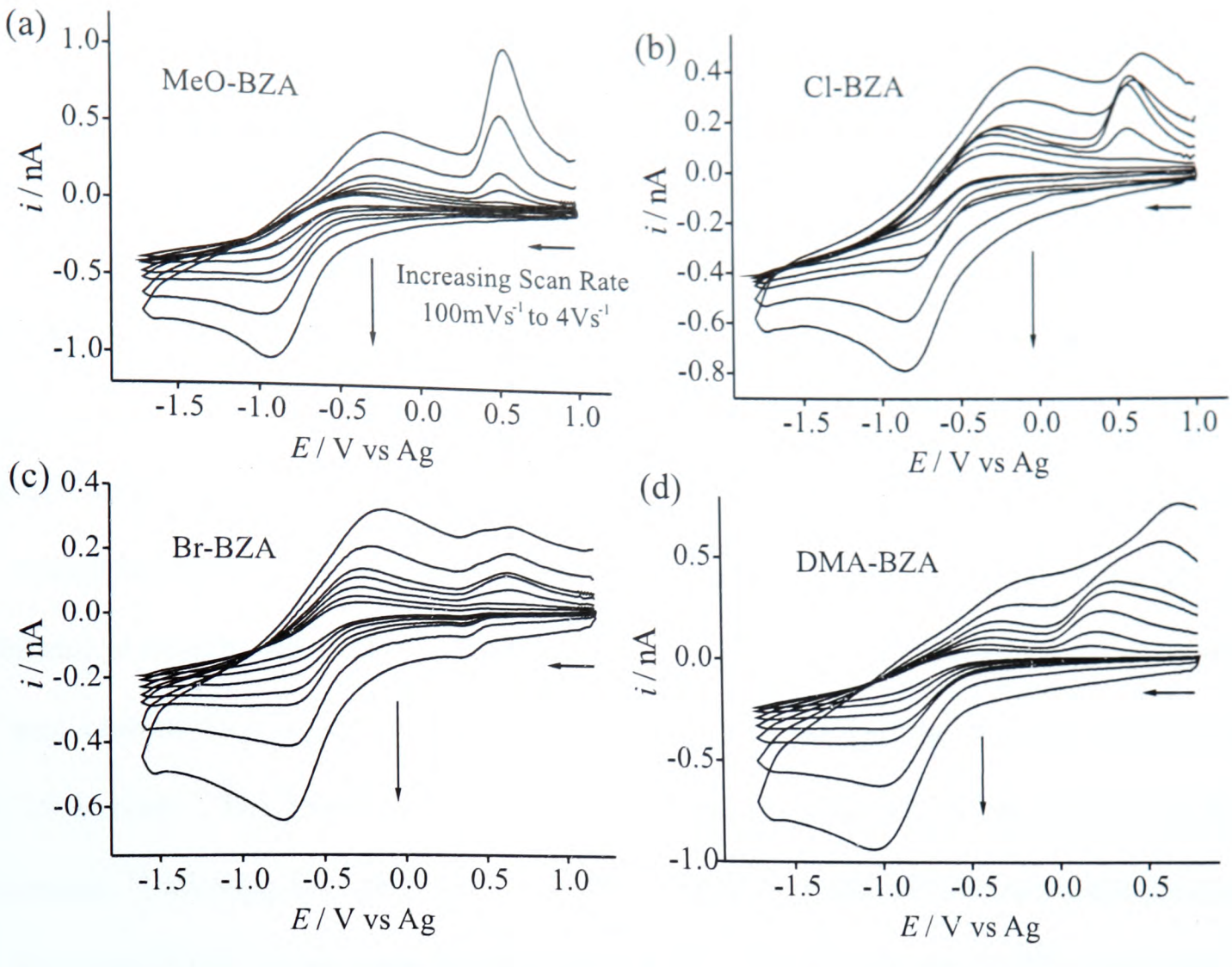

Figure 11.10: Typical cyclic voltammetry obtained over a range of scan rates (0.1, 0.2, 0.4, 0.7, 1, 2 and 4 V s^{-1}) for the reduction of saturated solutions of various substituted BZAs in $[C_4mpyrr][NTf_2]$ on a 10 μm diameter Pt electrode at 298 K.

than that observed for the BZA proton (Figure 11.2c), suggesting a lower solubility of the substituted BZAs. The voltammetry is somewhat similar to that of BZA, with a reduction peak at *ca.* -1 V and a corresponding broad oxidation peak assigned to the oxidation of adsorbed hydrogen. However, there is no evidence of the reductive 'pre-peak' (reduction of adsorbed protons), and activating the electrode at +1.5 V for 30 seconds did not influence the size or shape of the voltammograms obtained. In addition, there is a second oxidative 'back-peak' present in the voltammetry of all four substituted BZAs which was not present for the non-substituted form. It is thought that this peak is either the oxidation of bulk hydrogen, or the oxidation of the substituted benzoate anion. The oxidation of bulk hydrogen can be ruled out, since the peak potential of hydrogen oxidation was found to be at -0.03 V *vs* Fc/Fc^+

(at 4 V s^{-1}), and the potentials of the second oxidative peak on Figure 11.10a, b and c are *ca.* +0.25 V *vs* Fc/Fc^+. It is therefore suggested that the second oxidative peak following the reduction of substituted BZAs corresponds to the oxidation of the benzoate anion, which may be facilitated by electron-withdrawing substituents (Cl and Br) in the para-position. In the case of the electron-releasing substituents (OMe, DMA and DEA), it is possible that the methoxy and amino groups are protonated, rendering the substituent electron-withdrawing and facilitating the oxidation reaction. In the non-substituted case, no oxidation peak for the anion was seen.

Potential step chronoamperometry was performed on the reduction peak in all saturated solutions of substituted BZAs in $[C_4mpyrr][NTf_2]$. The potential was stepped from a position of zero current to a potential more negative than the peak and the transient was recorded for 10 seconds. The experimental transients were theoretically fit to the Shoup and Szabo expression,[15] allowing the calculation of diffusion coefficients and solubilities of each compound in $[C_4mpyrr][NTf_2]$. In all cases, the fitting was good (± 0.7 %), and the numbers obtained have been included in Table 11.1. As expected from the peak currents of the reduction peak, the solubilities of all five substituted BZAs were found to be significantly smaller than for the non-substituted BZA (see Table 11.1). The diffusion coefficients of each compound are approximately similar (*ca.* 2×10^{-11} m^2 s^{-1}), with a slight tendency to decrease with increasing size of the substituent.

Also included in Table 11.1 are the potentials for the reduction peak *vs* Fc/Fc^+. The reduction potential was found to vary between the different substituted BZAs, with Cl-BZA and Br-BZA appearing to be the easiest to reduce (-1.15 V *vs* Fc/Fc^+), followed by MeO-BZA (-1.25 V), BZA (-1.29 V) and finally the two dialkylamino BZAs (-1.45 and -1.46 V). This may represent the different electron donating/withdrawing power of the substituents. The second reduction peak (ii, reduction of the radical anion) was observed in the voltammetry all five compounds, and the potentials for the chloro, bromo and methoxy substituted BZAs (*ca.*

-2.68 V) were found to be similar to that of BZA (-2.69 V). but more positive than the two dialkylamino BZAs (*ca.* -2.88 V), suggesting that the presence of the dialkylamino groups may affect the thermodynamics of the second reduction.

11.3.4.1 Electrochemical Oxidation of 4-dimethylamino- and 4-diethylamino- benzoic acid

When studying the voltammetry for the reduction of the substituted BZAs, a sharp anodic feature was observed for the oxidation of 4-dimethylamino (and 4-diethylamino) benzoic acid in $[C_4mpyrr][NTf_2]$. This feature was not present in the methoxy-, chloro- and bromo- substituted and non-substituted forms of BZA, and therefore must be due to the oxidation of the dialkylamino group. Figure 11.11 shows the oxidation of a saturated solution of DMA-BZA in $[C_4mpyrr][NTf_2]$ at a range of scan rates on a Pt electrode of diameter 10 μm. Similar voltammetry was also observed for the oxidation of DEA-BZA, but the voltammetry has not been included here. As seen in Figure 11.11, the oxidation peak was sharp and electrochemically irreversible, and the appearance of two to three reduction peaks were observed on the reverse sweep at higher scan rates (4 V s^{-1}). These features are similar to that observed by Kotkar and Srivastava[35] for the oxidation of 4-aminobenzoic acid on carbon paste electrodes in acidic buffer solution. They suggest that the oxidation peak is due to the one-electron oxidation of the amino group to the free radical (C_6H_5-$N^{\bullet}H$), which combines with another free radical to give a dimer (with a benzidine-like structure), and again undergoes oxidation by two electrons to form an azo compound. On the reverse sweep, they observed a reversible reduction peak, which was assigned to the reduction of polymerized 4-aminobenzoic acid on the electrode surface.[35] In this work, although there are alkyl substituents on the amine group, it is possible that substituted polyaniline is being formed on the Pt electrode surface *via* the radical cation (C_6H_5-$N^{\bullet+}R_2$), due to the similar voltammetric features observed.

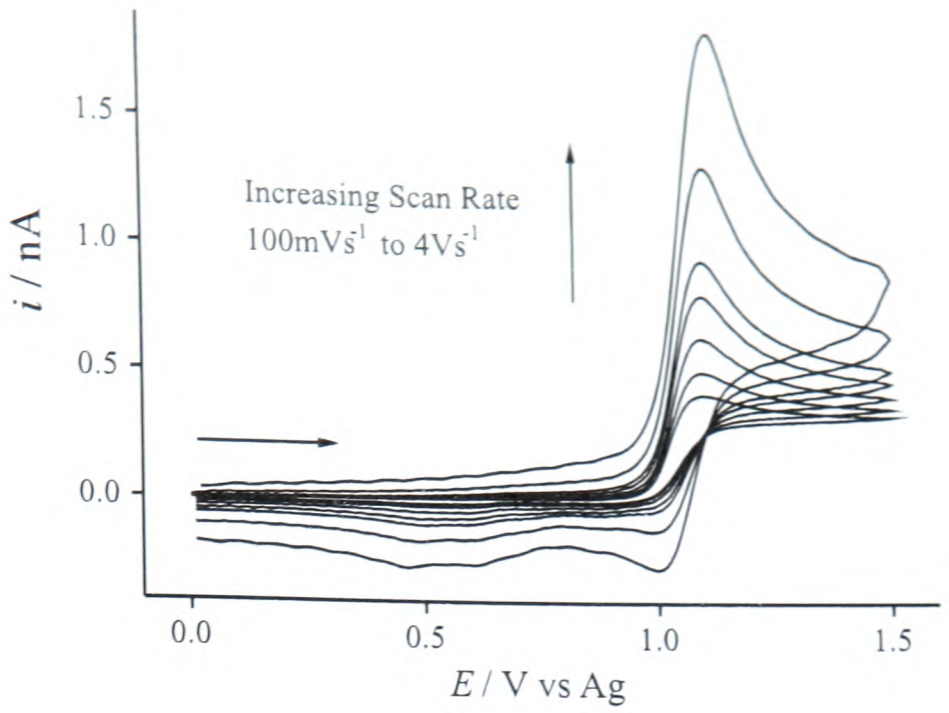

Figure 11.11: Cyclic voltammetry obtained over a range of scan rates (0.1, 0.2, 0.4, 0.7, 1, 2 and 4 V s^{-1}) for the oxidation of a saturated solution of DMA-BZA in $[C_4mpyrr][NTf_2]$ on a 10 μm diameter Pt electrode at 298 K.

11.4 Conclusions

Cyclic voltammetry for BZA reduction was found to be similar in all six RTILs, with a main reduction peak following a CE mechanism (the position of which depends mainly on the nature of the RTIL anion), a reductive 'pre-peak' (reduction of adsorbed protons) and an oxidative 'back-peak' (oxidation of adsorbed hydrogen). A further reduction peak at more negative potentials was assigned to the reversible reduction of the BZA radical anion. The potentials of the proton reduction peak were found to vary when BZA was substituted in the para position and when the electrode was changed from Pt to Au. However, the potential of the radical anion peak was similar on both Pt and Au, and for the substituted BZAs, except in the case of the two dialkylamino BZAs. An additional oxidative 'back-peak' was observed following the reduction of the methoxy, chloro, bromo and dialkylamino substituted BZAs, tentatively assigned to the oxidation of the benzoate anion, facilitated by electron-withdrawing substituents on the benzene ring. In addition, the voltammetry for the oxidation of two dialkylamino BZAs suggests the possible formation of substituted polyaniline on the Pt electrode surface.

References

[1] He, W.; Silvester, D. S.; Streeter, I.; Aldous, L.; Hardacre, C. and Compton, R. G., *J. Phys. Org. Chem.*, 2008, page Accepted for publication.

[2] Silvester, D. S.; He, W.; Aldous, L.; Hardacre, C. and Compton, R. G., *J. Phys. Chem. C*, 2008, **112**, 12966–12973.

[3] Barradas, R. G.; Kutowy, O. and Shoesmith, D. W., *Electrochim. Acta*, 1974, **19**, 49–56.

[4] Daniele, S.; Ugo, P.; Mazzocchin, G. A. and Bontempelli, G., *Anal. Chim. Acta*, 1985, **173**, 141–148.

[5] Treimer, S. E. and Evans, D. H., *J. Electroanal.Chem.*, 1998, **455**, 19–27.

[6] Vielstich, W. and Jahn, D., *Z. Elektrochem.*, 1960, **64**, 43–44.

[7] Albery, W. J. and Bell, R. P., *Proc. Chem. Soc.*, 1963, **6**, 169–70.

[8] Barrette Jr., W. C. and Sawyer, D. T., *Anal. Chem.*, 1984, **56**, 653–657.

[9] Streeter, I. and Compton, R. G., *J. Electroanal. Chem.*, 2008, **615**, 154–158.

[10] Daniele, S.; Lavagnini, I.; Baldo, M. A. and Magno, F., *Anal. Chem.*, 1998, **70**, 285–294.

[11] Daniele, S.; Baldo, M. A.; Bragato, C.; Abdelsalam, M. E. and Denuault, G., *Anal. Chem.*, 2002, **74**, 3290–3296.

[12] Fleischmann, M.; Lasserre, F.; Robinson, J. and Swan, D., *J. Electroanal. Chem.*, 1984, **177**, 97–114.

[13] Ji, X.; Silvester, D. S.; Aldous, L.; Hardacre, C. and Compton, R. G., *J. Phys. Chem. C*, 2007, **111**, 9562–9572.

[14] Compton, R. G. and Banks, C. E., *Understanding Voltammetry*, World Scientific, Singapore, 2007.

[15] Shoup, D. and Szabo, A., *J. Electroanal. Chem. Interfacial Electrochem.*, 1982, **140**, 237–245.

[16] Paddon, C. A.; Silvester, D. S.; Bhatti, F. L.; Donohoe, T. J. and Compton, R. G., *Electroanalysis*, 2007, **19**, 11–22.

[17] Rogers, E. I.; Silvester, D. S.; Poole, D. L.; Aldous, L.; Hardacre, C. and Compton, R. G., *J. Phys. Chem. C*, 2008, **112**, 2729–2735.

[18] Hotta, T.; Nii, S.; Yajima, T. and Kawaizumi, F., *Chem. Eng. Technol.*, 2007, **30**, 208–213.

[19] Catchpole, O. J. and King, M. B., *Ind. Eng. Chem. Res.*, 1994, **33**, 1828–37.

[20] Evans, R. G.; Klymenko, O. V.; Price, P. D.; Davies, S. G.; Hardacre, C. and Compton, R. G., *ChemPhysChem*, 2005, **6**, 526–533.

[21] Evans, R. G.; Klymenko, O. V.; Saddoughi, S. A.; Hardacre, C. and Compton, R. G., *J. Phys. Chem. B*, 2004, **108**, 7878–7886.

[22] Barrosse-Antle, L.; Silvester, D. S.; Aldous, L.; Hardacre, C. and Compton, R. G., *J. Phys. Chem. B*, 2008, **112**, 3398–3404.

[23] O'Mahony, A. M.; Silvester, D. S.; Aldous, L.; Hardacre, C. and Compton, R. G., *J. Phys. Chem. C*, 2008, **112**, 7725–7730.

[24] Dobinson, G. C.; Mason, R. and Russell, D. R., *Chem. Commun.*, 1967, **2**, 62–63.

[25] Faithful, B. D. and Wallwork, S. C., *Chem. Commun.*, 1967, **23**, 1211.

[26] Sengul, A., *Turk. J. Chem.*, 2005, **29**, 571–578.

[27] Siew, L. C. and Sundheim, B. R., *J. Phys. Chem.*, 1969, **73**, 4135–4141.

[28] Chantooni Jr., M. K. and Kolthoff, I. M., *J. Phys. Chem.*, 1974, **78**, 839–846.

[29] Silvester, D. S.; Ward, K. R.; Aldous, L.; Hardacre, C. and Compton, R. G., *J. Electroanal. Chem.*, 2008, **818**, 53–60.

[30] Rogers, E. I.; Silvester, D. S.; Jones, S. E. W.; Aldous, L.; Hardacre, C.; Russell, A. J.; Davies, S. G. and Compton, R. G., *J. Phys. Chem. C*, 2007, **111**, 13957–13966.

[31] Silvester, D. S.; Rogers, E. I. and Compton, R. G., *'Reference Electrodes for use in RTILs' in Electrodeposition from Ionic Liquids*, ed. Endres, F, MacFarlane, D. R. and Abbot, A., Wiley, Weinheim Germany, 2008.

[32] Grützner, G. and Kuta, J., *Pure Appl. Chem.*, 1984, **56**, 461–466.

[33] Zhang, J. and Bond, A. M., *Anal. Chem.*, 2003, **75**, 2694–2702.

[34] Buick, A. R.; Kemp, T. J.; Neal, G. T. and Stone, T. J., *Chem. Commun.*, 1968, **21**, 1331–2.

[35] Kotkar, R. M. and Srivastava, A. K., *Sens. Act. B*, 2006, **119**, 524–530.

Overall Conclusions of this Thesis

This thesis has looked at the electrochemical behaviour of a number of solid, liquid and gaseous species dissolved in a range of room temperature ionic liquid solvents. In general, the results indicate that many compounds (*e.g.* bromide, nitro derivatives, ammonia) display similar reactions and mechanisms in RTILs as in aprotic solvents such as MeCN, DMF and DMSO. However other species (*e.g.* nitrates, PCl_3, $POCl_3$) show remarkably different behaviour to traditional solvents. For nitrates, the electrochemical behaviour in RTILs much more closely resembles the behaviour in high temperature nitrate melts than in conventional solvents. This makes RTILs very promising media for the study of inorganic compounds, and highlights the need for more investigations in this exciting area. It has also been shown that the nature of the RTIL anion has a very strong influence on its interaction with protons. Accordingly electrode processes in which these are released are sensitive to the RTIL nature. These results may provide a basis for understanding the pH properties of RTIL solvents, which cannot be determined using conventional methods.

In terms of using RTILs for real-world electrochemical applications, much more research is needed on the effect of atmospheric impurities on the physical properties of RTILs. It is noted that all of the experiments in this thesis were performed in highly pure ionic liquids under a controlled atmosphere, where effects from moisture and gaseous impurities were minimised. However, in order to scale these up for commercial purposes (*e.g.* for use in gas sensors), the behaviour of electroactive species should be investigated under atmospheric conditions and in the presence of differing amounts of moisture to resemble the conditions in a variety of climates. If such investigations are carried out and appear promising, this could allow the use of RTILs as low-volatility electrolytes in practical sensors.

Typeset using LaTeX